Calix[4]pyrrole Based Receptors for the Recognition of Ion Pairs

Ricardo Molina Muriel

UNIVERSITAT ROVIRA i VIRGILI

Calix[4]pyrrole Based Receptors for the Recognition of Ion Pairs

RICARDO MOLINA MURIEL

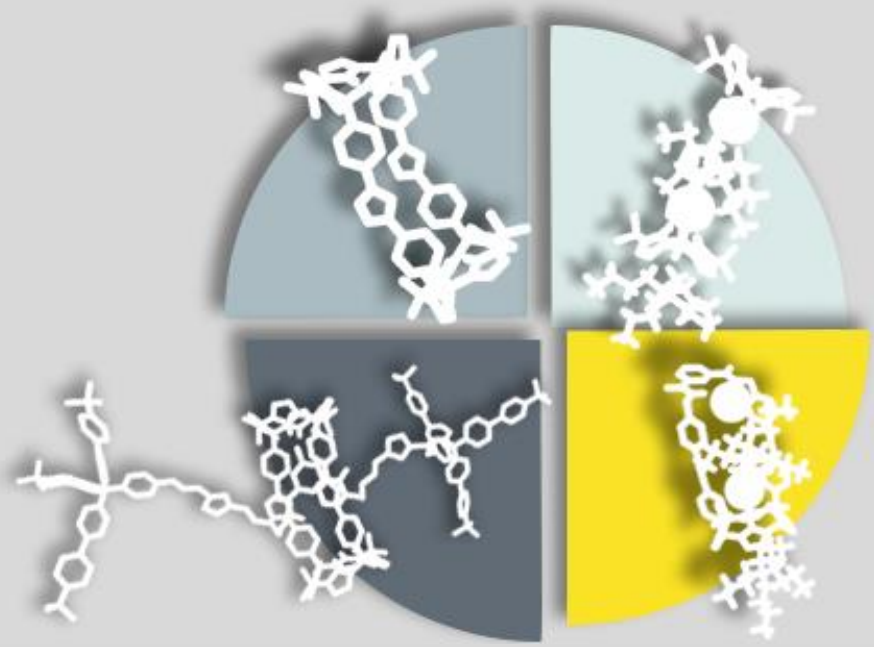

DOCTORAL THESIS
2020

UNIVERSITAT ROVIRA I VIRGILI
Calix[4]pyrrole Based Receptors for the Recognition of Ion Pairs
Ricardo Molina Muriel

UNIVERSITAT ROVIRA I VIRGILI
Calix[4]pyrrole Based Receptors for the Recognition of Ion Pairs
Ricardo Molina Muriel

DOCTORAL THESIS

Ricardo Molina Muriel

CALIX[4]PYRROLE BASED RECEPTORS FOR THE RECOGNITION OF ION PAIRS

Supervised by Prof. Pablo Ballester Balaguer

UNIVERSITAT
ROVIRA i VIRGILI

Tarragona

2020

UNIVERSITAT ROVIRA I VIRGILI
Calix[4]pyrrole Based Receptors for the Recognition of Ion Pairs
Ricardo Molina Muriel

ICIQ
Institut Català d'Investigació Química

Av. Països Catalans, 16
43007 Tarragona, Spain
Tel. (+34) 977 920 200
email: iciq@iciq.es

UNIVERSITAT ROVIRA i VIRGILI
Dept. de Química Analítica i Química Orgànica

Carrer de Marcel·lí Domingo, 1
43007 Tarragona, Spain
Tel. (+34) 977 55 97 69
email: sdn4@urv.cat

I STATE that the present study, entitled "Calix[4]pyrrole based receptors for the recognition of ion pairs", presented by Ricardo Molina Muriel for the award of the degree of Doctor, has been carried out under my supervision at the Institute of Chemical Research of Catalonia (ICIQ).

Tarragona, November 2020

Doctoral Thesis Supervisor

Prof. Pablo Ballester Balaguer

UNIVERSITAT ROVIRA I VIRGILI
Calix[4]pyrrole Based Receptors for the Recognition of Ion Pairs
Ricardo Molina Muriel

«*Los dioses no tuvieron más sustancia que la que tengo yo. Yo tengo, como ellos, la sustancia de todo lo vivido y de todo lo por vivir. No soy presente sólo, sino fuga raudal de cabo a fin. Y lo que veo a un lado y otro, en esta fuga, rosas, restos de alas, sombra y luz, es sólo mío, recuerdo y ansia míos, presentimiento, olvido. ¿Quién sabe más que yo, quién puede, ha podido, podrá decirme a mí qué es mi vida y mi muerte, qué no es? Si hay quien lo sabe, yo lo sé más que ése, y si lo ignora, más que ése lo ignoro. Lucha entre este saber y este ignorar es vida, su vida, y es la vida*»

Juan Ramón Jiménez

«*Más sabe el que vive sin querer saber que el que quiere saber sin vivir*»

Benito Pérez Galdós

«*Hay cosas encerradas dentro de los muros que, si salieran de pronto a la calle y gritaran, llenarían el mundo*»

Federico García Lorca

UNIVERSITAT ROVIRA I VIRGILI
Calix[4]pyrrole Based Receptors for the Recognition of Ion Pairs
Ricardo Molina Muriel

Acknowledgements

La presente tesis es un resumen de parte de los resultados obtenidos en estos más de cuatro años de investigación. Fuera de estas páginas quedan, por razones obvias, las experiencias personales vividas dentro y fuera del laboratorio PB4. Sirvan estas páginas como agradecimiento a todas esas personas que han dado fruto a tantos momentos inolvidables.

En primer lugar, quiero dar las gracias a mi supervisor **Pau Ballester**. Cuando ya tenía un pie fuera de Tarragona, me diste la oportunidad de unirme a tu grupo de investigación con un proyecto que me apasionaba. Tuve siempre muy presente durante estos cuatro años lo que me dijiste en esa primera reunión: «*Tener el título de doctor no te hará más inteligente, no es más que un papel. Lo que aprendas con tu trabajo estos años es lo que te llevarás a casa; de ti depende*». A pesar de las innumerables dificultades, siempre estuviste dispuesto a ayudar y a enseñarme, con suma paciencia, cómo se lleva a cabo la investigación de más alto nivel. Gracias por todo el apoyo que me has dado durante este largo periodo de aprendizaje. Con tu supervisión y consejo, me has ayudado a conocer tanto la química supramolecular como a mí mismo. Me faltarían líneas para agradecértelo tanto como mereces. Muchísimas gracias.

La ayuda de la doctora **Gemma Aragay** ha sido imprescindible para la elaboración de esta tesis. Los primeros pasos dentro de un laboratorio son siempre complicados, pero Gemma estaba ahí para guiarme por este laberinto de matraces, espectros de RMN y referencias… A lo largo de estos años, tu ayuda con la interpretación de los resultados más extravagantes, algunos aún sin explicación (los 30 ITC en acetona mandan saludos), fue inestimable. No creo que olvide nunca esas visitas a la oficina a las 7.30 h de la mañana, llevando un espectro lleno de tachones, que a menudo seguían con la formulación de teorías y explicaciones surrealistas y solían terminar con un «*esto a Pau no le va a convencer*». Por tu paciencia, tus ganas de ayudar, tu amabilidad y por el aceite de calidad a bajo precio, gracias Gemma.

A lo largo de estos años el PB4 ha sido un ir y venir de investigadores de todos los lugares del mundo. Esta mezcolanza intercultural es el caldo de cultivo perfecto para un crecimiento personal y profesional que difícilmente habría alcanzado en cualquier otro sitio. Mi agradecimiento a todos y cada uno de los miembros de este grupo.

Muchísimas gracias a los doctores Daniel Hernández, Jordi Aguilera, Frank Arroyave, Ryo Sekiya, Alejandro Díaz-Moscoso, Rajesh Pudi y Ramón Romero por vuestra compañía en la primera etapa de mi tesis. Si este grupo ha sido grande y se ha mantenido fuerte en nuestro campo durante estos años, es por la implicación y el esfuerzo de todos vosotros.

Gracias también a **Beatriz Martin** por su inestimable ayuda desde el primer día. Gracias por estar siempre disponible y ayudarme en todos los problemas, administrativos o no, que surgen en el día a día de un laboratorio de investigación. Siempre nos atiendes con una sonrisa que, imagino, debe ser difícil mantener cuando te acosan diariamente con peticiones de todo tipo. Muchas gracias por todo.

Gracias a **Luis** por su ayuda y consejo, así como por los buenos momentos pasados dentro y fuera del laboratorio. Tu pasión por la química y forma de ver la vida me ha enseñado mucho en estos años. Gracias por la compañía en esos tristes cafés de sábado por la mañana. Gracias también a la persona que tuve sentada a mi vera durante estos años: **Guillem**. Gracias por haber sido siempre tan natural y auténtico conmigo, en lo bueno y en lo malo. En más de una ocasión me hizo falta un poco de realidad (de la de ahí fuera) para poner los pies en la tierra. Gracias por tu guasa, por el *trap* decadente, por tu capacidad de hablar de todo, y por la brasa que me has dado con la política. Después de esto, como solías decir: «*Yo ya, de relax…*» Ahora le toca a *la* **Giulia**. No se podría entender mi paso por este laboratorio sin mencionar a esta persona. Tuvimos una conexión prácticamente inmediata desde que coincidimos en Cambridge, y es que resulta fácil identificar y conectar con aquellos que comparten tus mismas taras. Gracias por tantísimos momentos; casi que necesitaría una tesis aparte para enumerarlos… Por las pausas para el *YogiTea*, por los momentos *Gallo*®, por las miradas a cámara, por tu lucha contra lo *unacceptable*, por pasarte por Huelva y por ser tan pesada, gracias. Recuerda: «*You are ~~un~~limited*». Gracias a **Lluis** por hacer del laboratorio un lugar mejor. Tenías a tu alrededor un aura de buen rollo y tranquilidad que no he visto en nadie. Siempre implicado en todo y dejándote la piel tanto en el laboratorio como de fiesta por Tarragona. Nunca olvidaré tu chaqueta de postdoc ni tus pósteres, directos al primer premio. Gracias por tu positivismo, por ser el único que conocía las referencias de la España más cañí de los 90, por las ensaimadas, por tu amistad y por los «*¡Venga chavales!*». Larga vida a la reina emérita del PB4. Desde la mismísima Bogotá, Colombia, mandaron al analista estrella, al mero mero, al máster de la química, mi mompirri: **Felipe**. Muchísimas gracias Felipe por tu inestimable amistad. No podría haber tenido un mejor vecino de cabina. Hemos pasado interminables horas de

columna charlando sobre historias inverosímiles: de aventuras en el Amazonas, atracos en puentes, citas para hablar de las noticias, profesoras de química-física con la cabeza ida y nuestros amigos con Nobel. Nos hemos comportado como verdaderos críos, llegando muy lejos con tal de hacer un chiste o una gracieta sin gracia. Contigo aprendí que repetir el mismo chiste mil veces puede seguir siendo divertido, y que todo momento de nuestra vida puede adaptarse a una escena de los Simpsons. Por todos esos momentos dentro y fuera del PB4 y por tu ayuda cuando más la necesitaba: muchas gracias. Te debo una ensaimada de crema. Thanks to **Dragos** for making life in the PB4 an interesting survival experience. I have never met a person with so little self-value for his own well-being, which makes working with you always a fun experience. In all seriousness, thank you for always been there to discuss work and non-chemistry related stuff. It was always a pleasant experience having you nearby, a little (no pun intended) know-it-all with whom I could discuss the most interesting aspects of life, from politics to videogames. Thank you for everything, my half-cyborg friend, and have a nice time back in Rome. Thank you also to **Qingqing** who, at the beginning, had the worst luck in the lab: having to share the fumehood with me during more than a year! I hope I didn't drive you crazy with my extreme organization of the fumehood. I could not have asked for a better person to share it with, as you were always super nice to me and an easy-going person. I tried to teach you the little I knew in your first months in the lab and I really hope you learnt something valuable from me. Thank you for your patience, your positivism and your Chinese tea! You always had something to give me; I hope I gave you back as much as you did. Thanks to **Kaisa** for her help with everything I asked her for. For being a beacon of professionalism and life-job balance which I admire to this day. Hope you had a great time with us and you could enjoy a bit of the Spanish/Catalan culture and weather with your family. Thanks for everything. Thanks to **Pedro** for arriving in the best moment. You shed a new kind of light in the PB4, one that shined as no other one could, that changed the way I saw everything. Your overall vibe of not-giving-a-damn and positivism is truly contagious. Thank you for being always there when needed and trying to make everything as nice as possible. This final period would have been a challenge without your presence here. Thank you to the best dancer at this side of the Atlantic. Thanks also to **Chiara**, the second incorporation from the «*ITN*» boys. What to say? Your cheerfulness and over-the-top happy attitude is so overwhelming that you always made me feel like the grumpy person I am! Thank you for your friendship, for your annoying music that I never liked, for being so kind and authentic and for trying to cheer me up. I really appreciate you Chiara, don't let me be misunderstood! Finally, thanks to the

last PhD student that joined the PB4, **Andrea**. Thank you for your company and friendship. Even when we have not been together for a long period I have really enjoyed every minute of it and I am looking forward to many more. I hope we can share many more moments in the future, many more coffees in *Raffa* all together, and many more laughs. Thank you for everything my... «*¿come si dice? My friend-e*».

I also want to tank every person that spend a short period of time with us in the PB4. Even when you only were there for three to six months, you all contributed to who I am today. Gracias a los summer fellows Aina Fito, Lorena Baranda e Inmaculada Sampere. Compartí campana con vosotras y disfruté cada momento de esos tres veranos. Gracias por todo. Thanks to the internship PhD and also the master students: Ferdinando Malagreca the pizzaiolo, Sven van Vliet, part of you stays in Salou (more precisely your jacket), Diana Vargas for bringing to the lab the good Colombian moves and a kind personality, Giacomo Berton for all the funny stories we shared with you (and for the bowl you give me for the kitchen) and Stefania Gambaro for your friendship in the little time we had together. Many thanks also to Jorn, Anna, David, Jia, Angelina and Sebastian for your time spent in the PB4.

Many thanks also for the people who shared their time with me from outside the PB4: Belén, Laura, Terry and Daniel. Thank you very much for investing your time on me on the first two years of my time at ICIQ. You really helped me when I need it more and I will always be grateful for that. Thank you.

Muchísimas gracias también a las unidades de apoyo del ICIQ. A los chicos de RMN Isra, Kerman y Gabriel por su infinita amabilidad, ayuda y paciencia. Al personal de Chromtae Marta, Simona y Meritxell por su rápida disponibilidad y eficacia. Muchas gracias también a las integrantes de la unidad de masas Noemí, Vanessa y Charly. En especial gracias a Noemí por enseñarme a utilizar sin miedo un espectrómetro de masas y, por supuesto, por ayudarme a congeniar con el gato. En general, gracias al ICIQ por prestar las instalaciones para desarrollar las labores de investigación que han dado fruto a esta tesis.

I would also like to thank Professor Christoph Schalley for giving me the opportunity to do a short-period internship on his research group. Maybe it was not the bests of times to do it, but I still enjoyed my time in Berlin and in the FUB. Many thanks for your kindness and help. Also thanks to all the group members, especially Daniel

Stares and Andreas Springer for their help and for teaching me how to use the instruments. Thanks also to Cristina Mozaceanu for her company and sharing with me her life experiences in the FUB.

Vielen Dank für meinen Freund **Sussane Simon**. Danke für alles, dass du machtest in Berlin für mir. Danke, dass du mir Yoga und Deutsch beigebracht hast. Danke auch für die leckeren Kuchen und Geschichtsstunden. Ich werde meine Zeit in Berlin nie vergessen. Bitte sag hallo zu Fergus für mich.

Gracias también a mis amigos onubenses, que siempre han estado ahí dispuestos a acompañarme en mis idas y venidas por mi Huelva. Gracias también por las innumerables charlas por Discord y acompañarme en mis ratos libres para despejarme de tanta química. Muchas gracias a **Cristina**, **Andrés**, **Enrique**, **Carmen**, **Ángel**, **Ana** e incluso a **Jorge** (!). Los ratos con vosotros me han hecho sentir en mi tierra hasta en la fría y oscura Berlín.

Por último, muchísimas gracias a mi familia. Gracias a todos por vuestro cariño y paciencia. En especial, gracias a mis padres por el inmenso esfuerzo, tanto económico como emocional, que siempre invirtieron en mí. Gracias a mis hermanas por su apoyo y estar siempre disponibles en los malos ratos. Gracias también a mis dos cuñados, también por el apoyo y la guasa que traen. También gracias a mis sobrinos que, aunque aún no puedan leer estas líneas, espero que en un futuro encuentren entre ellas la explicación de por qué su tito nunca pasaba por casa.

El trabajo contenido en esta tesis ha sido posible gracias a la financiación otorgada por el Gobierno de España/Ministerio de Economía y Competitividad (MINECO) y al Fondo Europeo de Desarrollo Regional (FEDER) (CTQ2017-84319-P and BES-2016-076617).

UNIVERSITAT ROVIRA I VIRGILI
Calix[4]pyrrole Based Receptors for the Recognition of Ion Pairs
Ricardo Molina Muriel

A Pablo y Ariadna,

UNIVERSITAT ROVIRA I VIRGILI
Calix[4]pyrrole Based Receptors for the Recognition of Ion Pairs
Ricardo Molina Muriel

Table of Contents

UNIVERSITAT ROVIRA I VIRGILI
Calix[4]pyrrole Based Receptors for the Recognition of Ion Pairs
Ricardo Molina Muriel

General Introduction

UNIVERSITAT ROVIRA I VIRGILI
Calix[4]pyrrole Based Receptors for the Recognition of Ion Pairs
Ricardo Molina Muriel

1.1 Ion-pairs recognition

An ion pair consist of a two-particle aggregate formed by one negatively charged atom or molecule, an anion, and a positively charged one, a cation (**Figure 1.1**). In the gas phase, both particles are bound together due to the strong and attractive Coulombic interactions that arise between them.[1] In recent years, we have experienced increasing interest towards the recognition of charged species by synthetic receptors in the field of supramolecular chemistry. This is a direct effect of the investigations of the crucial role that anions and cations play in biological processes.[2,3] Indeed, a myriad of supramolecular architectures have been described through the last decades with the sole purpose of mimicking and studying the interactions that anions and cations stablish with more complex biological receptors such as proteins.

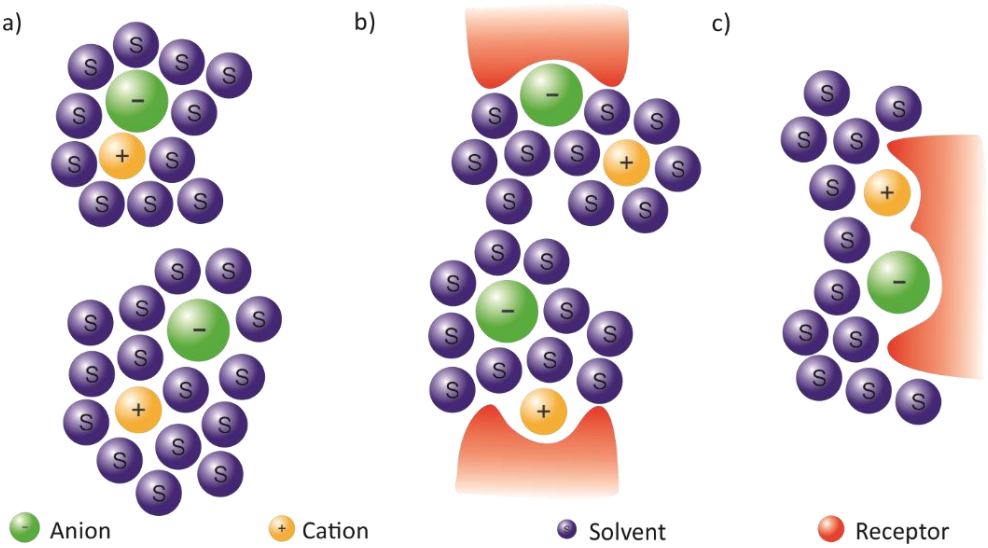

Figure 1.1. Schematic drawings of ion pairs and its complexes. a) Close contact (top) and solvated (bottom) ion pair; b) anion (top) and cation (bottom) receptors with solvated counterion and c) ion pair receptor.

Cation recognition is typically achieved through the establishment of cation-π and Coulombic interactions between the host and the cation of interest. Neutral synthetic receptors for cations usually bear electron rich aromatic rings as well as heteroatoms possessing lone pairs, such as nitrogen or oxygen atoms, able to stablish favourable electrostatic interactions with the cation.[4] However, due to the small size, high surface charge density and the similar shape of most relevant inorganic cations (such as Na^+ or Li^+), the design of the receptors for cations tends

to be simpler than for its anionic analogues. The most widely used synthetic receptors for cation binding are crown-ether and its derivatives.[5,6]

Synthetic receptors for anions, on the other hand, need to be carefully designed to obtain a suitable binding site that fulfil the coordination requirements of the anion to be bound. [7,8] This is due to the wide variety in shape and size of most common anions studied in supramolecular chemistry, e.g. spherical halide anions compared to lineal cyanate or trigonal-planar nitrate anion. The binding processes of neutral anion receptors are driven by the establishment of weak non-covalent interactions such as hydrogen bonds,[9] halogen bonds[10,11,12] and anion-π interactions with electron deficient aromatic rings,[13,14] among others.[15] Despite the high synthetic cost of anion receptors, the complementarity between the carefully designed host and the anion results in high affinity constant values and great selectivity towards the anion of interest.

Although the separate recognition of cations and anions has been proved feasible throughout the years, there is an increasing interest in the concomitant recognition of the ion pair. However, there are some intrinsic difficulties associated with ion pair binding. First, one must overcome the attractive Coulombic interactions that rules the ion-pairing equilibrium.[16] The Coulombic interaction is directly dependant on the dielectric constant of the media. In summary, one can assume that the Coulombic interaction is prevalent in low dielectric constant solvents, such as chloroform. The ion pairing constant (K_{ip}) is thus highly dependent on the solvent system. On the contrary, in solvent systems with high dielectric constant, such as polar and protic solvents as water or methanol, the ion-pairing equilibrium will be shifted towards the dissociated ion pair. This leads to the second challenge to overcome for solvated anions: desolvation. Both the anion and the cation are surrounded by a solvation shell in high dielectric constant solvents. The energy required to break the solvation shell must be compensated by the intermolecular interactions established between the anion and the host in the complex. In addition, it has been shown that the cation serves to modulate the binding affinity and selectivity of the receptor towards the anion, what is now known as the "counterion effect".[17,18,19] However, the "counterion effect" is also solvent dependent, as cations are usually well solvated in polar media. Still nowadays, the development of heteroditopic receptors able to bind the cation and the anion simultaneously remains challenging.

Significant advances have been made in the synthesis and binding studies of ditopic receptors for ion-pairs in the last twenty years. [20,21,22,23,24] In some cases, the binding of the cation in the ditopic receptor produces intrinsic conformational changes that favour the binding of the anion, or vice-versa. In other cases, a stabilizing Coulombic interaction between the two charged particles arises due to the close proximity of the anion and the cation. In both cases, this produces an increase in the binding affinity constant towards the anion if compared to the value obtained with monotopic receptors.

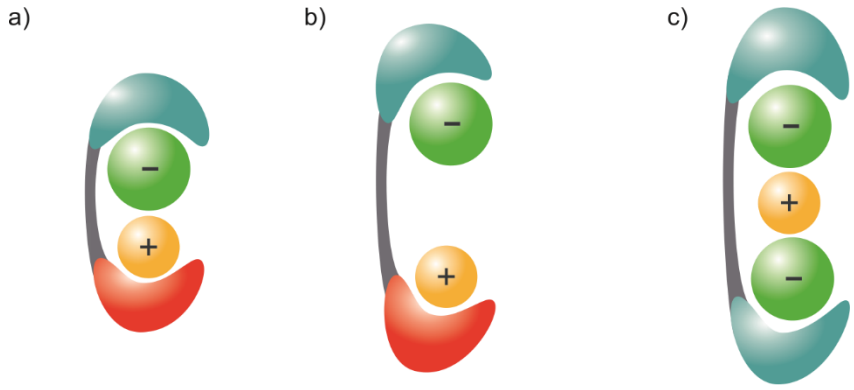

Figure 1.2. Schematic representation of the different arrangements observed in the formation of complexes with heteroditopic receptors: close contact a), receptor separated b) and cascade complex c).

The change in binding affinity when both particles are concomitantly coordinated is referred as cooperativity effect. The accurate assessment of the cooperative effects requires the determination of the step-wise binding affinity constants of the system.[25] Cooperativity effects can be expressed as positive, negative or non-cooperative depending on the increase, decrease or no modification of binding affinity, respectively.[26]

In general terms, heteroditopic ion-pair receptors can be classified according to the binding arrangements displayed by the charged particles in the ion-paired complexes (**Figure 1.2**). Thus, in receptor-separated complexes, the two ions are bound in independent binding sites and are separate one from another (sometimes by a solvent molecule or the receptor's scaffold). In contrast, close contact complexes display both charged particles bound to their respective binding sites but remaining in contact and exhibiting a direct Coulombic interaction. Finally, cascade complexes involve the complexation of ion-pairs in an ion-triplet complex. The final complex consist of two bound anions or cations with a proper counterion

sandwiched between them. One of the anionic or cationic species of the ion-triplet cascade complex was initially bound to a homotopic receptor. This initial binding process produce the supramolecular hetero-ditopic receptor for the ion-pair.

As previously stated, in receptor separated ion-paired complexes the anion and the cation are bound apart displaying reduced, if any, Coulombic interactions between them. In this type of complexes, allosteric positive cooperativity was observed. In 2001, the group of Nabeshima reported the synthesis and binding studies of receptor **1**, based on two crown-ethers motifs covalently linked by a linear spacer containing two pyridyl bisamide units (**Figure 1.3**).[27] The authors proved the interaction of **1** with the cesium cation in a $CDCl_3$:CD_3CN 4:1 solution mixture by means of ^1H NMR titration experiments and ESI-MS analysis. The obtained results supported the formation of 1:1 and 1:2 complexes. In particular, the 1:1 complex **Cs⊂1** was produced when an equimolar ratio of **1** and cesium was used. The precursor of the cesium cation was the corresponding BArF salt. The BArF counteraction displayed reduced coordinating capabilities to the bis-amide units of

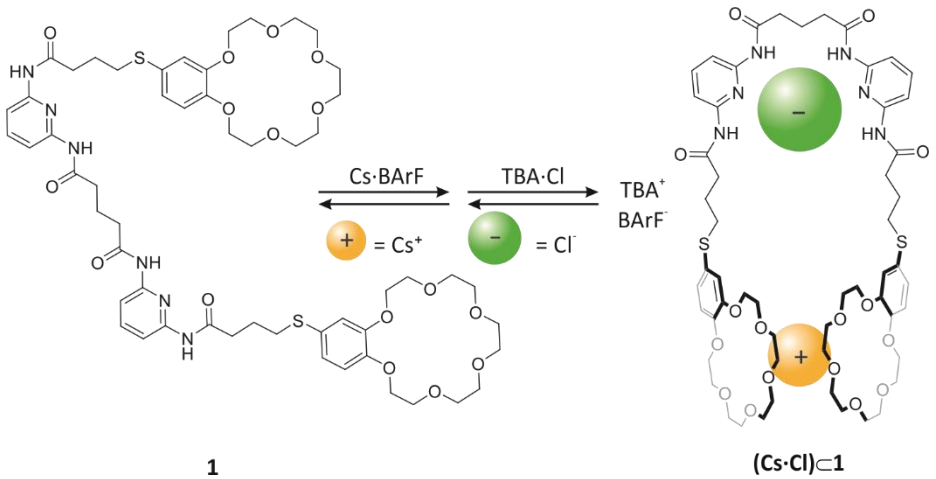

Figure 1.3. Schematic drawing of Nabeshima's tweezer receptor **1** binding Cs·Cl

the receptor. In the 1:1 complex, the cesium cation was sandwiched between the two crown-ether units of the receptor. This binding mode induced a conformational change of the receptor generating a preorganized anionic binding site. The anionic binding site is defined by the two 1,3 bis-pyridyl amide units of the spacer. The addition of more than one equivalent of the salt produced the formation of the 1:2 complex, **Cs_2⊂1**. Interestingly, the addition of TBA·Cl or TBA·Br salts to the pre-formed 1:1 complex, **Cs⊂1**, generated ion-paired counterparts in which the halide

established four hydrogen bonding interactions with the amide groups. In the presence of 1 equivalent of cesium, the calculated binding affinity for the halide binding increased in one order of magnitude in comparison to the value obtained for **1** alone. This result evidenced the existence of a positive allosteric effect in the anion binding, which was mainly provided by the preorganization of the receptor.

Allosteric cooperativity in ion-pairs binding is not only related to conformational changes in the heteroditopic receptor. In some cases, the binding of one charged particle may generate significant changes in the electronic environment of the receptor. As a result, the binding affinity towards the second binding partner may be modified. Using this approach, the group of Schubert described in 2017 ion-pair binding studies using a crown ether receptor bearing an iodo-triazole unit inserted in the cyclic structure (**Figure 1.4**).[28] The iodo-triazole unit of the cyclic receptor was envisaged to participate in the binding of halides through the establishment of halogen bonding interactions.[10,11,12] Using ^{1}H and ^{13}C NMR spectroscopy, the authors studied the binding affinity of the receptor towards sodium and iodide in separate CD_2Cl_2:CD_3CN 3:1 solvent mixtures. The precursor salts of the investigated ions contained non-coordinating counterions: the BPh_4^- anion, in the case of the sodium, and TBA^+ cation, in the case of iodide. The obtained results revealed the existence of very weak interactions between both coordinating ions (Na^+ and I^-) and receptor

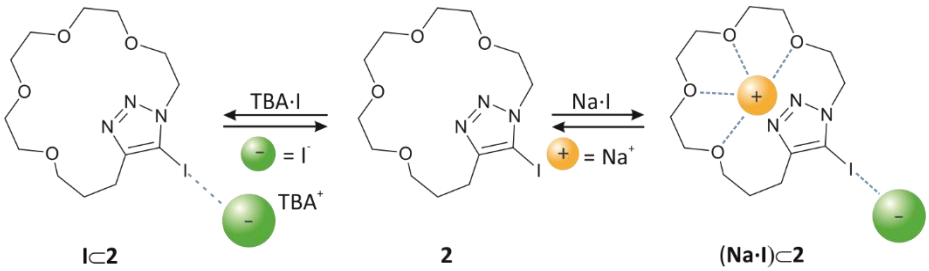

Figure 1.4. Schematic representation of the iodide binding process observed Schubert's triazole-based receptor **2**.

2. The reduced size complementarity between the Na^+ cation and the crown ether unit of the receptor was put forward as the main reason of the observed weak interaction. In the case of the iodide anion, the authors rationalized the observed weak interactions as the contribution of different factors: the low basicity and charge density of the anion and the charge-neutrality of the receptor and the iodo-triazole unit. Next, the authors studied the capability of receptor **2** to act as heteroditopic receptor for the binding of Na·I. In the performed titration

experiments, the authors observed complexation-induced shifts (CIS) in the chemical shift value of the carbon atom in the triazole ring that is attached to the iodine. This result supported the involvement of the triazole unit in the binding of the salt. They did not observe chemical shift changes in the carbon spectra of the titrations experiments carried out with TBA·I. The authors estimated that the binding affinity constant for the sodium iodide complex formed with **2** was in the order of 10^2 M^{-1}. The different behaviour of receptor **2** in response to the used salts i.e. Na·I, Na·BPh_4 and TBA·I was rationalized considering the modification of the π-electron cloud of the triazole unit induced by the coordination of the sodium cation to the crown ether. The initial formation of the cationic complex Na⊂**2** would favour the coordination of the iodide to the iodine atom of the triazole unit through a halogen bonding interaction.

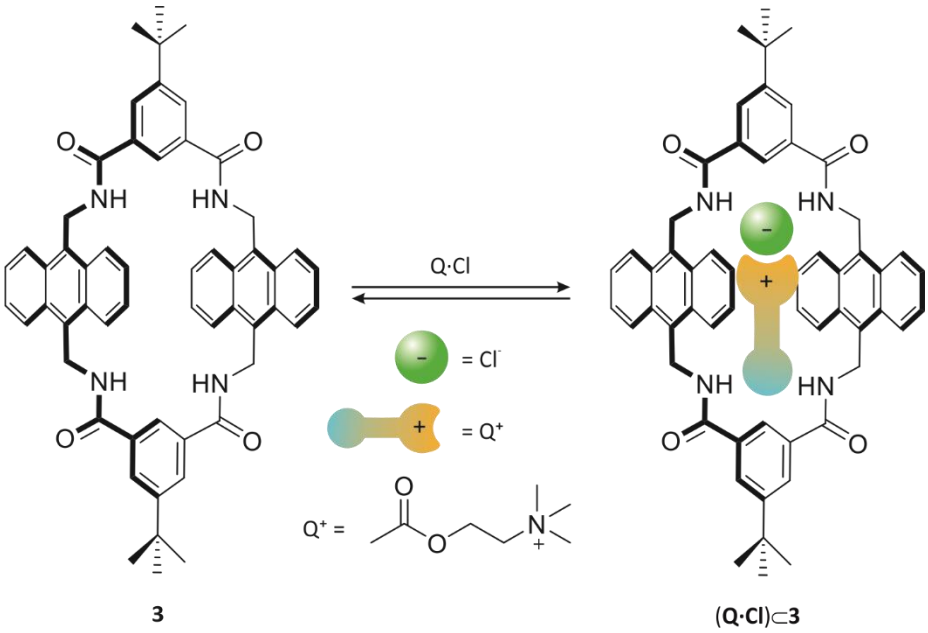

Figure 1.5. Schematic representation of the three particle aggregates obtained with heteroditopic receptor **3** described by Smith and coworkers.

In close contact ion-paired complexes, the stabilizing Coulombic interaction established between the bound charged particles can also generate allosteric positive cooperativity in the binding process. Recently, the group of Smith described the synthesis and binding studies of the tetralactam-based macrocycle **3**. Compound **3** is a ditopic receptor featuring two binding sites for anions (**Figure 1.5**).[29] Interestingly, the titration experiments, performed using ^{1}H NMR spectroscopy, of

receptor **3** with the BarF salt of acetyl choline **Q·BArF** and TBA·Cl in chloroform solution did not reveal the existence of chemical shift changes in the proton signals of the receptor. These findings indicated that receptor **3** displayed a reduced binding affinity for either the organic acetyl choline cation, $\mathbf{Q}^+$, and the inorganic chloride anion Cl^- in separate solutions. However, the addition of chloride salt of acetylcholine, **Q·Cl**, to a chloroform solution of receptor **3** produced significant complexation induced shifts in the protons signals of the receptor. This observation supported the formation of the (**Q·Cl**)⊂**3** complex. The formation of the complex was rationalized by the inherent capabilities of the ditopic acetyl choline cation $\mathbf{Q}^+$. At one end, the acetyl choline cation bears an ester unit capable of interaction with the NHs of one of the bis-amide units of the receptor. At the opposite end of its alkyl chain, the ditopic acetyl choline cation $\mathbf{Q}^+$ presents a quaternary ammonium group. The tetralkylammonium group established Coulombic interactions with the chloride bound in the distal bis-amide binding site of receptor **3**. The obtained complex (**Q·Cl**)⊂**3** displayed a close contact binding geometry featuring an increase of two orders of magnitude in the binding constant in comparison to the TBA·Cl counterpart.

As described in the examples above, Coulombic interactions play an important role in the energetic stabilization of ion-paired complexes. An approach to enhance these interactions is the design of cage covalent receptors featuring inner cavities that force the close contact of the ion-pair. In this respect, the group of Martinez demonstrated the capability of a hemicryptophane in the binding of ion-pairs in chloroform solution.[30] Receptor **4** is based on a cryptophane unit covalently connected to a C_3 tris-urea motif (**Figure 1.6**). The ditopic covalent cage **4** was structurally very similar to a predecessor that was developed by the same group, which displayed a smaller inner cavity. Receptor **4** was able to bind halide anions deriving from TBA salts with high affinities. Remarkably, the TBA^+ cation seemed not to be involved in the binding event. However, the lager inner volume of receptor **4** allowed the co-inclusion of the TMA^+ cation with the bound chloride. The resulting ternary complex displayed a close-contact ion paired binding geometry. Moreover, titration experiments performed with a series of halide anions and a pre-formed **TMA**⊂**4** complex revealed that the binding affinity for the halide was increased by more than one order of magnitude compared to that of **4**. These findings were rationalized by the authors in terms of the stabilizing Coulombic interactions established in the close-contact binding geometry of the halide complexes of **4** with the TMA^+ cation. In the close-contact geometry complexes, the anion was bound in

the tris-urea motif by the establishment of multiple hydrogen bonding interactions. In turn, the cation was located in the shallow and electron rich aromatic cavity defined by the cyclophane unit. The binding of the TMA^+ cation was stabilized due to the π-π, CH-π and cation-π interactions stablished with the receptor, as well as the attractive Coulombic interactions with the bound anion.

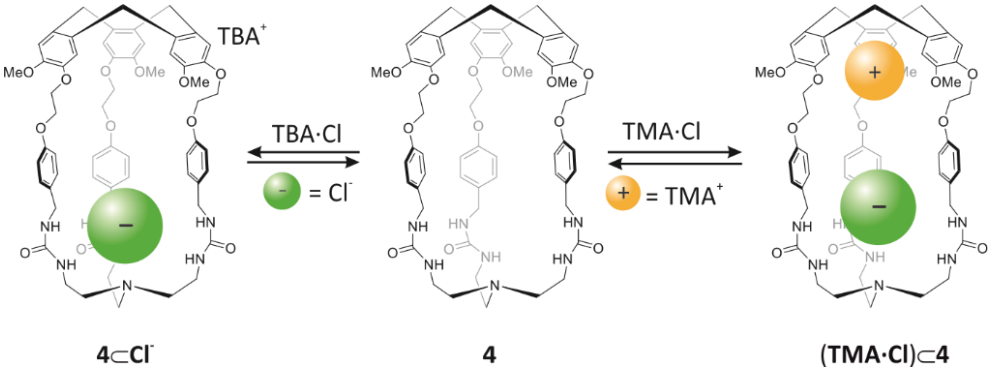

Figure 1.6. Schematic representation of the 1:1 and 1:2 complexes obtained between Martinez's receptor **4** with TBA·Cl and TMA·Cl.

Cascade complexes are a special case of ion-paired complexes. These molecular aggregates consist in three or more charged particles bound in the receptor's cavity stabilized by Coulombic interactions. Thus, the ion triplet is bound inside the receptor's cavity in a close-contact binding geometry. Covalent receptors able to bind ion triplets in a cascade-like manner are not common. The inclusion of, at least, two covalently linked binding sites that can locate the three charged particles in a close contact geometry requires a careful molecular design. Due to its intrinsic structural properties, self-assembled heteroditopic receptors are often used for the generation of ion-pair complexes featuring triplet cascade geometry. The first example of a receptor capable of binding an ion triplet was published in 2010 by the group of Lüning.[31] The tritopic macrocycle **5** consisted of two isophthalamide units covalently linked by two ethylene glycol chains (**Figure 1.7**). The conformationally flexible structure of **5** allowed its adaptability in the binding of the triplet. The properties of receptor **5** to bind a series of halide salts in a $CDCl_3$:DMSO 95:5 solvent mixture were evaluated using ^1H NMR titration experiments. Interestingly, receptor **5** selectively bound $Ca{\cdot}Cl_2$. The ternary complex (**$Ca{\cdot}Cl_2$**)⊂**5** displayed cascade geometry. The two chloride anions were hydrogen-bonded to each one of the two bis-amide motifs of the receptor. The Ca^{2+}cation was sandwiched between the two chlorides. In addition, the calcium cation established cation-dipole interactions with

the oxygen atoms of the glycol chains and Coulombic interactions with the bound chlorides. The selectivity displayed by receptor **4** to the calcium chloride salt was attributed by the authors to the greater match in size if compared to other studied alkali salts, e.g. magnesium, lithium or sodium, among others.

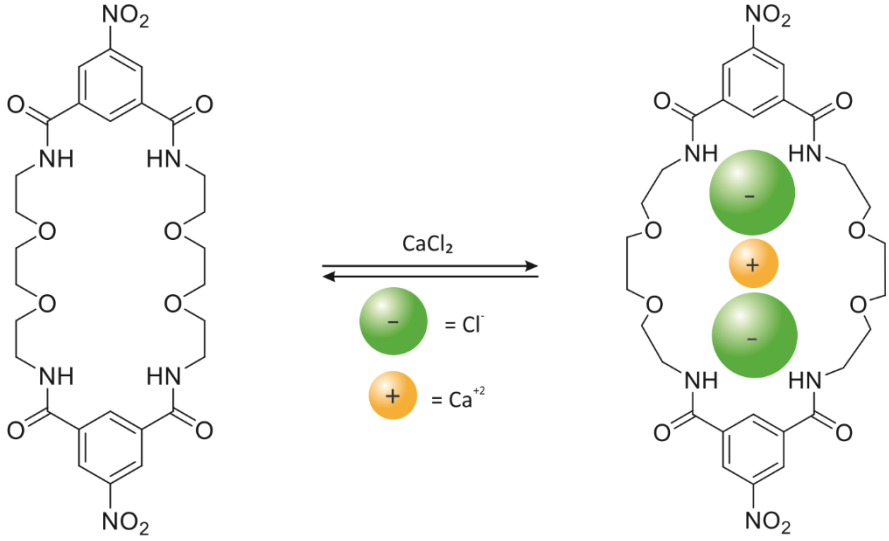

Figure 1.7. Schematic representation of Lunings's macrocyclic receptor **5** and the cascade complex formed with $CaCl_2$.

The group of Jabin described a macro-oligocyclic receptor able to form cascade complexes in CD_3OD:$CDCl_3$ 1:1 solution with sulfate salts of organic cations.[32] The reported bis(calix[6]arene) receptor contained three thiourea alkyl spacers (**Figure 1.8**). Using ^1H NMR spectroscopy, the authors demonstrated the reduced properties of receptor **6** for the binding of various ions in the form of $TBA^+ \cdot X^{n-}$ salts, with X^{n-} = SO_4^{2-}, NO^{3-}, or Cl^- in $CDCl_3$. Similar conclusions were derived from the experiments carried out with $PrNH_3^+Pic^-$. These results were explained by invoking the lack of preorganization of the flexible receptor. Interestingly, the simultaneous addition of both salts $TBA^+ \cdot SO_4^{2-}$ and $PrNH_3^+Pic^-$ induced the formation of a ternary cascade complex corresponding to the stoichiometric formula $[(\mathbf{PrNH_3^+})_2 \cdot \mathbf{SO_4^{2-}}] \subset \mathbf{6}$, both in $CDCl_3$ and CD_3OD:$CDCl_3$ 1:1 mixtures. Analogous ternary cascade complexes were observed in the ^1H NMR titration experiments of **6** with the sulfate salts of a series of monoalkylammonium salts $(RNH^{3+})_2 \cdot SO_4^{2-}$ (R = Et, Pr, Hex, or Dodec). In the obtained complexes, the sulfate anion was located in the middle of receptor **6**, sandwiched between the two bound mono-alkyl ammonium ions. In turn, the

ammonium ions were bound in the distal calix[6]arene aromatic cups of the receptor. The ammonium cations were stabilized by establishing cation-π interactions with the aromatic panels of the calix[6]arene, as well as hydrogen bonding interactions with their methoxy groups. In addition to this, the thiourea units of receptor **6** wrapped around the sandwiched sulfate anion, providing the greater thermodynamic stability to the complex. The binding geometry of the cascade complex in the solid state was supported by X-Ray analysis of a single crystal. Interestingly, the cascade complex displayed helical chirality owing to the arrangement of the thiourea unit around the bound anion. The supramolecular chirality was transferred to the calix[6]arene cores and ultimately felt by the bound ammonium cations.

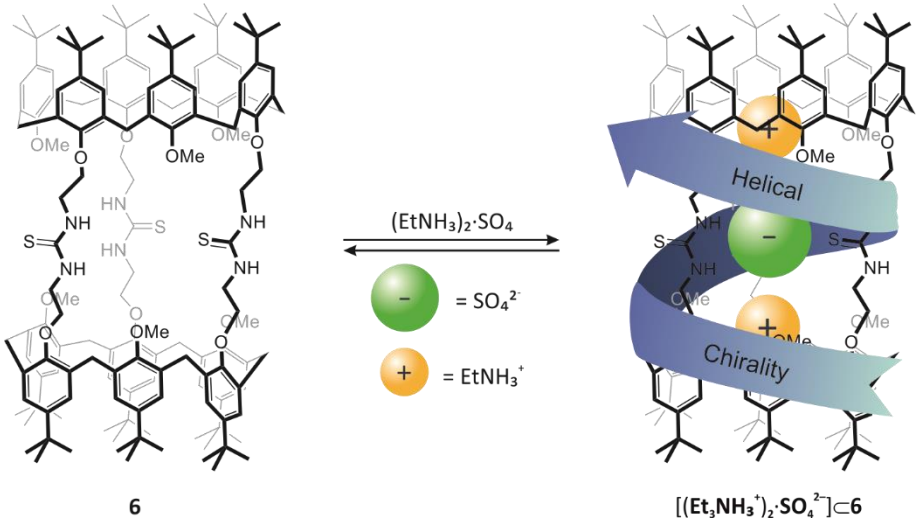

Figure 1.8. Schematic representation of Jarbin's bis(calix[6]arene) receptor binding $(EtNH_3)_2{\cdot}SO_4$ in a cascade-like binding geometry.

1.2. Calix[4]pyrrole as receptors

Calix[4]pyrroles (C4P) are macrocyclic structures consisting of four pyrrole rings covalently connected by four sp^3 carbon atoms. These non-planar structures were first synthetized by Baeyer in 1886 by the acid catalysed condensation of pyrrole with acetone.[33] However, it was not until more than a century later, in the year 1996, in which the ion binding capabilities of the most basic C4P structure, the octamethyl C4P, were properly investigated by the group of professor Sessler.[34]

C4P receptors might exist in solution as four conformational isomers depending on the relative orientation of the pyrrole rings (**Figure 1.9**). According to the stability of the conformers, from higher to lower, they can adopt a 1,3-alternate conformation, a partial cone, 1,2-alternate and cone conformation. The stability of the conformers can be rationalize by the repulsive electrostatic interactions between the adjacent pyrrole rings. However, in the absence of a binding guest molecule, the distribution of the four different conformations is highly dependent on the polarity of the solvent. Hence, in the presence of a polar solvent such as acetonitrile, C4P adopt the cone conformation due to the coordination of a solvent molecule in the C4P core. This is also the preferred conformation observed in the complexes obtained with neutral and charged molecules.[35]

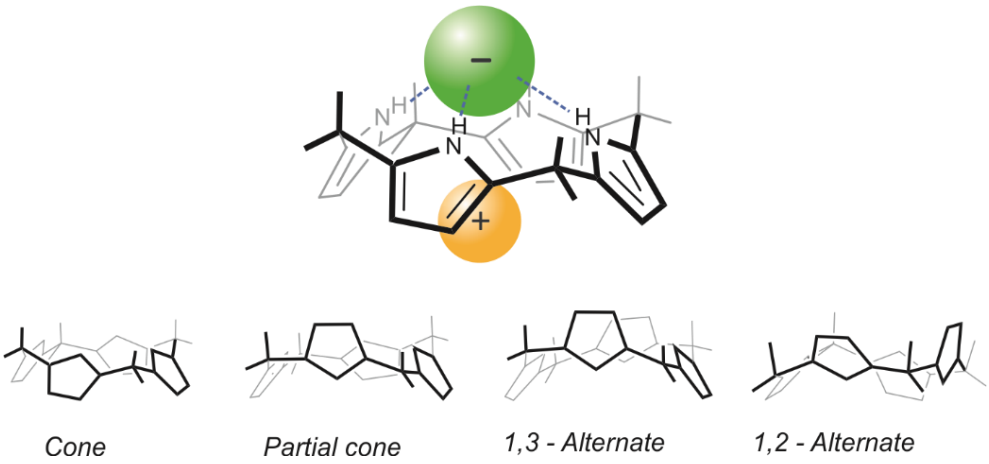

Figure 1.9. Top – Octamethyl C4P binding an ion pair in the cone conformation. Bottom – Schematic drawings of the four different conformational isomers of a C4P.

One of the most remarkable features of C4P macrocycles is their ability to act as heteroditopic receptors. In this regard, the binding capabilities of C4P are due to its structural properties. Additionally, the NH groups of the pyrrole rings can act as hydrogen bond donors. When the C4P adopts the cone conformation, the four NH groups converge to generate a binding site suitable for the coordination of electron-rich polar neutral molecules and anions. The binding event is driven by the establishment of hydrogen bonding interactions with the analyte (**Figure 1.9**). On the other hand, the cone conformation generates an electron-rich aromatic cup opposite to the hydrogen-bonded guest. This electron-rich region can engage in cation-π, CH-π and π-π interaction with polar neutral guests and cations. These properties confer C4P receptors the ability to bind a great variety of neutral and

charged species.[36,37,38,39] As a result, various practical applications have been found for these heteroditopic receptors such as membrane transport and signalling devices, [40,41,42,43] among others.[44,45]

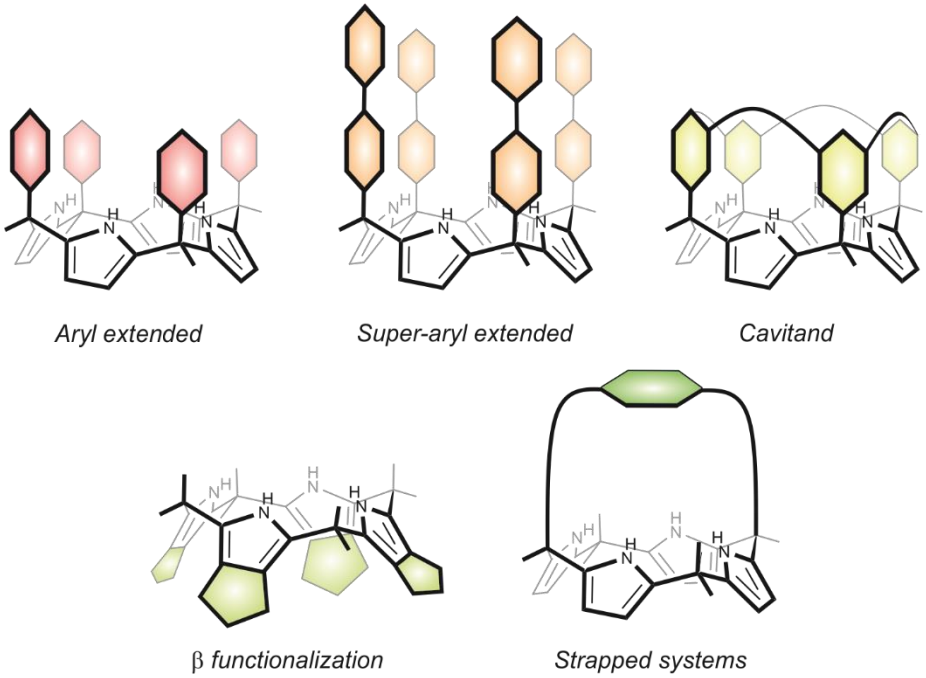

Figure 1.10. Schematic representations of the different derivatization possibilities of calix[4]pyrroles.

In addition to the intrinsic properties of the basic C4P core, higher affinity and selectivity can be achieved by the direct derivatization of the macrocycle. Indeed, a myriad of C4P based receptors have been presented along the years (**Figure 1.10**). These receptors are based on the addition of new structural motifs into the C4P upper and/or lower rims. Some of the incorporated units are able to stablish non-covalent interactions with the bound guest. With the exception of β-functionalized C4Ps, the general strategy for the synthesis of C4P-based receptors is the direct functionalization on the *sp*^{3} *meso* carbon position. Aryl and super-aryl- extended C4P are one of the most common examples of these functionalized receptors. At the same time, a pre-organized and more rigid receptor can be achieved by the covalent linkage of upper rim extensions, as is the case for strapped and cavitand derivatives.

The derivatization on the β position of the pyrrole ring in C4P systems serves to extend the lower rim of the macrocycle. These receptors present greater properties for binding cations and electron deficient molecules in the shallow aromatic cavity

defined by the functionalized pyrrole units. Although examples in literature of β-functionalized C4P are scarce, the vast majority of them are focused on the incorporation of electron rich aromatic groups.[46,47,48] Nevertheless, some examples exist in which β-modification is obtained alongside with *meso*- substitution.[49] In recent years, the group of professor Sessler has presented β-substituted tetrathiafulvalene and benzotetrathiafulvalene TTF-C4P receptor derivatives capable of binding halide salts, as well as neutral electron deficient molecules (**Figure 1.11**).[50,51,52] In these receptors, the binding of an anion locks the TTF-C4P core in the cone conformation in apolar solvents. This generates a bowl-shaped cavity in the lower rim that can strongly bind sizeable cations, such as TBA^+. The cation is stabilized by cation-π interactions with the TTF framework, while still in close contact with the bound anion. An enhancement in binding affinity was observed and it was related to a highly positive allosteric effect. On the other hand, when the receptor is free in solution, the system can freely rotate to adopt a 1,3-alternate conformation. In this conformation, the distal TTF groups are oriented in the same directions defining two-opposed sandwich-like cavities. The 1,3-alternate conformer of TTF C4P derivatives was shown to form 1:2 complexes with electron deficient molecules such as trinitrobenzene, trinitrotoluene and picric acid. The guests "slip into" the cavities and were sandwiched between two TTF walls. The bound guest were stabilized by charge transfer interactions and hydrogen bonding with two of the NHs of the C4P core.

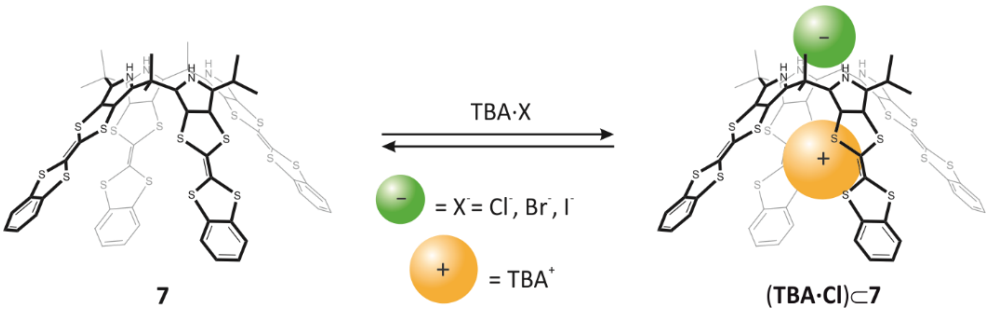

Figure 1.11. Sessler's β-substituted calix[4]pyrrole binding halide salts of TBA.

The derivatization of C4P in the *meso*-positions can lead to an enhancement of its binding affinity. A particular case of *meso*-substituted C4P are aryl extended (AE-C4P) and super-aryl extended (SAE-C4P) derivatives. These macrocycles are produced by the incorporation of aryl substituents at the *meso*-positions of the C4P scaffold. This substitution produces different configurational isomers. Moreover, depending on the degree of functionalization at the *meso*-positions AE-C4P and SAE-

CEP can be divided in "four-walls" and "two-walls" C4P derivatives. In the "four-wall" series, one aromatic substituent is appended at each of the four sp^3 *meso*-carbons. The different relative orientation of the *meso*-aromatic walls produces the existence of "four wall" receptors as four possible configurational isomers: $\alpha\alpha\alpha\alpha$, $\alpha\alpha\alpha\beta$, $\alpha\beta\alpha\beta$ and $\alpha\alpha\beta\beta$. On the other hand, "two-wall" C4P receptors bear only two aryl-substituents at opposite *meso*-carbons. For this reason, they exist as two conformers: $\alpha\alpha$ and $\alpha\beta$. A recent example of "four-wall" SAE-CAP was described by our group.[53] In this manuscript, a series of SAE-C4P functionalized both at their upper and lower rims were used for the complexation of small polar molecules in water solution. The solubility of the SAE-C4Ps in water was achieved through the incorporation of eight charged or ionizable groups to their scaffolds: carboxylic acid groups for **8** and pyridinium or imidazolium groups for **9** and **10**, respectively (**Figure 1.12**). The authors investigated the formation of inclusion complexes with a series of pyridyl *N*-oxides derivatives in water solution. Thermodynamically and kinetically

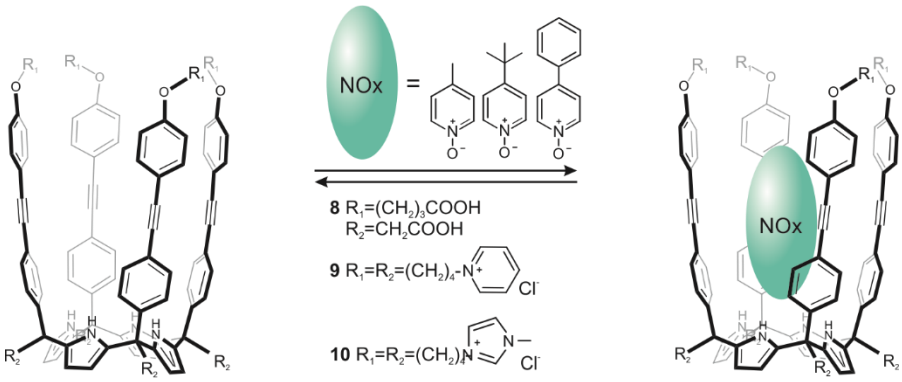

Figure 1.12. SAE-C4P **8**, **9** and **10** synthetized recently by our group binding three of the *N*-oxide guests studied.

stable 1:1 inclusion complexes were obtained with all the studied guests. Binding constants in the range 10^5 to 10^9 M^{-1} were calculated for the inclusion complexes. The formed complexes were stabilized by hydrogen bonding interactions between the oxygen atom of the pyridyl *N*-oxide and the NHs of the C4P core. In addition, the guest engaged in π- π and CH- π interactions with the aromatic walls of the receptor. Interestingly, isothermal titration calorimetry (ITC) experiments revealed a linear relationship between the size of the non-polar *para*- substituent in the pyridyl *N*-oxide and the free energy of the complex. Indeed, the free energy of the complex increased in response to a larger surface area of the *para*-substituent of the *N*-oxide. A difference of ~4.5 kcal mol^{-1} was measured between the free energy values of the

complexes of receptors **8** and **9** with the *p*-phenyl substituted and non-substituted pyridyl *N*-oxide, respectively. The obtained results were rationalized by invoking the role of the hydrophobic effect on binding: a larger non-polar surface of the *para*-substituent is translated into a thermodynamically more stable 1:1 complex.

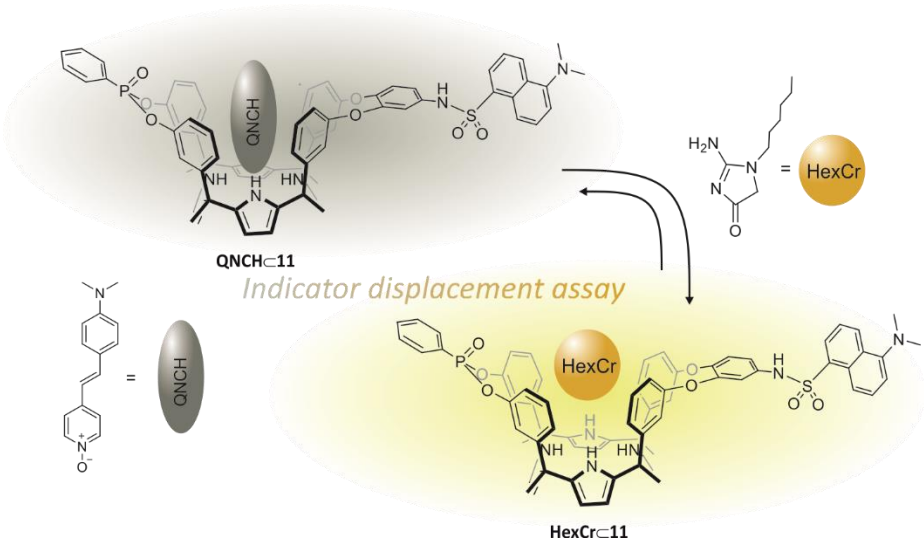

Figure 1.13. Schematic representation of the indicator displacement assay experiments performed for the sensing of creatinine developed by our group.

Cavitand-like receptors are produced by the incorporation of bridging units to the AE-C4P scaffolds. The bridging units covalently link two adjacent aromatic walls. Compared to the SAE-C4P counterparts, AE-C4Ps and its cavitand derivatives display a shallower aromatic cavity making the pyrrole NHs located at the closed-end more exposed to the bulk solution. At the same time, the cavitand architecture produces a more preorganized and conformationally rigid structure. Recently, our group disclosed AE-C4P cavitand **11** bearing two different bridging units at its upper rim.[54] The phosphonate group was incorporated with the intention of stablishing non-covalent interactions between its inwardly directed PO group and the included guest. The dansyl-amide fluorophore was covalently attach to the bridging phenyl unit with the aim to generate a molecular sensor. Unfortunately, guest binding did not produce noticeable changes in the absorption and emission spectra of the free receptor. In any case, the fluorescent receptor **11** was used in the sensing and quantification of creatinine (**Cr**) and its more lipophilic version hexyl-creatinine (**HexCr**) using an indicator displacement assay (IDA) (**Figure 1.13**). Firstly, by means of ^{1}H NMR and ITC experiments, the authors demonstrated the formation of 1:1

inclusion complexes between **11** and **HexCr** in chloroform solution. The formed complex was characterized with an affinity constant value of $K_a = 4.5 \pm 0.4 \times 10^5\ M^{-1}$. The formation of the **HexCr⊂11** complex was driven by the establishment of multiple non-covalent interactions. In addition to the CH-π and hydrogen bonding interactions previously described for the AE-C4P scaffold. The bound creatinine was also involved in a hydrogen bonding interactions with the oxygen atom of the inwardly directed phosphonate group. The formation of stable inclusion complex with the black-hole quencher **QNCH** was also confirmed by means of fluorescence titration and ITC experiments, yielding a binding affinity constant value of $K_a = 1.2 \pm 0.5 \times 10^7\ M^{-1}$. Additionally, at micromolar concentration the fluorescence of receptor **11** (λ_{max} = 341 nm), was completely quenched by the addition of 2 equivalent of **QNCH**. In the IDA experiments, the incremental addition of **HexCr** to a pre-formed 1:1 inclusion complex, **QNCH⊂11,** produced an increase in the fluorescence. This result is due to the displacement and substitution of the quencher bound in the inner cavity of the receptor by a molecule of hexyl-creatinine. Similar results were obtained when using Cr. Structurally related bis-phosphonate cavitands were also described by our group. These receptors bound neutral polar molecules in both organic and water media.[55]

Strapped C4P are a special class of *meso*-functionalized C4P bearing two opposed substituents. These receptors feature a covalent connection between *meso*-substituents by means of an upper-rim strap. Using this synthetic methodology, rigid and preorganized C4P receptors, featuring an additional binding site in the strap, are produced. The inherent preorganization and rigidity of the strapped C4Ps facilitates adopting the cone conformation, thus enhancing their anion binding capabilities. Additionally, the close arrangement of two inequivalent binding sites in their scaffolds induces cooperative effects in the binding of ion pairs in close-contact geometry.[56,57,58] Recently, Sessler's group reported binding studies based on strapped C4P receptors.[59,60] Strapped C4P receptors **12** and **13** were introduced (**Figure 1.14**). A phenantroline unit was appended at the upper rim of the receptors as binding unit of the strap. The amide groups present in receptor **13** (but not in **12**) were envisaged to assist in the binding of halide anions (F^-, Br^-, Cl^- and I^-) and various oxoanions (HCO_3^-, $H2PO_4^-$, HSO_4^- and SO_4^{2-}). The precursor salts of the anions contained TBA^+ and TEA^+ cations as counter-ions. The binding experiments were performed in chloroform and 15% aqueous DMSO solutions. Remarkably, in chloroform solution, the majority of the anionic complexes of receptor **12** featured slightly larger binding constant values compared to the analogues with receptor **13**.

For example, the binding constant values measured by ^{1}H NMR titrations experiments towards Br^- was K_a = 3.38 x 10^2 ± 0.25 M^{-1} for **12** and K_a = 0.56 x 10^2 ± 0.04 M^{-1} for **13**. An exception of the trend was observed in the binding of chloride and bicarbonate. This striking result was rationalized by the authors invoking the existence of competitive intramolecular interactions between the amide NHs of **13** and the nitrogen atom of the phenantroline unit of the strap. This hydrogen-bonding interaction proved to be stronger in chloroform solution. This hypothesis was substantiated with the results of the binding studies performed in more polar solvents. Thus, the preferred binding of the anions to receptor **12** compared to **13** changed in the binding experiments performed in 15% D_2O in DMSO. In this solvent mixture, the binding constant values of the anions for receptor **12** decreased substantially. In fact, with the exception of F^-, no binding was detected for **12** and the anions series. In contrast, the investigated anionic complexes of the amide functionalized C4P-strapped **13** experienced an increase in the binding affinity. For example, in the case of the bicarbonate anion, the calculated binding constant increased from K_a = 4.8 x 10^3 M^{-1} in chloroform solution to $K_a > 10^4$ M^{-1} in 15% DMSO-D_2O solution. This increase in binding strength must be related to the effect played by the solvent. Most likely, in 15 % DMSO D_2O solution the intramolecular hydrogen-bonding interactions of **13** weakened and allowed the amide groups to engage in intermolecular hydrogen bonding interactions with the anionic guests.

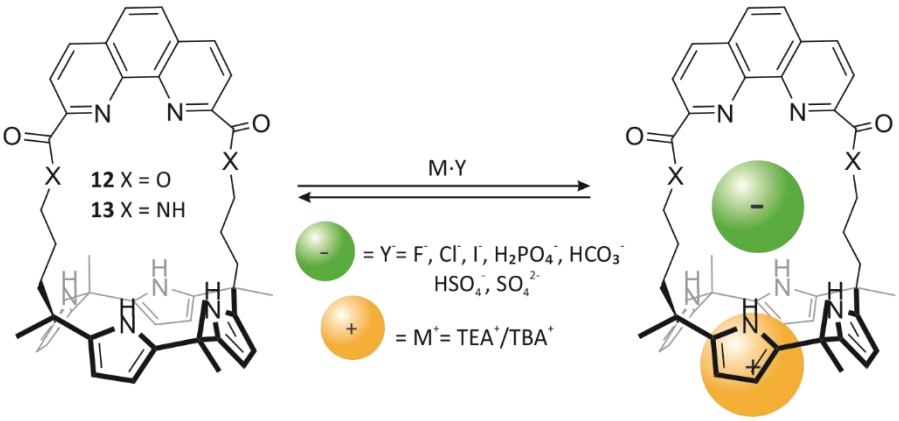

Figure 1.14. Schematic drawings of strapped C4P receptors **12** and **13** designed by Sessler for the binding of ion pairs.

When the strap incorporated at the upper rim of the C4P scaffold is another C4P, the receptors are referred as bis(calix[4]pyrrole) (BC4P).[57] These receptors display a large inner cavity having multiple binding sites. Consequently, BC4P are capable of

binding more than one guest between the two converging C4P units. The binding of the guests can be assisted by polar groups present in the functionalized walls of the receptor (vide infra). Owing to the difficult design and high synthetic costs of these macro-oligocyclic receptors, the number of examples found in literature are scarce.

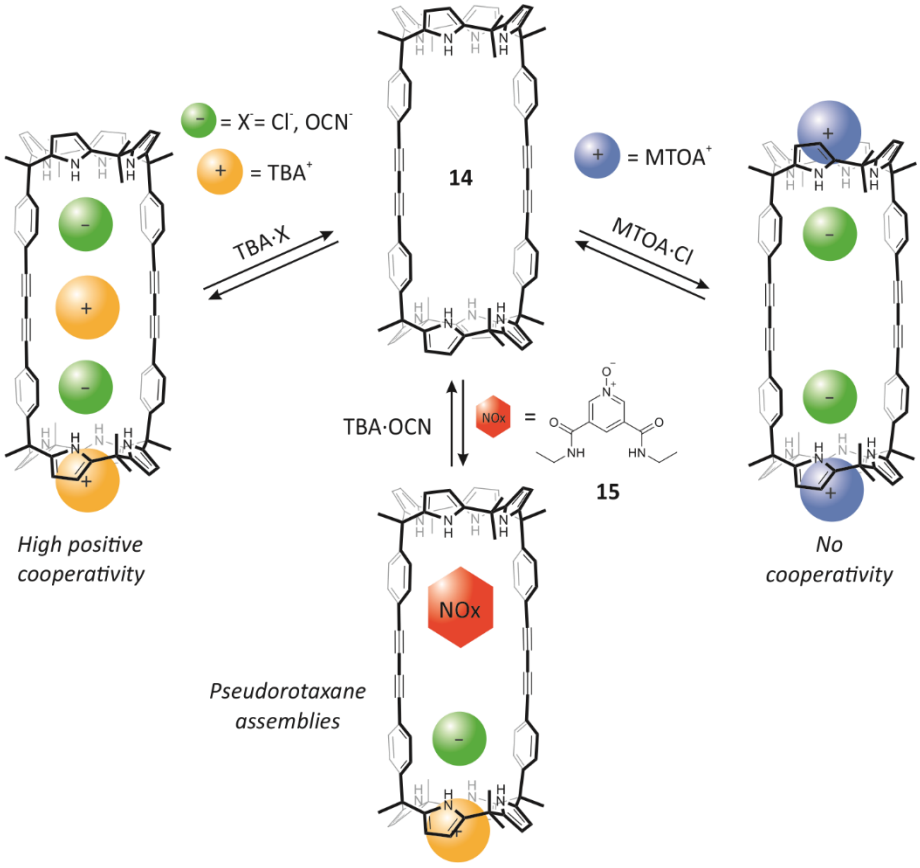

Figure 1.15. Schematic drawings of Ballester's B4CP symmetric macrocycle **14** used for the formation of 2:1 complexes and pseudorotaxane architectures.

The first synthetized BC4P receptor was reported by our group in 2012.[61] The BC4P macrocycle **14** was obtained by a double Hay coupling reaction of two terminal alkyne AE-C4P (**Figure 1.15**). Although originally the reaction was claimed to be templated by one equivalent of bis-pyridyl bis-*N*-oxide, later studies demonstrated a reduced template effect of the *N*-oxide. The rigid and symmetric oligocycle was shown to be threaded by suitable lineal guest i.e. 3,5-bis-amide pyridyl *N*-oxides **15** in $CDCl_3$ solution. The formation of ternary complexes (**15·X**)⊂**14** (X= Cl, OCN) was demonstrated using ^{1}H NMR spectroscopy. The pseudorotaxane topology of the

self-assembled complexes **15⊂14** was produced by the establishment of hydrogen bonding interactions between the oxygen atom of the *N*-oxide and the four NHs of one of the C4P units of the receptor. In these assemblies, the lineal component experienced a pirouetting motion inside the receptors cavity. The bound *N*-oxide exchanged between the two identical binding sites of **14**, as well as between the free counterpart, in binding equilibria that at r.t. showed fast dynamics on the ^{1}H NMR chemical shift timescale. The subsequent addition of one equivalent of a suitable anionic tetraalkylammonium salt produced the quantitative formation of a four particles assembly (**15·X·TBA**)⊂**14**. In this complex, the anion was bound in the binding pocket defined by the two amide protons of the lineal component and the four NHs of one of the C4P binding sites of **14**. The cation was located opposite to the bound anion and included in the external, aromatic and electron rich cavity defined by the pyrrole rings of the C4P core in cone conformation. Experimental support to the proposed binding geometry was derived from 1D ^{1}H NMR spectroscopy experiments as well as the analysis of the ROESY and DOSY spectra of the equimolar mixture of components.

The same oligocylic receptor **14** was later employed in binding studies of tetraalkylmmonium salts in $CDCl_3$ solution.[62] Receptor **14** bound TBA·Cl and TBA·OCN salts forming ion-quartet complexes that displayed cascade-like arrangement of three ions. This binding geometry was evidenced in solution using ^{1}H NMR spectroscopy experiments. The cascade-like structure of the ion-quartet complexes was also revealed in the solid state by means of X-Ray diffraction of single crystals (**Figure 1.15**). One of the ion pairs was bound in a close-contact binding geometry while the other showed a receptor-separated binding mode. The overall binding affinity constants for the five-particles complexes were calculated by ITC experiments. In the case of TBA·OCN a binding affinity value of $K_{2:1}$= 1.5 ± 0.3 × 10^{11} M^{-2} was determined. In the case of TBA·Cl the calculated value was $K_{2:1}$= 1.9 × 10^9 M^{-2}. The assessment of the cooperativity effect in the complexation process required the use of a reference compound. To this end, the authors used a simple "two-wall" *para*-alkynyl AE-C4P receptor. The binding constant values determined for the two salts to the reference receptor were compared (K_{ref}). Defining the cooperativity factor as $\alpha = K_{2:1} / K_{ref}^2$, the two complexes were characterized as having a large positive allosteric cooperativity. The TBA^+ cation sandwiched between the two bound anions served to cancel any repulsive Coulombic interactions that could arise between them. Titration experiments of receptor **14** with MTOA·Cl provided striking different results. Firstly, a host-separated binding mode was

observed for the two bound ion pairs, as revealed by X-Ray diffraction analysis of single crystals and ^{1}H NMR spectroscopic studies. These findings were rationalized in terms of the superior complementarity of the methyl group of the $MTOA^+$ cation and the external bowl-shaped cup defined by the pyrrole rings of the C4P core in cone conformation. Using ITC experiments, the stepwise binding constant value of $K_{average}$ = 4.9±1 × 10^4 M^{-1} was determined. The calculated value indicated that no significant cooperativity was taking place in the formation of the complex.

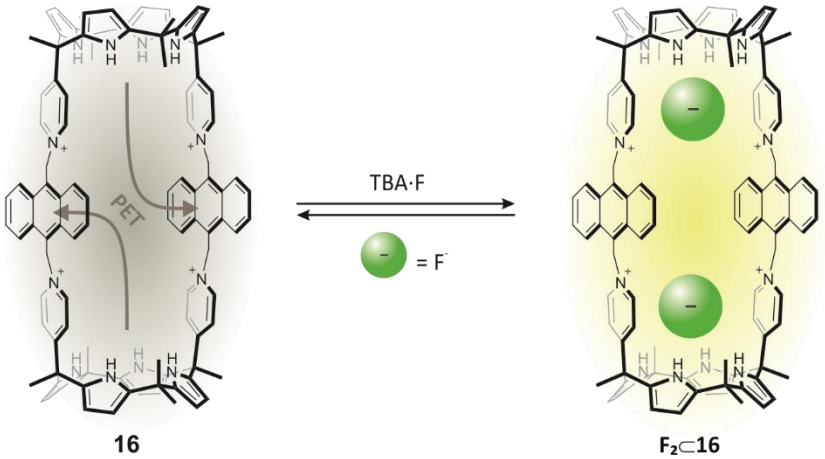

Figure 1.16. Schematic representation of Lee's fluorescent macrocycle **16** involved in the binding of fluoride anions in acetonitrile solution.

The two spacers covalently connecting the C4P units of BC4P receptors can incorporate photoactive components. The photoactive groups would serve to probe the formation of the complexes using absorption and/or emission spectroscopy. Having this consideration in mind, the group of Lee disclosed in 2015 a new tetracationic BC4P receptor possessing an anthracene unit in the spacer (**Figure 1.16**).[63] Receptor **16** formed 1:1 and 1:2 complexes in CD_3CN solution. F^- was selectively bound over Cl^- and I^-, as inferred from the results obtained in fluorescence spectroscopy titration experiments. The selectivity of the receptor towards fluoride was rationalized by the conformational restrictions of the system. They observed a fluorescence "turn-on" of the receptor exclusively upon addition of the fluoride salt. According to the authors, the binding of the anion produced conformational changes in the receptor that disrupted the π-π interactions that caused the quenching of the fluorescence. These conformational changes also favoured the binding of the second fluoride anion. This conclusion was also supported by the observation of a 300-fold increase in the binding constant value

for the second fluoride. Thus, ITC experiments returned K_1 = 1.91 x 10^5 M^{-1} for the first binding event and K_2 = 5.95 x 10^7 M^{-1} for the second event. This result evidenced the high allosteric cooperativity displayed by the receptor in the binding of fluoride.

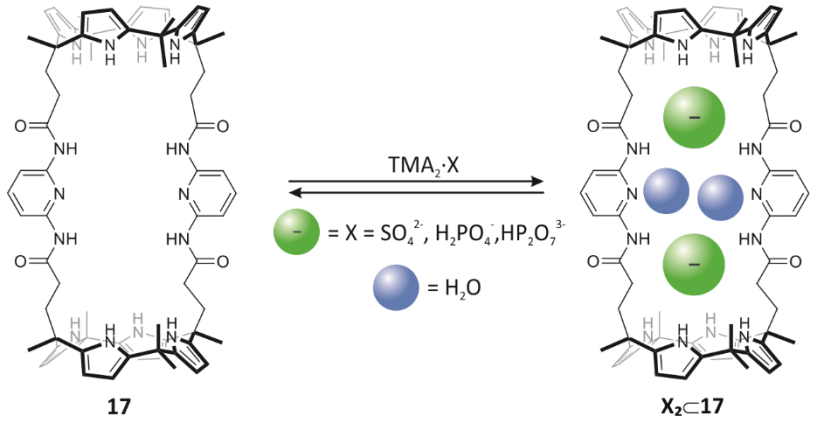

Figure 1.17. Schematic drawings of Sessler's macrocycle **17** in the formation of 2:1 complexes with oxoanions.

Another recent example of BC4P receptor was described by the group of Sessler in 2017.[64] In contrast to the previous BC4P receptors, macrocycle **17** was synthesized by the multiring acid catalysed condensation of acetone with a bis-dipyrromethane containing a 2,6-diamidopyridine derivative as spacer (**Figure 1.17**). The authors envisaged that the spacer selected for the linking of the two hemispheres of the tri-cyclic receptor could also be involved in the binding of ion pairs. The results of ^{1}H NMR titrations experiments indicated that receptor **17** produced 1:2 complexes with relatively large oxoanions such as SO_4^{2-}, $H_2PO_4^-$ and $HP_2O_7^{3-}$ (as TBA or TMA salts) in a CD_2Cl_2:MeOD 9:1 mixtures. This finding was also supported by the results obtained in UV titration experiments carried in DCE and DCE:MeOD 9:1 mixtures. Interestingly, the X-Ray diffraction of single crystals obtained for the complexes of **17** with $H_2PO_4^-$ and SO_4^{2-} revealed the existence of two water molecules bridging the bound anions. The stepwise binding constant values for the complex formation were determined using ITC experiments. The 1:1 complex was characterized by stability constants of the order of K_a= 10^4 - 10^6 M^{-1} for the coordination of $H_2PO_4^-$ and $HP_2O_7^{3-}$, respectively. These large magnitudes were rationalized by the stabilization of the complexes through the formation of up to twelve hydrogen-bonding interactions between the receptor and the bound oxoanion. Nevertheless, the second binding event, leading to the formation of the 1:2 complex, displayed in both cases slightly lower magnitudes. The observed negative allosteric cooperativity

was assigned do the repulsive Coulombic interactions arising between the two bound anions.

1.3. Rotaxanes: synthesis and recognition of charged species

Mechanically interlocked molecules (MIM) are supramolecular architectures consisting of one or more molecules entangled by a mechanical bond.[65] The components forming the MIM are locked together and can only be brought apart by the cleavage of at least one covalent bond, yielding the separated components or the untangled molecule. The components of MIM are held together by non-covalent interactions. Due to the weak nature of these interactions, molecular motions are often present in these architectures. MIMs can be divided according to its topological features into catenanes,[66] rotaxanes,[67] knots[68] and Borromean rings (**Figure 1.18**).[69,70] Over the past decades, the interest for the syntheses of these architectures using supramolecular assistance has experienced a tremendous growth. These synthetic efforts and the potential applications of the resulting architectures were recognized in 2016 with the Nobel Prize in chemistry being awarded to Prof. Fraser Stoddart, Prof. Ben Feringa and Prof. Jean-Pierre Sauvage "for the design and synthesis of molecular machines".[71]

The intrinsic structural properties of these supramolecular architectures often generate functionalized three-dimensional binding pockets able to engage in molecular recognition events. In addition, the relative motions (translation and rotation) of the components of interlocked molecules have been exploited to generate molecular switches and primitive molecular machines.

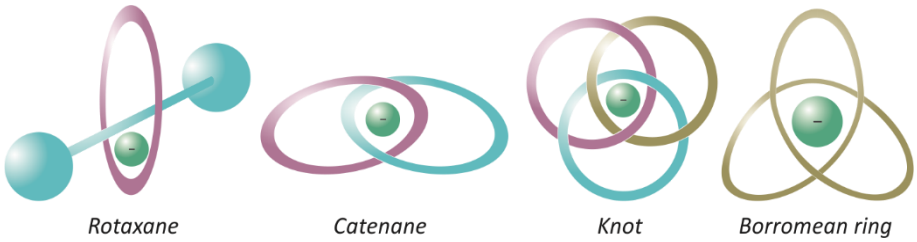

Figure 1.18. Schematic representation of MIMs as anion receptors.

MIMs are attractive to scientists for their potential applications. However, Nature already offers many examples of functional MIMs. [72,73,74,75,72,73] For example, DNA is known to adopt catenane and knot topologies in the replication process inside the cell.[76,77] In addition, DNA also assemble in rotaxane-like structures in combination

with the protein λ-Exonuclease. The protein wraps the DNA strain in the replication and reparation processes.[78]

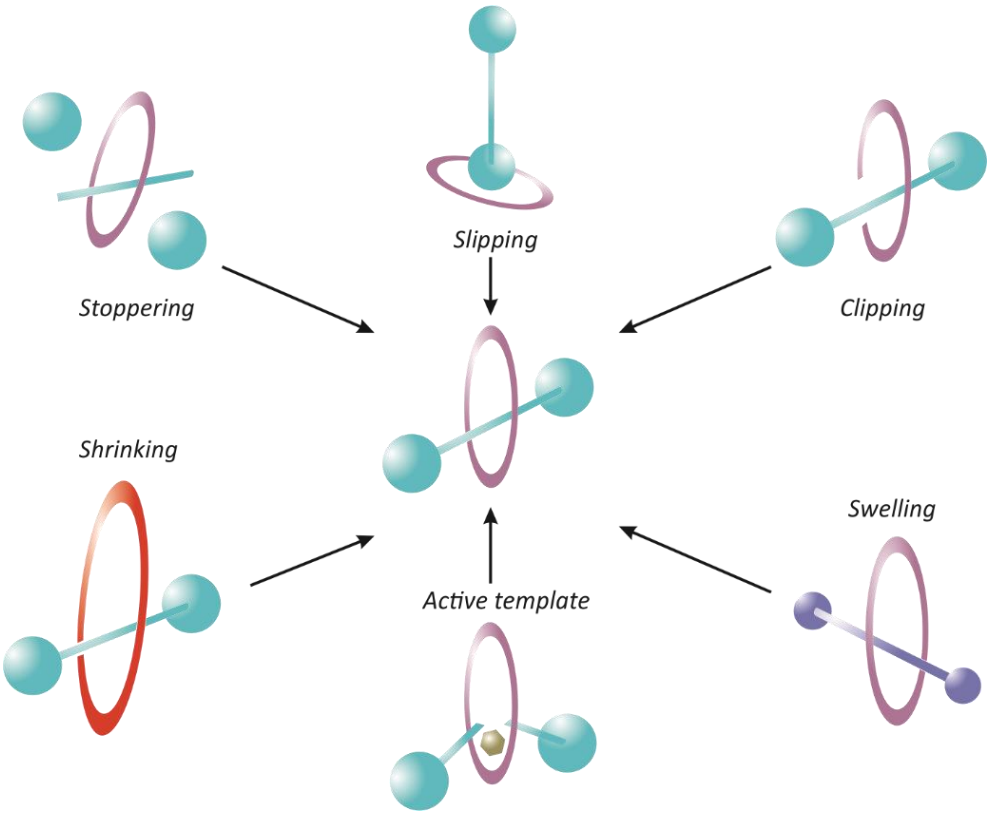

Figure 1.19. Schematic representation of the different synthetic routes used to obtain rotaxane assemblies.

Rotaxanes are MIM that consists on a macrocyclic unit threaded by a lineal component, an axle that bears sterically bulky groups – commonly known as stoppers – at both ends to prevent the disassembly of the interlocked components. Non-covalent interactions are often stablished between the thread and the macrocycle owing to the supramolecular assistance employed in the synthesis of the interlocked assembly. The incorporation of a second recognition site in the axle leads to the so-called "two station" rotaxanes, often used in the design of molecular machines or switches. Indeed, in "two station" rotaxanes the macrocyclic component can switch between the stations in response to an external stimuli, such as light or a pH change.[79,80] The inclusion of an additional macrocycle or axle generates [*n*]rotaxane architectures, where *n* is the number of components that forms the assembly. An important family of assemblies closely related to rotaxane

are pseudorotaxanes. These are supramolecular complexes formed by one macrocycle threaded by a lineal component. In contrast to rotaxane architectures, the lineal component does not bear bulky stoppers to prevent the dethreading process. Thus, the complex and its free components are in equilibrium. Rotaxane architectures are obtained by applying different synthetic procedures that can be divided in three major groups: covalent modification, slipping and catalyst template synthesis (**Figure 1.19**).[81]

Rotaxane synthesis by covalent modification implies the establishment of non-covalent interactions between the precursors of the axle and the macrocycle. Generation of a 1:1 complex between the precursors precedes a covalent modification step that locks the molecular structure. This is the case for the clipping, capping, swelling and shirking strategies. In the clipping approach, the open macrocycle interacts with the axle prior closure of the ring. The axle, already bearing sterically bulky groups at both ends, presents a recognition site able to interact reversibly with the opened macrocycle. Closure of the complexed macrocycle generates the rotaxane. [82] In a similar manner, in the capping strategy the axle precursor, with no stoppers incorporated, threads the macrocyclic component to generate a pseudorotaxane assembly. The incorporation of the stoppers into the axle grants the interlocked structure.[83] In both the swelling and the shrinking strategies, the stoppered axle and the macrocycle generates a 1:1 complex. However, the pseudorotanxae complex can disassemble due to the poor size complementarity between the macrocycle and the bulky stopper. The covalent modification to increase the size of the stoppers – swelling – or reduce the size of the macrocycle – shrinking – generates the interlocked architecture.[84,85]

In the slipping approach, the size complementarity between the stoppers and the macrocycle is exploited in a different manner. In this case, the stoppered axle is unable to thread the macrocyclic component due to the greater size of the stoppers. In order to surpass the energy barrier to thread the stoppered axle, more energy is provided to the system in the form of higher temperature or pressure. Under these conditions, the lineal component is able to “slip” through the ring and reach a kinetic trap that locks the architecture as the rotaxane.[86]

Finally, the active template strategy implies the use of an external reagent that templates and catalyses the reaction that forms the interlocked structure. In this case, an external reagent establishes non-covalent interactions with both the macrocycle and the axle precursors. At the same time, this external reagent serves

to catalyze the reaction to generate the stoppered axle. As the reaction takes place inside the macrocyclic structure, the axle remains threaded through the ring to generate the rotaxane. The catalyst is then released to the bulk solution.[87]

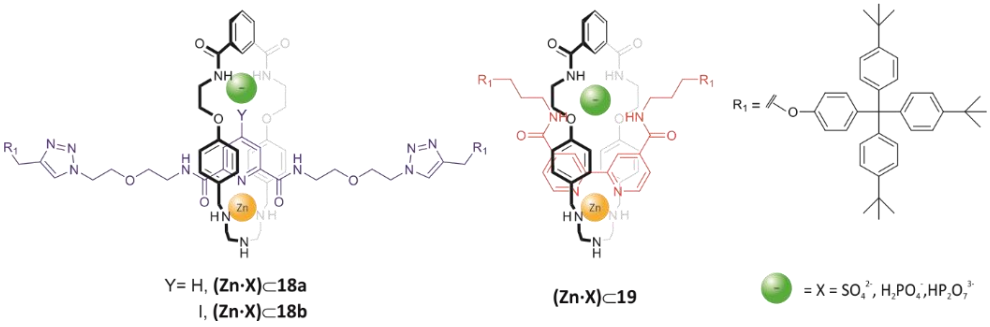

Figure 1.20. Schematic representation of Beer's isophthalamide based rotaxanes **18a-b** and **19** binding ion pairs.

Rotaxane architectures can serve as heteroditopic receptors for the binding of ion pairs.[72] Indeed, the topology of the system often generates three-dimensional binding pockets that can allocate both the anion and the cation. The interlocked structures offer greater selectivity and affinity compared to the non-interlocked counterparts. A recent example of rotaxanes as ion pair receptors comes from the group of Beer.[88] They synthesized three rotaxanes based on a similar macrocycle, **18a-b** and **19** (**Figure 1.20**). In all cases, the macrocycle featured an isophthalamide binding unit able to interact with anions. A trisamine was inserted in the opposite region of the macrocycle, with the aim of engaging in the binding of metal cations. The three rotaxane architectures differed in the structure of the threaded axle. In the case of **18b**, the axle was based on a 4-iodopyridyl-2,6-dicarbonyl pyridine derivative. In **19**, a 2,2-bipyridyl-4,4-bis-amide functionalised axle was used. For **18a-b**, the rotaxane assemblies were obtained following a bis-stoppering strategy mediated by a double Cu(I) catalyzed azide-alkyne cycloaddition (CuAAC). In contrast, for **19** a mono-stoppering strategy was followed. An amide coupling reaction was used as the key step of the rotaxane formation. Interestingly, in all cases the threading of the axle was assisted by the use of a Cu(II) cation previously coordinated to the tris-amine unit of the macrocycle. The Cu(II) was removed prior to the purification of the heteroditopic rotaxanes. The addition of a $Zn(ClO_4)_2$ to the rotaxanes generated 1:1 Zn(II)-complexes with the cation located in the metallic binding site of the heteroditopic receptors. This was evidenced by HR-MS and ^1H NMR spectroscopy studies. Next, the anion binding properties of the Zn(II)-complexed rotaxanes towards halide and various oxoanions were studied by ^1H

NMR titration experiments. Complex **Zn⊂19** selectively bound AcO^- over Cl^-, Br^-, I^- and NO_3^- in $CDCl_3$:CD_3OD 1:1 mixtures. These findings were interpreted by the authors as a possible direct coordination of the anion to the Zn(II) metal. In the case of the Zn(II) complexes of **18a-b**, the authors found a slightly preference for the recognition of Br^- in a $CDCl_3$:CD_3OD:D_2O 45:45:10 mixture. Interestingly, small differences were observed between the binding properties of the Zn(II) complexes of **18a** and **18b**. The iodine-substituted Zn(II)-rotaxane complex **Zn⊂18b** displayed a modest improvement in the affinity constant values. The bulky iodine substituents was not involved in halogen bonding interactions. Instead, the formed complexes were mainly stabilized by hydrogen bonding and Coulombic interactions. Nevertheless, the binding selectivity of the Zn(II)-complexed rotaxane towards anions was attributed to the better shape and size complementarity between the anions and the three dimensional anionic binding-site present in the heteroditopic receptors.

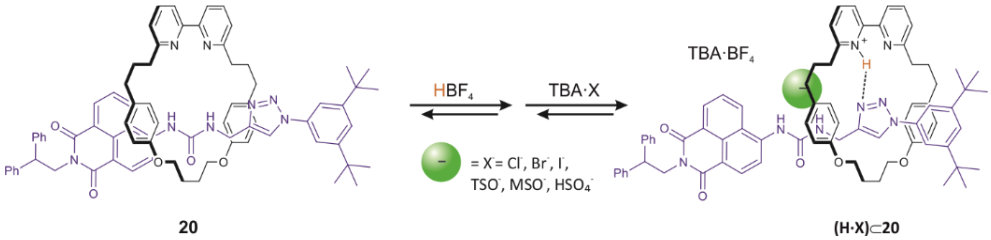

Figure 1.21. Schematic representation of Goldup's rotaxane **20** shuttling in the binding of HX type ion pairs.

In some cases, the binding of an ion pair to a rotaxane receptor can induce molecular motions. Indeed, the ion-pair binding can provoke the displacement of the macrocyclic component along the axle into a different recognition site. The group of Goldup observed this phenomenon, known as shuttling, in one of his most recent publications.[89] The authors reported the active template synthesis of [2]rotaxane **20** by means of a mono-stoppering CuAAC reaction. The receptor consisted on a macrocycle decorated with a 2,2-bipyridyl-4,4-bis-amide unit and an axle with two stations: an urea and a triazole group (**Figure 1.21**). In addition, a naphthalimide unit was used as a stopper in order to monitor the binding events by means of UV-Vis spectroscopy. In a 1:1 mixture of $CDCl_3$:CD_3CN, the macrocyclic component of the [2]rotaxane was found to be encircling the urea group by establishing hydrogen bonding interactions between the NHs and the nitrogen atoms of the bispyridine unit. The results of the ^1H NMR analysis of the structure of the rotaxane in solution were supported by the X-Ray diffraction of a single crystal. In addition, UV-Vis

experiments performed in the same solvent revealed an increase in the absorbance at λ = 380 nm, further supporting the formation of the complex.

Interestingly, the addition of a panel of anions did not produce noticeable changes in the UV-Vis and the ^{1}H NMR spectra of the rotaxane. The poor ability of the receptor to bind anions was attributed to the strong intramolecular interaction between the bispyridine unit of the macrocycle and the urea group of the axle. The authors envisaged that the protonation of the bispyridine unit should induce the urea group to be free and engage in intermolecular interactions with the anions. Indeed, the addition of HBF_4 produced the shuttling of the protonated macrocycle to the triazole station, as evidenced from the ^{1}H NMR and UV-Vis spectra. To further support this claim, the X-Ray diffraction of a single crystal of **HBF_4⊂20** showed close-contact distances between the bispyridine and the triazole proton of the axle, as well as between one of the nitrogen atoms of the triazole and the protonated one in the bis-pyridine. The properties of **HBF_4⊂20** in the binding of TBA ion pairs was probed using ^{1}H NMR and UV-Vis spectroscopy titrations. As expected, the addition of basic anions such as AcO^- and F^- restored receptor **20** with no anion binding observed. The use of less basic anions generated 1:1 complexes with a binding constant value up to 10^4 M^{-1} for the Cl^- anion. A general increase in binding affinity was observed when the results were compared with those obtained for the free axle. In addition, **20·HBF_4** displayed a greater shape and size selectivity due to the crowded surroundings of the urea motif. Smaller and spherical anions, such as Cl^- and Br^-, were preferred over tetrahedral HSO_4^- or the larger mesylate MSO^-.

As previously discussed, C4P are exceptional receptors for the binding of ion pairs. It is then sensible to believe that rotaxane assemblies based on C4Ps could exhibit improved binding capabilities for ion-pairs. However, in the vast literature of rotaxanes only one example is found involving C4Ps components.[90] In 2017 our group reported the synthesis and binding studies of a [2]rotaxane based on a BC4P cyclic component. This cyclic component was already investigated for the self-assembly of [2]pseudorotaxanes.[61] The synthesis of rotaxane **21** was achieved through a stoppering strategy. A stable 1:1 complex was formed in solution between the cyclic component **14** and the unstoppered axle, containing a pyridyl *N*-oxide binding motif. The double CuAAC reaction of the terminal azide groups of the axle with the alkyne-derivative bearing a bulky ter-biphenyl substituent produced the rotaxane receptor **21** in an acceptable yield (**Figure 1.22**). ^{1}H NMR studies in $CDCl_3$ solution revealed that the axle was involved in a pirouetting exchange between the

two equivalent binding sites of the BC4P macrocycle. The exchange was intermediate on the ^{1}H NMR chemical shift timescale. By means of ^{1}H NMR experiments, the properties of the [2]rotaxane to bind tetraalkylammonium salts of cyanate, chloride and nitrate were investigated. In all the cases, thermodynamically and kinetically highly stable 1:1 complexes were obtained. The anion was coordinated in the polar inner cavity of the receptor, where up to six NHs converge

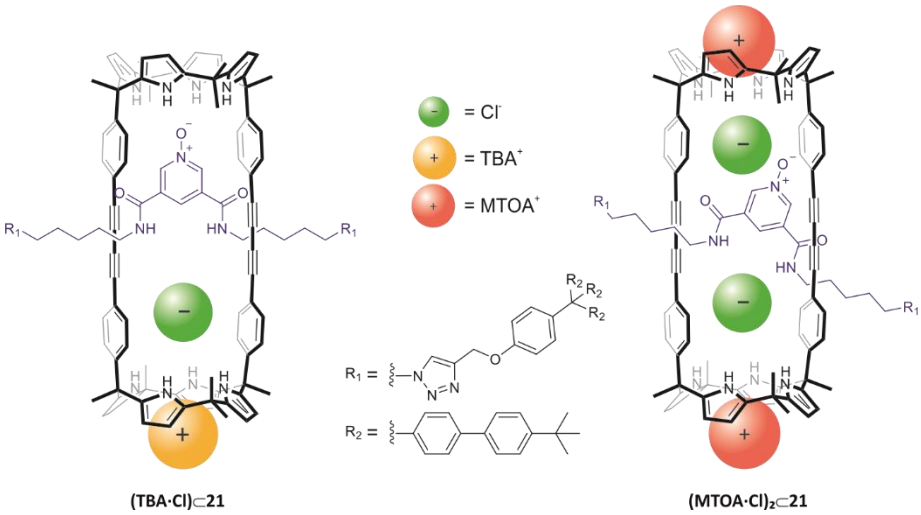

Figure 1.22. Schematic drawing of calix[4]pyrrole based [2]rotaxane **21** developed by our group and the complexes formed with chloride salts.

(two from the axle and four from the C4P core). In addition, the cation was located in the electron rich aromatic cavity defined by the pyrrole rings of the C4P unit binding the anion. The cation binding was stabilized by CH-π and cation-π interactions. Interestingly, the addition of more than one equivalent of MTOA·Cl produced the formation of a 2:1 complex; it is believed that the chloride anion can compete with the *N*-oxide for the binding with the C4P. This generates a new complex in which the axle is partially displaced outside of the macrocyclic component. The thermodynamic parameters of the 1:1 complexes were assessed using ITC experiments. The binding processes of all studied ion pairs were driven by enthalpy. This was expected considering that **21** is a hydrogen bonding receptor operating in non-polar and non-protic media. The values determined for the binding constants revealed a higher affinity towards the cyanate salt of TBA compared to that of nitrate and chloride. These findings were rationalized owing to a better size and shape complementarity between the cylindrical anion and the polar cavity of the rotaxane. In addition, a three order of magnitude increase was observed in the

bidning affinity of the rotaxane for MTOA·Cl with respect to the TBA counterpart. This difference was related to the better match in shape of the MTOA cation, having a methyl group that can be included in the shallow aromatic cavity defined by the pyrrole ring of the C4P cone conformation.

1.4. ESI-MS in supramolecular chemistry

Mass spectrometry (MS) is an analytical technique that can be used for the accurate determination of the exact mass of a molecular ion. This technique has become a common tool for the characterization of synthetic products. Modern high-resolution MS instruments can go further and reveal the isotopic pattern of the ionic species, which we may consider as its fingerprint. Beyond basic characterization, MS can also be used to probe the formation of supramolecular assemblies in the gas phase and the strength of the involved interactions. The MS analysis includes a first step that implies the formation and vaporization of a charged species derived from the molecule or supramolecule of interest, the so-called ionization process. In this process, upon the introduction of the ion in a low-pressure area, the solvation shell is lost. This results in the formation of a gas-phase ion. Thus, the intrinsic properties and characteristics of the supramolecular assemblies can be altered: the binding energy, the selectivity and the geometry differ from the species in solution. In general terms, non-covalent interactions that can compete with the solvent are strengthened in the gas phase, such as hydrogen bonding interactions. On the other hand, hydrophobic interactions are diminished in the gas phase in the absence of water molecules. In addition to this, the ionization process often produces the fragmentation of the supramolecular architecture, regenerating the separated components or even producing new ones.

Although there are many methods for the ionization process, the most widely used for the study of supramolecular architectures and complexes is Electrospray Ionization (ESI). ESI can be considered one of the softest methods of ionization in mass spectrometry due to the mild conditions used and the low fragmentation observed in these experiments. This methodology has proved to be useful for the analysis of biologically relevant species, granting Professor Fenn the Nobel Prize in chemistry in 2002 for “the development of methods for identification and structure analyses of biological macromolecules”.[91] In this ionization method, a solution containing the analyte is ejected through a thin steel capillary. The capillary is connected to an opposing plate charged with an electric potential of ~5 kV (**Figure 1.23**). The solution is propelled forming a Taylor-cone shape at the tip of the needle

that generates a stream of small droplets containing the charged analyte. The desolvation of the ion due to the high vacuum and the charge repulsion inside the droplet produces the subsequential shrinkage. This process is repeated until the solvent-free molecular ion is obtained with little to no fragmentation.[92,93,94] The ions generated are often present in multicharged states due to further protonation or deprotonation in the needle. In addition, in some cases, clusters are generated with anions or cations present in the solvent, such as chloride or sodium.

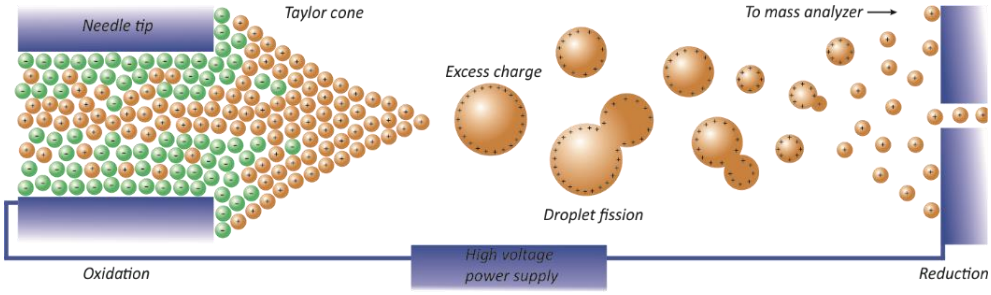

Figure 1.23.Diagram of an ESI-MS ion source working in positive mode.

The detection of the ionic supramolecular assemblies and complexes is highly dependent on the experimental conditions. Two of the major factors that have to be taken into account before running the experiments are the solvent choice and the concentration.[95] Regarding the solvent, it is sensible to expect that polar solvents can damper the establishment of non-covalent interactions in solution, e.g. disfavouring the formation of the complex if polar interactions play an important role. However, the use of non-polar solvents is detrimental for the stabilization of the charged particles. These solvents usually present low dielectric constants not appropriate to transfer the electric field generated in the ionization source. High dilution conditions, often mandatory to avoid signal saturation, can negatively affect the formation of ionic complexes. Low values in the binding affinity constant to generate host-guest aggregates will translate in a negligible amount of the complex when working in high dilution conditions. Furthermore, higher concentration solutions could favour the formation of adducts, often generated by non-specific binding of host and guest.

The study of supramolecular assemblies by ESI-MS can provide accurate and insightful information on the formation of non-covalent complexes by detection of the ion peak. Furthermore, beyond the characterization of the complexes, information on the conformational properties, topology and stability can be inferred

from ESI-MS experiments.[96,97,98] The geometry and stability of a supramolecular complex can be assessed in Tandem-MS experiments by attending to collision induced dissociation (CID). In the CID experiments described in this thesis, the gas-phase ion is mass-selected and transported to a collision cell using an electric field. The high-speed ions impact with a stationary inert gas such as N_2. The kinetic energy is transformed into internal energy, ultimately producing the fragmentation of the molecule if a collision energy threshold is reached. The obtained fragmentation pattern gives information of the overall connectivity of the supramolecular architecture, as well as the stability of the non-covalent interactions.

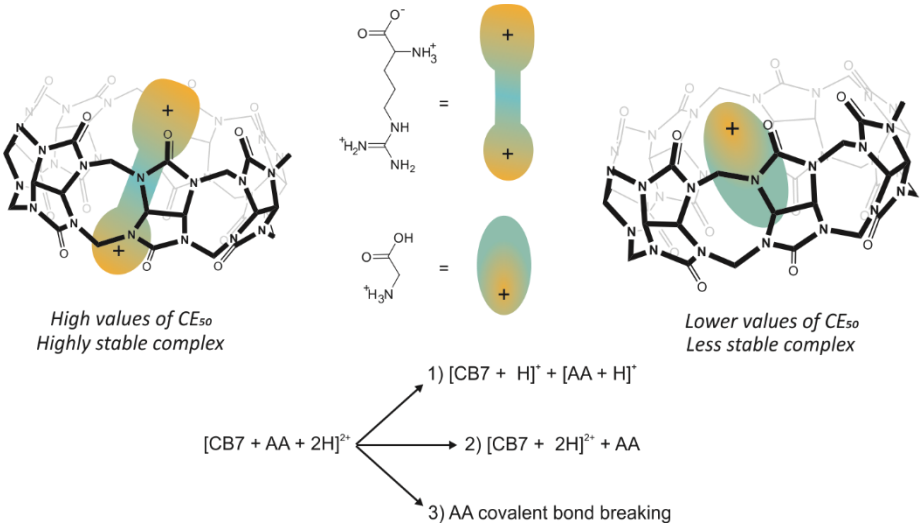

Figure 1.24. Top) Schematic representation of the complexes formed between CB7 and protonated arginine and lysine. Bottom) Different fragmentation pathways observed in the MS experiments.

A recent publication from the group of Kovalenko shows the potential applications of tandem-MS experiments to assess the stability of supramolecular complexes.[99] In this work, several CID experiments were performed to investigate the stability of the complexes formed between cucurbit[7]uril (CB7) and a series of aminoacids (**Figure 1.24**). The formation of complexes $[H+A+2H]^{2+}$ was confirmed by the detection of the ion peak in the ESI-MS experiments. The subsequent fragmentation in the MS-MS experiments followed three different pathways: 1) a charge separation process, 2) aminoacid dissociation and 3) covalent bond cleavage of the aminoacid. For complexes obtained with non-basic aminoacids, processes 1) and 2) were proved to occur simultaneously. This was inferred from the comparison of the collision energy needed to fragment the parent ion to a 50% extent ($E_{CM(50\%)}$), which proved to be similar (between 0.9 and 1.1 eV). These findings were rationalized by

the similar activation barrier for charge separation and dissociation events to take place. Remarkably, some differences were observed depending on the proton affinity of the aminoacids. In general terms, those complexes formed with aminoacids with a higher proton affinity, such as glycine, underwent a fragmentation process that followed pathway 2). The authors explained the prevalent dissociation pathway by the existence of a bridging proton that connected both the aminoacid and the CB7. If the proton affinity is high enough in the bound aminoacid, the dissociation occurs by sequestration of the bridging proton. CID experiments of the complexes formed with aminoacids bearing two protonable sites, such as lysine and arginine, returned higher values of $E_{CM(50\%)}$. In addition, these complexes dissociated following pathway 3), covalent bond leakage. These results were interpreted by invoking the superior binding affinity of the aminoacids that could now interact with both polar portals of the CB7 to form a highly thermodynamically and kinetically stable aggregate.

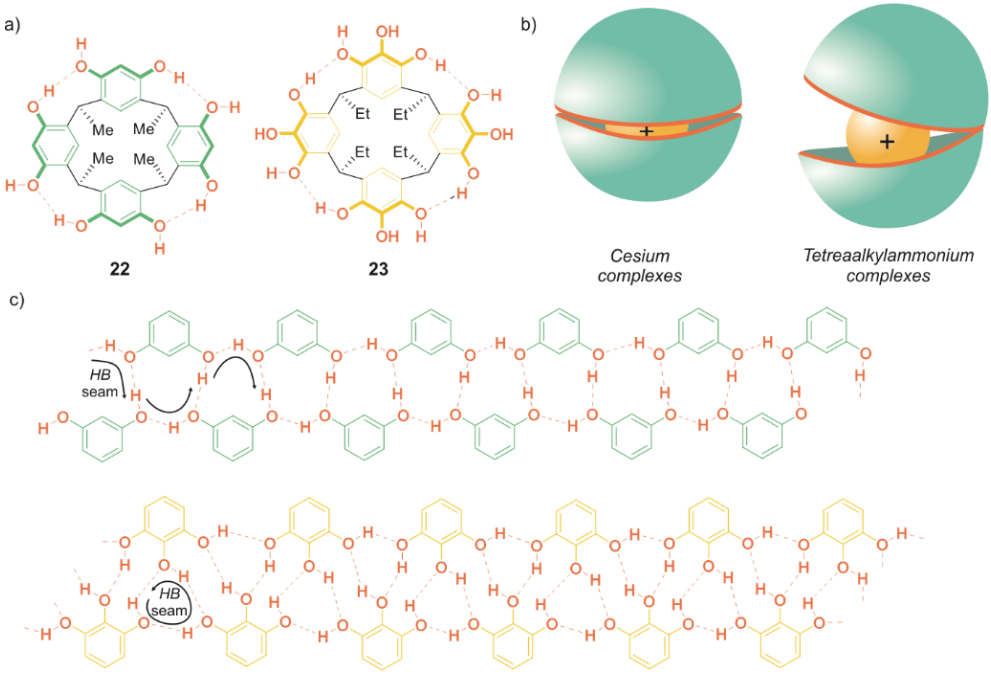

Figure 1.25. Schematic representation of resorcinarenes **22** and **23** a), three dimensional models of the complexes obtained with cesium and tetraalkylammonium salts b) and representation of the hydrogen bond belt for the capsules obtained with **22** (top) and **23** (bottom).

A variation of tandem-MS that have proved to be useful for supramolecular chemistry are H/D exchange experiments. These experiments function in a similar

manner as tandem-MS, although the gas-phase ion does not fragment in the collision chamber. Instead, a deuterated reagent is introduced in the chamber and is left to exchange with the ion molecule for a defined time-period. This process can also take place on the detector in the case of FT-ICR instruments or inside an orbitrap. In any case, the mass selected ion suffers subsequent proton-deuterium exchanges that are dependent on the proton affinities of both the ion and the deuterated reagent. For a successful exchange to occur the proton affinities of both reactants have to be similar. In addition, the non-covalent interactions that the proton is involved in, such as hydrogen bonding, can damper the exchange rate.[100] The resulting mass spectrum presents additional $[M+n]^{n+}$ ion peaks depending on the exchanged protons. This technique is generally used in supramolecular chemistry to assess the formation of complexes and the different conformers, as well as to study the hydrogen bonding interactions presents in the assembly. [97]

H/D exchange experiments were used to assess the formation of capsular assemblies in a 2011 manuscript from the group of Schalley.[101] In this work, two different resorcinarene receptors were employed to generate capsular assemblies assisted by templating cations, i.e. cesium and ammonium salts (**Figure 1.25a**). The experiments were carried out by the introduction of deuterated methanol in the detector of an FT-ICR instrument. Capsular assemblies were obtained in all cases, regardless of the presence and size of the cation (**Figure 1.25b**). Interestingly, they observed that using reso-macrocycle **22** with cesium as templating agent generated a capsular assembly that experimented fast H/D exchange. However, a significant decrease in the exchange rate was observed when tetrametyl or tetraetylammonium cations were employed as template. These findings were rationalize by means of the existence of a hydrogen bond belt in the capsule that favours the exchange. This continuous hydrogen bond belt could only be generated with smaller cations such as cesium, as encapsulated cations with a greater size situate both components too far apart from each other. In a proposed mechanism, the methanol molecule is inserted in the continuous hydrogen bond seam. The concerted mechanism for the H/D exchange requires no charge separation, as the electrons are redistributed along the hydrogen bond seam, facilitating consequent exchanges in the capsule (**Figure 1.25c**). However, in the case of the pyro-resorcinarene **23**, a small percentage of exchange was detected even with the encapsulation of the ammonium cations. This result was explained in terms of the formation of an unexpected hydrogen bond pattern that held together the assembly. Indeed, formation of a pattern of six-member rings of hydrogen bonds

along the capsule equatorial was deducted by DFT calculations. The H/D exchange could still be feasible without a detrimental charge separation step. The exchange would be followed by the rearrangement of the capsule to form a new six-membered ring of hydrogen bonds to repeat the process until full exchange was achieved.

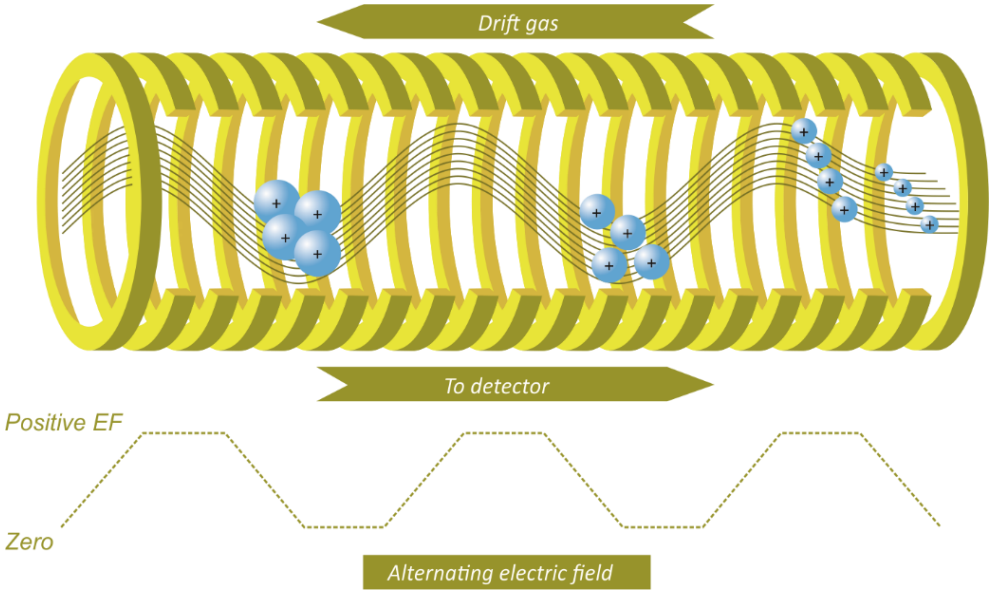

Figure 1.26. Diagram of a TW-IMS instrument.

A powerful tool derived from MS for supramolecular chemistry is Ion Mobility Mass Spectrometry (IMS). In this technique, ions with identical mass to charge ratio are separated according to its size and conformation, in a similar way as electrophoresis does so in the condensed phase.[102] In general, there are three different ways of performing IMS experiments based on the instrumentation: drift tube ion mobility, traveling wave ion mobility and field asymmetric ion mobility.[103] In drift tube experiments, the gas-phase ions travel through a metal tube subjected to a voltage of approximately 5-100 V that facilitates the acceleration of the particles. Inside the tube, an inert gas cause low-energy collision with the moving ions that hinder their advance through the cylinder; more compacted ions will undergo fewer collisions resulting in lower drift times, while the ones with a greater size will arrive later.[104] Traveling wave ion mobility is the method used in the experiments described in this thesis (**Figure 1.26**). In this methodology, ions are transported through a sequence of parallel rings that are subjected to an alternating radiofrequency voltage. A voltage wave pushes the ions towards the detector. At the same time, an inert gas

flow pushes them in the opposite direction. The ions with greater size tend to fall off from the top of the wave while the smaller ones are pushed through the tube resulting in lower drift times.[105] Finally, in field asymmetric ion mobility the charged particles are pushed perpendicularly to an alternating electric field generated by two electrodes opposing each other. In addition, a compensation voltage is applied to evade ions from reaching the electrodes and being neutralized. In this method, the ions are separated by its mobility by the manipulation of the compensation voltage.[106] The use of IMS in the field of supramolecular chemistry is nowadays centred on the separation of species with identical mass that can adopt different conformations, as in the case of photoswitchable receptors.[107] Outside supramolecular chemistry, this technique has also found applications in other fields such as biological systems[108] or coordination chemistry.[109]

1.5. Aim of the thesis

The main objective of this work has been the coordination of ion pairs in organic media. For this purpose, we envisaged the use of synthetic receptors based on C4P binding sites. In cone conformation, C4P receptors present a polar binding site generated by four converging pyrrole NH groups. In the structures of the AEC4P and SAEC4P receptors, this polar binding site closes one end of the deep and polar aromatic cavity that is defined by their cone conformation. The opposed end of the cavity remains opens. In addition, the C4P binding site is optimal for the coordination of negatively charged ions and neutral polar molecules through the formation of multiple hydrogen-bonds. Simultaneously, the pyrrole rings of the C4P in cone conformation shape a shallow and electron rich aromatic cavity opposed to the hydrogen-bonded bound guest. This second binding site is suitable for the binding of cations and electron poor molecules. We expected that the incorporation of C4P units in BC4P receptors and strapped systems would allow the binding of more than one ion-pair. Moreover, the spatial proximity of binding sites in the above-mentioned multitopic receptors could favour the binding of several ions owing to positive cooperativity effects. These effects may arise from positive Coulombic and/or hydrogen bonding interactions established between the bound particles that are charged and in close proximity. The synthesis of receptors featuring [2]rotaxane topology and containing as cyclic components BC4P receptors could potentially enhance the binding affinity of the ion-pairs due to the three dimensional polar environments that are generated in the interlocked structures.

O.1) Synthesis and binding studies of a BC4P receptor

Previously, we reported the synthesis of a symmetric and conformationally rigid BC4P receptor that was able to bind quartets of tetraalkylammonium anion salts in chloroform solution. In order to improve the binding selectivity towards quartets of ion-pairs with smaller anions, we designed and proposed the synthesis of a macrocycle bearing shorter linkers as bridging unit between its two C4P binding sites. This strategy was expected to generate a heteroditopic receptor with a reduced inner volume. We also wanted to study the binding properties of the new receptor towards quartets of tetraalkylammonium ion-pairs. This study should help us to entangle the cooperativity effects, if any, that are operative in the binding of multiple charged particles by the B4CP receptor in chloroform solution.

O.2) Formation of MIM based on a B4CP receptor

We envisaged the formation of mechanically interlocked molecules (MIM) using the previously synthetized BC4P receptor as cyclic component. We expected that the three-dimensional polar cavity provided by the planned receptor featuring [2]rotaxane topology should increase the binding affinity towards the tetraalkylammonium ion-pairs compared to their separate components or simple C4P receptors. The synthesis of the [2]rotaxane structure would involve a capping procedure and the use of a bis-amide pyridyl-*N*-oxide as lineal component. On the one hand, pyridyl *N*-oxides display high affinity towards C4P binding sites. On the other hand, bulky tris(bis-phenyl) stoppers were used with even larger BC4P macrocycles to prevent the dethreading of the axle. We expected a change in the selectivity of the newly designed interlocked receptor compared to the previous [2]rotaxanes receptors developed by the group. The smaller size and unsymmetrical nature of the cyclic component used in this work was expected to generate a three dimensional polar binding site with different binding properties for ion-pairs. The synthesis of the [2]rotaxane receptor and the study of its binding properties should be preceded by investigations on the self-assembly of the corresponding [2]pseudorotaxane precursors and their binding properties towards ion pairs.

O.3) Synthesis and binding studies of a bisamidopyridyl strapped C4P

Inspired by the structures of the strapped C4P receptors published by professor Sessler and others, we imagined the use of a bis-amidopyridyl strapping unit to obtain an unprecedented SAE-C4P strapped receptor. In contrast to the examples described in literature, the new receptor would present a greater inner cavity that

would allow for the binding of ion dimers and triplets. At the same time, we sought to develop a multitopic receptor for ion-multiplets featuring two distinct anionic binding sites. We expected that the new receptor design would offer different binding affinities and selectivities for the complexation of ion-pairs compared to the parent counterparts.

1.6. Outline of the thesis

The present thesis is divided in six chapters. In chapter one, a general introduction of the topic of the currents thesis is presented. Discussion regarding ion pair receptors, calix[4]pyrroles, mechanically interlocked molecules and concepts about ESI-MS techniques used in this thesis are provided. At the same time, literature examples about those same topics are presented to give context and perspective on the results herein described. In chapter two, the design and synthesis of a BC4P receptor featuring triazole ring as linkers is presented in detail. The use of a template agent had a dramatic effect on the outcome of the coupling reaction of the two C4P units. Indeed, up to three different species were isolated depending on the shape and size of the ditopic guest used as template: the desired BC4P, an opened dimeric product and a tetrameric macrocycle. Binding studies of the synthesized BC4P in chloroform solution with neutral ditopic guests are also presented. Chapter three extends the binding studies of the BC4P receptor in chloroform towards ion pairs. The binding of the heteroditopic receptor with various tetraalkylammonium salts was studied using NMR, ITC and ESI-MS experiments. We observed different binding geometries for the 2:1 complexes depending on the used ion-pair. The cooperativity of the binding system was also studied and it was shown to be dependent on the binding geometry of the complexes. In chapter four, the self-assembly of pseudorotaxane assemblies is investigated using the previously discussed BC4P. Using a bis-amide pyridyl-*N*-oxide as a lineal component, [2]pseudorotaxane assemblies were stabilized by coordination to tetraalkylammonium ion pairs. The unsymmetrical receptor displayed a discrimination in the binding of either the anion or the lineal component in its two distinct binding sites. We also present the synthesis of a [2]rotaxane and the binding studies with ion-pairs. The receptor was obtained by a stoppering procedure. We used a double CuAAC reaction of the bound axle to attach the bulky stoppers based on terbutyl bisphhenyl units. The ability of the [2]rotaxane to bind tetraalkylammonium ion-pairs in chloroform solution was also explored. The results of NMR, ITC and ESI-MS experiments supported the formation of ion-paired 1:1 complexes. Related binding discrimination processes as detected in the [2]pseudorotaxane precursors assemblies were observed. Finally,

chapter six is focused on the synthesis of a strapped SAE-C4P receptor. Contrary to what we did in the case of the BC4P receptor, the macrocycle was obtained by the acid catalysed condensation reaction of the parent bis-dipyrromethane. In the NMR and ESI-MS experiments performed, we observed the formation of 2:1 complexes with all the studied ammonium salts. Nevertheless, the obtained 2:1 complexes displayed different binding geometries in response to the nature of the alkylammonium cation of the salt.

1.7. References and notes

[1] Marcus, Y.; Hefter, G., Ion Pairing. *Chem. Rev.* **2006,** *106* (11), 4585-4621.
[2] Burton, R. F., Inorganic ion pairs in physiology: Significance and quantitation. *Comparative Biochemistry and Physiology Part A: Physiology* **1983,** *74* (4), 781-785.
[3] Berend, K.; van Hulsteijn, L. H.; Gans, R. O. B., Chloride: The queen of electrolytes? *Eur. J. Intern. Med.* **2012,** *23* (3), 203-211.
[4] Ma, J. C.; Dougherty, D. A., The Cation–π Interaction. *Chem. Rev.* **1997,** *97* (5), 1303-1324.
[5] Pedersen, C. J., Cyclic polyethers and their complexes with metal salts. *J. Am. Chem. Soc.* **1967,** *89* (26), 7017-7036.
[6] Reetz, M. T.; Niemeyer, C. M.; Harms, K., Crown Ethers with a Lewis Acidic Center: A New Class of Heterotopic Host Molecules. *Angew. Chem. Int. Ed.* **1991,** *30* (11), 1472-1474.
[7] Gale, P. A.; Howe, E. N. W.; Wu, X.; Spooner, M. J., Anion receptor chemistry: Highlights from 2016. *Coord. Chem. Rev.* **2018,** *375*, 333-372.
[8] Chen, L.; Berry, S. N.; Wu, X.; Howe, E. N. W.; Gale, P. A., Advances in Anion Receptor Chemistry. *Chem* **2020,** *6* (1), 61-141.
[9] Choi, K.; Hamilton, A. D., Macrocyclic anion receptors based on directed hydrogen bonding interactions. *Coord. Chem. Rev.* **2003,** *240* (1), 101-110.
[10] Gilday, L. C.; Robinson, S. W.; Barendt, T. A.; Langton, M. J.; Mullaney, B. R.; Beer, P. D., Halogen Bonding in Supramolecular Chemistry. *Chem. Rev.* **2015,** *115* (15), 7118-7195.
[11] Cavallo, G.; Metrangolo, P.; Pilati, T.; Resnati, G.; Sansotera, M.; Terraneo, G., Halogen bonding: a general route in anion recognition and coordination. *Chem. Soc. Rev.* **2010,** *39* (10), 3772-3783.
[12] Metrangolo, P.; Meyer, F.; Pilati, T.; Resnati, G.; Terraneo, G., Halogen Bonding in Supramolecular Chemistry. *Angew. Chem. Int. Ed.* **2008,** *47* (33), 6114-6127.
[13] Schottel, B. L.; Chifotides, H. T.; Dunbar, K. R., Anion-π interactions. *Chem. Soc. Rev.* **2008,** *37* (1), 68-83.
[14] Frontera, A.; Gamez, P.; Mascal, M.; Mooibroek, T. J.; Reedijk, J., Putting Anion–π Interactions Into Perspective. *Angew. Chem. Int. Ed.* **2011,** *50* (41), 9564-9583.
[15] Schneider, H.-J., Binding Mechanisms in Supramolecular Complexes. *Angew. Chem. Int. Ed.* **2009,** *48* (22), 3924-3977.
[16] Quintanar-Guerrero, D.; Allémann, E.; Fessi, H.; Doelker, E., Applications of the Ion-Pair Concept to Hydrophilic Substances with Special Emphasis on Peptides. *Pharm. Res.* **1997,** *14* (2), 119-127.
[17] Sessler, J. L.; Gross, D. E.; Cho, W.-S.; Lynch, V. M.; Schmidtchen, F. P.; Bates, G. W.; Light, M. E.; Gale, P. A., Calix[4]pyrrole as a Chloride Anion Receptor: Solvent and Countercation Effects. *J. Am. Chem. Soc.* **2006,** *128* (37), 12281-12288.
[18] Shukla, R.; Kida, T.; Smith, B. D., Effect of Competing Alkali Metal Cations on Neutral Host's Anion Binding Ability. *Org. Lett.* **2000,** *2* (20), 3099-3102.
[19] Hua, Y.; Ramabhadran, R. O.; Uduehi, E. O.; Karty, J. A.; Raghavachari, K.; Flood, A. H., Aromatic and Aliphatic CH Hydrogen Bonds Fight for Chloride while Competing Alongside Ion Pairing within Triazolophanes. *Chem. Eur. J.* **2011,** *17* (1), 312-321.
[20] He, Q.; Vargas-Zúñiga, G. I.; Kim, S. H.; Kim, S. K.; Sessler, J. L., Macrocycles as Ion Pair Receptors. *Chem. Rev.* **2019,** *119* (17), 9753-9835.

[21] McConnell, A. J.; Beer, P. D., Heteroditopic Receptors for Ion-Pair Recognition. *Angew. Chem. Int. Ed.* **2012,** *51* (21), 5052-5061.
[22] Kim, S. K.; Sessler, J. L., Ion pair receptors. *Chem. Soc. Rev.* **2010,** *39* (10), 3784-3809.
[23] Gale, P. A., Anion and ion-pair receptor chemistry: highlights from 2000 and 2001. *Coord. Chem. Rev.* **2003,** *240* (1), 191-221.
[24] Kirkovits, G. J.; Shriver, J. A.; Gale, P. A.; Sessler, J. L., Synthetic Ditopic Receptors. *J. Inclusion Phenom. Macrocyclic Chem.* **2001,** *41* (1), 69-75.
[25] Thordarson, P., Determining association constants from titration experiments in supramolecular chemistry. *Chem. Soc. Rev.* **2011,** *40* (3), 1305-1323.
[26] von Krbek, L. K. S.; Schalley, C. A.; Thordarson, P., Assessing cooperativity in supramolecular systems. *Chem. Soc. Rev.* **2017,** *46* (9), 2622-2637.
[27] Nabeshima, T.; Hanami, T.; Akine, S.; Saiki, T., Control of Ion Binding by Cooperative Ion-Pair Recognition Using a Flexible Heterotopic Receptor. *Chem. Lett.* **2001,** *30* (6), 560-561.
[28] Tepper, R.; Schulze, B.; Bellstedt, P.; Heidler, J.; Görls, H.; Jäger, M.; Schubert, U. S., Halogen-bond-based cooperative ion-pair recognition by a crown-ether-embedded 5-iodo-1,2,3-triazole. *Chem. Commun.* **2017,** *53* (14), 2260-2263.
[29] Li, D.-H.; Smith, B. D., Shape-Selective Recognition of Quaternary Ammonium Chloride Ion Pairs. *J. Org. Chem.* **2019,** *84* (5), 2808-2816.
[30] Delecluse, M.; Colomban, C.; Moraleda, D.; de Riggi, I.; Duprat, F.; Michaud-Chevallier, S.; Dutasta, J.-P.; Robert, V.; Chatelet, B.; Martinez, A., Positive Cooperative Effect in Ion-Pair Recognition by a Tris-urea Hemicryptophane Cage. *Chem. Eur. J.* **2019,** *25* (13), 3337-3342.
[31] Eckelmann, J.; Saggiomo, V.; Sönnichsen, F. D.; Lüning, U., The first supramolecular ion triplet complex. *New J. Chem.* **2010,** *34* (7), 1247-1250.
[32] Moerkerke, S.; Le Gac, S.; Topić, F.; Rissanen, K.; Jabin, I., Selective Extraction and Efficient Binding in a Protic Solvent of Contact Ion Triplets by Using a Thiourea-Based Bis-Calix[6]arene Receptor. *Eur. J. Org. Chem.* **2013,** *2013* (24), 5315-5322.
[33] Baeyer, A., Ueber ein Condensationsproduct von Pyrrol mit Aceton. *Ber. Dtsch. Chem. Ges.* **1886,** *19* (2), 2184-2185.
[34] Gale, P. A.; Sessler, J. L.; Král, V.; Lynch, V., Calix[4]pyrroles: Old Yet New Anion-Binding Agents. *J. Am. Chem. Soc.* **1996,** *118* (21), 5140-5141.
[35] Wu, Y.-D.; Wang, D.-F.; Sessler, J. L., Conformational Features and Anion-Binding Properties of Calix[4]pyrrole: A Theoretical Study. *J. Org. Chem.* **2001,** *66* (11), 3739-3746.
[36] Bhatt, K. D.; Shah, H. D.; Modi, K. M.; Narechania, M. B.; Patel, C., Calix[4]pyrrole virtuous sensor: a selective and sensitive recognition for Pb(II) ions by spectroscopic and computational study. *Supramol. Chem.* **2019,** *31* (4), 268-282.
[37] Kim, S. K.; Sessler, J. L., Calix[4]pyrrole-Based Ion Pair Receptors. *Acc. Chem. Res.* **2014,** *47* (8), 2525-2536.
[38] Rather, I. A.; Wagay, S. A.; Hasnain, M. S.; Ali, R., New dimensions in calix[4]pyrrole: the land of opportunity in supramolecular chemistry. *RSC Adv.* **2019,** *9* (66), 38309-38344.
[39] Kim, D. S.; Sessler, J. L., Calix[4]pyrroles: versatile molecular containers with ion transport, recognition, and molecular switching functions. *Chem. Soc. Rev.* **2015,** *44* (2), 532-546.
[40] Gale, P. A., From Anion Receptors to Transporters. *Acc. Chem. Res.* **2011,** *44* (3), 216-226.
[41] Gale, P. A.; Hursthouse, M. B.; Light, M. E.; Sessler, J. L.; Warriner, C. N.; Zimmerman, R. S., Ferrocene-substituted calix[4]pyrrole: a new electrochemical sensor for anions involving CH···anion hydrogen bonds. *Tetrahedron Lett.* **2001,** *42* (38), 6759-6762.

[42] A. Gale, P.; A. Gale, P.; J. Twyman, L.; I. Handlin, C.; L. Sessler, J., A colourimetric calix[4]pyrrole–4-nitrophenolate based anion sensor†. *Chem. Commun.* **1999,** (18), 1851-1852.
[43] Miyaji, H.; Anzenbacher Jr, P.; L. Sessler, J.; R. Bleasdale, E.; A. Gale, P., Anthracene-linked calix[4]pyrroles: fluorescent chemosensors for anions. *Chem. Commun.* **1999,** (17), 1723-1724.
[44] Bhatt, K. D.; Shah, H. D.; Modi, K. M.; Narechania, M. B.; Patel, C., Calix[4]pyrrole virtuous sensor: a selective and sensitive recognition for Pb(II) ions by spectroscopic and computational study. *Supramol. Chem.* **2019,** *31* (4), 268-282.
[45] Abbas, I.; Shamseddine, H.; Hammud, H. H., Diethyl ether-modified calix[4]pyrrole receptor: thermodynamics of lead cation complexation – lead extraction from water by its polymer. *Complex Metals* **2014,** *1* (1), 57-68.
[46] Bähring, S.; Root, H. D.; Sessler, J. L.; Jeppesen, J. O., Tetrathiafulvalene-calix[4]pyrrole: a versatile synthetic receptor for electron-deficient planar and spherical guests. *Org. Biomol. Chem.* **2019,** *17* (10), 2594-2613.
[47] Nielsen, K. A.; Cho, W.-S.; Lyskawa, J.; Levillain, E.; Lynch, V. M.; Sessler, J. L.; Jeppesen, J. O., Tetrathiafulvalene-Calix[4]pyrroles: Synthesis, Anion Binding, and Electrochemical Properties. *J. Am. Chem. Soc.* **2006,** *128* (7), 2444-2451.
[48] Park, J. S.; Sessler, J. L., Tetrathiafulvalene (TTF)-Annulated Calix[4]pyrroles: Chemically Switchable Systems with Encodable Allosteric Recognition and Logic Gate Functions. *Acc. Chem. Res.* **2018,** *51* (10), 2400-2410.
[49] Chahal, M. K.; Labuta, J.; Březina, V.; Karr, P. A.; Matsushita, Y.; Webre, W. A.; Payne, D. T.; Ariga, K.; D'Souza, F.; Hill, J. P., Knock-on synthesis of tritopic calix[4]pyrrole host for enhanced anion interactions. *Dalton Trans.* **2019,** *48* (41), 15583-15596.
[50] Park, J. S.; Bejger, C.; Larsen, K. R.; Nielsen, K. A.; Jana, A.; Lynch, V. M.; Jeppesen, J. O.; Kim, D.; Sessler, J. L., Synthesis and recognition properties of higher order tetrathiafulvalene (TTF) calix[n]pyrroles (n = 4–6). *Chem. Sci.* **2012,** *3* (9), 2685-2689.
[51] Nielsen, K. A.; Cho, W.-S.; Jeppesen, J. O.; Lynch, V. M.; Becher, J.; Sessler, J. L., Tetra-TTF Calix[4]pyrrole: A Rationally Designed Receptor for Electron-Deficient Neutral Guests. *J. Am. Chem. Soc.* **2004,** *126* (50), 16296-16297.
[52] Park, J. S.; Le Derf, F.; Bejger, C. M.; Lynch, V. M.; Sessler, J. L.; Nielsen, K. A.; Johnsen, C.; Jeppesen, J. O., Positive Homotropic Allosteric Receptors for Neutral Guests: Annulated Tetrathiafulvalene–Calix[4]pyrroles as Colorimetric Chemosensors for Nitroaromatic Explosives. *Chem. Eur. J.* **2010,** *16* (3), 848-854.
[53] Escobar, L.; Ballester, P., Quantification of the hydrophobic effect using water-soluble super aryl-extended calix[4]pyrroles. *Org. Chem. Front.* **2019,** *6* (11), 1738-1748.
[54] Sierra, A. F.; Hernández-Alonso, D.; Romero, M. A.; González-Delgado, J. A.; Pischel, U.; Ballester, P., Optical Supramolecular Sensing of Creatinine. *J. Am. Chem. Soc.* **2020,** *142* (9), 4276-4284.
[55] Peñuelas-Haro, G.; Ballester, P., Efficient hydrogen bonding recognition in water using aryl-extended calix[4]pyrrole receptors. *Chem. Sci.* **2019,** *10* (8), 2413-2423.
[56] Lee, C.-H.; Miyaji, H.; Yoon, D.-W.; Sessler, J. L., Strapped and other topographically nonplanar calixpyrrole analogues. Improved anion receptors. *Chem. Commun.* **2008,** (1), 24-34.
[57] Peng, S.; He, Q.; Vargas-Zúñiga, G. I.; Qin, L.; Hwang, I.; Kim, S. K.; Heo, N. J.; Lee, C.-H.; Dutta, R.; Sessler, J. L., Strapped calix[4]pyrroles: from syntheses to applications. *Chem. Soc. Rev.* **2020,** *49* (3), 865-907.

[58] Wagay, S. A.; Rather, I. A.; Ali, R., Functionalized calix[4]pyrroles: Emerging class of ion-pair receptors in supramolecular chemistry. *Materials Today: Proceedings* **2020**.
[59] He, Q.; Williams, N. J.; Oh, J. H.; Lynch, V. M.; Kim, S. K.; Moyer, B. A.; Sessler, J. L., Selective Solid–Liquid and Liquid–Liquid Extraction of Lithium Chloride Using Strapped Calix[4]pyrroles. *Angew. Chem. Int. Ed.* **2018,** *57* (37), 11924-11928.
[60] Heo, N. J.; Oh, J. H.; Lee, J. T.; He, Q.; Sessler, J. L.; Kim, S. K., Phenanthroline-strapped calix[4]pyrroles: anion receptors displaying affinity reversal as a function of solvent polarity. *Org. Chem. Front.* **2020,** *7* (3), 548-556.
[61] Valderrey, V.; Escudero-Adán, E. C.; Ballester, P., Polyatomic Anion Assistance in the Assembly of [2]Pseudorotaxanes. *J. Am. Chem. Soc.* **2012,** *134* (26), 10733-10736.
[62] Valderrey, V.; Escudero-Adán, E. C.; Ballester, P., Highly Cooperative Binding of Ion-Pair Dimers and Ion Quartets by a Bis(calix[4]pyrrole) Macrotricyclic Receptor. *Angew. Chem. Int. Ed.* **2013,** *52* (27), 6898-6902.
[63] Saha, I.; Lee, J. H.; Hwang, H.; Kim, T. S.; Lee, C.-H., Remarkably selective, non-linear allosteric regulation of anion binding by a tetracationic calix[4]pyrrole homodimer. *Chem. Commun.* **2015,** *51* (26), 5679-5682.
[64] He, Q.; Kelliher, M.; Bähring, S.; Lynch, V. M.; Sessler, J. L., A Bis-calix[4]pyrrole Enzyme Mimic That Constrains Two Oxoanions in Close Proximity. *J. Am. Chem. Soc.* **2017,** *139* (21), 7140-7143.
[65] An Introduction to the Mechanical Bond. In *The Nature of the Mechanical Bond*, pp 1-54.
[66] Gil-Ramírez, G.; Leigh, D. A.; Stephens, A. J., Catenanes: Fifty Years of Molecular Links. *Angew. Chem. Int. Ed.* **2015,** *54* (21), 6110-6150.
[67] Xue, M.; Yang, Y.; Chi, X.; Yan, X.; Huang, F., Development of Pseudorotaxanes and Rotaxanes: From Synthesis to Stimuli-Responsive Motions to Applications. *Chem. Rev.* **2015,** *115* (15), 7398-7501.
[68] Fielden, S. D. P.; Leigh, D. A.; Woltering, S. L., Molecular Knots. *Angew. Chem. Int. Ed.* **2017,** *56* (37), 11166-11194.
[69] Pan, M.; Su, C.-Y., Coordination assembly of Borromean structures. *Cryst. Eng. Comm.* **2014,** *16* (34), 7847-7859.
[70] Lu, Y.; Zhang, H.-N.; Jin, G.-X., Molecular Borromean Rings Based on Half-Sandwich Organometallic Rectangles. *Acc. Chem. Res.* **2018,** *51* (9), 2148-2158.
[71] Leigh, D. A., Genesis of the Nanomachines: The 2016 Nobel Prize in Chemistry. *Angew. Chem. Int. Ed.* **2016,** *55* (47), 14506-14508.
[72] Erbas-Cakmak, S.; Leigh, D. A.; McTernan, C. T.; Nussbaumer, A. L., Artificial Molecular Machines. *Chem. Rev.* **2015,** *115* (18), 10081-10206.
[73] Kassem, S.; van Leeuwen, T.; Lubbe, A. S.; Wilson, M. R.; Feringa, B. L.; Leigh, D. A., Artificial molecular motors. *Chem. Soc. Rev.* **2017,** *46* (9), 2592-2621.
[74] Langton, M. J.; Beer, P. D., Rotaxane and Catenane Host Structures for Sensing Charged Guest Species. *Acc. Chem. Res.* **2014,** *47* (7), 1935-1949.
[75] Mena-Hernando, S.; Pérez, E. M., Mechanically interlocked materials. Rotaxanes and catenanes beyond the small molecule. *Chem. Soc. Rev.* **2019,** *48* (19), 5016-5032.
[76] Hudson, B.; Vinograd, J., Catenated Circular DNA Molecules in HeLa Cell Mitochondria. *Nature* **1967,** *216* (5116), 647-652.
[77] Krasnow, M. A.; Stasiak, A.; Spengler, S. J.; Dean, F.; Koller, T.; Cozzarelli, N. R., Determination of the absolute handedness of knots and catenanes of DNA. *Nature* **1983,** *304* (5926), 559-560.

[78] Kovall, R.; Matthews, B. W., Toroidal Structure of λ-Exonuclease. *Science* **1997,** *277* (5333), 1824-1827.
[79] Antonio, R.; Ugo, C.; Antonino, C.; Giovanni, R., Recent Developments on Rotaxane-Based Shuttles: An Update to 2010. *Curr. Org. Chem.* **2012,** *16* (2), 127-160.
[80] Schröder, Hendrik V.; Schalley, C. A., Electrochemically switchable rotaxanes: recent strides in new directions. *Chem. Sci.* **2019,** *10* (42), 9626-9639.
[81] Evans, N. H., Recent Advances in the Synthesis and Application of Hydrogen Bond Templated Rotaxanes and Catenanes. *Eur. J. Org. Chem.* **2019,** *2019* (21), 3320-3343.
[82] Saura-Sanmartin, A.; Martinez-Cuezva, A.; Pastor, A.; Bautista, D.; Berna, J., Light-driven exchange between extended and contracted lasso-like isomers of a bistable [1]rotaxane. *Org. Biomol. Chem.* **2018,** *16* (38), 6980-6987.
[83] David, A. H. G.; García-Cerezo, P.; Campaña, A. G.; Santoyo-González, F.; Blanco, V., [2]Rotaxane End-Capping Synthesis by Click Michael-Type Addition to the Vinyl Sulfonyl Group. *Chem. Eur. J.* **2019,** *25* (24), 6170-6179.
[84] Ko, J.-L.; Ueng, S.-H.; Chiu, C.-W.; Lai, C.-C.; Liu, Y.-H.; Peng, S.-M.; Chiu, S.-H., Using a Threading-Followed-by-Swelling Approach to Synthesize [2]Rotaxanes. *Chem. Eur. J.* **2010,** *16* (23), 6950-6960.
[85] Hsueh, S.-Y.; Ko, J.-L.; Lai, C.-C.; Liu, Y.-H.; Peng, S.-M.; Chiu, S.-H., A Metal-Free "Threading-Followed-by-Shrinking" Protocol for Rotaxane Synthesis. *Angew. Chem. Int. Ed.* **2011,** *50* (29), 6643-6646.
[86] Lee, J.-J.; White, A. G.; Baumes, J. M.; Smith, B. D., Microwave-assisted slipping synthesis of fluorescent squaraine rotaxane probe for bacterial imaging. *Chem. Commun.* **2010,** *46* (7), 1068-1069.
[87] Echavarren, J.; Gall, M. A. Y.; Haertsch, A.; Leigh, D. A.; Marcos, V.; Tetlow, D. J., Active template rotaxane synthesis through the Ni-catalyzed cross-coupling of alkylzinc reagents with redox-active esters. *Chem. Sci.* **2019,** *10* (30), 7269-7273.
[88] Brown, A.; Mennie, K. M.; Mason, O.; White, N. G.; Beer, P. D., Copper(ii)-directed synthesis of neutral heteroditopic [2]rotaxane ion-pair host systems incorporating hydrogen and halogen bonding anion binding cavities. *Dalton Trans.* **2017,** *46* (39), 13376-13385.
[89] Denis, M.; Qin, L.; Turner, P.; Jolliffe, K. A.; Goldup, S. M., A Fluorescent Ditopic Rotaxane Ion-Pair Host. *Angew. Chem. Int. Ed.* **2018,** *57* (19), 5315-5319.
[90] Romero, J. R.; Aragay, G.; Ballester, P., Ion-pair recognition by a neutral [2]rotaxane based on a bis-calix[4]pyrrole cyclic component. *Chem. Sci.* **2017,** *8* (1), 491-498.
[91] Fenn, J. B., Electrospray Wings for Molecular Elephants (Nobel Lecture). *Angew. Chem. Int. Ed.* **2003,** *42* (33), 3871-3894.
[92] Kebarle, P.; Tang, L., From ions in solution to ions in the gas phase - the mechanism of electrospray mass spectrometry. *Anal. Chem.* **1993,** *65* (22), 972A-986A.
[93] Kebarle, P., A brief overview of the present status of the mechanisms involved in electrospray mass spectrometry. *J. Mass Spectrom.* **2000,** *35* (7), 804-817.
[94] Wortmann, A.; Kistler-Momotova, A.; Zenobi, R.; Heine, M. C.; Wilhelm, O.; Pratsinis, S. E., Shrinking Droplets in Electrospray Ionization and Their Influence on Chemical Equilibria. *J. Am. Soc. Mass Spectrom.* **2007,** *18* (3), 385-393.
[95] Benkestock, K.; Sundqvist, G.; Edlund, P.-O.; Roeraade, J., Influence of droplet size, capillary–cone distance and selected instrumental parameters for the analysis of noncovalent protein–ligand complexes by nano-electrospray ionization mass spectrometry. *J. Mass Spectrom.* **2004,** *39* (9), 1059-1067.

[96] Cera, L.; Schalley, C. A., Supramolecular reactivity in the gas phase: investigating the intrinsic properties of non-covalent complexes. *Chem. Soc. Rev.* **2014,** *43* (6), 1800-1812.
[97] Winkler, H. D. F.; Dzyuba, E. V.; Schalley, C. A., Gas-phase H/D-exchange experiments in supramolecular chemistry. *New J. Chem.* **2011,** *35* (3), 529-541.
[98] Qi, Z.; Heinrich, T.; Moorthy, S.; Schalley, C. A., Gas-phase chemistry of molecular containers. *Chem. Soc. Rev.* **2015,** *44* (2), 515-531.
[99] Kovalenko, E.; Vilaseca, M.; Díaz-Lobo, M.; Masliy, A. N.; Vicent, C.; Fedin, V. P., Supramolecular Adducts of Cucurbit[7]uril and Amino Acids in the Gas Phase. *J. Am. Soc. Mass Spectrom.* **2016,** *27* (2), 265-276.
[100] Hunter, E. P. L.; Lias, S. G., Evaluated Gas Phase Basicities and Proton Affinities of Molecules: An Update. *J. Phys. Chem. Ref. Data* **1998,** *27* (3), 413-656.
[101] Winkler, H. D. F.; Dzyuba, E. V.; Sklorz, J. A. W.; Beyeh, N. K.; Rissanen, K.; Schalley, C. A., Gas-phase H/D-exchange reactions on resorcinarene and pyrogallarene capsules: Proton transport through a one-dimensional Grotthuss mechanism. *Chem. Sci.* **2011,** *2* (4), 615-624.
[102] Lanucara, F.; Holman, S. W.; Gray, C. J.; Eyers, C. E., The power of ion mobility-mass spectrometry for structural characterization and the study of conformational dynamics. *Nature Chem.* **2014,** *6* (4), 281-294.
[103] Kanu, A. B.; Dwivedi, P.; Tam, M.; Matz, L.; Hill Jr., H. H., Ion mobility–mass spectrometry. *J. Mass Spectrom.* **2008,** *43* (1), 1-22.
[104] Kemper, P. R.; Dupuis, N. F.; Bowers, M. T., A new, higher resolution, ion mobility mass spectrometer. *Int. J. Mass Spectrom.* **2009,** *287* (1), 46-57.
[105] Shvartsburg, A. A.; Smith, R. D., Fundamentals of Traveling Wave Ion Mobility Spectrometry. *Anal. Chem.* **2008,** *80* (24), 9689-9699.
[106] Guevremont, R., High-field asymmetric waveform ion mobility spectrometry: A new tool for mass spectrometry. *J. Chromatogr. A* **2004,** *1058* (1), 3-19.
[107] Wollschläger, J. M.; Schalley, C. A., Ion Mobility Mass Spectrometric Investigation on the Photoisomerization of a 4,4'-Diamidoazobenzene Model. *ChemPhotoChem* **2019,** *3* (6), 473-479.
[108] Ben-Nissan, G.; Sharon, M., The application of ion-mobility mass spectrometry for structure/function investigation of protein complexes. *Curr. Opin. Chem. Biol.* **2018,** *42*, 25-33.
[109] Christie, L. G.; Surman, A. J.; Scullion, R. A.; Xu, F.; Long, D.-L.; Cronin, L., Overcoming the Crystallization Bottleneck: A Family of Gigantic Inorganic {Pdx}L (x=84, 72) Palladium Macrocycles Discovered using Solution Techniques. *Angew. Chem. Int. Ed.* **2016,** *55* (41), 12741-12745.

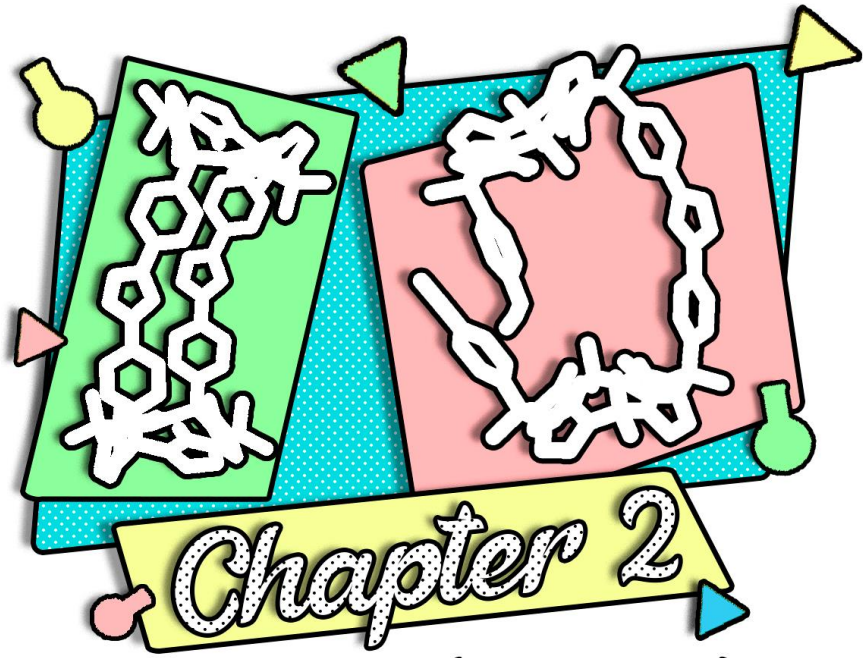

Design and synthesis of a bis(calix[4]pyrrole) receptor

Unpublished results

UNIVERSITAT ROVIRA I VIRGILI
Calix[4]pyrrole Based Receptors for the Recognition of Ion Pairs
Ricardo Molina Muriel

2.1 Introduction

Historically, synthetic supramolecular receptors such as macrocycles and molecular interlocked molecules (MIMs) were obtained through low-yield statistical approaches. Statistical approaches were based on the random mechanical collision of the reacting molecules in solution, e.g. the two terminal groups of a lineal molecule reacting to generate a macrocyclic supramolecule.[1,2] The outcome of these reactions was highly dependent on the concentration, high dilution conditions favoring the formation of the macrocycle over the oligomeric products. The obtained low yields prompted for the development of new synthetic methodologies.[3] Nowadays, the majority of the synthetic procedures towards supramolecular receptors are based on the use of a template.[4,5]

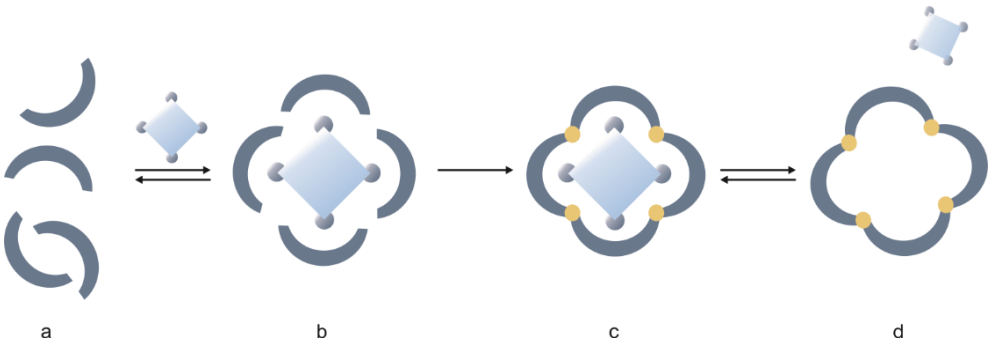

Figure 2.1. Schematic representation of the templated synthesis of supramolecular receptors. a) Precursor of the receptor, b) supramolecular complex established with the template, c) formation of covalent bonds to generate the receptor and d) release of the template.

A template molecule serves as a mold to generate supramolecular architectures.[6] The precursors of a macrocyclic receptor are brought in close proximity and with the correct spatial orientation by interacting with the template (**Figure 2.1a**).[7,8] The interactions stablished are generally weak and reversible such as ion-dipole,[9] hydrogen bonding[10] and π-π interactions,[11] although covalent interactions may also be used.[12] The complementarity in size and shape of the template with the reacting partners and the product dictates the outcome of the reaction (**Figure 2.1b**). The formation of a supramolecular entity between precursors and template increases the local concentration of the reacting groups of the precursors, ultimately favoring the covalent linking reaction that yields the supramolecular receptor (**Figure 2.1c**). Afterwards, the template is released into the bulk solution by the addition of a competitive guest or can remain trapped within the receptors cavity (**Figure 2.1d**). Although the templated synthesis of supramolecular receptors has been extensively

used along the recent decades, it is worth mentioning the work performed by the group of Anderson in this area.[13] In one of his most recent manuscript, porphyrin based nanorings were obtained using the unprecedented cooperative binding of two stacked six-legged templating agents.[14]

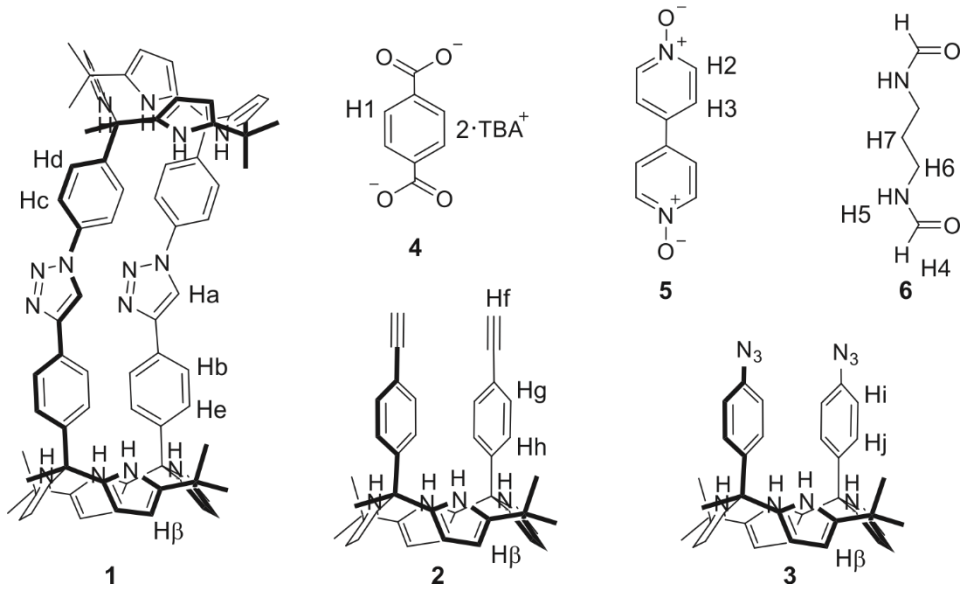

Figure 2.2. Line-drawing structures of BC4P macrocycle **1**, C4P receptors **2** and **3** and guests terephthalate (TPH) **4**, 4,4-bipyridine-*N*,*N*-dioxide (BPNOx) **5** and N,N'-(propane-1,3-diyl)diformamide (DFA) **6**.

In this chapter, we aimed at synthetizing a bis(calix[4]pyrrole) (BC4P) oligocyclic macrocycle bearing triazole rings as linkers, receptor **1** (**Figure 2.2**). Up to date, four examples of BC4P macrocycles covalently connected by two arms can be found in literature.[15,16,17,18,19] BC4P architectures can be synthetized following two methodologies: a macrocyclization reaction involving two C4P units or an acid-catalyzed condensation of two bis-dipyrromethane units.[20,21] We explored the first strategy, based on the previous experience of the group in the synthesis of BC4P receptors. We surmised that for the synthesis of receptor **1**, the use of a suitable template would be mandatory to minimize the formation of oligomeric products. We investigated by means of ^{1}H NMR spectroscopy and HPLC analysis the effects exerted by different templates in the synthesis of receptor **1**. We evaluated the properties of the used templates for the quantitative assembly of 1:2 complexes with the C4P reacting units at mM concentrations. Our expectations were that template effect will become even more relevant once the first intermolecular

reaction between the C4P units has occurred. Finally, we also studied the formation of 1:1 complexes between the synthesized receptor **1** and a series of ditopic guests, some of them already used as templates.

2.2. Results and discussion

2.2.1. Design and synthesis

The synthesis of BC4P receptor **1** was envisioned through the Copper(I)-catalyzed alkyne-azide cycloaddtion (CuAAC) coupling reaction of C4P units **2** and **3**. The synthesis of precursors **2** and **3** was previously described by our group elsewhere.[16,22] The choice of a CuAAC reaction between an alkyne substituted C4P and its terminal azide analogue was not trivial. The CuAAC reaction has emerged as a robust "click chemistry" procedure for the synthesis of supramolecular receptors.[23] This is due to the mild conditions employed, the wide variety of functional groups that tolerates and the high obtained yields.[24,25]

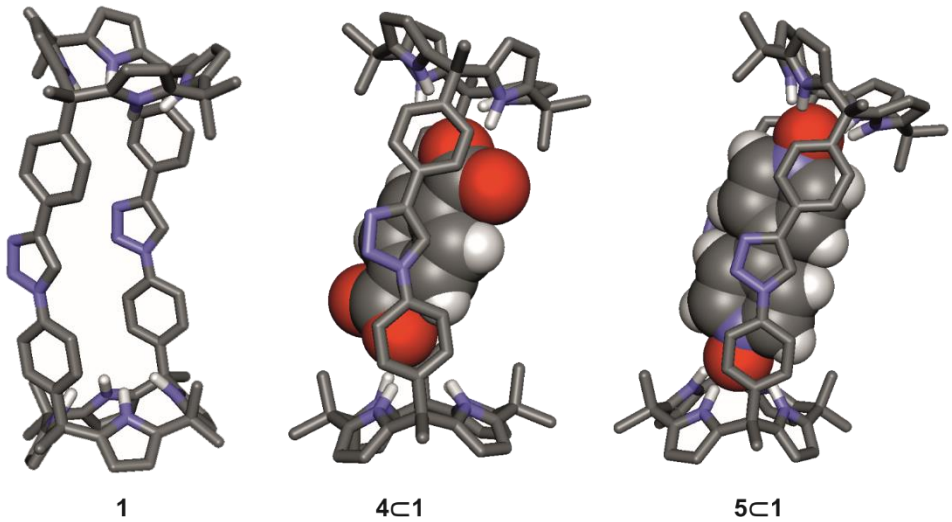

Figure 2.3. Energy-minimized structures (MM3) of macrocyclic receptor **1** (left), complex **4⊂1** (middle) and complex **5⊂1** (right).[26]

The template molecule used for the coupling reaction had to fulfill a series of geometric and electronic properties in order to favor the macrocyclization product. The nature of the required inter- and intramolecular reactions leading to the macrocycle demanded the use of a ditopic guest able to interact concomitantly with both C4P cores. The templating agent was required to bear electronic rich groups,

that is hydrogen bond acceptor groups, capable of engaging in non-covalent interactions with the pyrrole NHs in the C4P core of **2** and **3**. In this regard, C4P receptors are well known for their ability to bind oxygen atoms of carbonyl groups (e.g. acid, ester or amide functionalization) and of *N*-oxides derivatives. [27,28,29] In addition, the shape and size of the template had to be taken into account. As a rule of thumb, we surmised that the ditopic template had to be able to fit inside the polar cavity of receptor **1**. A distance of 11.3 Å (N-H···H-N) between C4P units was measured in the energy-minimized structure of receptor **1** (**Figure 2.3**). This distance set the maximum length of the putative template molecule. A shorter template would position the reacting groups of C4P **2** and **3** in an unfavorable arrangement to achieve an optimum transition state geometry for both the initial intermolecular and the subsequent and more important intramolecular macrocyclization reaction.

Taking into account all the previous requirements, we selected the bis-carboxylate salt of terephthalic acid **4** (TPH) and 4,4-bipyridine-*N*,*N*-dioxide **5** (BPNOx) as possible templates. The measured O···O atom distances of 9.904 Å and 10.004 Å in the energy minimized structure of compounds **4** and **5**, respectively, fulfilled the size requirements of receptor **1** (**Figure 2.3**). Indeed, the energy-minimized structures for the inclusion complexes **4**⊂**1** and **5**⊂**1** advocated for an ideal match in size and shape. Prior to undertake the synthetic attempts for the preparation of the BC4P receptor **1**, we performed ^{1}H NMR titration experiments in order to study the formation of 2:1 assemblies between both C4P units and the selected templates, **4** and **5**, at millimolar concentrations. We surmised that the formation of receptor **1** would be preceded by the assembly in solution of an initial 2:1 complex and more importantly the subsequent 1:1 complex deriving from the first intermolecular coupling. Once the 2:1 heterocomplexes comprising **4** and **5** are assembled, the azide and alkyne moieties are close in space to favor its coupling. Following the initial intermolecular reaction, the bound template also places the two additional unreacted groups of the 1:1 complex in the right orientation to favor the second intramolecular reaction. This will favor to the formation of BC4P **1** to the expenses of polymeric aggregates deriving from competing intermolecular reactions of the 1:1 complexes. We selected acetonitrile as the solvent for the ^{1}H NMR titration experiments, as well as for the coupling reaction, in order to favor the cone conformation of the C4P over the alternate and partial cone counterparts, which in turns favor the coordination of the template molecule.

We started our ^{1}H NMR spectroscopy studies of the formation of the hetero-dimeric 2:1 assemblies using template **4**, the bis-tetrabutylammonium (TBA) salt of therephthalic acid. In acetonitrile solution and at mM concentration, we expected that the ion pairing equilibria of the carboxylate salt would be significantly shifted towards the dissociated form.[30] Acetonitrile is a polar solvent and the TBA^+ cation can be nicely solvated by several acetonitrile molecules thus reducing the Coulombic interaction between the charged particles. The energy minimized structure of the 2:1 complex formed by two molecules of C4P and **4**, shows that the TPH dianion is slightly tilted with respect to the C4P units (**Figure 2.4**). In the structures used for the molecular modelling of the complex, the negative charge of the carboxylate groups is mainly located in one of the oxygen atoms. This limitation results from the use of force field calculations (MM3) in our modelling studies. We assigned a negative charge to deprotonated oxygen atom of the carboxylate anion. This led to a more favorable coordination of the negatively charged oxygen with the C4P NH core. However, in reality the negative charge of the carboxylate group should be equally delocalized between the two oxygen atoms (resonance from of the carboxylate). The charge resonance reduces the charge density available on a single oxygen atom. This effect could be detrimental for the binding affinity of the templating agent. It is expected that the hydrogen-bonding accepting capabilities of

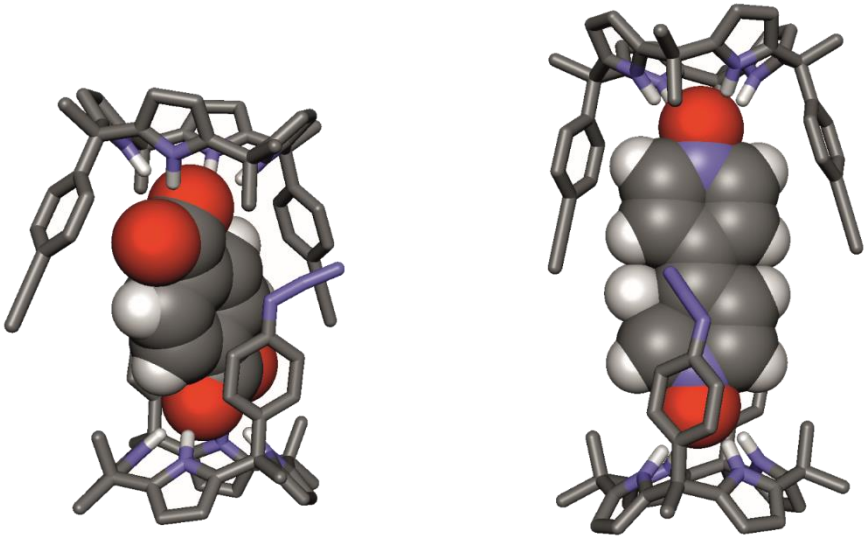

Figure 2.4. Energy-minimized structures (MM3) of heterocomplex **4**⊂**2·3** (left) and **5**⊂**2·3** (right).[31]

functional groups or ions increase with an increase in charge density. For a mono-charged residues, this means that the smaller the residue the larger its charge density.

The ^{1}H NMR spectrum of terminal alkyne C4P **2** in acetonitrile-d_3 solution shows sharp and well-defined proton signals (**Figure 2.5**). The β-pyrrolic protons, Hβ, resonate as two sharp triplets centered at 5.6 and 5.9 ppm. The aromatic protons Hg and Hh, and the terminal alkyne proton Hf appear at 7.4, 6.9 and 3.4 ppm, respectively. In addition, the NH protons resonate as a broad signal at 7.8 ppm. The addition of 0.25 equivalent of a solution of template **4** produced dramatic changes in the ^{1}H NMR spectrum of the free receptor. Many signals experienced broadening, as observed for Hβ and Hf. This broadening was even more pronounced in the case of proton Hh, which broadened beyond detection. The observed broadening is attributed to the dynamic exchange process of receptor **2** between free and bound states being intermediate on the ^{1}H NMR chemical shift timescale. The coordination of **4** with **2** is also supported by the appearance of a new signal at 11.6 ppm. This signal is assigned to the NH protons of bound C4P **2**. The bound C4P NHs are involved in hydrogen bonding interactions with the carboxylate groups of template **4**. The methylene protons *alpha* to the nitrogen in the TBA^+ cation appeared at 3.1 ppm. Along the course of the titration, this signal increased in intensity but did not experience significant chemical shift changes. The unaltered chemical shift of TBA^+ indicates that the cation is not extensively involved in the binding process. The addition of up to 0.5 equivalent of the template **4** produced the sharpening of all the proton signals of the C4P **2** receptor. At this point, the NH proton signal attributed to the bound C4P **2** was exclusively observed. We also observed a singlet at 7.0 ppm that was assigned to the aromatic protons H1 of the TPH **4**. This signal was already observed in the presence of 0.25 equivalent of **4** but it was slightly more sharper. At the equimolar ratio of **2** and **4**, the aromatic proton H1 split in two separate broad singlets. The proton signals of the bound receptor displayed reduced changes when the concentration of **4** was increased from 0.5 equivalent to 1.0 equivalent.

Taken together, the obtained results indicated the quantitative formation of complex **4**⊂(**2**)$_2$ in the presence of 0.5 equivalent of **4**. The initial addition of 0.25 equivalent of **4** produced a dynamic chemical exchange between the free C4P **2** and the bound counterpart in the **4**⊂(**2**)$_2$ complex, that showed slow exchange dynamics for some of the protons i.e. NH and fast (Hg) or intermediate (Hh and Hβ) for others.

In the complex **4**⊂(**2**)$_2$, the TPH dicarboxylate **4** coordinates one C4P **2** receptor in each one of its carboxylate groups. The interaction between the carboxylates and the C4Ps is based on four simultaneous hydrogen bonding interactions. The results in solution are not conclusive with respect to the mono- or ditopic interaction of the carboxylate and the C4P core. In any case, these hydrogen bonding interactions are supported by the dramatic chemical shift change experienced by the NH protons of bound **2**. The bound NHs moved downfield approximately $\Delta\delta$ = 3.8 ppm, after the addition of 0.5 equivalent of **4**. Because the assembly of **4**⊂(**2**)$_2$ is quantitative under stoichiometric conditions at mM concentration, we were not able to derive conclusions in relation to the existence of possible cooperative allosteric effects during its formation.

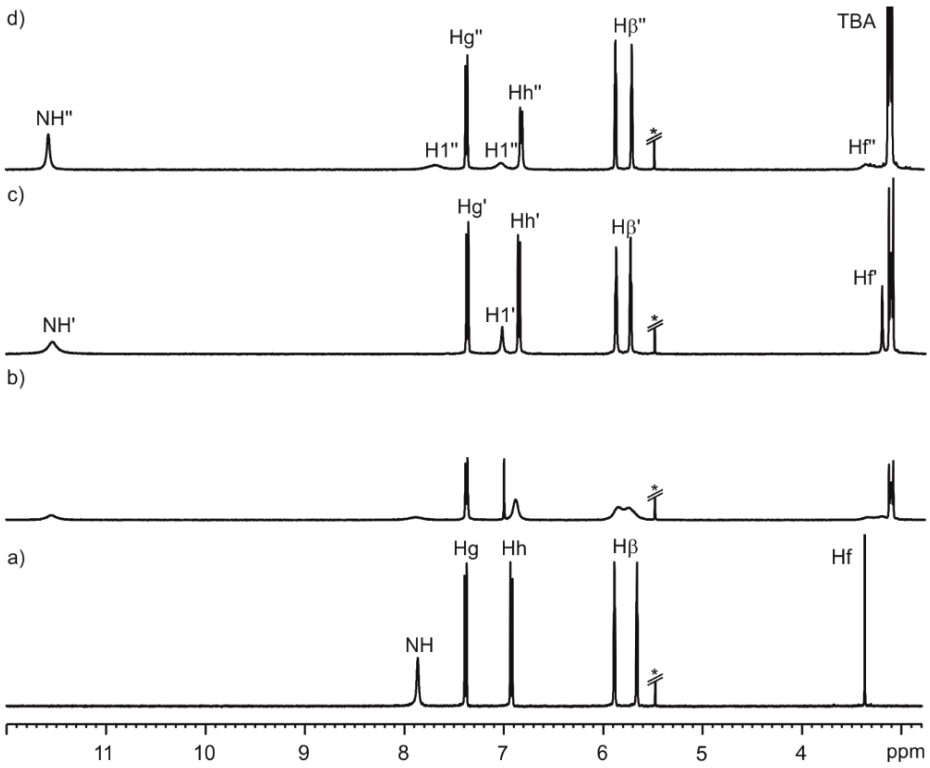

Figure 2.5. Selected region of the ^{1}H NMR spectra (400 MHz, 298 K, CD_3CN) acquired during the titration experiment of receptor **2** (a) with incremental additions of TPH **4**: 0.25 equivalent (b), 0.5 equivalent (c), and 1 equivalent (d). Primed letter correspond to complex **4**⊂(**2**)$_2$; doubled primed letters correspond to complex **4**⊂**2**. See Figure 2.2 for proton assignments. *Residual solvent signal.

Upon the addition of 1 equivalent of **4**, the proton signal H1 for the bound dicarboxylate resonated as two separate singlets. We rationalized this observation

by assuming that in the presence of 1 equivalent of **4** the homo-dimeric **4**⊂(**2**)$_2$ complex is fully disassembled and the corresponding 1:1 complex **4**⊂**2** is the exclusive species formed in solution. This result hints to the existence of a negative allosteric effect in the assembly of the homodimer **4**⊂(**2**)$_2$.

The symmetry and dynamics of the homodimeric complex **4**⊂(**2**)$_2$ produced the observation of the aromatic proton H1 of bound **4** as a singlet. In contrast, the aromatic protons of bound **4** in the 1:1 complex are not chemically equivalent and resonate as two separate signals. The set of two protons *alpha* to the bound carboxylate group are buried in the aromatic cleft defined by complexed receptor **2** in cone conformation. There they experience the magnetic anisotropy produced by the *meso*-phenyl substituents and shift upfield. The other two aromatic protons of bound **4** are almost fully exposed to the bulk solution.

Identical results were obtained in the ^{1}H NMR titration experiments performed with the azide C4P analogue **3**. The NH proton signal of the homo-dimeric assembly **4**⊂(**3**)$_2$ resonated at 11.6 ppm after the addition of 0.5 equivalent of template **4**. The disassembly of the homodimer produced the 1:1 complex **4**⊂**3**. This fact was evidenced by the splitting of the proton signal H1 of bound **4** in the equimolar mixture of the two components, **4** and **3** (see Experimental Section).

Once the quantitative assembly of the homodimers **4**⊂(**2**)$_2$ and **4**⊂(**3**)$_2$ was confirmed to take place at mM concentration and working under stoichiometric control, we investigated the putative assembly of the hetero-dimeric counterpart **4**⊂**2·3**. We prepared two solutions in acetonitrile-d_3 containing the two homodimeric assemblies. To this end, we used 1:0.5 mixtures of C4Ps **2** and **3** with respect to the TPH salt **4**. The quantitative assembly of the homodimers was confirmed by ^{1}H NMR spectroscopy. Next, the two solutions were mixed to obtain a mixture of the three components, **2**, **3** and **4**, in a 1:1:1 ratio. The ^{1}H NMR spectrum of the resulting mixture showed some protons as broad and ill-defined signals. This result was indicative of the existence of a dynamic equilibrium between the different assemblies in solution. The dynamics of the exchange processes were either fast or intermediate on the ^{1}H NMR chemical shift timescale (**Figure 2.6**). The solution mixture was cooled down to 238 K. This produced the sharpening of all the signals in the registered ^{1}H NMR spectrum. Most likely, at this temperature most exchange dynamics became slow on the chemical shift time scale. In order to assess the extent of the formation of the heterodimeric assembly, we recorded a ^{1}H NMR spectra of homodimers **4**⊂(**3**)$_2$ and **4**⊂(**2**)$_2$ also at 238 K. By comparison of the three

spectra, we were able to assign the proton signals corresponding to the heterodimer **4**⊂**2·3**. As could be expected, proton H1 of bound **4** in the heterodimer **4**⊂**2·3** resonated as two separate sharp singlets at 7.0 and 6.9 ppm. This is indicative of the different magnetic environments provided by the two C4P components in the heterodimer complex **4**⊂**2·3**. The integral values of selected proton signals assigned to the three different complexes (Hf, H1 and NH) allowed the calculation of the species distribution as 0.6 : 0.2 : 0.2 for **4**⊂**3·2**, **4**⊂(**2**)$_2$ and **4**⊂(**3**)$_2$. This result is in agreement with an almost statistical distribution of almost isoenergetic assemblies. These results confirmed the formation of heterodimer **4**⊂**3·2** in a significant extent and augur well for the use of the TBA salt of **4** as template for the synthesis of receptor **1**.

Next, we investigated the formation of the heterodimeric assembly assisted by template **5**, 4,4-bipyridine-*N*,*N*-dioxide (**Figure 2.4**). Molecular modelling studies of the heterodimer **5**⊂**3·2** revealed that in the ternary complex the two C4P units were located relatively close in space. This arrangement of the C4Ps could be beneficial for the use of **5** as template in the synthesis of the macrocyclic receptor **1**.

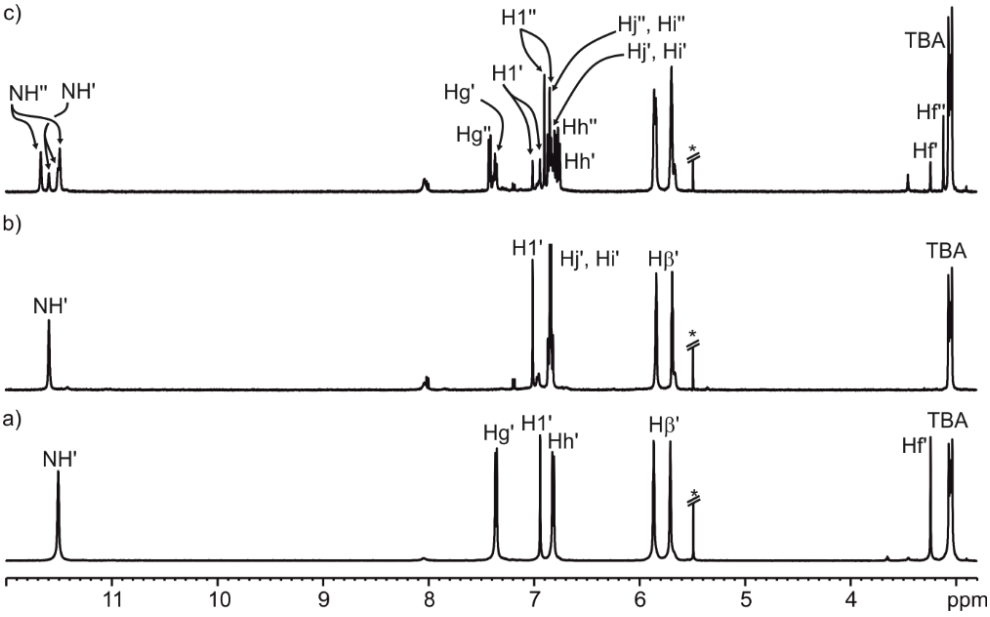

Figure 2.6. Selected region of the ^{1}H NMR spectra (400 MHz, 238 K, CD_3CN) of the homodimeric assemblies **4**⊂(**2**)$_2$ (a), **4**⊂(**3**)$_2$ (b) and the mixture of the two homodimers (primed signals) that produces the emergence of the heterodimer assembly **4**⊂**2·3** (doubled primed signals) (c). See Figure 2.2 for proton assignments. *Residual solvent signal.

However, we obtained striking different results in the ^{1}H NMR spectroscopy studies of the assembly of the heterodimer **5**⊂**3·2** compared to those described above for the **4**⊂**3·2** counterpart. The addition of template **5** to separate solutions of receptors **2** and **3** produced minor changes in the ^{1}H NMR spectra of the free receptors (see Experimental Section). In particular, the proton signals assigned to the aromatic walls of **2** and **3** did not show significant chemical shifts changes when titrated with template **5**. A reduced binding of template **5** was inferred from the slight downfield shift ($\Delta\delta$ = 0.7 ppm) detected for the proton signals of the pyrrole NHs along the course of the titration. The proton signals corresponding to the beta pyrrolic protons Hβ also experienced minor chemical shift changes due to complexation. A similar behavior was observed for the aromatic proton signals of template **5** (H2 and H3). The observed changes in proton chemical shifts did not reach saturation even in the presence of a large excess of **5**.

Taken together, these results suggest the formation of complexes **5**⊂**2** and **5**⊂**3** to a reduce extent in the titration conditions. Moreover, the complexes experience a fast exchange regime on the ^{1}H NMR chemical shift timescale with their free components. Likewise, we did not obtain evidence supporting the formation of homodimeric complexes **5**⊂(**2**)$_2$ and **5**⊂(**3**)$_2$. The low binding affinity determined for **5** towards C4Ps **2** and **3** is responsible for the assembly of the 2:1 homodimer to a very reduced extent in the used conditions (1 mM concentration of the C4Ps and 0.5 equivalent of **5** added). As observed for **4**, the incremental addition of **5** favors the formation of the 1:1 complexes.

Prompted by the promising results obtained in the experiments carried out with the TPH salt, we performed the CuAAC reaction of C4Ps **2** and **3** in the presence of an of **4**. We suspended in dry and degassed acetonitrile an equimolar amount of the two C4Ps, **2** and **3**, and 0.5 equivalent of the TPH salt **4**. Next, we added 1.5 equivalent of CuI as catalyst and ten drops of freshly distilled triethylamine. The resulting orange solution was left stirring at room temperature for four hours. Macrocycle **1** was isolated as a pale yellow solid in a remarkable 30 % yield after purification of the crude by column chromatography (silica) using a 4% mixture of EtOAc in $CHCl_3$ as eluent.

Receptor **1** was fully characterized by a complete set of high-resolution spectra (1D and 2D NMR experiments as well as ESI-HRMS). The ^{1}H NMR spectrum of the BCP macrocycle **1** in $CDCl_3$ solution showed sharp and well-defined proton signals (**Figure 2.7a**). Receptor **1** possesses two 2W-C4P units that are chemically non-equivalent

owing to the 1,4-substituted triazole used as spacer. Thus, we observed two separate signals for the pyrrole NHs of each unit. The NHs resonated at δ = 6.97 and 6.91 ppm. The aromatic protons Hb–e appeared as four signals, similarly to the β-pyrrole protons Hβ . The triazole proton Ha appeared as a singlet at δ = 8.7 ppm.

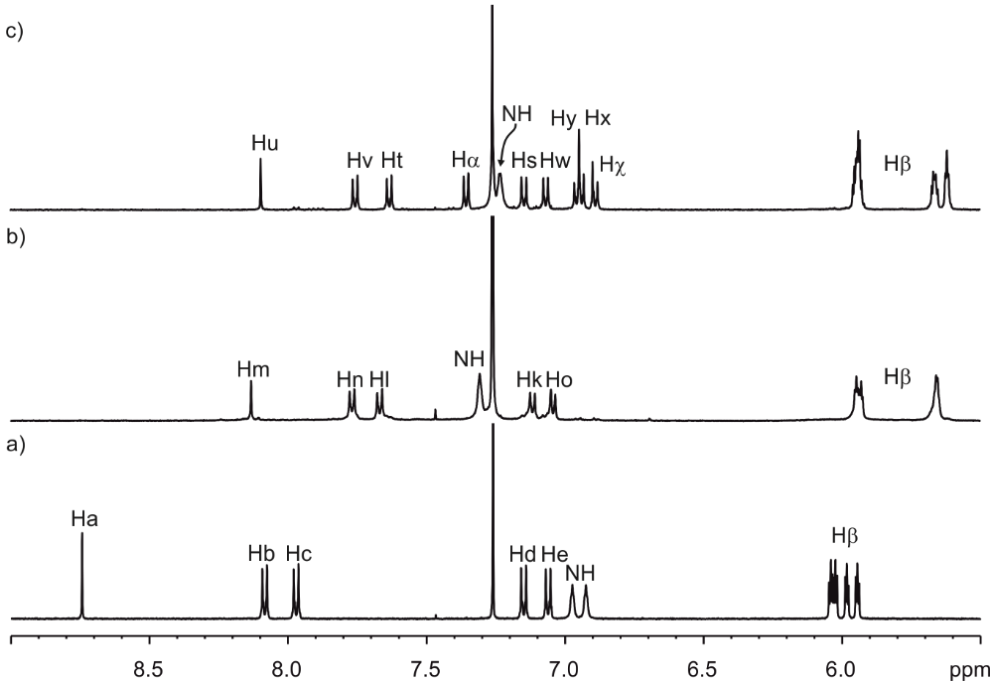

Figure 2.7. Selected region of the ^{1}H NMR spectra (400 MHz, 298 K, CD_3Cl) of receptor **1** a), tetramer **7** b) and open dimer **8** c). See Figure 2.2 and 2.9 for proton assignments.

Once the macrocyclic receptor **1** was isolated, we evaluated the effect that the different templates had in the outcome of the reaction producing the compound. For this reason, we performed several CuAAC reactions between **2** and **3** in the presence of TPH salt **4**, BPNOx **5** and without the use of any template.

2.2.2. Detailed analyses of the template effect on the synthesis of **1**

All macrocyclization reactions were performed following the conditions described above for the synthesis of **1** with TPH as template (*vide supra*). The real-time monitoring of all reactions involved the analysis by HPLC of different aliquots. Aliquots were withdrawn before and immediately after the addition of the copper catalyst. Two more aliquots were taken after two and four hours of reaction.

Macrocyclization reaction templated by TPH dianion **4**

The HPLC trace of the first aliquot analyzed before the addition of the catalyst showed two major peaks with retention times of 3.4 and 3.3 min. These peaks corresponded to C4P units **2** and **3**, respectively (see Experimental Section). The HPLC trace of the aliquot taken immediately after the addition of the catalyst, displayed a new major peak with a retention time of 4.0 min. Interestingly, the new peak was not present in the HPLC trace of the aliquot corresponding to two hours of reaction. After four hours, the reaction was quenched and worked-up because the HPLC traces of the aliquots taken at 2 and 4 hours were identical and indicative of reaction completion. The HPLC trace of the reaction crude displayed the presence of four major peaks with retention times of 4.8, 5.9, 10.7 and 13.5 min (**Figure 2.8**). We identified the peak eluting at 5.9 min as receptor **1**. We isolated fractions of the other three peaks by means of semi-preparative HPLC purification. The ^{1}H NMR analyses of the isolated fractions suggested that the compounds eluting with retention times of 4.8 and 10.7 min were oligomeric species, which we did not characterize.

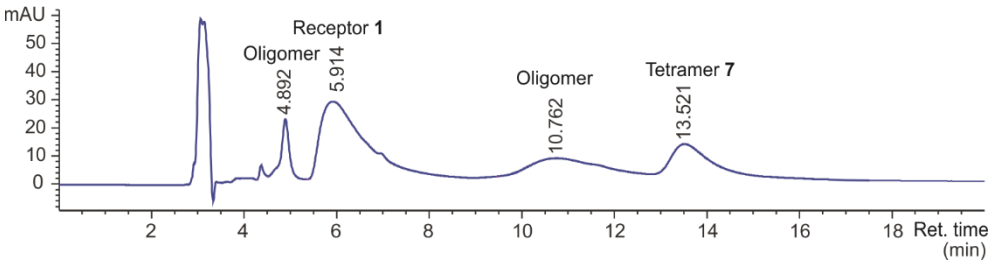

Figure 2.8. HPLC trace of the analysis of the crude obtained in the CuAAC reaction between C4P **2** and **3** in the presence of one equivalent of TPH **4**.

The ^{1}H NMR spectrum of the fraction eluting at 13.5 min was similar to that of receptor **1** (**Figure 2.7b**). We observed four doublets resonating between 7.8 and 7.0 ppm and one sharp singlet at 8.1 ppm. This observation suggested us that this fraction contained a pure product displaying C_{2v} symmetry. Macrocycle **1** also shows a ^{1}H NMR spectrum in agreement with C_{2v} symmetry. For this reason, we hypothesize that the isolated product was a larger macrocyclic compound containing the same units, which is C4Ps **2** and **3** covalently connected by triazole spacers. The exact mass of the compound coincided with that of the tetramer receptor **7** (**Figure 2.9**). It is worth mentioning that structurally related macrocycles have been previously obtained in our group. [32] The dimerization reaction between

two mono-reacted C4Ps **2** and **3**, compound **8**, would explain the formation of **7**. This finding suggested that the TPH template is not ideal to favor the intramolecular reaction in the supramolecular complex TPH⊂**8**. The ^{1}H DOSY experiment in $CDCl_3$ solution assigned a diffusion constant of D = 3.60± 0.06 x 10^{-10} m^2 s^{-1} to the tetramer **7**. This value corresponds to a diffusing spherical object having a hydrodynamic radius of 11.5 Å. The analogous calculated hydrodynamic radius for **1** was 9.14 Å

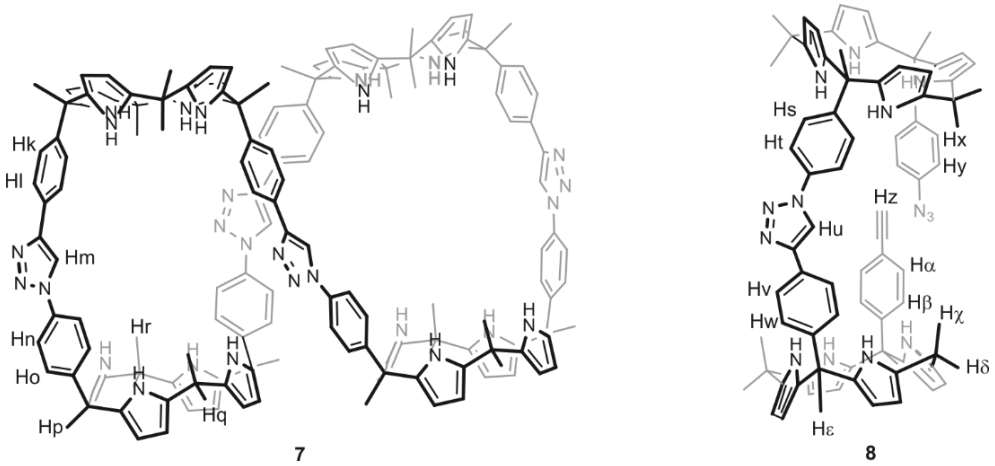

Figure 2.9. Line-drawing structures of tetramer **7** and dimeric product **8**.

(D = 4.52± 0.06 x 10^{-10} m^2 s^{-1}). Macrocycle **7** was fully characterized by a set of high resolution spectra (see Experimental Section).

Macrocyclization reaction templated by BPNOx **5**

The CuAAC coupling reaction of C4P units **2** and **3** in the presence of an equimolar amount of BPNOx **5** produced significant different results. The addition of BPNOx **5** to the reaction vessel produced the appearance of a yellow solid that remained in suspension throughout the course of the reaction. The HPLC trace of the aliquot taken after addition of the catalyst showed peaks of low intensity that were attributed to oligomeric species. The peak corresponding to **1** also displayed low intensity (see Experimental Section). The analysis of the aliquot taken after four hours revealed complete consumption of the starting materials and that **1** and **7** were present in minimal amounts. These results suggested the formation of insoluble polymeric compounds as the major products of the reaction using **5** as template. We hypothesize that BPNOx **5**, if any, imposes a negative template effect towards formation of receptor **1.**

Macrocyclization reaction in the absence of template

We surmised that carrying out the CuAAC reaction without the use of a template would mainly produce the formation of a mixture of oligomeric aggregates. Thus, the reaction mixture should be similar to that obtained with BNOx **5** if the *N*-oxide lacks of any templating effect. From the results obtained using TPH and **5** as templates, we concluded that the assembly of 1:1 complex between the mono-reacted product **8** and the used template was mandatory in order to obtain **1** as the major reaction product. Interestingly, the HPLC trace of the first aliquot taken after the addition of the catalyst for the non-templated reaction revealed a broad peak with a retention time of 4.1 min (see Experimental Section). It is important to note here that a similar peak was initially detected in the first HPLC trace of the reaction

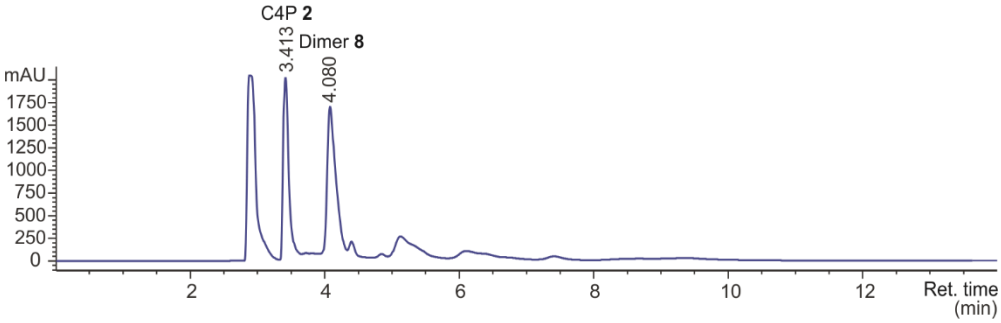

Figure 2.10. HPLC trace of the analysis of the crude obtained in the CuAAC reaction between C4P **2** and **3** in the absence of any template.

using TPH **4** as template. However, in the non-templated reaction conditions the peak at 4.1 min remained present throughout the course of the reaction (4 h). This peak corresponded to the major peak present in the HPLC trace of the reaction crude (**Figure 2.10**). Gratifyingly, using semipreparative HPLC purification, we were able to isolate the compound corresponding to the major peak. The ^{1}H NMR spectrum in $CDCl_3$ solution of the isolated solid corresponded to a pure compound (**Figure 2.7c**). The spectrum showed two sharp singlets resonating at 8.10 ppm and 3.05 ppm. Both signals had similar integral values and we assigned them to one proton in a triazole ring and one proton of a terminal alkyne. In addition, eight sharp doublets appeared between 7.8 and 6.8 ppm. We assigned these signals to the aromatic protons of the *meso*-phenyl substituents of the C4P units. The number of protons signals is in agreement with a reduced symmetry for the isolated compound and suggests a non-cyclic structure. Taken together, all the above observations are indicative of the formation of the non-cyclized dimer **8** (**Figure 2.9**). This compound is formed by the single intermolecular CuAAC reaction of C4P units **4** and **5.** The

structure of **8** was fully characterized by a set of high resolution spectra. A ^{1}H DOSY experiment performed in $CDCl_3$ solution assigned a diffusion constant of D = 4.55 ± 0.07 x 10^{-10} m^2 s^{-1} to **8**. This value is in good agreement with the one determined for **1** and supports the similar size of both species in solution (see Experimental Section).

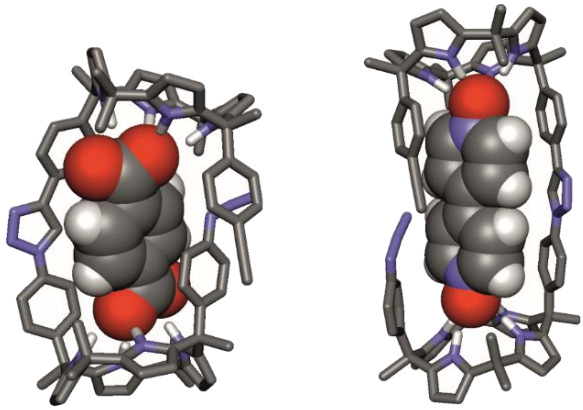

Figure 2.11. Energy-minimized structures (MM3) of complexes **4⊂8** (left) and complex **5⊂8** (right).

The isolation of the heterodimer **8** in the coupling reaction carried out without template indicated that: 1) the formation of a ternary 2:1 complex with a template was not mandatory to favor the first intermolecular "click" reaction and 2) a template was necessary to promote the intramolecular "click" reaction between the reacting groups of **8**. Thus, we propose that the reaction mechanism leading to the formation of the macrocycle **1** is based on a first CuAAC intermolecular reaction between C4P units **2** and **3**. This reaction occurs through random collision between the azide and alkyne units independently of the presence of a template. In the absence of template, the non-cyclic dimer **8** is stable in solution and is the major isolated product. Most likely, a second intramolecular "click" reaction is not favored for **8** owing to its conformational properties. As the reaction time is increased, competitive intermolecular "click" reactions between **8** dimers led to the formation of polymeric by-products (see Experimental Section). The addition of a suitable template dramatically changes the outcome of the reaction. The presence of TPH **4** in solution induces the formation of the 1:1 complex **4⊂8**. In this complex, the alkyne and azide reacting groups of the C4P units are adequately oriented, as suggested by the energy-minimized structure (**Figure 2.11**), to favor an intramolecular CuAAC coupling reaction between them. This reaction produces **1** as

the major reaction product. This intramolecular reaction competes with the intermolecular CuAAC coupling between two **4**⊂**8** complexes. The subsequent intramolecular reaction of the open tetramer would explain the formation of tetramer **7**. On the other hand, the presence of BPNOx **5** either disfavors the formation of **8** or induces its rapid oligomerization. The energy-minimized structure of the **5**⊂**8** complex, due to the length of the lineal template, displays the reacting terminal alkyne and azide in an orientation that is not adequate for their intramolecular reaction (**Figure 2.12**). Moreover, the poor solubility of the oligomerization product favors the rapid consumption of the C4P units.

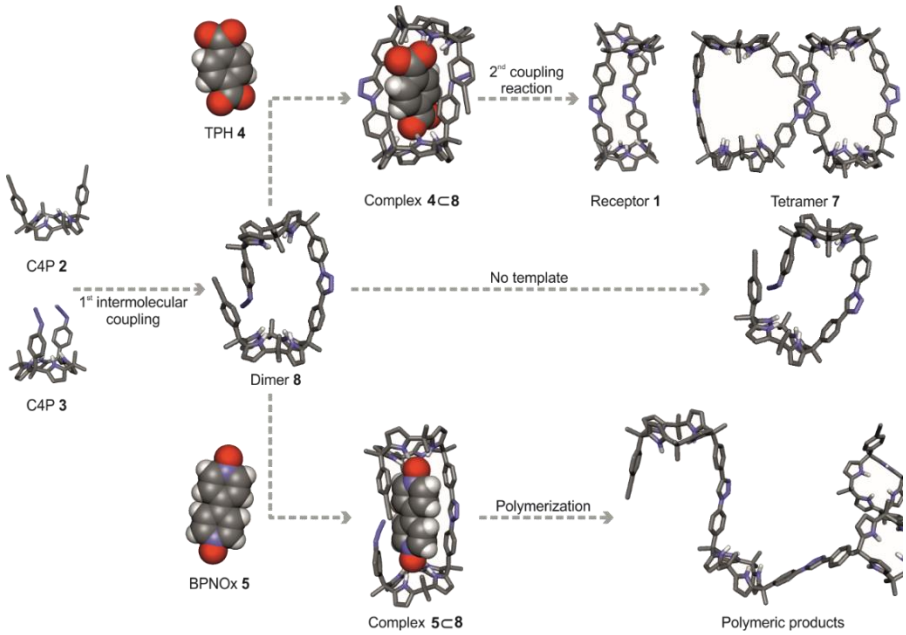

Figure 2.12. Schematic representation of the proposed mechanism for the synthesis of receptor **1**, tetramer **7** and dimeric product **8**.

To further investigate the effect that TPH **4** and BPNOx **5** have in the intramolecular CuAAC reaction of **8**, we performed macrocyclization reactions using **8** formed "in situ" as starting material. C4Ps **2** and **3** were reacted under standard conditions in the absence of template. We confirmed by HPLC analysis the formation of the acyclic dimer **8** immediately after the addition of the copper catalyst (see Experimental Section). After that, we added one equivalent of either TPH **4** or BPNOx **5** to separate reaction vessels. The HPLC traces of the aliquot taken immediately after addition of the templates reveal the disappearance of the peak

attributed to **8**. However, different results were obtained depending on which of the templates was used. Firstly, addition of BPNOx **5** produced the appearance of a yellow precipitate indicative of polymer formation. Indeed, the HPLC analysis of the reaction crude is consistent with the exclusive presence of oligomeric products. On the other hand, the addition of **4** produced the appearance of the peak attributed to macrocycle **1**.[33] This result confirmed that the intramolecular coupling reaction took place only in the presence of **4** and using **8** as starting material.[34] These results were interpreted in terms of the superior capabilities of template TPH over BPNOx to favor the CuAAC closing reaction of intermediate **8** to generate BCP receptor **1**. In addition, our findings prove that the template effect is exerted at the level of the intramolecular reacted compound **8** and the formation of the corresponding 1:1 complex **4**⊂**8**. The role played by **4** in the assembly of the 2:1 complex **4**⊂**2**·**3** seems to be not relevant for the isolation of **8** or its intramolecular reacted product **1**.

2.2.3. Binding of ditopic guests

We investigated the binding properties of receptor **1** towards a series of ditopic guests namely TPH **4**, BPNOx **5** and DFA **6**. Addition of incremental amounts of guest **4** to a millimolar solution of receptor **1** in $CDCl_3$ produced the broadening of all the proton signals of the receptor. This is indicative of an intermediate chemical exchange process on the ^{1}H NMR chemical shift timescale between free and bound receptor (**Figure 2.13**). The proton signals of the receptor **1** sharpened after addition of an excess of the TPH dianion. We probed the formation of the **4**⊂**1** complex using variable temperature experiments on a 1:0.5 mixture of receptor **1** and TPH **4** in chloroform solution. The ^{1}H NMR spectrum of the mixture at 233 K shows sharp and well-defined proton signals. At this temperature, the exchange between the free and the bound receptor becomes slow on the ^{1}H NMR chemical shift timescale. We confirmed the 1:1 stoichiometry of the complex by integration of the proton signals of the two involved species. Likewise, we calculated a binding affinity constant of $2.2 \pm 0.3 \times 10^4\ M^{-1}$ for the **4**⊂**1** complex using the integral values of the proton signals Hc and H1 assigned to free and bound receptor.

Next, we titrated receptor **1** with BPNOx **5**. Unfortunately, the addition of approximately one equivalent of **5** to a $CDCl_3$ solution of **1** originated the formation of an insoluble precipitate. Most likely, an insoluble complex is formed in $CDCl_3$. Consequently, we could not investigate further the binding system.

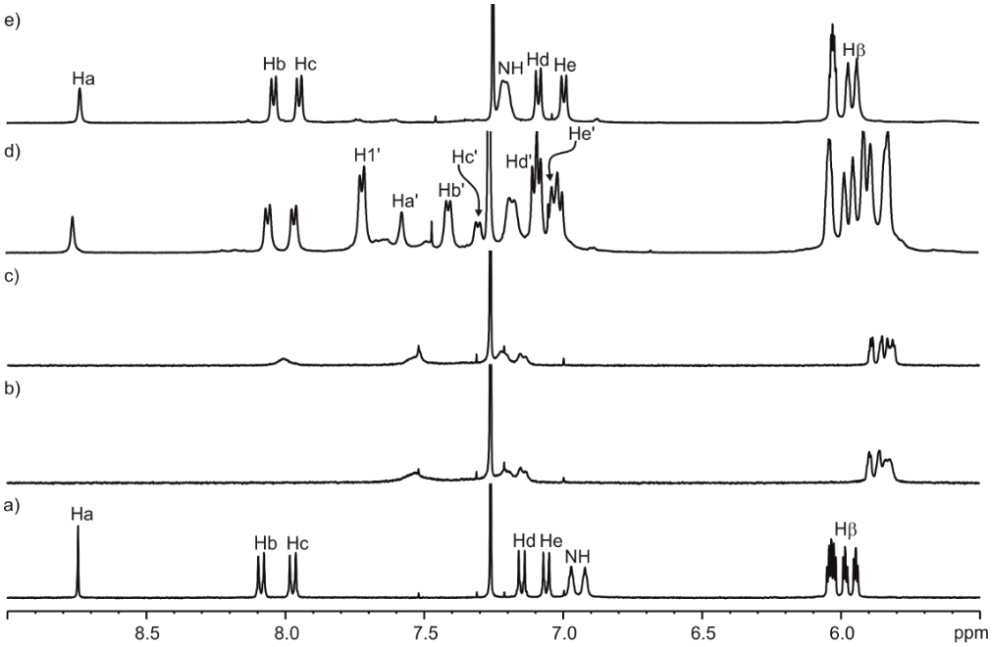

Figure 2.13. Selected region of the ^{1}H NMR spectra (400 MHz, CD_3Cl) of free receptor **1** (a) and after the addition of 1 b) and 2 equivalent c) of TPH **4** at 298 K. Low temperature experiments (233 K) of a 1:0.5 mixture of receptor **1** and TPH **4** d) and free receptor for comparison e). Primed signals correspond to protons of complex **4**⊂**1**. See Figure 2.2 for protons assignments.

For the binding studies of DFA **6** it is worth noting that secondary formamides exist in solution as two possible isomers depending on the relative orientation of the *N* substituents. In solution, the *trans* isomer of secondary amides is more stable than the *cis* analogue.[35,36] This is mostly due to steric reasons and to the establishment of additional polar interactions. However, due to the significant energetic barrier for the interconversion, $\Delta G‡ \geq 20$ kcal·mol^{-1}, the isomerization process is slow on the ^{1}H NMR chemical shift timescale and separate proton signals are observed for both isomers.[37] We were interested in studying the binding preference of receptor **1** towards DFA **6** as it could exist in three possible isomers: *trans*,*trans*; *cis*,*trans* and *cis*,*cis*.[38,39] We performed simple molecular modelling studies in order to provide information about the most plausible geometry adopted by the neutral guest inside receptor **1**. Molecular modelling studies suggested that the *cis*,*cis* isomer would favor the formation of complex **6**⊂**1**. The cis,cis conformer of **6** locates in the fully extended conformation of the alkyl spacer both oxygen atoms in a perfect orientation to form hydrogen-bonding interactions with pyrrole NHs of both C4P units in **1** (**Figure 2.14**).

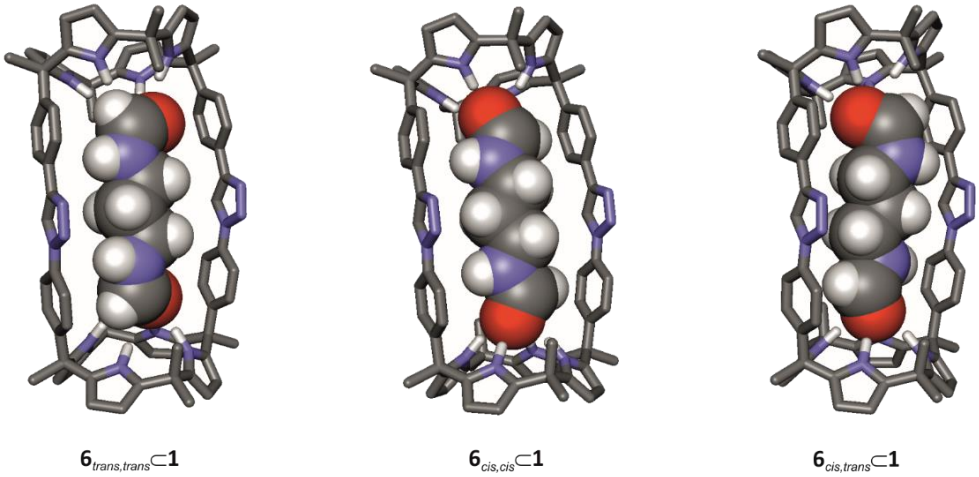

Figure 2.14. Energy-minimized structures (MM3) of the complexes formed between receptor **1** and the trans,trans (left), the cis,cis (middle) and the cis,trans (right) isomers of **6**.

The ^{1}H NMR spectrum of a 2 mM solution of guest **6** in $CDCl_3$ showed two sharp signals resonating at 8.2 and 8.0 ppm that were attributed to the formyl proton (H5) in the *trans*,*trans* and the *cis*,*trans* isomers, respectively (**Figure 2.15**). According to the values of the integrated proton signals, we obtained a *trans*,*trans* to *cis*,*trans* ratio of 89:11. The signal corresponding to the *cis*,*cis* isomer could not be detected due to its low intensity. It is also worth noting that the *trans* proton in the *cis*,*trans* isomer coincides with that of *trans*,*trans* isomer. This was taken into account for the calculation of the ratio between isomers.

The incremental addition of a solution of DFA **6** to a 2 mM solution of receptor **1** in $CDCl_3$ induced dramatic changes in some of the proton signals of the macrocycle (**Figure 2.15**). More precisely, the proton signals of the aromatic walls closer to the binding site, Hb and Hc, broadened and shifted upfield. A similar behavior was observed for the proton signal associated with the triazole spacer Ha. The gradual chemical shift changes of these signals progressed as the concentration of DFA **6** was increased. Interestingly, the NH proton signals of BCP **1** broadened beyond detection. Taken together, these results advocate for the formation of a complex between **1** and **6**. Interestingly, the proton signal of the *trans*,*trans* DFA at 8.2 ppm grew in intensity along the course of the titration and did not experience chemical shift changes. The binding equilibrium display mixed chemical exchange dynamics intermediate on the ^{1}H NMR chemical shift timescale depending on the signals taken in consideration.

For the protons displaying fast chemical exchange, the obtained titration data were mathematically analyzed using the software HypNMR 2008 (version 4.0.66). The fit to a theoretical one to one binding model was good and returned an apparent binding constant value of K_{app} = 1.1 ± 0.1 x 10^2 M^{-1} (see Experimental Section). It is worth noting that the calculated binding constant value is a weighted average of the binding constants for the three possible complexes that could form in solution: **6**$_{trans,trans}$ ⊂**1**, **6**$_{cis,trans}$ ⊂**1** and **6**$_{cis,cis}$ ⊂**1**.

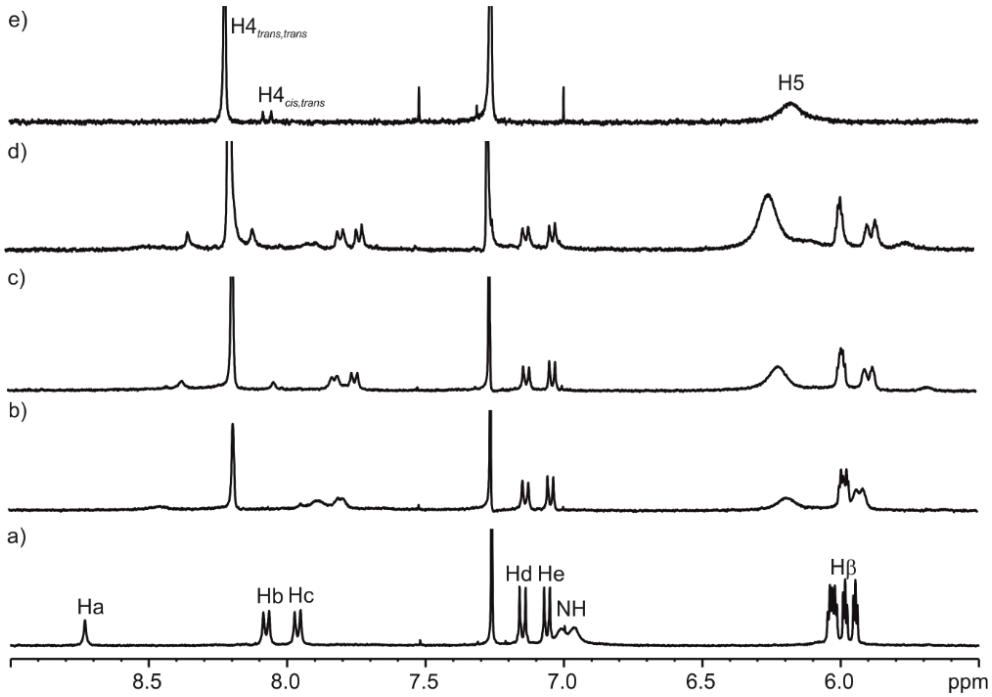

Figure 2.15. Selected region of the ^{1}H NMR spectra (400 MHz, 298K, CD_3Cl) of free receptor **1** (a) and after the addition of 4 b) and 8 c) and 12 d) equivalent of DFA **6** e). See Figure 2.2 for protons assignments.

To better assess the binding affinity of receptor **1**, we analyzed the titration data using a mathematical binding model that assumed the exclusive formation of a 1:1 complex with the *cis*,*trans* isomer of **6**. We fixed the values of the equilibrium constant between the two isomers (K_{iso}) and the chemical shifts of the analyzed proton signals in free and bound **1**. The value for K_{iso} was extracted from the integral values of the proton signals of the two isomers as K_{iso} = **6**$_{trans,trans}$/**6**$_{cis,trans}$ = 89/11 = 8.1. The fit of the experimental data to this binding model returned a binding constant value of 3.1 ± 1.0 x 10^3 M^{-1} (see Experimental Section). The difference of one order of magnitude between K_{app} and K [**6**$_{cis,trans}$⊂**1**] illustrates the importance

of assuming more elaborate binding models when the target isomer exists to a minor extent in solution. The binding of $\mathbf{6}_{cis,cis}$ to **1** is not considered in the used binding model. This limitation is not expected to affect the apparent binding constant determined owing the low concentration of this isomer. On the other hand, we assume higher values for the binding affinity constant of complex *K* [$\mathbf{6}_{cis,cis}\subset\mathbf{1}$].

The difference of one order of magnitude between *K*[**4**⊂**1**] and *K*[**6**⊂**1**] can be rationalized by the superior capabilities of the carboxylates of guest **4** to act as an hydrogen bond acceptor groups compared to the neutral groups in the alkyl bis-formamide. In addition, guest **4** is conformationally rigid and can engage in the establishment of π-π and aromatic CH-π interactions with the aromatic walls of BCP receptor **1**.

2.3. Conclusions

We have reported the synthesis of a BC4P oligocyclic macrocycle, receptor **1**, bearing triazole rings as linkers. We prepared receptor **1** by the templated double CuAAC reaction of two 2W-C4P units, **2** and **3**, featuring a terminal alkyne and azide groups, respectively. We selected tetrabutylammonium terephthalate **4** and bispyridine *N*-oxide **5** as templates due to their good fit in terms of size and shape with the final macrocyclic structure. First, we studied the formation of homo and heterodimeric 2:1 assemblies using TPH **4** and BPNOx **5** and calix[4]pyrroles **2** and **3**. The ^{1}H NMR spectrum of an equimolar CD_3CN mixture of **2**, **3** and TPH **4** showed the formation of 2:1 homo and hetero-dimeric assemblies in an almost statistical distribution (20:20:60, **4**⊂(**2**)$_2$: **4**⊂(**3**)$_2$: **4**⊂**3·2**). However, analogous ^{1}H NMR binding studies with BPNOx **5** showed more reduced changes in the proton signals assigned to the free host and free guest. Most likely, this is due to a reduced binding affinity of **5** to the 2W C4P in this experimental conditions.

The CuAAC reaction of 2W C4P units **2** and **3** in the presence of TPH **4** afforded macrocycle **1** in a remarkable 30% yield.

The effect of the template in the macrocyclization reaction was evaluated using HPLC analysis. Macrocyclization reaction in the absence of template produced compound **8** in 14% yield. Compound **8** is the product of one single intermolecular reaction between calix[4]pyrroles **2** and **3** (i.e. non-cyclized product).

Macrocyclization in the presence of TPH **4** produced macrocycle **1** in a 30% yield together with tetramer **7** (4% yield) and other oligomeric products. Analogous reaction conditions in the presence of BPNOx **5** instead of **4** immediately produced a precipitate in the reaction mixture. Interestingly, the same results were obtained when using compound **8** as starting material and templates **4** and **5**. These results point out that the template effect is exerted mostly by the formation of 1:1 **4⊂8** complex and not from the initial hetero-dimeric assemblies.

Next, we moved on to study the template effect in the macrocyclization reaction by HPLC analysis. We ran several macrocyclization reactions in the presence of TPH **4**, BPNOx **5** and in the absence of any template. For our surprise, we could isolate open oligomer **8** in the macrocyclization reaction without the use of any template. This finding proved that for the synthesis of receptor **1**, the formation of the heterodimeric assembly was not mandatory. On the contrary, a first intermolecular reaction between the two C4P prompted by random collision of the two units generates intermediate **8**. Then, template **4** assists on the second CuAAC reaction by the formation of 1:1 complex **4⊂8**, locating the reacting units close in space to favor the intramolecular reaction that generates **1**. In addition, we found that two units of intermediate **7** could react intermolecularly to obtain tetrameric receptor **7**, isolated in the CuAAC reaction in the presence of template **4**. Carrying the CuAAC reaction in the presence of template **5** only produced the formation of precipitates.

Finally, the binding properties of **1** towards ditopic guests **4**, **5** and **6** were evaluated by means of ^{1}H NMR experiments in $CDCl_3$ solution. We demonstrated that BC4P **1** was able to form kinetically and thermodynamically stable complexes with TPH **4** and DFA **6**. On the other hand, analogous titrations with BPNOx **5** resulted in the formation of an insoluble complex.

We determined a difference of one order of magnitude between K[**4⊂1**] and K[**6⊂1**]. We attributed this difference to the superior hydrogen bond acceptor propertied of carboxylates compared to the neutral formamide groups of **6**. Moreover, guest **4** can also establish π-π and aromatic CH-π interactions with the aromatic walls of **1**.

We calculated the binding constant values for the complexes **4⊂1** and **6⊂1** and observed an increase of two orders of magnitude for the TPH complex. These results were rationalized in terms of the greater hydrogen bond acceptor properties of TPH **4**, as well as its ability to engage in π-π interactions with receptor **1**. Finally, we have

demonstrated the importance of considering elaborate binding models for the determination of binding constants when different equilibria take place in solution and more importantly when the target compound exists to a minor extent in solution.

2.4. Experimental section

2.4.1. General information and instruments

Reagents were obtained from commercial suppliers and used without further purification unless otherwise stated. All solvents were commercially obtained and used without further purification. Dry solvents were taken from a solvent system MB SPS 800. CH_3CN and NEt_3 were dried, distilled and degassed by three freeze-pump-thaw cycles before used in the CuAAC reactions. Routine ^1H NMR and $^{13}C\{^1H\}$ NMR spectra were recorded on a Bruker Avance 300 (300 MHz for ^1H NMR and 75 MHz for ^{13}C NMR), Bruker Avance 400 (400 MHz for ^1H NMR and 100 MHz for ^{13}C NMR), Bruker Avance 500 (500 MHz for ^1H NMR and 125 MHz for ^{13}C NMR) or Bruker Avance 500 with cryoprobe (500 MHz for ^1H NMR and 125 MHz for ^{13}C NMR). Deuterated solvents were purchase from Sigma Aldrich. Chemical shifts are reported in ppm using residual solvent peaks as reference. Coupling constant values J are given in Hz. COSY, NOESY, ROESY, HMQC and HMBC experiments were recorded to help with the assignment of ^1H and ^{13}C signals. High-resolution mass spectra (HRMS) were obtained on a Bruker HPLC-TOF (MicroTOF Focus) and Bruker HPLC-QqTOF (MaXis Impact) using the ionization mode indicated for each compound. IR spectra were recorded on a Bruker Optics FTIR Alpha spectrometer equipped with a DTGS detector, KBr beamsplitter at 4 cm^{-1} resolution using a one bounce ATR accessory with diamond windows. Melting points were measured on a MP70 Melting Point System Mettler Toledo. HPLC analysis were done in an Agilent® 1200 system using a Waters Spherisorb® 5.0 μm silica column and a 35% EtOAc in DCM mixture of solvents. Column chromatography was performed with silica gel technical grade, pore size 60 Å, 230-400 mesh particle size, 40-63 μm particle size and thin layer chromatography (TLC) analysis on silica gel 60 F254.

2.4.2. Synthesis and characterization data

BC4P Receptor 1. α,α-Bis-4-[ethynylphenyl]calix[4]pyrrole **2** (57 mg, 0.095 mmol, 1 equivalent) and α,α-Bis-4-[azidephenyl]calix[4]pyrrole **3** (60 mg, 0.095 mmol, 1 equivalent) were dissolved in 50 mL of dry and degassed acetonitrile. CuI (25 mg, 0.132 mmol, 1.4 equivalent), tetrabutylammonium terephthalate **4** (61 mg, 0.095

mmol, 1 equivalent), and 0.5 mL of freshly distilled triethylamine were added. The reaction was stirred at room temperature for 4 h. After that, 50 mL of dichloromethane was added to the reaction crude. The organic phase was washed three times with 100 mL of water and later dried with anhydrous Na_2SO_4, filtered, and concentrated under reduced pressure to give a brown solid. Purification of the crude by silica column chromatography using a 4% mixture of EtOAc in $CHCl_3$ (Rf = 0.4) afforded **1** as a white solid (35 mg, 30% yield). ^{1}H NMR (500 MHz, $CDCl_3$, 298 K) δ 8.75 (s, 2H, Ha), 8.08 (d, 4H, J = 8.0 Hz, Hb), 7.97 (d, 4H, J = 8.7 Hz, Hc), 7.15 (d, 4H, J = 8.7 Hz, Hd), 7.06 (d, 4H, J = 8.0 Hz, He), 6.99 (br, 4H, NHs), 6.95 (br, 4H, NHs), 6.06–5.92 (m, 16H, Hβ), 2.04 (s, 12H, Hf), 1.53 (s, 12H, Hg), 1.45 (s, 12H, Hh). ^{13}C {^{1}H} NMR (125 MHz, $CDCl_3$, 298 K) δ 148.6, 147.6, 137.5, 137.2, 136.2, 135.9, 135.9, 129.0, 128.8, 128.0, 126.1, 120.0, 117.8, 106.1, 105.6, 105.4, 105.2, 44.9, 44.9, 35.9, 35.8, 30.7, 30.6, 30.2, 30.2, 29.3, 29.2. FTIR (ATR): $\bar{\upsilon}_{max}$ (cm^{-1}) = 3443 (amine N–H stretching), 2970 (alkene C–H stretching), 1214 (amine C–N stretching), 1039 (alkene C═C bending), 788 (alkene C═C bending). HR-MS (MALDI-TOF-MS) m/z calculated for $C_{80}H_{77}N_{14}$ $[M - H]^-$ 1233.6461, found 1233.6479. mp >270 °C (decomp).

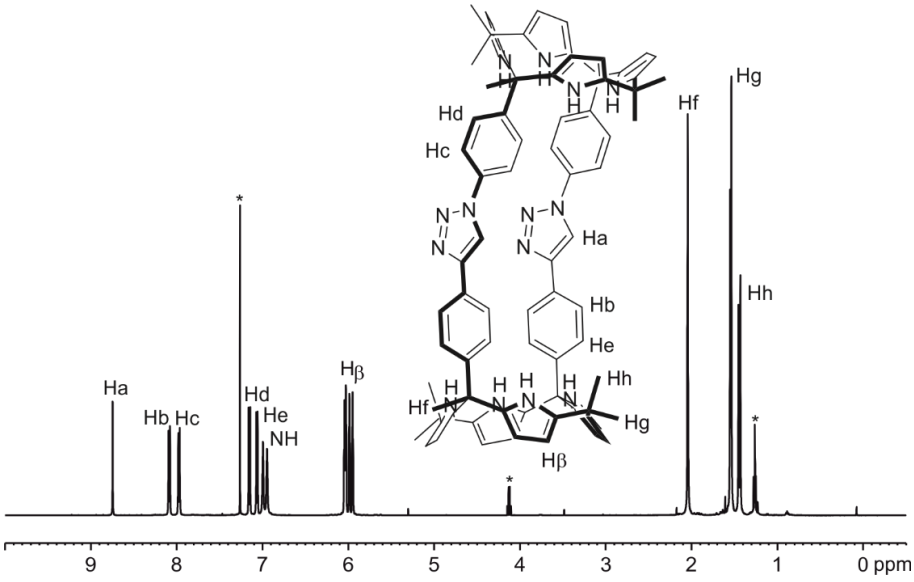

Figure 2.16. ^{1}H NMR (500 MHz, $CDCl_3$, 298 K) spectrum of a 2 mM solution of BC4P macrocycle **1** with the corresponding proton assignments. *Residual solvent peaks.

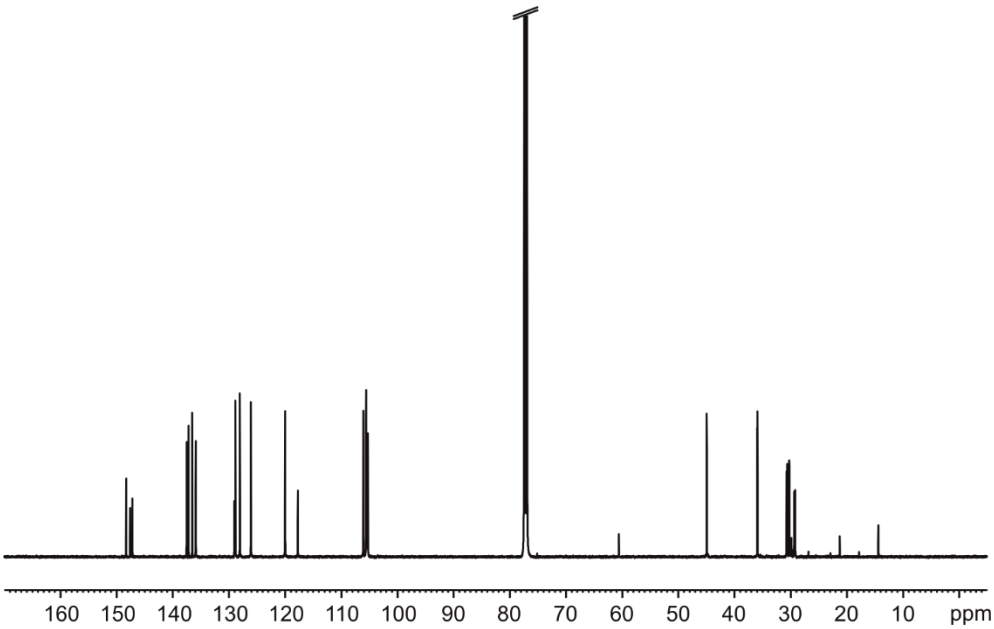

Figure 2.17. ^{13}C NMR (125 MHz, $CDCl_3$, 298 K) spectrum of a 2 mM solution of BC4P macrocycle **1**.

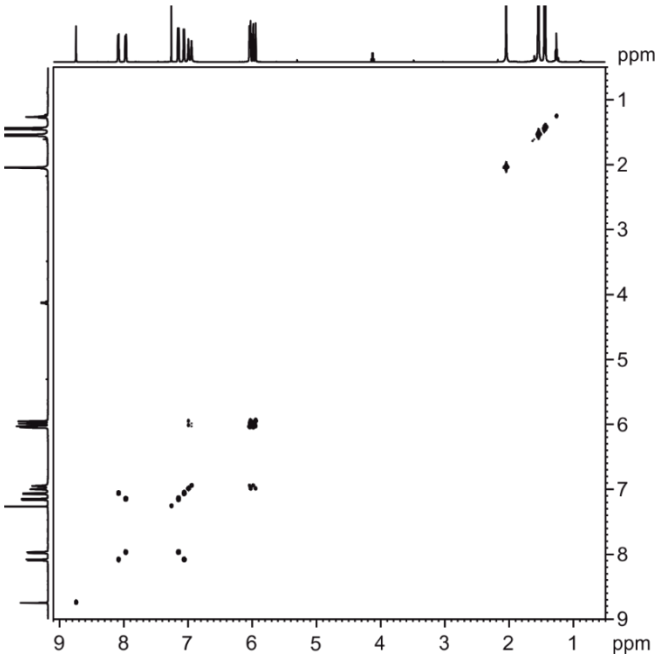

Figure 2.18. $^{1}H - {}^{1}H$ COSY (500 MHz, $CDCl_3$, 298 K) spectrum of a 2 mM solution of BC4P macrocycle **1**.

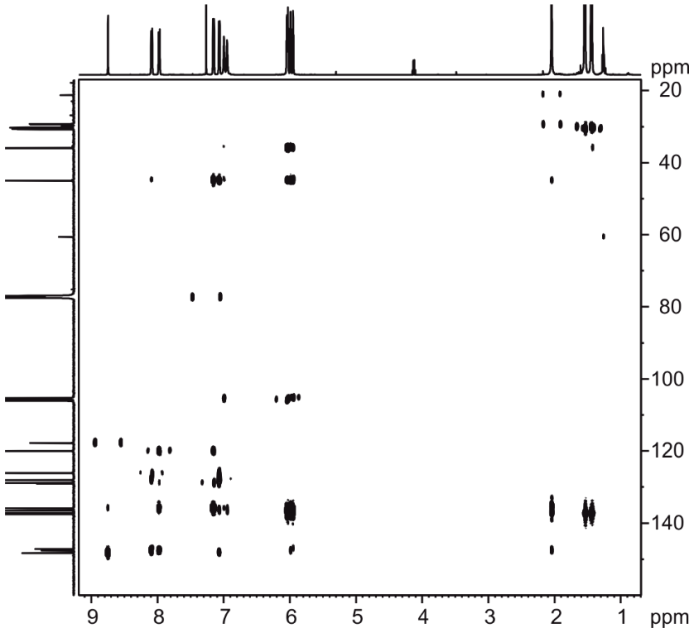

Figure 2.19. ^{1}H - ^{13}C HSQC (500 MHz, $CDCl_3$, 298 K) spectrum of a 2 mM solution of BC4P macrocycle **1**.

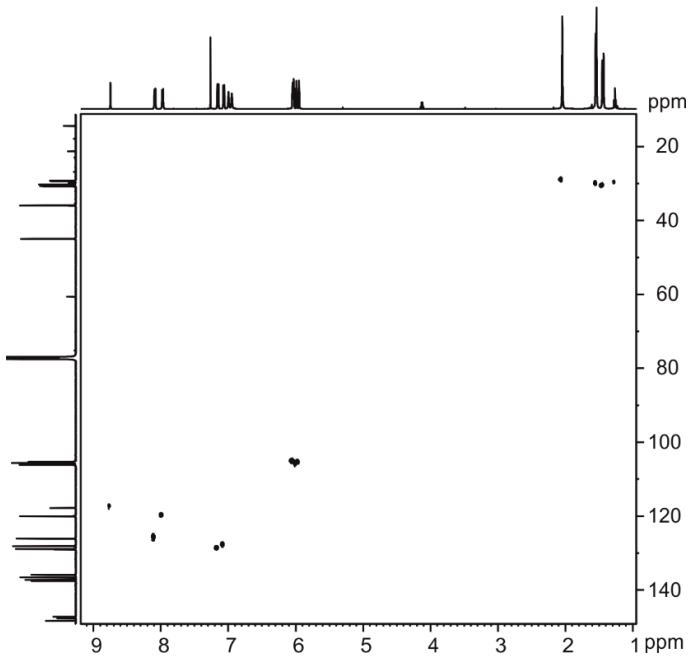

Figure 2.20. ^{1}H-^{1}H HMBC (500 MHz, $CDCl_3$, 298 K) spectrum of a 2 mM solution of BC4P macrocycle **1**.

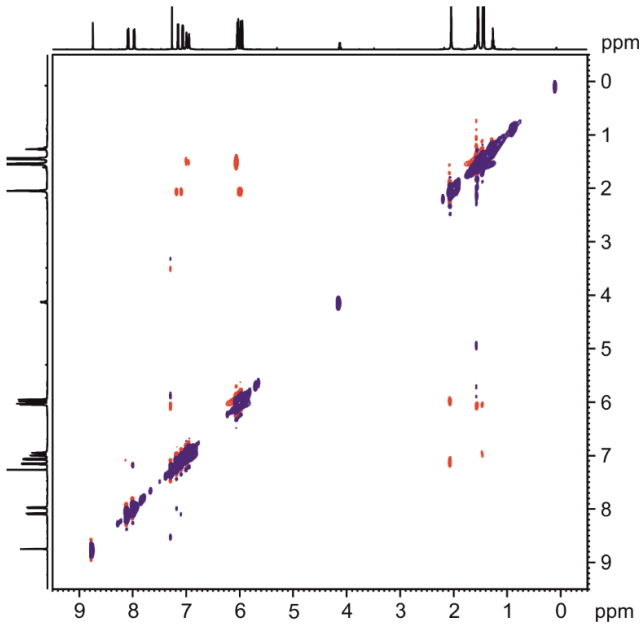

Figure 2.21. ^{1}H – ^{1}H ROESY (500 MHz, $CDCl_3$, 298 K, spin-lock = 0.3 s) spectrum of a 2 mM solution of BC4P macrocycle **1**.

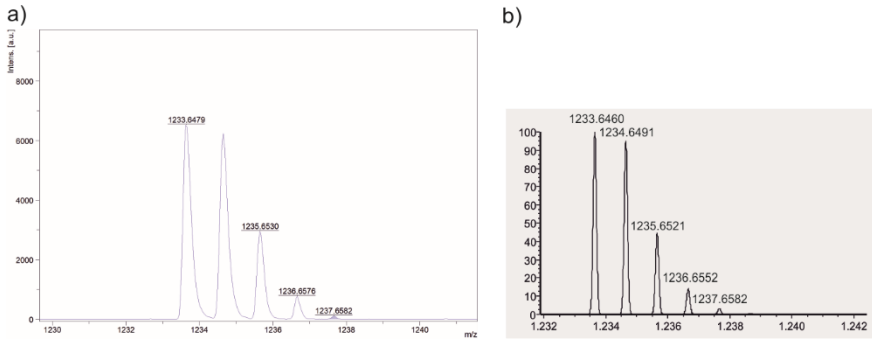

Figure 2.22. Experimental (a) and theoretical (b) isotopic distribution for BC4P molecular ion [**1**-H]$^{-}$.

Tetramer 7. α,α-Bis-4-[ethynylphenyl]calix[4]pyrrole **2** (47 mg, 1 equivalent) and α,α-Bis-4-[azidephenyl]calix[4]pyrrole **3** (50 mg, 1 equivalent) were dissolved in 40 mL of dry and degassed acetonitrile. CuI (23 mg, 1.5 equivalent), tetrabutylammonium terephthalate **4** (51 mg, 1 equivalent), and 0.5 mL of freshly distilled triethylamine were added. The reaction was stirred at room temperature for 4 h. After that, 50 mL of dichloromethane was added to the reaction crude. The organic phase was washed three times with 100 mL of water and later dried with anhydrous Na_2SO_4, filtered, and concentrated under reduced pressure to give a

brown solid. Purification of the crude by HPLC semi-preparative silica column using a 35% EtOAc in Hexane mixture afforded **7** as a brown solid (10 mg, 4% yield). ^{1}H NMR (500 MHz, $CDCl_3$, 298 K) δ 8.13 (s, 4H, Hm), 7.76 (d, 8H, *J* = 8.5 Hz, Hn), 7.66 (d, 8H, *J* = 8.9 Hz, Hl), 7.30 (br, 16H, NHs), 7.11 (d, 8H, *J* = 8.9 Hz, Hk), 7.04 (s, 8H, *J* = 8.2 Hz, Ho), 5.93 (m, 16H, Hβ), 5.65 (m, 16H, Hβ) 1.94 (s, 24H, Hq), 1.65 (s, 24H, Hr), 1.50 (s, 24H, Hp). ^{13}C {^{1}H} NMR (125 MHz, $CDCl_3$, 298 K) δ 148.1, 138.7, 138.6, 136.3, 135.8, 128.8, 128.0, 125.0, 119.2, 106.2, 103.3, 103.1, 44.6, 44.5, 32.0, 30.74, 29.6, 29.3, 27.6, 27.2, 27.1, 22.6, 14.1. FTIR (ATR): $\bar{\upsilon}_{max}$ (cm^{-1}) = 3415 (amine N–H stretching), 2972 (alkene C–H stretching), 1705 (triazole C=N stretching), 1220 (amine C–N stretching), 1036 (alkene C═C bending), 768 (alkene C═C bending). HR-MS (ESI-TOF-MS) m/z calculated for $C_{160}H_{156}N_{28}$ $[M - 2H]^{2-}$ 1233.6802, found 1233.6450. mp >270 °C (decomp).

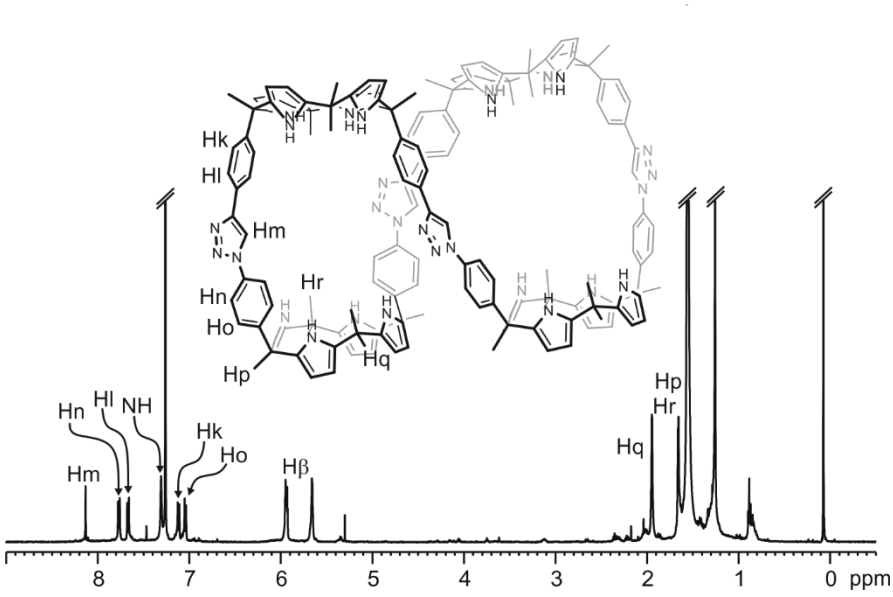

Figure 2.23. ^{1}H NMR (500 MHz, $CDCl_3$, 298 K) spectrum of tetramer **7** with proton assignments.

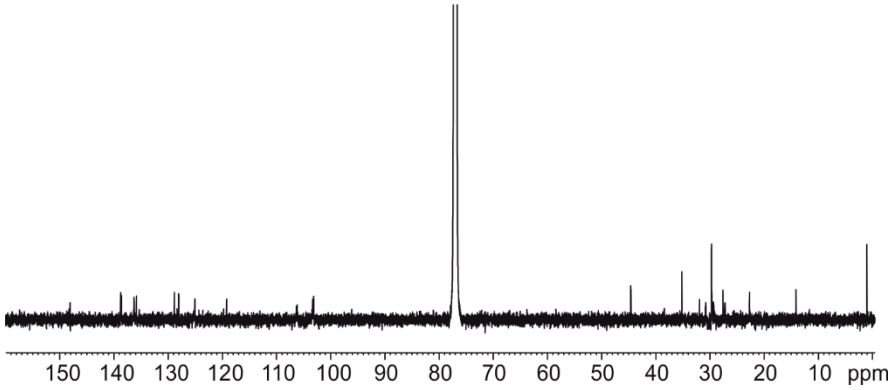

Figure 2.24. ^{13}C NMR (125 MHz, $CDCl_3$, 298 K) spectrum of tetramer **7**.

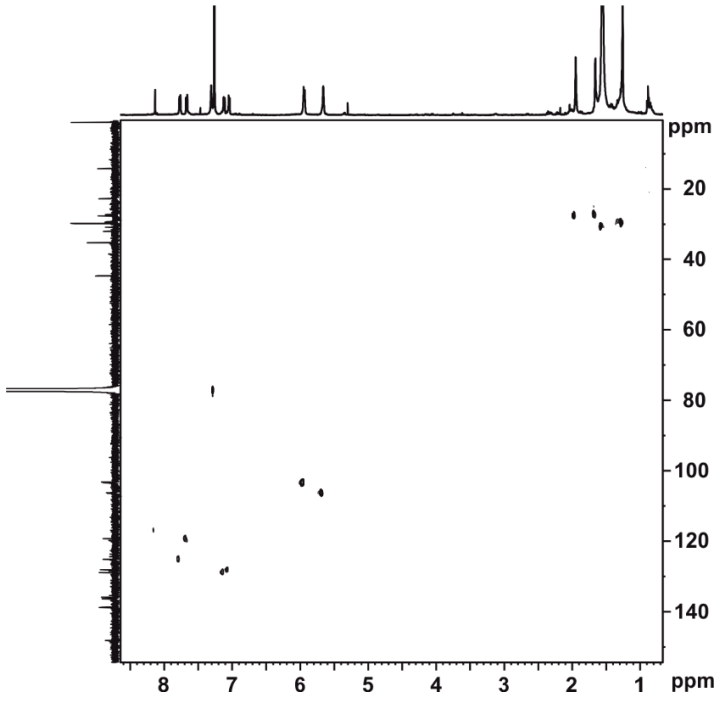

Figure 2.25. ^{1}H-^{13}C HSQC (500 MHz, $CDCl_3$, 298 K) spectrum of tetramer **7**.

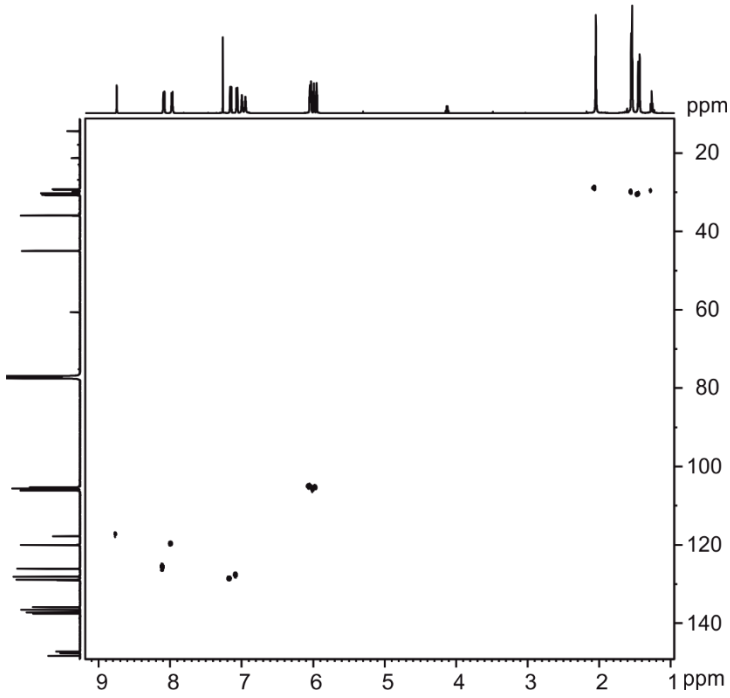

Figure 2.26. ^{1}H-^{1}H HMBC (500 MHz, $CDCl_3$, 298 K) spectrum of tetramer **7**.

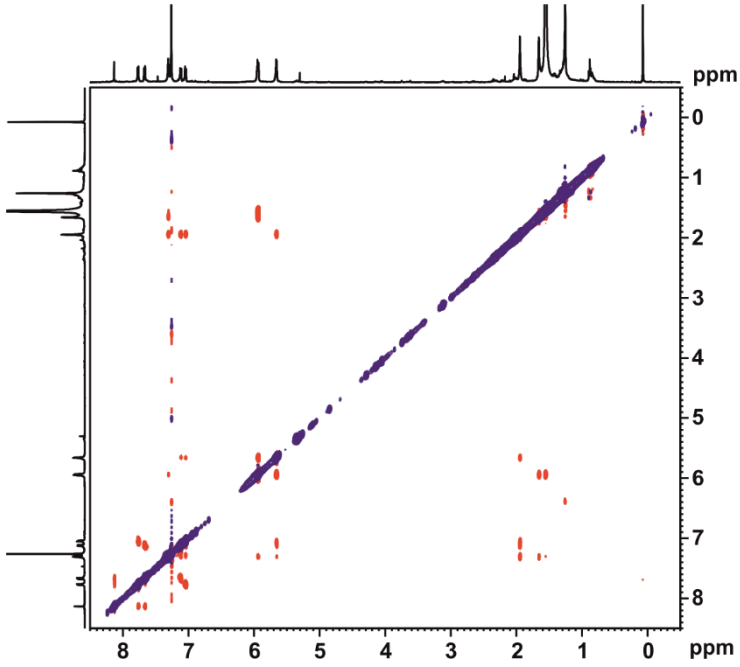

Figure 2.27. ^{1}H-^{1}H ROESY (500 MHz, $CDCl_3$, 298 K, spin-lock = 0.3 s) spectrum of tetramer **7**.

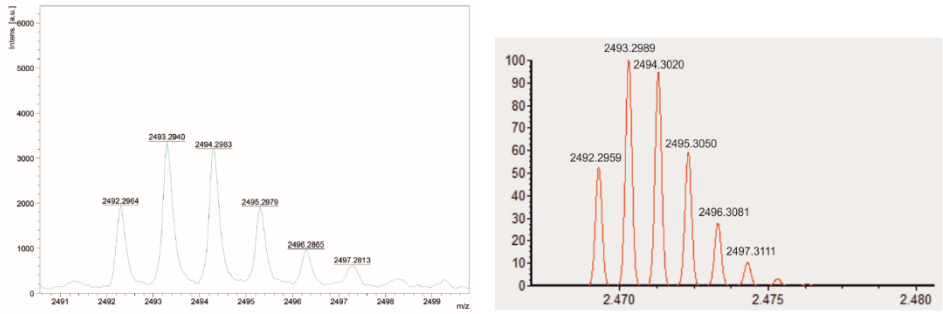

Figure 2.28. Experimental (a) and theoretical (b) isotopic distribution for [**7**+Na]$^+$.

Dimer 8. α,α-Bis-4-[ethynylphenyl]calix[4]pyrrole **2** (47 mg, 1 equivalent) and α,α-Bis--4-[azidephenyl]calix[4]pyrrole **3** (50 mg, 1 equivalent) were dissolved in 33 mL of dry and degassed acetonitrile. CuI (23 mg, 1.5 equivalent) and 0.3 mL of freshly distilled triethylamine were added. The reaction was stirred at room temperature for 4 h. After that, 50 mL of dichloromethane was added to the reaction crude. The organic phase was washed three times with 100 mL of water and later dried with anhydrous Na_2SO_4, filtered, and concentrated under reduced pressure to give a brown solid. Purification of the crude by HPLC semi-preparative silica column using a 30% EtOAc in Hexane mixture afforded **7** as a yellow clear solid (5 mg, 5% yield). ^{1}H NMR (500 MHz, $CDCl_3$, 298 K) δ 8.05 (s, 1H, Hu), 7.75 (d, 2H, *J* = 8.0 Hz, Hv), 7.63 (d, 2H, *J* = 8.5 Hz, Ht), 7.35 (d, 2H, *J* = 8.5 Hz, Hα), 7.23 (br, 8H, NHs), 7.14 (d, 2H, *J* = 8.5 Hz, Hs), 7.06 (d, 2H, *J* = 8.2 Hz, Hw), 6.95 (d, 2H, , *J* = 8.2 Hz, Hy), 6.94 (d, 2H, *J* = 8.2 Hz, Hx), 6.88 (d, 2H, *J* = 8.5 Hz, Hχ), 5.94 (m, 8H, Hβ-pyrrole), 5.66 (m, 4H, Hβ), 5.61 (m, 4H, Hβ), 3.02 (s, 1H, Hz), 1.92 (d, 6H, *J* = 2.4 Hz, Hϕ), 1.87 (d, 6H, *J* = 2.4 Hz, Hχ), 1.63 (s, 12H, Hε), 1.54 (s, 12H, Hδ). ^{13}C {1H} NMR (125 MHz, $CDCl_3$, 298 K) δ 139.1, 139.0, 138.9, 136.7, 136.4, 136.2, 129.1, 128.3, 127.8, 125.5, 120.1, 118.6, 106.3, 103.7, 103.7, 103.6, 44.9, 35.5, 30.4, 30.1, 28.3, 28.1. FTIR (ATR): $\bar{\upsilon}$ max (cm^{-1}) = 3419 (amine N–H stretching), 2966 (alkene C–H stretching), 2112 (alkyne C≡C stretching and azide stretching), 1219 (amine C–N stretching), 1035 (alkene C═C bending), 767 (alkene C═C bending). HR-MS (HPLC-TOF-ESI$^-$) m/z calculated for $C_{80}H_{77}N_{14}$ $[M - 2H]^{2-}$ 616.3194, found 616.3193. mp >250 °C (decomp).

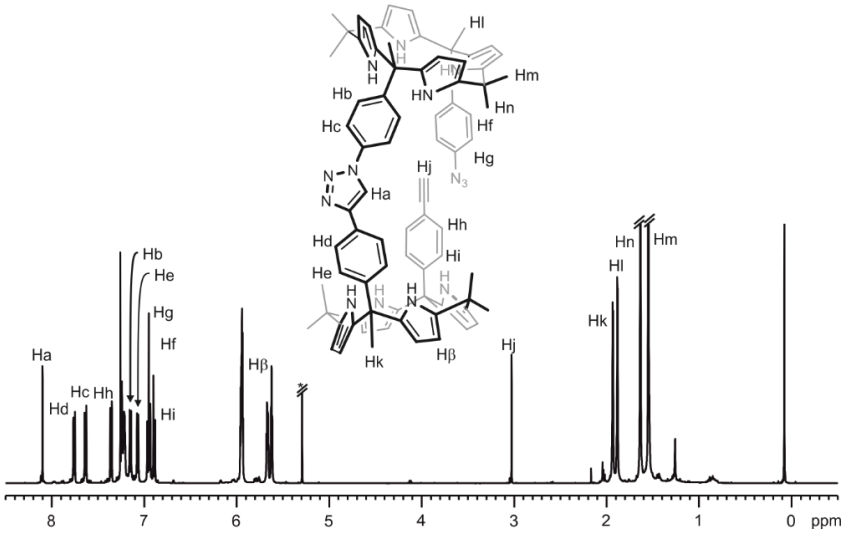

Figure 2.29. ^{1}H NMR (500 MHz, $CDCl_3$, 298 K) spectrum of dimer **8** with proton assignments.

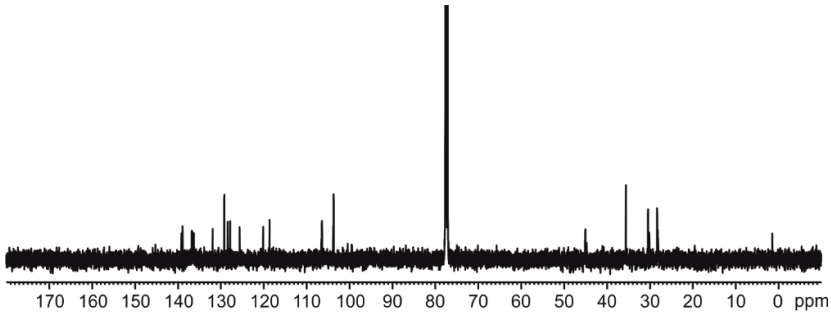

Figure 2.30. ^{13}C NMR (125 MHz, $CDCl_3$, 298 K) spectrum of dimer **8**.

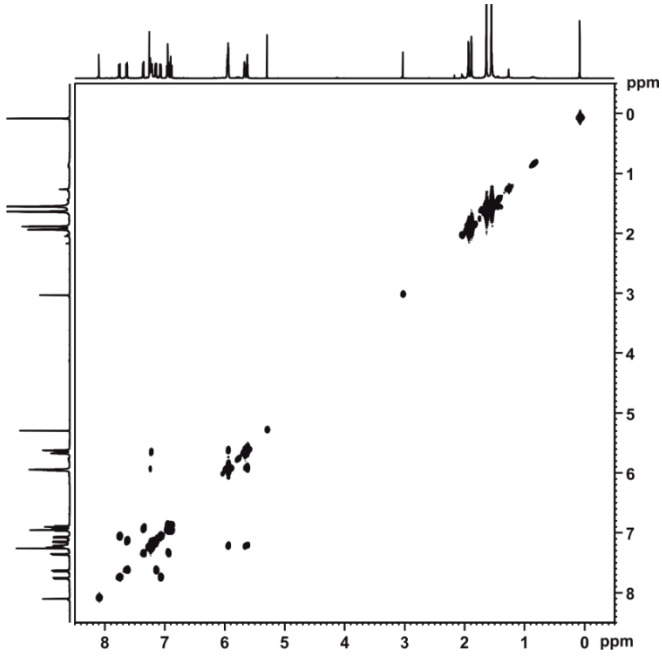

Figure 2.31. ^{1}H-^{1}H COSY (500 MHz, $CDCl_3$, 298 K) spectrum of dimer **8**.

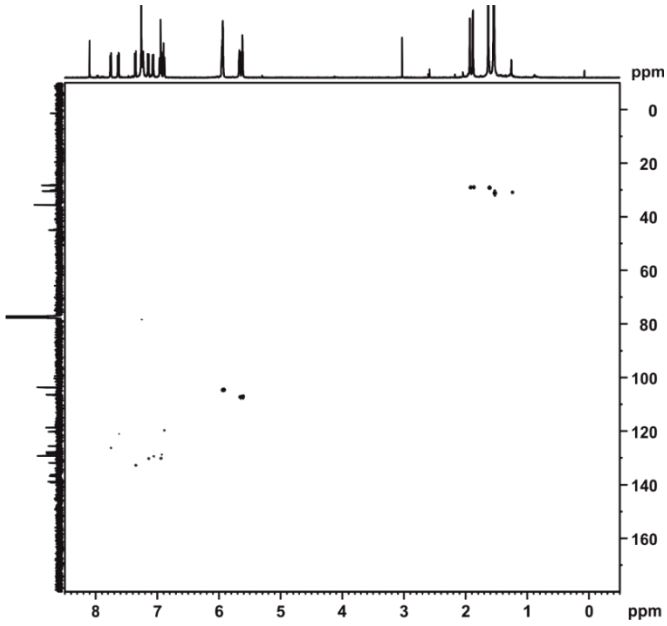

Figure 2.32. ^{1}H-^{13}C HSQC (500 MHz, $CDCl_3$, 298 K) spectrum of dimer **8**.

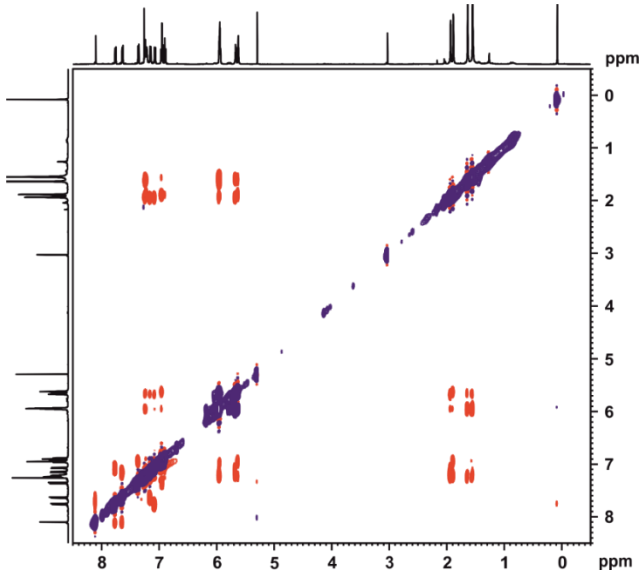

Figure 2.33. ^{1}H-^{1}H ROESY (500 MHz, $CDCl_3$, 298 K, spin-lock = 0.3 s) spectrum of dimer **8**.

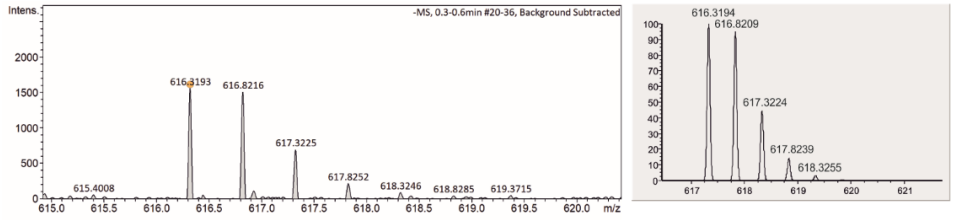

Figure 2.34. Experimental (a) and theoretical (b) isotopic distribution for dimer **8**.

2.4.3. DOSY Experiments

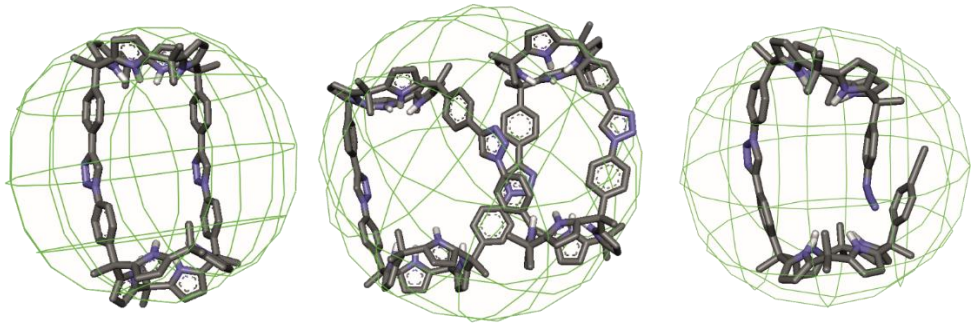

Figure 2.35. Energy minimized structures of the different architectures described in this chapter with a wire-frame sphere to indicate the volume derived from the DOSY analysis.

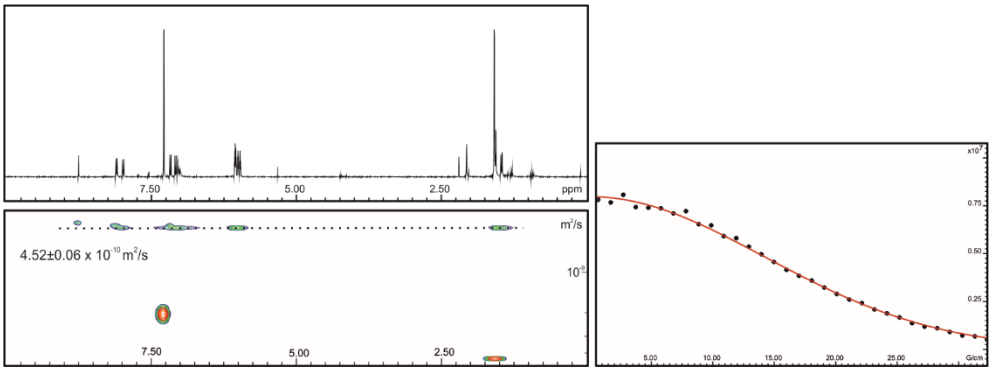

Figure 2.36. (left) ^{1}H pseudo 2D plot of DOSY (500 MHz, 298K, $CDCl_3$) of macrocycle **1** (D20 = 0.15 s, P30 = 1 ms). (right) Fit of the decay of the signal of proton Ha to a mono-exponential function using Dynamics Center software from Bruker. Errors are indicated as standard deviation.

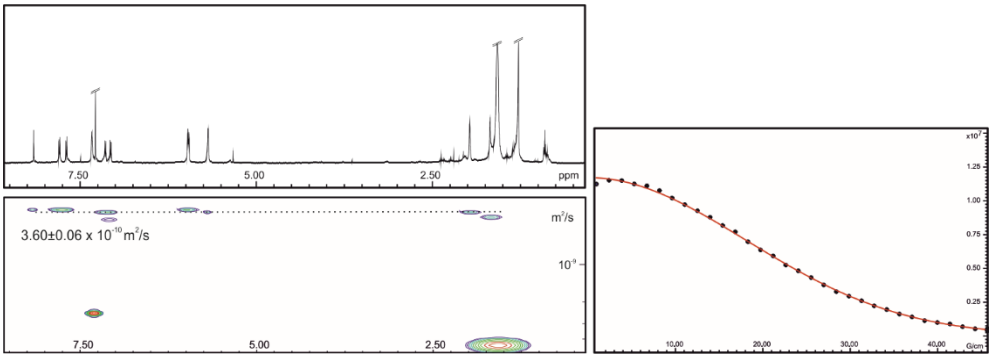

Figure 2. 37. (left) ^{1}H pseudo 2D plot of DOSY (500 MHz, 298K, $CDCl_3$) of tetramer **7** (D20 = 0.15 s, P30 = 1 ms). (right) Fit of the decay to a mono-exponential function. Errors are indicated as standard deviation.

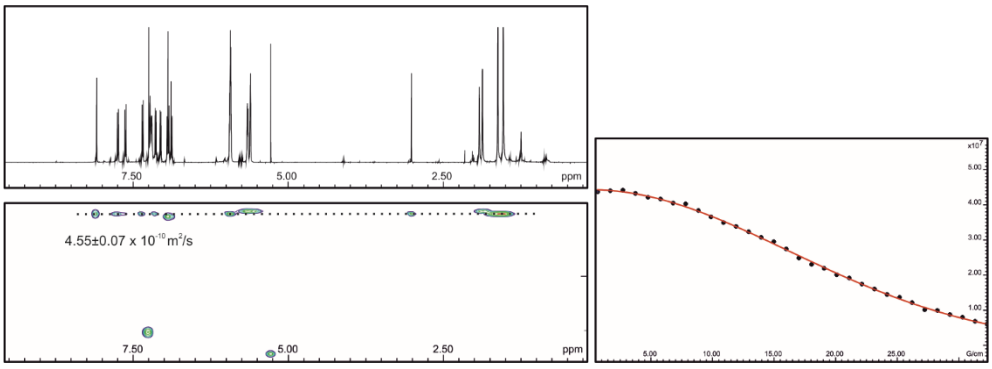

Figure 2. 38. (left) ^{1}H pseudo 2D plot of DOSY (500 MHz, 298K, $CDCl_3$) of macrocycle **1** (D20 = 0.15 s, P30 = 1 ms). (right) Fit of the decay to a mono-exponential function. Errors are indicated as standard deviation.

2.4.4. ^{1}H NMR titration experiments

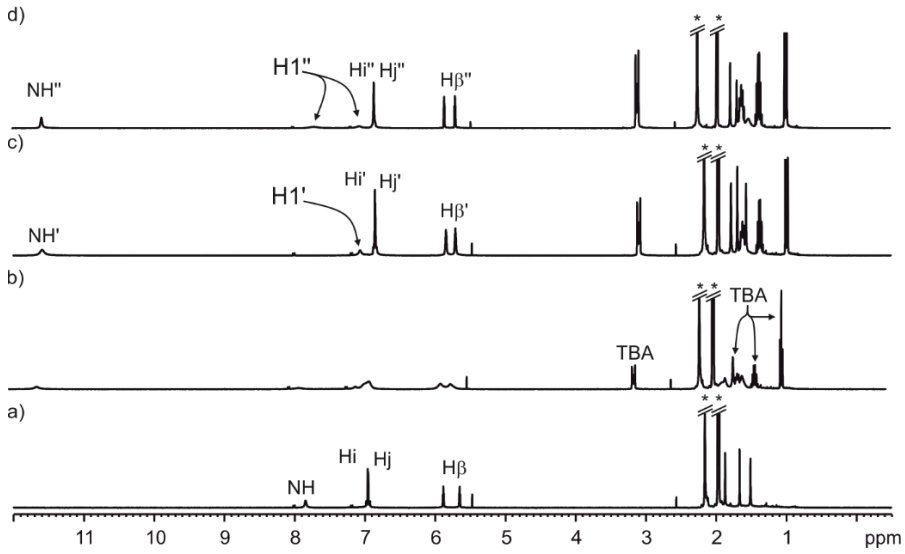

Figure 2.39. ^{1}H NMR spectra (400 MHz, 298 K, CD_3CN) acquired during the titration experiment of receptor **3** (a) with incremental additions of TPH **4**: 0.25 equivalent (b), 0.5 equivalent (c), and 1 equivalent (d) with assigned diagnostic signals. Primed letter correspond to complex **4**⊂**3**$_2$; doubled primed letters correspond complex **4**⊂**3**. Proton H1 correspond to the two magnetically inequivalent proton signals of guest **4**. See Figure 2.2 for proton assignments. *Residual solvent signal.

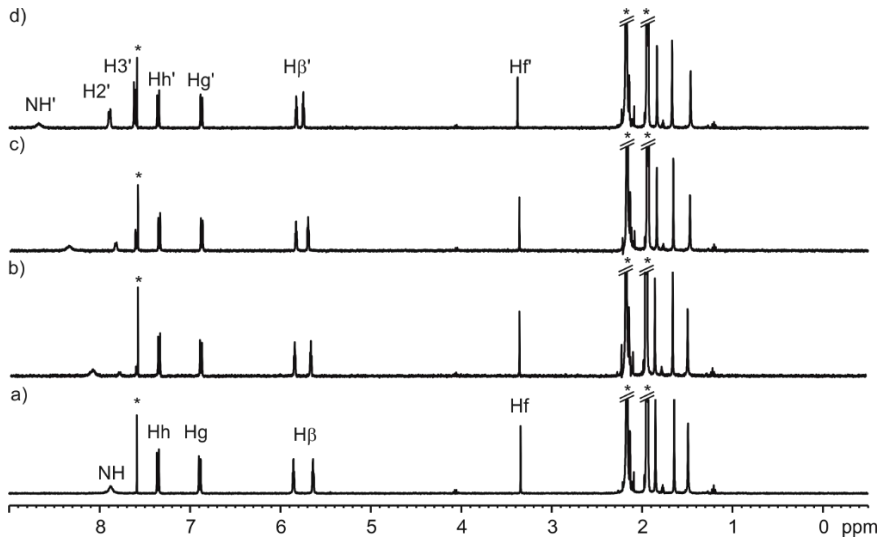

Figure 2.40. ^{1}H NMR spectra (400 MHz, 298 K, CD_3CN) acquired during the titration experiment of receptor **2** (a) with incremental additions of BPNOx **5**: 0.25 equivalent (b), 0.5 equivalent (c), and 1 equivalent (d) with assigned diagnostic signals. Primed letter correspond to signals of complex formed between **2** and BPNOx **5**. See Figure 2.2 for protons assignments. *Residual solvent signal.

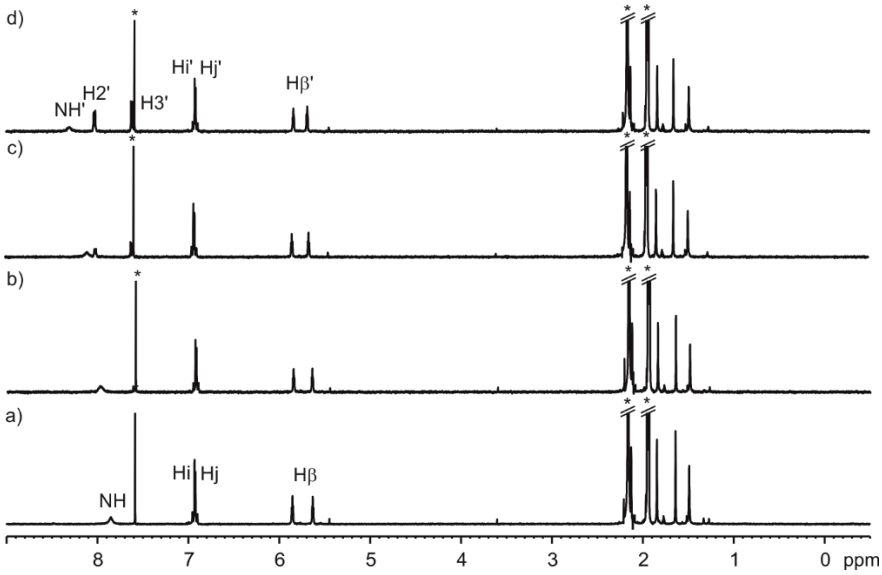

Figure 2.41. ^{1}H NMR spectra (400 MHz, 298 K, CD_3CN) acquired during the titration experiment of receptor **3** (a) with incremental additions of BPNOx **5**: 0.25 equivalent (b), 0.5 equivalent (c), and 1 equivalent (d) with assigned diagnostic signals. Primed letter correspond to signals of complex formed between **3** and BPNOx **5**. See Figure 2.2 for protons assignments. *Residual solvent signal.

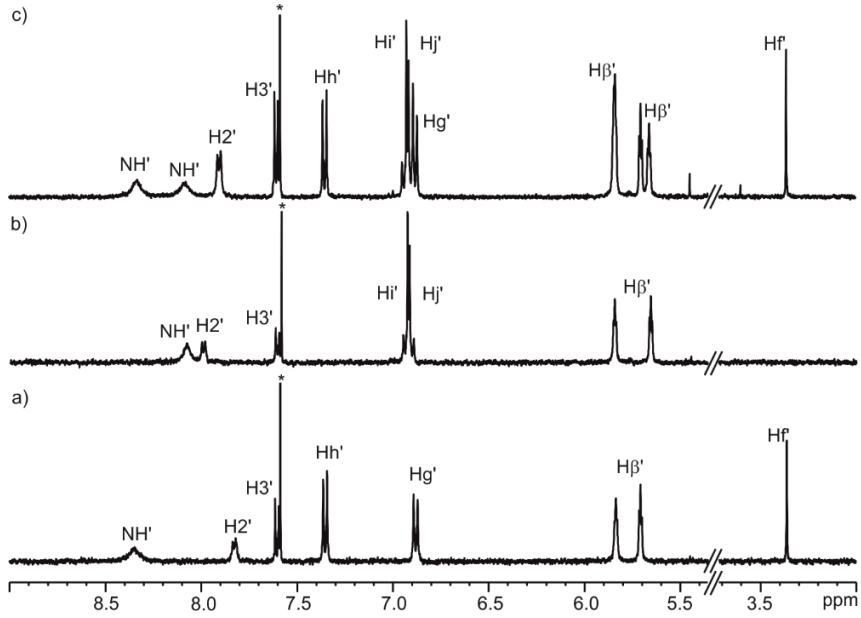

Figure 2.42. Selected region of the ^{1}H NMR spectra (400 MHz, 298 K, CD_3CN) of 2:1 mixture of C4P **2** and BPNOx **5** a) C4P **3** and BPNOx **5** b) and the 1:1:1 mixture of the three components. Primed letter correspond to complex to the 1:1 complexes. See Figure 2.2 for protons assignments. *Residual solvent signal.

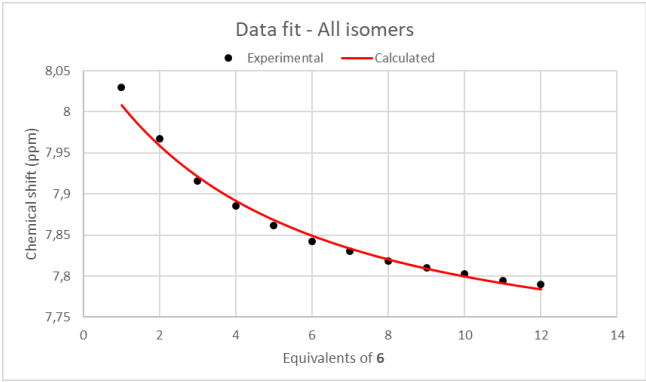

Figure 2.43. Fit of the chemical shift changes experience by the signal for proton Hc of **1** during the titration experiment with DFA **6** using a theoretical 1:1 binding model that considers the complexation with all isomers of **6**. HypNMR 2008 software (version 4.0.66) was used for the mathematical fit.

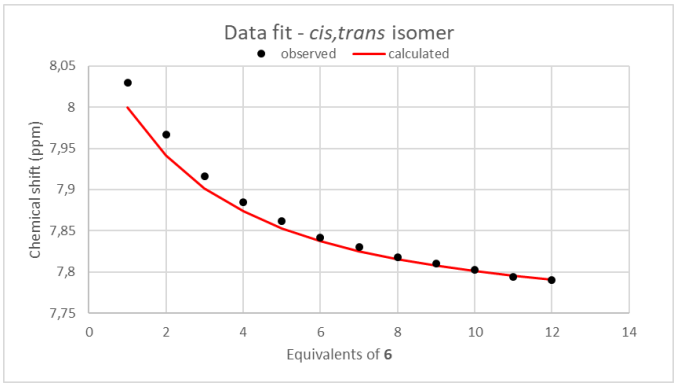

Figure 2.44. Fit of the chemical shift changes experience by the signal for proton Hc of **1** during the titration experiment with DFA **6**. Manually adjusted to a theoretical binding model that considered the two isomeric forms of **6** with K_{iso} = 8.1 and the exclusive binding of the *cis*,*trans* isomer.

For the calculated chemical shifts values it was necessary to calculate the amount of free *cis,trans* isomer at each point of the titration experiment. For this, we used the next relationship attending at the definition of the binding equilibrium constants and mass balances:

$$[B] \overset{K_{iso}}{\rightleftharpoons} [A] \qquad K_{iso} = \frac{[A]}{[B]} \; ; \; [A] = K_{iso}[B]$$

$$[H_F] + [B] \overset{\beta}{\rightleftharpoons} [HB] \qquad \beta = \frac{[HB]}{[H_F][B]} \; ; \; [HB] = \beta[H_F][B]$$

[B] = *cis,trans* isomer
[A] = *trans,trans* isomer
[H] = Host
[G] = Guest
$[X_T]$ = Total X
$[X_F]$ = Free X

$$[H_T] = [H_F] + [HB] = [H_F] + \beta[H_F][B] = [H_F](1+\beta[B]) \; ; \; [H_F] = \frac{[H_T]}{1+\beta[B]}$$
$$[G_F] = [A]+[B] = K_{iso}[B]+[B] = [B](1+K_{iso})$$
$$[G_T] = [G_F] + [HB] = [B](1+K_{iso}) + \beta[H_F][B] \quad (\textit{Assumes [HA] = 0})$$

$$[G_T] = [B](1+K_{iso}) + \frac{\beta[H_T][B]}{1+\beta[B]} \; ; \; [G_T] - [B](1+K_{iso}) = \frac{\beta[H_T][B]}{1+\beta[B]}$$

$$([G_T] - [B]-[B]K_{iso})(1+\beta[B]) = \beta[H_T][B]$$
$$[G_T] + [G_T]\beta[B] - [B] - \beta[B]^2 - [B]K_{iso} - K_{iso}\beta[B]^2 - \beta[H_T][B] = 0$$

$$-(K_{iso}\beta+\beta)[B]^2 + ([G_T]\beta - 1 - K_{iso} - \beta[H_T])[B] + [G_T] = 0$$
(*Quadratic formula*)

2.4.5. HPLC analysis of the template effect

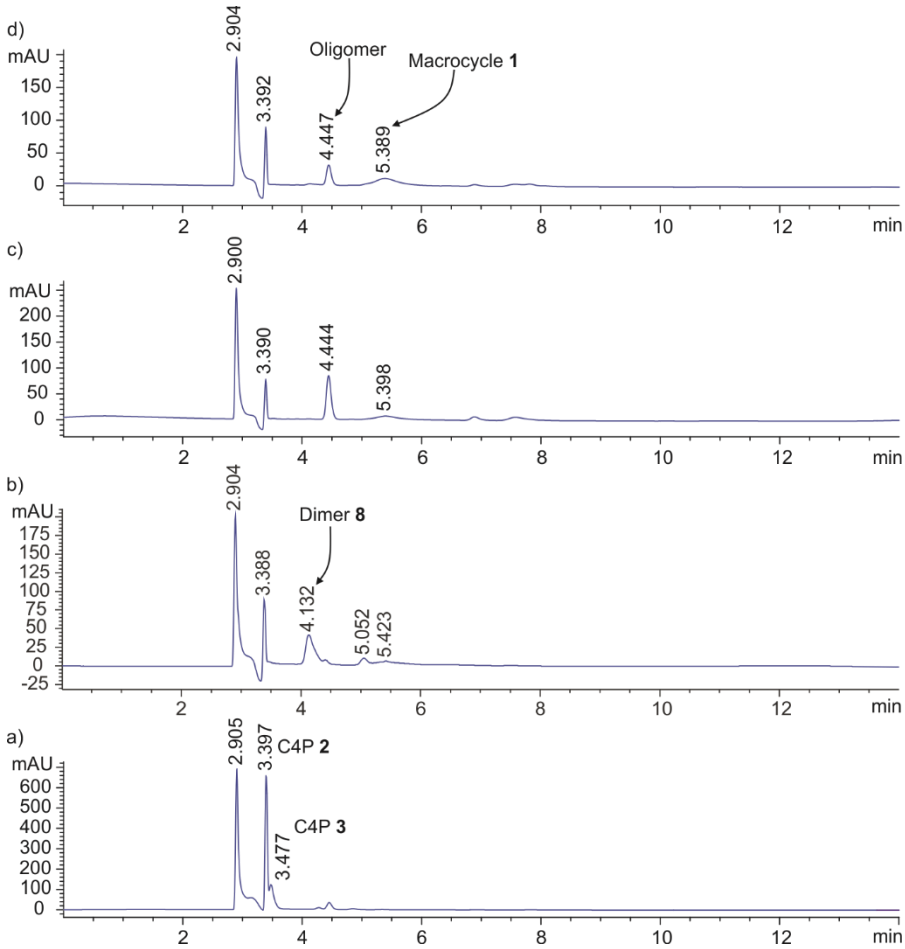

Figure 2.45. HPLC traces of the analysis of the aliquots extracted from the CuAAC reaction of an equimolar mixture of C4P **2** and **3** and TPH **4**. The aliquots were taken before the addition of the copper catalyst a) and 5 min. b) 2 hours (c) and 4 hours (d) after the addition of the copper catalyst. Some relevant signals are assigned.

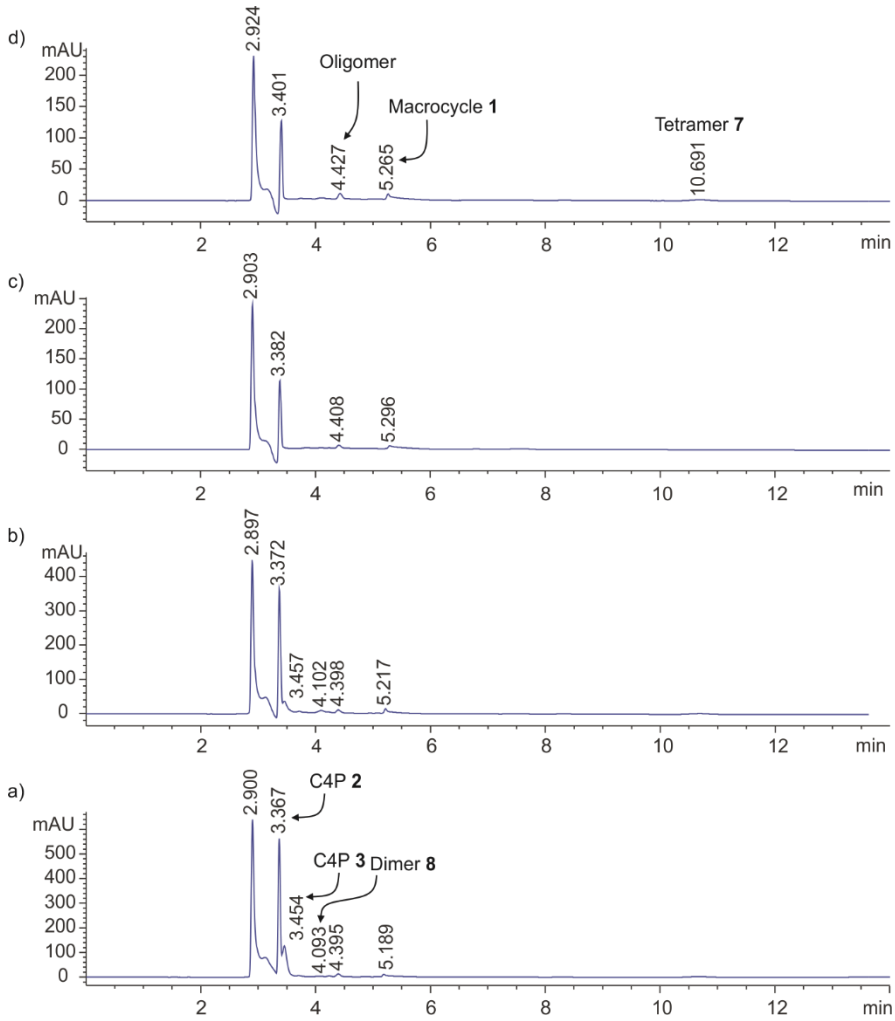

Figure 2.46. HPLC traces of the analysis of the aliquots extracted from the CuAAC reaction of an equimolar mixture of C4P **2** and **3** and BPNOx **5**. The aliquots were taken before the addition of the copper catalyst a) and 5 min. b) 2 hours c) and 4 hours d) after the addition of the copper catalyst. Some relevant signals are assigned.

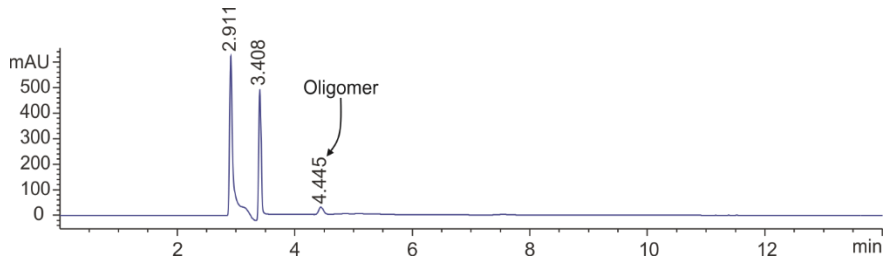

Figure 2.47. HPLC trace of the analysis of the crude obtained in the CuAAC reaction between C4P **2** and **3** in the presence of BPNOx **5**.

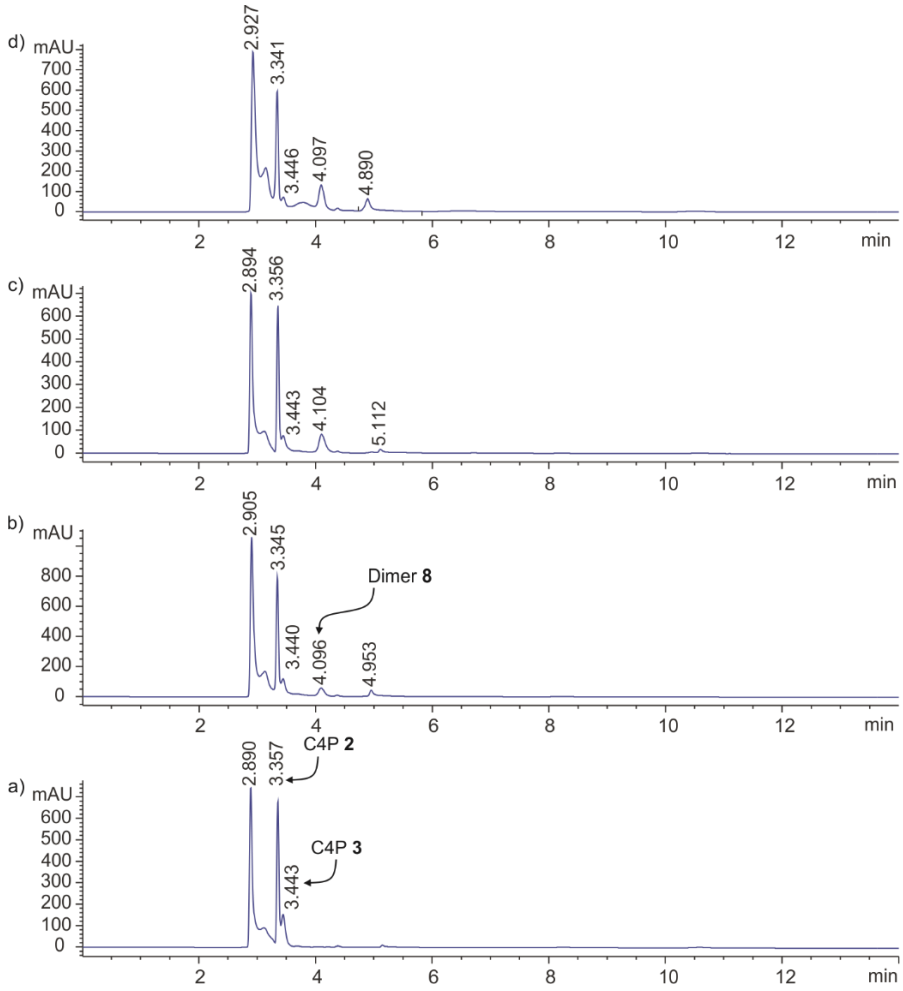

Figure 2.48. HPLC traces of the analysis of the aliquots extracted from the CuAAC reaction of an equimolar mixture of C4P **2** and **3**. The aliquots were taken before the addition of the copper catalyst a) and 5 min. b) 2 hours c) and 4 hours d) after the addition of the copper catalyst. Some relevant peaks are assigned.

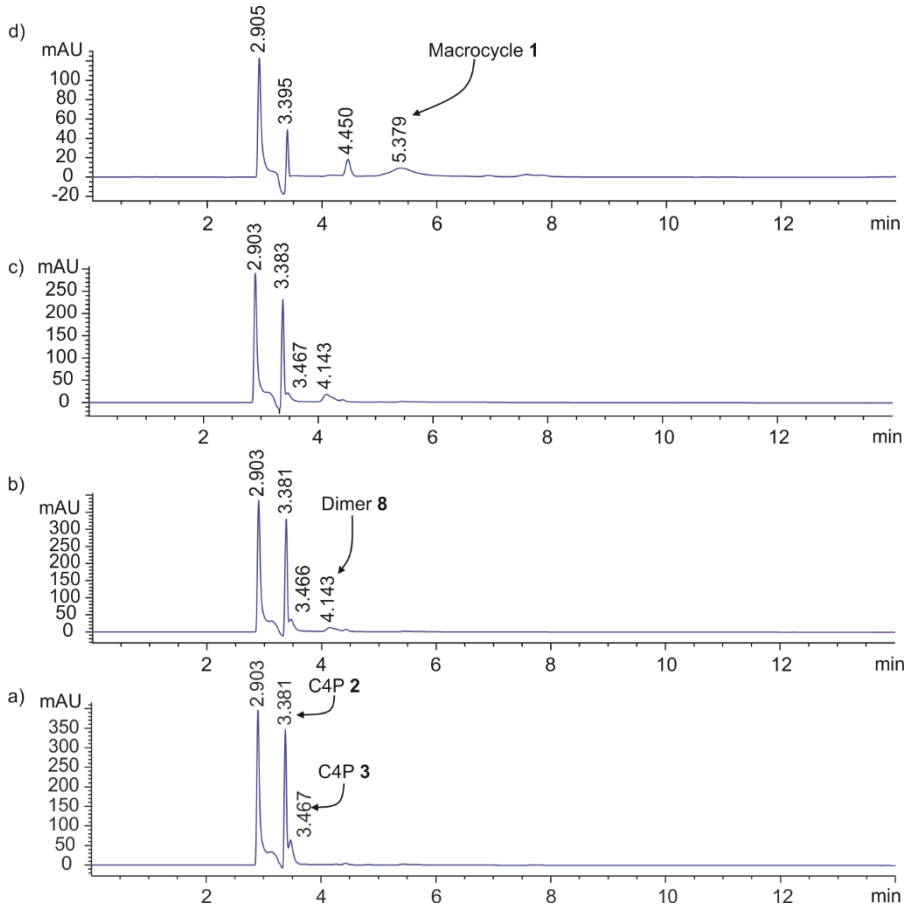

Figure 2.49. HPLC traces of the analysis of the aliquots extracted from the CuAAC reaction of an equimolar mixture of C4P **2** and **3**. The aliquots were taken before the addition of the copper catalyst a) and 5 min. b) and one hour c) after the addition of the catalyst. One additional aliquot was taken and analysed after the addition of one equivalent of TPH **4** d). Some relevant signals are assigned.

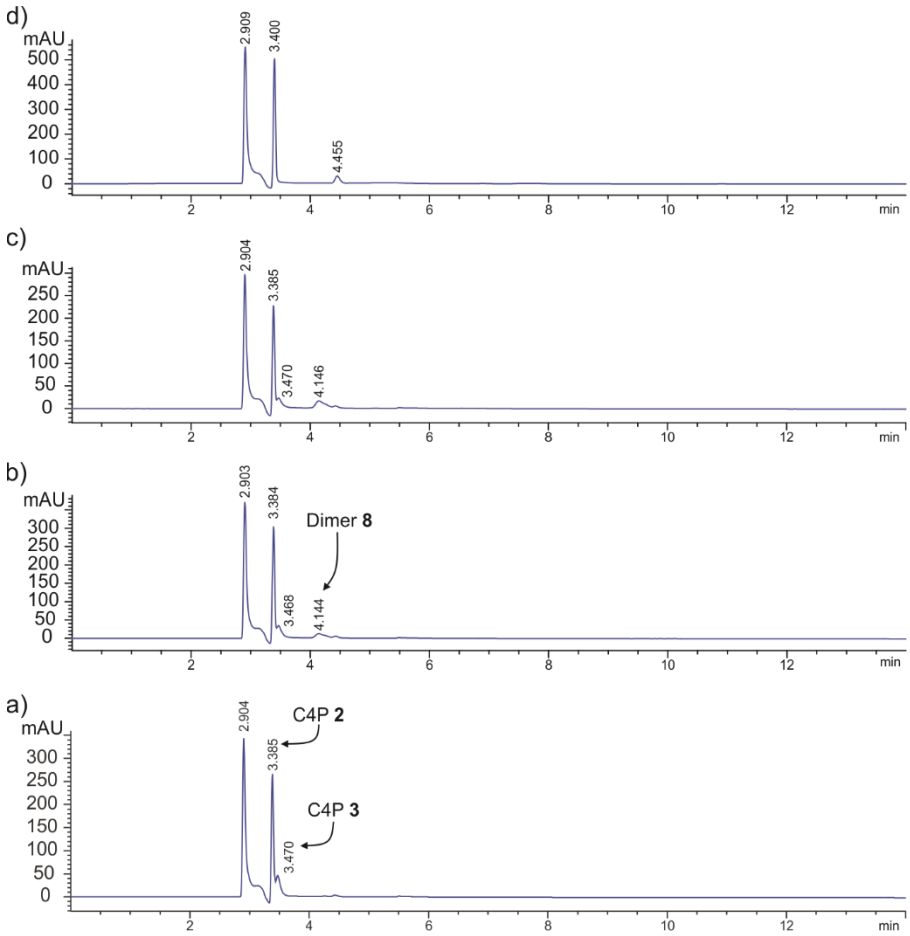

Figure 2.50. HPLC traces of the analysis of the aliquots extracted from the CuAAC reaction of an equimolar mixture of C4P **2** and **3**. The aliquots were taken before the addition of the copper catalyst a) and 5 min. b) and one hour c) after the addition of the catalyst. One additional aliquot was taken and analysed after the addition of one equivalent of BPNOx **5** d). Some relevant signals are assigned.

2.5. References and notes

[1] Wasserman, E., The preparation of interlocking rings: a catenane. *J. Am. Chem. Soc.* **1960,** *82* (16), 4433-4434.
[2] Agam, G.; Graiver, D.; Zilkha, A., Studies on the formation of topological isomers by statistical methods. *J. Am. Chem. Soc.* **1976,** *98* (17), 5206-5214.
[3] Pedersen, C. J., The Discovery of Crown Ethers (Noble Lecture). *Angew. Chem. Int. Ed.* **1988,** *27* (8), 1021-1027.
[4] Anderson, S.; Anderson, H. L.; Sanders, J. K. M., Expanding roles for templates in synthesis. *Acc. Chem. Res.* **1993,** *26* (9), 469-475.
[5] Furlan, R. L. E.; Otto, S.; Sanders, J. K. M., Supramolecular templating in thermodynamically controlled synthesis. *Proc. Natl. Acad. Sci. U. S. A.* **2002,** *99* (8), 4801-4804.
[6] Anderson, S. A., H. L., Templates in Organic Synthesis: Definitions and Roles. In *Templated Organic Synthesis*, 1999; pp 1-38.
[7] Laughrey, Z. R.; Gibb, B. C., Macrocycle Synthesis Through Templation. In *Templates in Chemistry II*, Schalley, C. A.; Vögtle, F.; Dötz, K. H., Eds. Springer Berlin Heidelberg: Berlin, Heidelberg, 2005; pp 67-125.
[8] Martí-Centelles, V.; Pandey, M. D.; Burguete, M. I.; Luis, S. V., Macrocyclization Reactions: The Importance of Conformational, Configurational, and Template-Induced Preorganization. *Chem. Rev.* **2015,** *115* (16), 8736-8834.
[9] Hamdan, F.; Tahoori, F.; Balalaie, S., Synthesis of novel cyclopeptides containing heterocyclic skeletons. *RSC Adv.* **2018,** *8* (59), 33893-33926.
[10] Ramos, S.; Alcalde, E.; Doddi, G.; Mencarelli, P.; Pérez-García, L., Quantitative Evaluation of the Chloride Template Effect in the Formation of Dicationic [14]Imidazoliophanes. *J. Org. Chem.* **2002,** *67* (24), 8463-8468.
[11] Gunter, M. J.; Farquhar, S. M., Neutral π-associated porphyrin [2]catenanes. *Org. Biomol. Chem.* **2003,** *1* (19), 3450-3457.
[12] Fischer, M.; Höger, S., Synthesis of a Shape-Persistent Macrocycle with Intraannular Sulfonate Groups. *Eur. J. Org. Chem.* **2003,** *2003* (3), 441-446.
[13] Bols, P. S.; Anderson, H. L., Template-Directed Synthesis of Molecular Nanorings and Cages. *Acc. Chem. Res.* **2018,** *51* (9), 2083-2092.
[14] Bols, P. S.; Rickhaus, M.; Tejerina, L.; Gotfredsen, H.; Eriksen, K.; Jirasek, M.; Anderson, H. L., Allosteric Cooperativity and Template-Directed Synthesis with Stacked Ligands in Porphyrin Nanorings. *J. Am. Chem. Soc.* **2020,** *142* (30), 13219-13226.
[15] Valderrey, V.; Escudero-Adán, E. C.; Ballester, P., Highly Cooperative Binding of Ion-Pair Dimers and Ion Quartets by a Bis(calix[4]pyrrole) Macrotricyclic Receptor. *Angew. Chem. Int. Ed.* **2013,** *52* (27), 6898-6902.
[16] Valderrey, V.; Escudero-Adán, E. C.; Ballester, P., Polyatomic Anion Assistance in the Assembly of [2]Pseudorotaxanes. *J. Am. Chem. Soc.* **2012,** *134* (26), 10733-10736.
[17] Saha, I.; Lee, J. H.; Hwang, H.; Kim, T. S.; Lee, C.-H., Remarkably selective, non-linear allosteric regulation of anion binding by a tetracationic calix[4]pyrrole homodimer. *Chem. Commun.* **2015,** *51* (26), 5679-5682.
[18] He, Q.; Kelliher, M.; Bähring, S.; Lynch, V. M.; Sessler, J. L., A Bis-calix[4]pyrrole Enzyme Mimic That Constrains Two Oxoanions in Close Proximity. *J. Am. Chem. Soc.* **2017,** *139* (21), 7140-7143.

[19] Xiong, S.; Chen, F.; Zhao, T.; Li, A.; Xu, G.; Sessler, J. L.; He, Q., Selective Inclusion of Fluoride within the Cavity of a Two-Wall Bis-calix[4]pyrrole. *Org. Lett.* **2020,** *22* (11), 4451-4455.
[20] Peng, S.; He, Q.; Vargas-Zúñiga, G. I.; Qin, L.; Hwang, I.; Kim, S. K.; Heo, N. J.; Lee, C.-H.; Dutta, R.; Sessler, J. L., Strapped calix[4]pyrroles: from syntheses to applications. *Chem. Soc. Rev.* **2020,** *49* (3), 865-907.
[21] Rather, I. A.; Wagay, S. A.; Hasnain, M. S.; Ali, R., New dimensions in calix[4]pyrrole: the land of opportunity in supramolecular chemistry. *RSC Adv.* **2019,** *9* (66), 38309-38344.
[22] Adriaenssens, L.; Estarellas, C.; Vargas Jentzsch, A.; Martinez Belmonte, M.; Matile, S.; Ballester, P., Quantification of Nitrate–π Interactions and Selective Transport of Nitrate Using Calix[4]pyrroles with Two Aromatic Walls. *J. Am. Chem. Soc.* **2013,** *135* (22), 8324-8330.
[23] Xu, L.; Li, Y.; Li, Y., Application of "Click" Chemistry to the Construction of Supramolecular Functional Systems. *Asian J. Org. Chem.* **2014,** *3* (5), 582-602.
[24] Liang, L.; Astruc, D., The copper(I)-catalyzed alkyne-azide cycloaddition (CuAAC) "click" reaction and its applications. An overview. *Coord. Chem. Rev.* **2011,** *255* (23), 2933-2945.
[25] Meldal, M.; Tornøe, C. W., Cu-Catalyzed Azide–Alkyne Cycloaddition. *Chem. Rev.* **2008,** *108* (8), 2952-3015.
[26] The energy-minimized structure was obtained using the software package Fujitsu Scigress Version 2.2.0. The structure was optimized by performing a geometry calculation using the implemented molecular mechanics force field with augmented MM3 parameters.
[27] Escobar, L.; Aragay, G.; Ballester, P., Super Aryl-Extended Calix[4]pyrroles: Synthesis, Binding Studies, and Attempts To Gain Water Solubility. *Chem.--Eur. J.* **2016,** *22* (38), 13682-13689.
[28] Moncelsi, G.; Escobar, L.; Dube, H.; Ballester, P., 2-(4'-Pyridyl-N-oxide)-Substituted Hemithioindigos as Photoresponsive Guests for a Super Aryl-Extended Calix[4]pyrrole Receptor. *Chem.--Asian J.* **2018,** *13* (12), 1632-1639.
[29] Peñuelas-Haro, G.; Ballester, P., Efficient hydrogen bonding recognition in water using aryl-extended calix[4]pyrrole receptors. *Chem. Sci.* **2019,** *10* (8), 2413-2423.
[30] Gagliardi, L. G.; Castells, C. B.; Ràfols, C.; Rosés, M.; Bosch, E., Static Dielectric Constants of Acetonitrile/Water Mixtures at Different Temperatures and Debye–Hückel A and a0B Parameters for Activity Coefficients. *J. Chem. Eng. Data* **2007,** *52* (3), 1103-1107.
[31] The energy-minimized structure was obtained using the software package Fujitsu Scigress Version 2.2.0. The structure was optimized by performing a geometry calculation using the implemented molecular mechanics force field with augmented MM3 parameters.
[32] Galán, A.; Aragay, G.; Ballester, P., A chiral "Siamese-Twin" calix[4]pyrrole tetramer. *Chem. Sci.* **2016,** *7* (9), 5976-5982.
[33] We did not observe formation of tetrameric receptor **7** using these conditions.
[34] The absence of the signal corresponding to the tetraolygomeric product is attributed to the low concentration of the aliquot analyzed in the HPLC system.
[35] Jorgensen, W. L.; Gao, J., Cis-trans energy difference for the peptide bond in the gas phase and in aqueous solution. *J. Am. Chem. Soc.* **1988,** *110* (13), 4212-4216.
[36] Martínez, A. G.; Vilar, E. T.; Fraile, A. G.; Martínez-Ruiz, P., A Computational and Experimental Study on the Relative Stabilities of Cis and Trans Isomers of N-Alkylamides in Gas Phase and in Solution. *J. Phys. Chem. A* **2002,** *106* (19), 4942-4950.
[37] Stewart, W. E.; Siddall, T. H., Nuclear magnetic resonance studies of amides. *Chem. Rev.* **1970,** *70* (5), 517-551.

[38] Li, Y.-S.; Escobar, L.; Zhu, Y.-J.; Cohen, Y.; Ballester, P.; Rebek, J.; Yu, Y., Relative hydrophilicities of cis and trans formamides. *Proc. Natl. Acad. Sci. U. S. A* **2019,** *116* (40), 19815.
[39] Escobar, L.; Díaz-Moscoso, A.; Ballester, P., Conformational selectivity and high-affinity binding in the complexation of N-phenyl amides in water by a phenyl extended calix[4]pyrrole. *Chem. Sci.* **2018,** *9* (36), 7186-7192.

UNIVERSITAT ROVIRA I VIRGILI
Calix[4]pyrrole Based Receptors for the Recognition of Ion Pairs
Ricardo Molina Muriel

Binding of ion-pairs by a bis(calix[4]pyrrole) receptor

Part of this chapter has been published in:

Molina-Muriel, R.; Aragay, G.; Escudero-Adán, E.; Ballester, P., *J. Org. Chem.* **2018**, *83*, 21, 13507–13514

UNIVERSITAT ROVIRA I VIRGILI
Calix[4]pyrrole Based Receptors for the Recognition of Ion Pairs
Ricardo Molina Muriel

3.1. Introduction

In recent decades, the field of supramolecular chemistry has witnessed increasing interest in ion recognition processes. This is due to the essential role that ions play in biology, chemistry and the environment.[1,2] The coordination of cationic species dominated the field in the early days of this research area, owing to the less demanding characteristics of the guests (size, structure and solvation energy). A myriad of synthetic receptors were disclosed capable of cation binding, most of them based on crown-ethers derivatives.[3] The design of synthetic anion receptors, however, progressed at a slower pace owing to the vast variety in size and shape of anionic species. Nevertheless, intense efforts are still invested on the synthesis of anion receptors due to its increasing presence in modern societies, i.e. nuclear waste and fertilizers.[4,5,6] Receptors able to bind both anions and cations at the same time evolved from the combination of both fields. Heteroditopic receptors feature binding sites directed to coordinate anions and cations concomitantly with greater affinity and selectivity than its monotopic analogues.[7,8,9,10] However, heteroditopic receptors come with an increased synthetic cost and a complex design inherent to its structural properties.[11,12] The final aim of these receptors is to mimic naturally occurring receptors such as proteins and disentangle the nature of its ion pair binding properties.[13,14]

Calix[4]pyrrole (C4P) are efficient heteroditopic receptors for ion pair binding in both wet and organic media.[15,16,17,18] The four converging NH groups of the receptor's cone conformation create an ideal binding site for anions and electron-rich neutral molecules. At the same time, the pyrrole rings in cone conformation define a shallow and electron rich cavity opposite to the bound anion that is optimal for cation binding through establishment of cation-π interactions mainly.[19,20] In this vein, we were interested in evaluating the properties of the macrocyclic bis-calix[4]pyrrole receptor **1** to coordinate ion pairs dimers (**Scheme 3.1**).

Bis(calix[4]pyrrole) (B4CP) receptors are well known for their ability to bind charged species. Recent work from the groups of Sessler, He and Lee showed the capabilities of these receptors to coordinate anions and ion dimers with high selectivity and affinity.[14,21,22] In previous years, we disclosed our investigations on the binding of tetraalkylammonium salts **2a-c** in $CDCl_3$ by BC4P receptor **3**, bearing two 1,3-diynyl spacers.[23,24] Receptor **3** formed 1:2 complexes with alkylammonium salts **2b** and **2c** by means of highly cooperative binding processes. Interestingly, the formed complexes featured cascade arrangements of close contact ion triplets. One of the

TBA^+ cations was sandwiched between the two bound anions (Cl^- or OCN^-) stabilized by electrostatic interactions. The other TBA^+ cation was bound in the aromatic cavity of the C4P, opposite to the bound anion, displaying a receptor-separated binding mode. On the other hand, using MTOA·Cl (**2a**) we obtained a 2:1 complex, (**2a**)$_2$⊂**3**, featuring a receptor-separated binding mode geometry for the two bound ion pairs. Moreover, the binding process showed no signs of cooperativity.

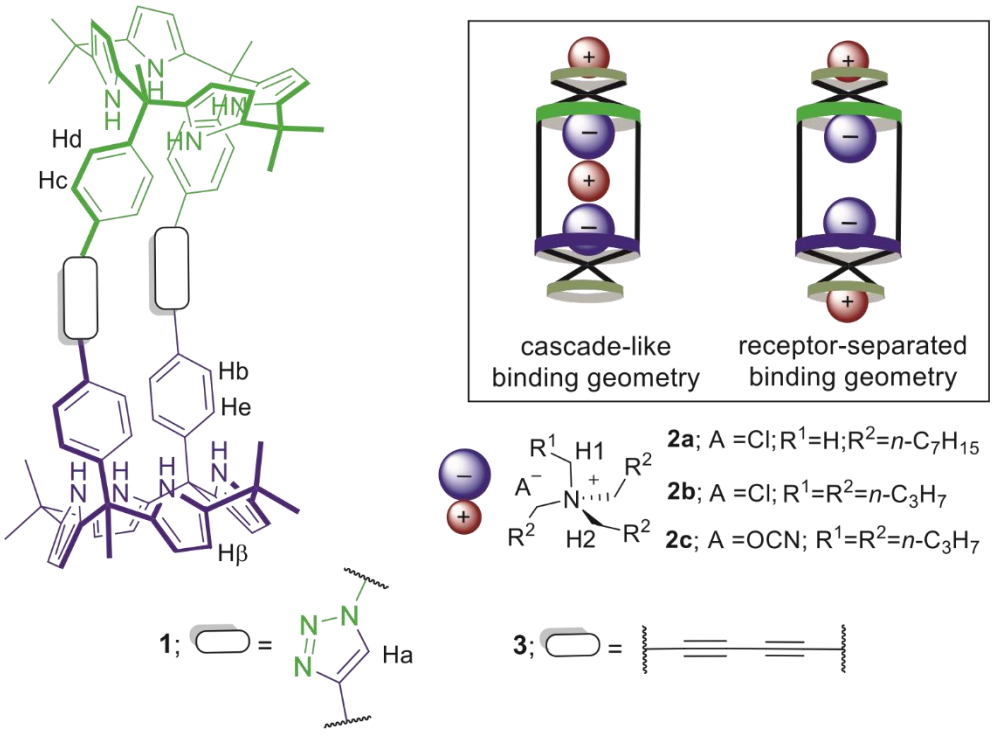

Scheme 3.1. Molecular structures of bis(calix[4]pyrrole) macrocycles **1** and **3** and the ion pairs used in the binding studies. Schematic representations of 2:1 binding geometries (inset).

We disclosed in the previous chapter the synthesis of a BC4P macrocycle obtained by the CuAAC coupling reaction of two C4P units, receptor **1**. We also described the ^{1}H NMR binding studies towards a series of ditopic guests, showing the ability of the receptor to generate thermodynamically and kinetically stable 1:1 complexes. In this chapter, we report the binding studies of receptor **1** towards tetraalkylammonium salts **2a-c**. We envisaged that BC4P **1** would be suitable for the generation of ion-triplet cascade complexes in solution owing to the proximity of its two binding sites. In addition, the reduced dimensions of receptor **1** compared to its analogue **3** may result in a different selectivity and cooperativity for the binding of ion-pair dimers. The binding of ion pairs will be probed by ^{1}H NMR titrations. The thermodynamic

parameters of the complexes will be measured by ITC experiments. Additionally, ESI-MS experiments will provide information on the stabilities of the complexes in the gas-phase.

3.2. Results and discussion

3.2.1. ^{1}H NMR binding studies with tetraalkylammonium salts **2a-c**

Despite the apparent structural similarities, BC4P **1** and its 1,3-diynyl analogue **3** present clear structural differences that will affect the binding affinity towards ion pairs **2a-c**. Macrocycle **1** presents a reduced cavity size compared to that of receptor **3**. Indeed, the N···N distance from the two distant C4P units is reduced by approximately 3 Å for receptor **1** compared to **3**. In addition, the bent shape of BC4P **1** for the Cv symmetry conformer that is generated by the 1,4-substitution on the triazole spacer, contrasts with the lineal arrangement of receptor **3**. Nevertheless, the C2 symmetry conformer of **1** also displays a lineal arrangement of the two binding sites (see Experimental Section). The triazole substitution generates also two inequivalent hemispheres with dissimilar binding sites, in contrast with the two identical binding sites displayed by **3**.

The ^{1}H NMR titration experiments were performed in chloroform solution at millimolar concentrations. It is known that in non-polar solvents C4P receptors generate ion-paired complexes with alkylammonium halide ion-pairs. The formed complexes display a receptor-separated binding geometry. The anion is coordinated to the four NHs of the calix[4]pyrrole core in the cone conformation. A suitable sized alkylammonium cation is included in the electron rich aromatic cavity defined by the pyrrole rings of the cone conformer, which is opposite to the bound anion. Additionally, C4P receptors present higher affinity towards the salts containing $MTOA^+$ cations compared to the TBA^+ counterparts. This is due to the better fit of the methyl group of the $MTOA^+$ cation in the electron-rich aromatic cavity of the C4P that is defined by the pyrrole rings in cone conformation.[25,26,27]

<u>Binding studies with methyltrioctylammonium chloride **2a**</u>

The ^{1}H NMR spectrum of a 2 mM solution in $CDCl_3$ of receptor **1** showed sharp and well-defined proton signals that are in agreement with C_2 and C_v symmetry (**Figure 3.1**). Most likely, in solution receptor **1** exists as a mixture of two conformers displaying a fast exchange on the proton ^{1}H NMR chemical shift timescale. The addition of 0.5 equivalent of MTOA·Cl produced the appearance of a new set of

sharp signals that were primarily assigned to receptor **1** in a complex of unknown stoichiometry with **2a**. Subsequent addition of **2a** provoked the increase in intensity of the new set of signals at the expenses of those associated with the free receptor. When an equimolar ratio of **1** and **2a** was reached only the set of signals assigned to the complex was observed. Interestingly, we noticed that one of the signals attributed to the NHs in receptor **1** shifted downfield to δ = 11.2 ppm while the other remained centered at δ = 7.1 ppm. These findings suggest that the chloride anion is bound exclusively to one of the two non-equivalent binding sites of receptor **1** through hydrogen bonding interactions with the pyrrole NHs. In addition, the proton signal associated with the methyl group of the $MTOA^+$ cation (H1) resonated at δ = 0.1 ppm while the one assigned to the methylene group *alpha* to the nitrogen atom (H2) appeared at δ = 2.0 ppm. The upfield shift experienced by these two signals with respect to its free counterpart ($\Delta\delta$ = -3.3 and -1.4 ppm, respectively) is indicative of its inclusion in the electron-rich aromatic cup of the C4Pin a 1:1 complex displaying receptor-separated geometry.

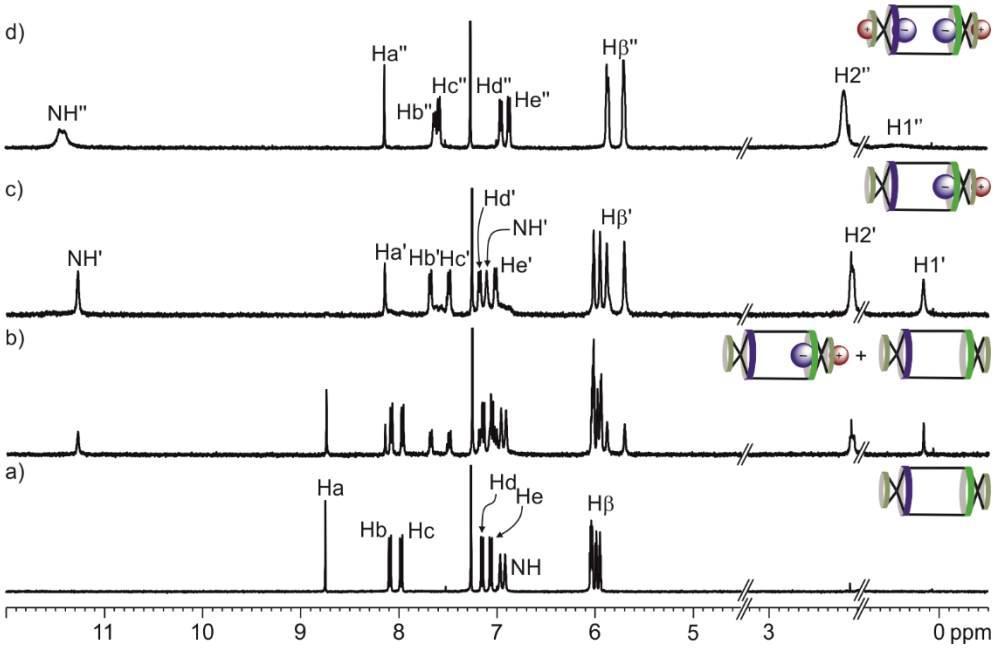

Figure 3.1. Selected region of the ^1H NMR spectra (400 MHz, $CDCl_3$, 298 K) of free receptor **1** (2 mM) (a) and incremental additions of MTOA·Cl (**2a**): 0.5 equivalent (b), 1.0 equivalent (c), and 2.0 equivalent (d). Primed letters correspond to **2a**⊂**1**, and double primed letters correspond to (**2a**)$_2$⊂**1**. See Scheme 3.1 for proton assignment.

In order to investigate the binding selectivity of the receptor, we performed DFT calculations (B3LYP/6-31G*) to assess the molecular electrostatic potential (MEP) at the center of the aromatic ring of the *meso*-aromatic substituent. The MEP value is related to the strength of interaction of a proton with the electron density of the molecule. As a rule of thumb, a negative value of the MEP corresponds to a repulsive interaction with an anion. The more negative the value is the more repulsive the interaction results, thus the energetic stability of the putative complex decreases. The DFT calculations assigned a MEP value at the center of the phenyl ring of the 4-methyl-1-*N*-phenyl-1,2,3-triazole and 1-methyl-4-*C*-phenyl-1,2,3-triazole of -11 and -19 kcal/mol, respectively (see Experimental Section). Thus, the chloride anion will preferentially bind the "two wall" aryl-extended C4P attached to the triazole ring through the nitrogen atom (*N*-substituted) than the one attached at the sp^2 carbon (*C*-Substituted).

Addition of more than 1 equivalent of MTOA·Cl produced the appearance of a new set of proton signals assigned to another complex of unknown stoichiometry. Incremental addition of **2a** provoked the increase in intensity of the new signals at the expenses of the original ones. When 2 equivalent were added, the second set of proton signals was the only one detected. At this point in the titration, two signals attributed to the NHs binding the Cl^- anion were detected at δ = 11.39 and 11.30 ppm, suggesting the formation of a 2:1 complex, (**2a**)$_2$⊂**1**. Addition of an excess of the MTOA·Cl salt did not produce additional changes in the signals associated to the bound receptor in the 2:1 complex. However, the proton signal assigned to the methyl group of the $MTOA^+$ cation (H1) experienced a dramatic broadening. We interpreted this observation as a result of the existence of a chemical exchange process between the bound and free $MTOA^+$ cation that showed intermediate dynamics on the ^{1}H NMR chemical shift timescale. Due to the increased amount of free $MTOA^+$ cation, the signal of the methyl group experiencing the intermediates exchange moved downfield towards the chemical shift value of the free cation.

Taken together, these results indicated the initial formation of a 1:1 complex. This complex was quantitatively formed when the equimolar ratio between receptor **1** and MTOA·Cl **2a** was reached. Complex **2a**⊂**1** displays a receptor-separated binding geometry with the chloride anion bound exclusively in the *N*-substituted hemisphere of receptor **1**. The complex experiences a slow exchange in the ^{1}H NMR chemical shift timescale with its free components, which may be also indicative of its high thermodynamic stability. Indeed, as the 1:1 complex is the only species

observed in the equimolar mixture of **2a** and **1**, we estimate the binding affinity constant as K[**2a**⊂**1**] > 10^4 M^{-1}.

The new set of proton signals that appeared after addition of more than 1 equivalent was attributed to the (**2a**)$_2$⊂**1** complex. As the concomitant formation of the two complexes was not observed in the early stages of the titration, we conclude that there is a large difference in the binding affinity constant for chloride between the two anionic binding sites of **1**. Moreover, the quantitative formation of (**2a**)$_2$⊂**1**after the addition of 2 equivalent of **2a** indicates that the overall binding affinity constant for the complex can be estimated as K[(**2a**)$_2$⊂**1**] > 10^8 M^{-2} . After addition of more than **1** equivalent of **2a**, we did not observed chemical shift changes in the signals assigned to the bound $MTOA^+$ cation (H1 and H2). This result supports that the binding of the second ion pair also takes place in a receptor-separated binding geometry. The methyl groups of the two bound $MTOA^+$ cations in the (**2a**)$_2$⊂**1** complex are included in the distal electron rich aromatic cups of the two different C4P binding units of **1**. However, they resonate as a single and highly upfield shifted broad singlet. We suggest that the two C4P cups provide similar magnetic environments.

In order to provide additional evidence for the receptor-separated binding geometry of the two ion-pairs involved in the (**2a**)$_2$⊂**1** complex, we performed a ROESY experiment using a solution containing a 2:1 mixture of **2a** and receptor **1** at mM concentrations (**Figure 3.2**). At this concentration and working under strict stoichiometric control the (**2a**)$_2$⊂**1** complex is quantitatively formed. We observed cross-peaks related to proximity in space between the proton signals assigned to the $MTOA^+$ cation and those associated with the β-pyrrole protons of **1**. At the same time, no cross-peaks were detected between the protons of the aromatic walls of **1** and those of the bound $MTOA^+$ cations. These observations are in agreement with the formation of a receptor-separated complex. The X-Ray diffraction analysis of a single crystal of the (**2a**)$_2$⊂**1** complex, which was grown by slow evaporation of a 1,2-difluorobenzene solution, also evidenced the receptor-separated binding geometry of the ion-pairs in the solid state.[28] The measured $Cl^-\cdots Cl^-$ atom distance in the crystal structure is 8.8 Å. This distance is too short for sandwiching the $MTOA^+$ cation between the two anions. However, the inclusion of an alkyl or methyl substituent between them is feasible (*vide infra*). Nevertheless, in the solid state, two molecules of solvent occupy the space between the two bound anions in the (**2a**)$_2$⊂**1** complex The receptor displays a *trans* geometry with respect to the two

triazole spacers, with the hydrogen attached to the sp^2 carbon atoms opposite to each other (**Figure 3.3**).

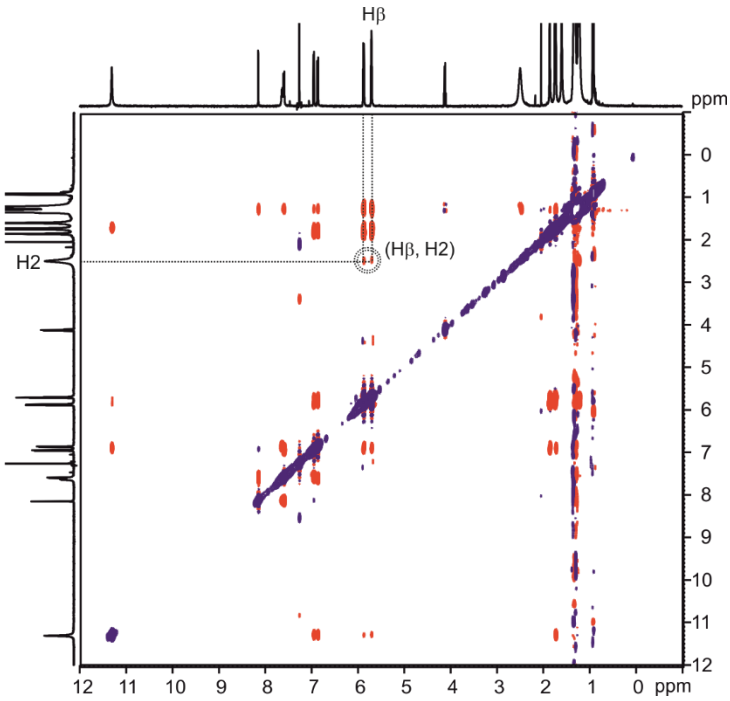

Figure 3.2. ^{1}H-^{1}H ROESY experiment (500 MHz, $CDCl_3$, 298 K, spin-lock = 0.3 s) of a 2:1 mixture of receptor **1** and MTOA·Cl (**2a**). Cross peaks between the *β*-pyrrole protons (Hβ) and the proton *alpha* to the nitrogen atom in the $MTOA^+$ cation (H2) are marked.

Binding studies with tetrabutylammonium salts **2b-c**

We moved next to the study of the binding affinity of receptor **1** towards the tetrabutylammonium salts of Cl^- (**2b**) and OCN^- (**2c**).

The addition of 0.5 equivalent of TBA·Cl to a 2 mM solution of macrocycle **1** in $CDCl_3$ produced broadening and upfield shift to all the proton signals of the free receptor (**Figure 3.4**). More precisely, the signal assigned to the NHs of the receptor broadened beyond detection. Concomitantly, we observed the appearance of a new set of signals that were assigned to the protons of the bound receptor in a complex of unknown stoichiometry. In the downfield region of the spectrum, we detected two signals resonating at δ = 11.3 and 11.45 ppm. We assigned these signals to the NH protons of the bound receptor in the newly formed complex. The methylene protons *alpha* to the nitrogen atom in the TBA^+ cation (H1) resonated at δ = 2.6 ppm.

This value represents an upfield shift ($\Delta\delta$ = -0.7 ppm) in comparison to the analogous signal in the free TBA^+ cation. This observation is indicative of the involvement of the TBA^+ cation in the binding process. The incremental addition of TBA·Cl produced an increase in intensity of the new set of signals to the expenses of those displaying broadening and upfield shift. When 2 equivalent of the ion pair were added, only the new set of signals was detected in the ^{1}H NMR spectrum of the mixture.

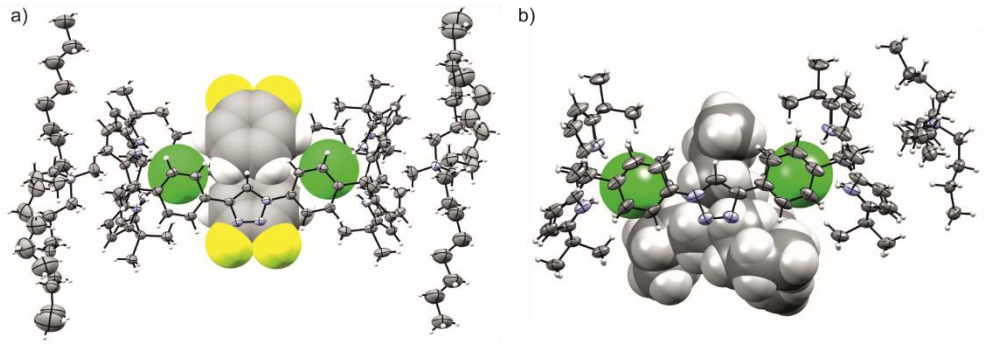

Figure 3.3. X-ray structure of the (**2a**)$_2$⊂**1** (a) and (**2b**)$_2$⊂**1** (b) complexes. Receptor **1**, $MTOA^+$ cation and "out" TBA^+ cation are shown as ellipsoids at 50% probability level and hydrogens as fixed-size spheres with a radius of 0.15 Å. Included chloride anions, solvent molecules and "in" TBA^+ cation are displayed as CPK representations.

Taken together, these results suggest the initial formation of a 1:1 complex, **2b**⊂**1**, which experiences a chemical exchange with the free counterparts in a dynamic range that is intermediate on the ^{1}H NMR chemical shift timescale. Almost concomitantly, a second complex is formed and produces a separate set of proton signals for the bound receptor. We assigned a 2:1 stoichiometry to this complex, (**2b**)$_2$⊂**1.** The pyrrole NHs of the (**2b**)$_2$⊂**1** complex resonate as two separate singlets in the downfield region of the ^{1}H NMR spectrum. The high downfield shift experienced by these protons is due to hydrogen bonding coordination with chloride anions. The NHs of the two anion binding sites of **1** are chemically non-equivalent and produce separate signals both in the free and bound states.

Considering that both complexes **2b**⊂**1** and (**2b**)$_2$⊂**1** were detected in solution in the early phases of the titration, we consider that the stepwise binding constants for the formation of the (**2b**)$_2$⊂**1** complex should be of the same order of magnitude. When 2 equivalent of TBA·Cl were added to the solution, the (**2b**)$_2$⊂**1** complex was exclusively observed. This result indicates that a global stability constant can be estimated as K[(**2b**)$_2$⊂**1**] > 10^8 M^{-2}. The obtained results are in striking contrast with those obtained for MTOA·Cl. Firstly, slow exchange dynamics ruled the binding

processes of both 1:1 and 2:1 complexes of MTOA·Cl with **1**. This observation supports a higher kinetic stability for the 1:1 complex of MTOA·Cl compared to that of TBA·Cl. In addition, the formation of the two complexes of **1** with MTOA·Cl was not concomitant. It followed a two-phase coordination process leading to a separate formation of the 1:1 and 2:1 under strict stoichiometric control. This behavior is consistent with the existence of a substantial difference between the magnitudes of the two stepwise binding affinity constants.

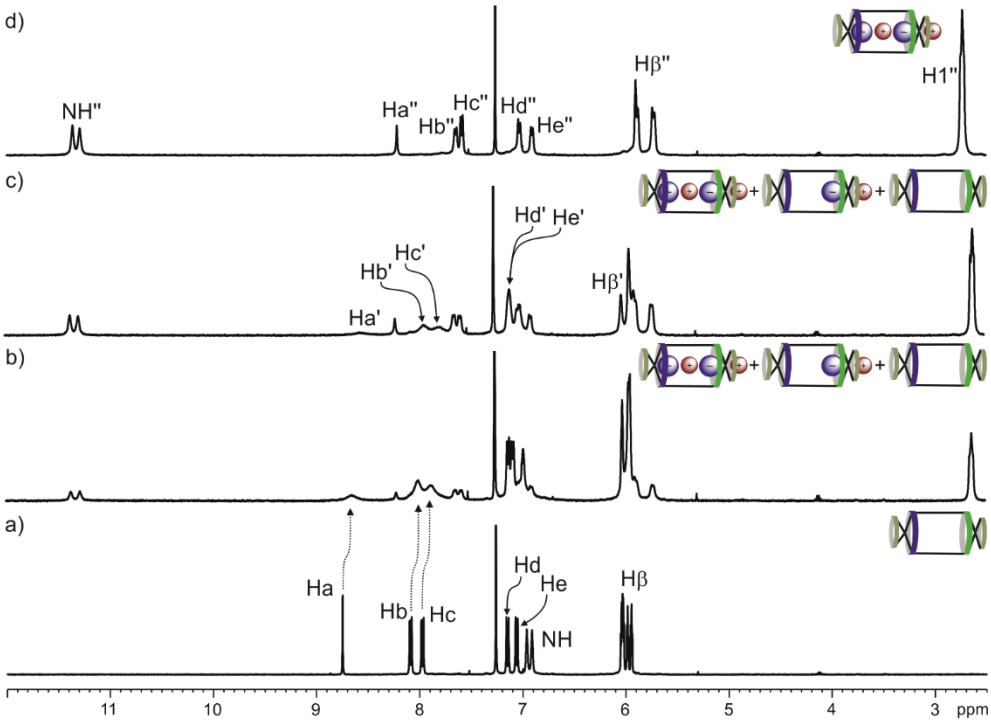

Figure 3.4. Selected region of the ^{1}H NMR spectra (400 MHz, $CDCl_3$, 298 K) of free receptor **1** (2 mM) (a) and incremental additions of TBA·Cl (**2b**): 0.5 equivalent (b), 1.0 equivalent (c), and 2.0 equivalent (d). Primed letters correspond to **2b**⊂**1**, and double primed letters correspond to (**2b**)$_2$⊂**1**. See Scheme 3.1 for proton assignment.

In the initial phase of the titration of **1** with TBA·Cl, i.e. up to the addition of 1 equivalent, the methylene protons *alpha* to the nitrogen atom of the cation (H1) gradually shifted upfield. We rationalize this behavior by the increase in concentration of bound TBA^+ in the 1:1 complex. In this complex, the bound TBA^+ is located in the aromatic cup opposite to the bound chloride of the C4P that is defined by the pyrrole rings. In this location, the H1 protons of TBA^+ experience the shielding effect produced by the pyrrole rings. The addition of more than 1 equivalent of TBA·Cl, **2b**, induced a downfield shift to the H1 signal. We attributed the change in

the chemical shift trend of H1 (biphasic behavior) to the formation of the 2:1 complex. As previously described for receptor **3**, we surmised that also for **1**, the TBA^+ cation of the second bound ion-pair is sandwiched between the two chloride ions included in the receptor's cavity. In short, the **(2b)$_2$⊂1** complex will display a cascade arrangement of an ion-triplet. The existence of a chemical exchange process, displaying fast dynamics on the ^{1}H NMR chemical shift timescale, between the sandwiched TBA^+ cation and other TBA cations included in the electron rich cavity defined by the pyrrole rings, either in the 1:1 or 2:1 complex, will explain the observed downfield shift for the TBA^+ signal when more than one equivalent of the salt is added to the receptor's solution.

We obtained similar results in the ^{1}H NMR titration experiments carried out with TBA·OCN **2c** (see Experimental Section). Further support for the formation of ion-paired cascade complexes **(2b)$_2$⊂1** and **(2c)$_2$⊂1** came from 2D ROESY experiments performed with separate solutions containing a 1:2 mixture of receptor **1** and the ion pairs **2b** and **2c**. Cross-peaks related to proximity in space were detected between the proton signals of the TBA^+ cation and the aromatic walls of the receptor, as well with its β-pyrrolic protons (**Figure 3.5**).

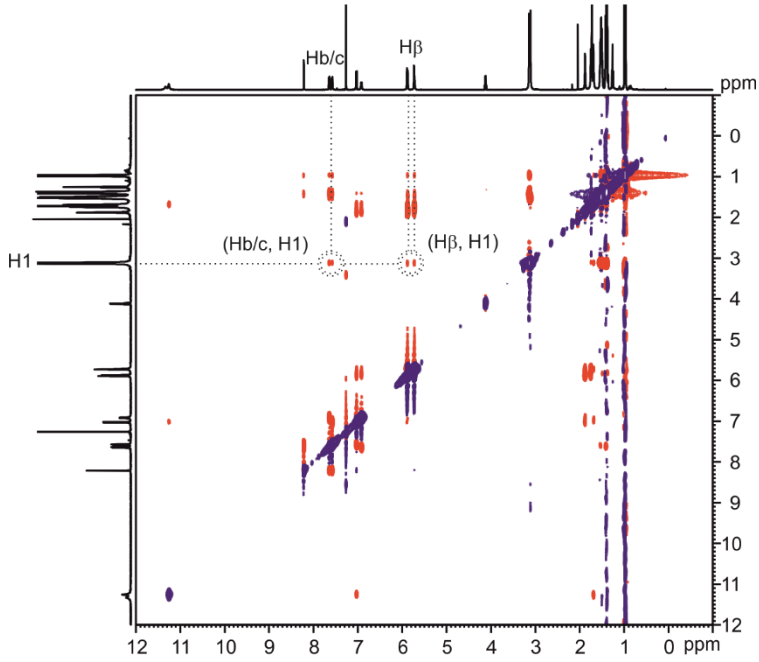

Figure 3.5. ^{1}H-^{1}H ROESY experiment (500 MHz, $CDCl_3$, 298 K, spin-lock = 0.3 s) of a 1:2 mixture of receptor **1** and TBA·Cl (**2b**). Cross peaks between the β-pyrrole protons (Hβ) and the proton *alpha* to the nitrogen atom in the TBA^+ cation (H1) are marked.

Single crystals grew from the slow evaporation of a solution in 1,3,5-trifluorobenzene containing a 1:2 molar ratio mixture of receptor **1** and **2b**. The X-ray structure of the (**2b**)$_2$⊂**1** complex revealed a cascade-like geometry of the ion-triplet in the solid state. This finding provided additional support to the proposed structure for the (**2b**)$_2$⊂**1** complex in solution, which was derived from the results of the ^{1}H NMR experiments performed in $CDCl_3$ (*vide supra*) (**Figure 3.3**). It is important to note, that we refer to the 2:1 complexes obtained with TBA^+, (**2b**)$_2$⊂**1** and (**2c**)$_2$⊂**1,** as displaying a "cascade-like" geometry. This is due to the partial inclusion of TBA^+ cation between the two anions of the ion trimer. In the case of the lineal and more symmetric receptor **3**, the 2:1 complexes obtained with TBA^+ displayed a perfect cascade geometry with the TBA^+ sandwiched and centered between the two chloride atoms. The greater inner volume of receptor **3** located the Cl^- anions in the 2:1 complexes 10.6 Å apart from each other with a Cl···N···Cl angle of 168°. In contrast, the complexes obtained with receptor **1** display a Cl···Cl distance 1.8 Å shorter, with a Cl···N···Cl angle of 123°. The reduced inner volume forces the TBA^+ cation to be partially sandwiched between the anions, with three of the four butyl chains protruding out of from the receptor. In this case, the receptor displays a *cis* geometry with respect to the triazole spacers (see Experimental Section).

3.2.2. Thermodynamic characterization of the ion-paired complexes formed with receptor **1** and the series of ion-pairs

We undertook ITC experiments in order to determine the thermodynamic parameters of the binding of the ion pairs **2a-c** by receptor **1**. In order to investigate the cooperativity of the binding event, if any, we wanted to compare the results obtained using receptor **1** with those obtained for the model receptors **4** and **5**. Receptors **4** and **5** are the analogous two-wall calix[4]pyrrole (2W-C4P) version of the two binding sites present in macrocycle **1** (**Figure 3.6**). C4P **4** is linked to the triazole unit trough a nitrogen atom while **5** is attached to a sp^2 triazole carbon atom. Along with the DFT calculations (*vide supra*), the binding studies of these receptors in chloroform will serve to disentangle the binding preference of ion pairs **2a-c** into each of the non-equivalent C4P binding sites of **1**. We determined the binding affinity constants of **4** and **5** towards MTOA·Cl **2c** using ITC experiments.[29] The data obtained were fit to a "one set of sites" theoretical binding model. The fits were good and returned the values for the binding affinity constants of K[**2a**⊂**4**] = 2.8 ± 0.5 × 10^4 M^{-1} and K[**2a**⊂**5**] = 6.5 ± 0.3 × 10^3 M^{-1} with an n value close to 1, as expected for the formation of 1:1 complexes. These results pointed out to a slightly

greater preference of **2a** towards the *N*-substituted C4P **4**. This preference can also be translated for the analogous binding site in receptor **1** over its *C*-substituted counterpart. We rationalize these results by invoking greater repulsive anion-π interactions for the chloride sandwiched between the more electron rich phenyl rings connected to the *p*-substituted triazole unit through the carbon atom instead of the nitrogen atom.[30,31]

Binding studies of receptor **1** with methyltrioctylammonium chloride **2a**

The sequential injection of a $CHCl_3$ solution of receptor **1** (8 mM) into a solution of ion pair **2a** (0.9 mM) produced a gradual release of heat. The normalized integrated values of the heat data displayed a binding isotherm with two noticeable inflection points, indicative of the existence of two distinct binding events. The inflection points were centered at a molar ratio **1**/**2a** of 0.5 and 1. Accordingly, the data obtained was fit to a theoretical binding model of two sequential binding sites using the Microcal ITC Data analysis module (**Figure 3.7**).

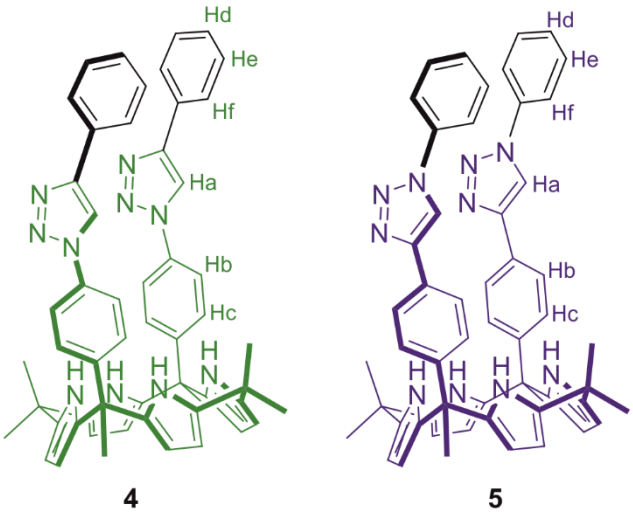

Figure 3.6. Molecular structures of calix[4]pyrrole receptors **4** and **5** used as reference systems.

The fit of the data returned values for the binding affinity constants K[**2a**⊂**1**] = 2.0 ± 0.5 × 10^6 M^{-1} and K[**2a**⊂**1**↔(**2a**)$_2$⊂**1**] = 2.0 ± 0.4 × 10^4 M^{-1}. The enthalpic contribution to each of the binding events was ΔH[**2a**⊂**1**] = -11.4 ± 1.6 kcal·mol^{-1} and ΔH[**2a**⊂**1**↔(**2a**)$_2$⊂**1**] = -5.1 ± 0.1 kcal·mol^{-1}, advocating for enthalpy driven binding events (**Table 3.1**).[32] Interestingly, the binding value obtained for the first binding

event is two orders of magnitude larger than the one obtained for the model receptor **4**. We rationalize these results in terms of the higher preorganization level of receptor **1** compared to simple "two wall" C4P receptor **4**. Indeed, model receptor **4** is conformationally more flexible than **1**. We surmise that the conformational changes that receptor **4** experiences in the binding of **2a** come at a higher entropic cost compared to **1**.[33] The value of the affinity constant for the second binding event with receptor **1** is two orders of magnitude smaller than that of the first one. This serves to explain why the formation of the complexes **2a**⊂**1** and (**2a**)$_2$⊂**1** occurred in two different phases of the titrations, as observed in the ^{1}H NMR titration experiments: the second binding site of receptor **1** does not participate in the binding event until the first is fully coordinated to the Cl^- anion.

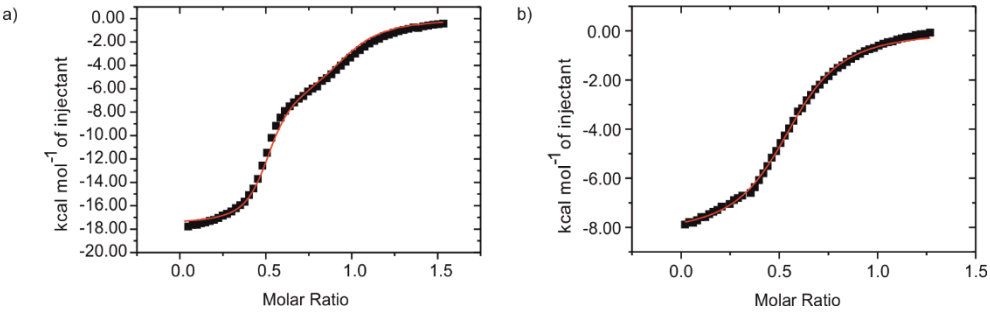

Figure 3.7. Binding isotherm (integrated and normalized heat data vs molar ratio) of the calorimetric titration of MTOA·Cl **2a** (a) and TBA·Cl **2b** (b) with **1** in chloroform solution. The data were fit to a theoretical "two sequential binding sites" model in the case of MTOA·Cl and to a "one set of sites" binding model for TBA·Cl (red line).

The cooperativity displayed by the formation of the **2:1** complexes was determined by calculating first the stepwise binding constants ratio. In the case of receptor **1**, we obtained *K*[**2a**⊂**1**] / *K*[**2a**⊂**1**↔(**2a**)$_2$⊂**1**] = 0.01. Next, we calculated the binding constants ratio for the two model receptors, **5** and **4**, *K*[**2a**⊂**5**] / *K*[**2a**⊂**4**] ~ 0.25. We assumed that the latter value should correspond to the cooperativity allosteric factor for receptor **1** if its two anion binding sites were totally independent i.e. the complexation of the first chloride does not influence that of the second one. We determined a normalized cooperativity factor for the formation of the 2:1 complexes, α_{norm}, as the quotient of the division of the two-above ratios. Hence, depending on the value calculated for α_{norm} , the formation of the 2:1 complex is said to display no cooperativity if $\alpha_{norm} = 1$, negative cooperativity if $\alpha_{norm} < 1$ and positive cooperativity in the case of $\alpha_{norm} > 1$. For the binding of **2a** with receptor **1**, we obtained α_{norm} = 0.01 / 0.25 = 0.04. This value indicates that the incorporation of

the two C4P receptors, **4** and **5**, in the covalent scaffold of **1** provokes a negative cooperativity in the binding of the second ion pair.

We rationalized this result by considering two different factors. Firstly, the short distance between the two bound chloride atoms of 8.6 Å originates repulsive electrostatic interactions disfavoring the binding of the second anion. These repulsive interactions might be reduced or even cancelled by the shielding effect of the solvent molecules, as observed in the X-ray structure of the (**2a**)$_2$⊂**1** complex (**Figure 3.3**). Secondly, the stronger repulsive anion-π interactions existing between the chloride bound in the C4P unit of **1** bearing the *C*-substituted *meso*-phenyl rings cannot be avoided owing to the conformational rigidity of the cyclic receptor. This limitation is in contrast to the binding of chloride by the model receptors **4** and **5**. These non-strapped receptors, being conformationally more flexible, can easily tune the distance between aromatic *meso*-substituents to reduce repulsive anion-π interactions. The intensification of the repulsive anion-π interactions in the binding of the second chloride by receptor **1** may also explain the determined negative allosteric cooperativity for the formation of the (**2a**)$_2$⊂**1** complex**,** α_{norm} ((**2a**)$_2$⊂**1**) < 1.

Table 3.1. Association Constant Values (M^{-2}) for the 2:1 Complexes of Tetraalkylammonium Salts **2a–c** with macrocycles **1** (this work) and **3** (ref 24). Measured in Chloroform Solution Using ITC Experiments. The Cooperativity Factors Calculated for the Second Binding Event are also tabulated. The α values for receptor **1** are normalized values.

	MTOA·Cl (**2a**)		TBA·Cl (**2b**)		TBA·OCN (**2c**)	
	K_a x 10^{-7}	α	K_a x 10^{-7}	α	K_a x 10^{-7}	α
1	4000	0.04	5.3	~4	68	~4
3	240	35	190	>10^5	15000	>10^5

The cooperativity displayed by receptor **1** in the binding of two ion-pairs of **2a** is remarkably different from the one assigned to the bis-alkynyl analogue **3** (**Table 3.1**). In the case of **3**, a large positive cooperativity was quantified for the binding of two ion-pairs of **2a**. This result could be explained by the larger size of the cavity of **3**, which allows the binding of the two Cl^- anions with reduced repulsive Coulombic interactions. In any case, the overall thermodynamic stability determined for the (**2a**)$_2$⊂**1** complex is of one order of magnitude larger than that of the (**2a**)$_2$⊂**3** complex. We explain this result by invoking the less repulsive anion-π interactions

that arise between the chloride and the *meso*-phenyls featuring the *para*-*N*-triazole substituent (MEP = -11 kcal·mol^{-1}) compared to those present in the *meso*-phenyls *para*-substituted with the butadynyl in receptor **3** (MEP = -18 kcal·mol^{-1}). Interestingly, the electronic modulation of the *meso*-phenyl rings in **3** is similar to the one experienced by the *para*-*C*-connected triazole substituent (MEP = -19 kcal·mol^{-1}) in receptor **1**. This reasoning implies that the formation of the 1:1 complex should be more favored in the case of receptor **1** than for receptor **3**. While the formation of the corresponding 2:1 complexes from the 1:1 counterparts should be energetically comparable or even less favorable for **1** (increased charge-charge interactions). Experimentally, we measured an increase of two orders of magnitude in the overall stability constant of the five-particle aggregate (**2a**)$_2$⊂**1** compared to (**2a**)$_2$⊂**3**.

Binding studies of receptor **1** with tetrabutylammonium salts **2b-c**

The incremental addition of a $CHCl_3$ solution of receptor **1** (11 mM) to separate solutions of ion pairs **2b** or **2c** (2 mM) in the same solvent produced the gradual release of heat of diminishing intensity. The normalized integrated values of the heat released generated a sigmoidal curve with an inflection point centered at a molar ratio **1**/**2b-c** of 0.5 (**Figure 3.7**). The observation of only one inflection point in the sigmoidal curves suggested the existence of two binding events with similar values of binding affinity constant. We analyzed the titration data using the theoretical binding model of "one set of sites" implemented in the Microcal ITC data analysis software. This model considers the existence of a set of identical binding sites in the receptor and returns averaged values for the binding affinity constants and the enthalpic contributions.[34] Thus, the overall stability constant for the formation of (**2b**)$_2$⊂**1** and (**2c**)$_2$⊂**1** was calculated by squaring the *K*a (average) value obtained and doubling the ΔH (average). The good fit of the experimental data to this binding model suggest that no cooperativity takes place in the binding of the two ion-pairs of TBA salts. The calculated values were *K*[(**2b**)$_2$⊂**1**] = 5.3 ± 0.1 × 10^7 M^{-2} and ΔH [(**2b**)$_2$⊂**1**] = −11.0 ±0.4 kcal·mol^{-1} for TBA·Cl and *K*[(**2c**)$_2$⊂**1**] = 6.7 ± 0.4 × 10^8 M^{-2} and ΔH [(**2c**)$_2$⊂**1**] = −18.6 ±0.8 kcal·mol^{-1} for TBA·OCN. These results are in complete agreement with the ones obtained in the ^{1}H NMR titration experiments, in which we observed the concomitant formation of the 1:1 and 2:1 complexes in the initial phases of the titration.

We also quantified the cooperativity displayed by receptor **1** in the binding of ion pair **2b** and **2c**. The analysis of the ITC data assigned identical values to the stepwise

binding constants for the formation of the 2:1 complexes. Assuming that the binding constants ratios, i.e. *K*[**2b**⊂**4**] / *K*[**2b**⊂**5**] and *K*[**2c**⊂**4**] / *K*[**2c**⊂**5**], are similar to the one determined in the case of MTOA·Cl *K*[**2a**⊂**5**] / *K*[**2a**⊂**4**] ~ 0.25.[29] We calculated a normalized cooperativity factor of α_{norm} = 1/0.25 = 4 for the binding of **2b** and **2c** to **1**. This cooperativity factor suggests that the binding of the two ion pairs **2b** and **2c** rendering the corresponding ion-pair quartet complex (**2b-c**)$_2$⊂**1** displays no-cooperativity. In short, the two binding sites of **1** behave totally independently.

The results obtained for the cooperativity factors of **1** in the binding of **2b** and **2c** are in striking contrast to those determined in the case of the bis-alkynyl analogue **3**. Receptor **3** displayed an impressively high positive binding cooperativity for the complexation of two ion-pairs of **2b** and **2c**. In addition, the overall binding constant values calculated for the complexes formed with receptor **3** were between 1 and 3 order of magnitudes larger than those measured for **1**.

In our previous studies with receptor **3**, we concluded that the 1:1 complexes **2b**⊂**3** and **2c**⊂**3** were exceptional heteroditopic receptors for the complexation of the second ion pair. The bound ion triplet in the 2:1 complexes, (**2b**)$_2$⊂**3** and (**2c**)$_2$⊂**3** displayed a perfect lineal cascade topology. The TBA^+ cation was perfectly sandwiched stabilized between the two bound anions. We already commented above that receptor **3** features a larger inner cavity compared to **1**.

In the case of receptor **1**, the triazole spacers do not locate the two C4P units at the ideal distance to coordinate the ion triplet Cl·TBA·Cl in a perfectly linear and sandwiched arrangement. Thus, in the 1:1 complexes, **2b**⊂**1** and **2c**⊂**1,** the heteroditopic binding site that is generated does not allow the coordination of the second ion dimer with a perfect cascade arrangement. This limitation is clearly observed in the X-ray diffraction analysis of the 2:1 complex, **2b**⊂**1** (**Figure 3.3**). The TBA^+ cation residing in close proximity to the bound chloride atoms in the 2:1 complex cannot establish ideal charge-charge interactions due to distance restrictions. The non-ideal arrangement of the ion-triplet produces a reduction in binding affinity for the second binding event. This reduction is also translated into the non-cooperative binding exhibited by **1** for the complexation of the TBA salts of chloride and cyanate. However, the partially sandwiched TBA^+ cation is involved in attractive electrostatic interactions with the two bound anions. As a result, the formation of the 1:2 complexes of **1** with the TBA salts, **2b** and **2c**, shows a reduced positive cooperativity in comparison to the complexes obtained with MTOA·Cl **2a**.

We also noticed a reduction of two orders of magnitude in the overall binding constant of (**2b**)$_2$⊂**1** compared to that of (**2a**)$_2$⊂**1**.This result was shocking owing to the large negative cooperativity displayed by **1** in the binding of **2a**, MTOA·Cl. We attributed this result to the previously discussed better fit of the methyl group of the $MTOA^+$ cation in the aromatic cup of the C4P unit compared to the TBA^+ counterpart. In addition, we observed significant differences between the thermodynamic stabilities of complexes (**2b**)$_2$⊂**1** and (**2c**)$_2$⊂**1**. The (**2c**)$_2$⊂**1** complex involving two OCN^- anions featured an affinity constant value that is one order of magnitude larger than that of the Cl^- counterpart, (**2b**)$_2$⊂**1**. We hypothesize that this difference might be due to the existence of more favorable dispersive interactions in the OCN^- complex or to the use of a too simplistic binding model for the ITC data analysis.[35]

3.2.3. Gas-phase characterization

In order to provide evidence of the formation of analogous five particle aggregates between receptor **1** and ion pairs **2a**-**c** in the gas phase, we performed ESI-MS analysis experiments of solutions containing a 1:2 receptor:guest molar ratio. We used the negative mode for the detection of the formed ions. According to the results obtained in the 1D/2D NMR and ITC experiments, as well as the X-ray analysis of the single crystals, the obtained complexes of **1** with the ion-pairs **2a-c** displayed a weakly bound TBA^+/$MTOA^+$ cation. This alkylammonium cation was located in the electron rich cavity defined by the pyrrole rings, which is opposed to the bound anion. The stabilization of the TBA^+/$MTOA^+$ cation in the binding site relies mainly on cation-π and CH-π interactions. On the other hand, Cl^- and OCN^- anions were coordinated to the NH core by the establishment of stronger hydrogen bonding interactions.

In this vein, we hypothesized that the transition of the 2:1 complexes from solution to the gas phase and subsequent ionization would imply the loss of the weakly bound cation, generating negatively charged complexes in the form of [**TBA·Cl$_2$⊂1**]$^-$, [**TBA·OCN$_2$⊂1**]$^-$ and [**MTOA·Cl$_2$⊂1**]$^-$.

We prepared a methanol solution at μM concentration of receptor **1** and MTOA·Cl **2a** in a strict 1:2 molar ratio. Gratifyingly, the ESI-MS spectrum in negative mode exhibited the presence of complex [**MTOA·Cl$_2$⊂1**]$^-$. The experimental isotopic pattern of the molecular ion matched the theoretical one (see Experimental Section). Similar results were obtained in the ESI-MS experiments in negative mode

of the analogue solutions prepared with ion pairs **2b** and **2c**. Indeed, we detected the ion peaks corresponding to the molecular ions [**TBA·Cl$_2$⊂1**]$^-$ and [**TBA·OCN$_2$⊂1**]$^-$, most likely generated upon the loss of the loosely bound "out" TBA$^+$ cation (see Experimental Section). Interestingly, in the ESI-MS experiments in negative mode performed with cyanate salt **2c**, we also observed the presence of an ion peak associated to a hetero-dimer [**TBA·Cl·OCN⊂1**]$^-$. Most likely, this species is generated

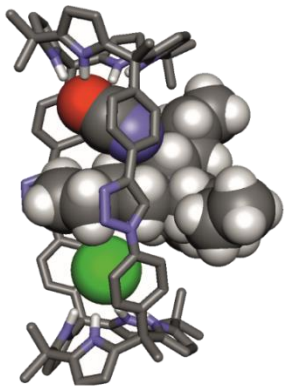

[**TBA·Cl·OCN⊂1**]$^-$

Figure 3.8. Energy-minimized structure (MM3) of hetero-dimer complex [**TBA·Cl·OCN⊂1**]$^-$.[36]

in the spectrometer due to the presence of residual Cl$^-$ anion in the methanol solution, the tip of the needle or the vial. We suspect that both anions in the complex are indeed coordinated into the C4P NH cores. The resulting bound ion triplet is expected to display a cascade-like arrangement similar to the homo-dimeric complexes aforementioned (**Figure 3.8**).

The gas-phase stabilities of the anionic 2:1 complexes were investigated in terms of Collision Induced Dissociation (CID) experiments. The obtained results in these experiments may mirror those obtained in solution. Nevertheless, the absence of solvent molecules is expected to affect the relative stabilities of charged complexes formed by polar and electrostatic interactions.[37] The gradual increase of the voltage applied at the entrance of the hexapole produced the fragmentation of complex [**MTOA·Cl$_2$⊂1**]$^-$ due to the rapid collision with N_2 molecules (**Figure 3.9**). The intensity of the ion peak was reduced as the complex disassembled due to non-covalent bond cleavage. Loss of MTOA·Cl generates the monocharged [**Cl⊂1**]$^-$ complex, as inferred from the presence of an ion peak at m/z = 1269.6360. Increasing further the applied voltage produced the disassembly of the 1:1 complex by the loss of H·Cl and the appearance of a new peak for the ion of the deprotonated

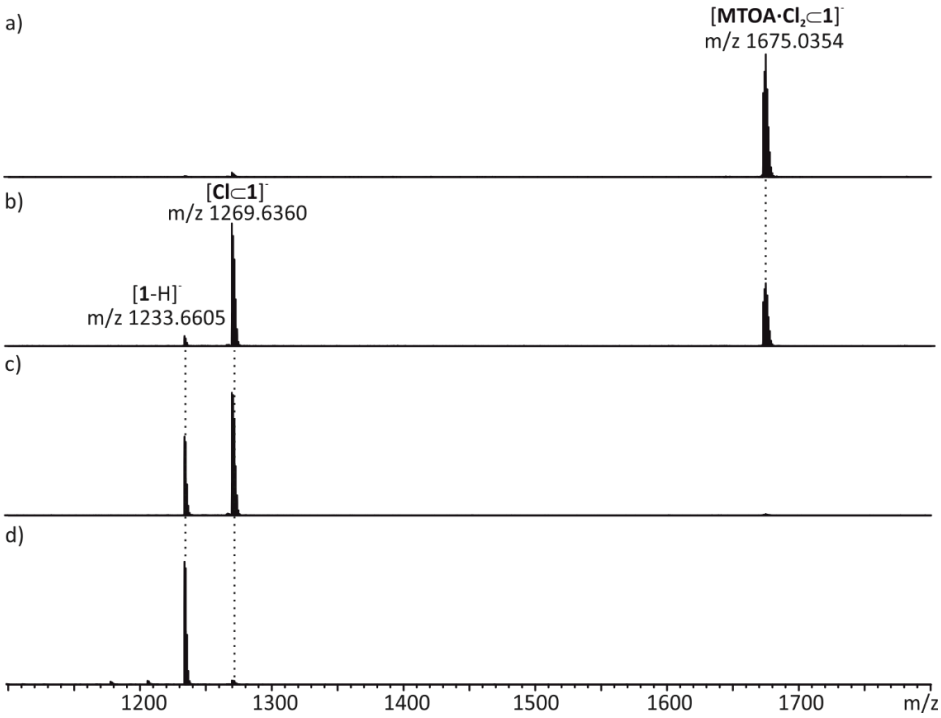

Figure 3.9. CID experiment performed with mass-selected ion [**MTOA·Cl$_2$⊂1**]$^-$ a) with CE of 35 V b), 48 V c) and 59 V d).

macrocycle [**1**-H]$^-$ at m/z = 1233.6605. We hypothesize that the chloride anion, bound by the pyrrole NHs of the C4P core, is lost by the concomitant deprotonation of a NH, despite the relatively high pKa value of the pyrrole ring (16.5).

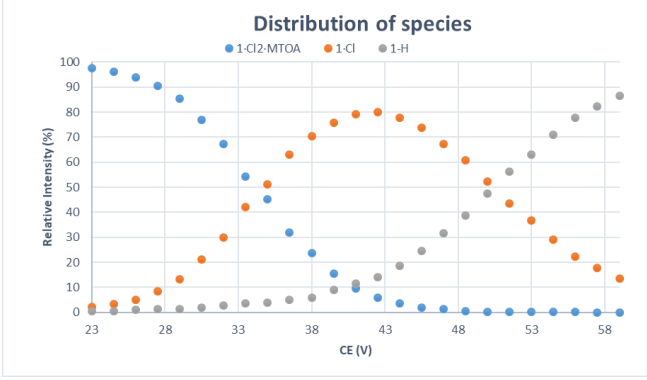

Figure 3.10. Relative intensity of the fragments observed in the CID experiment of complex **[MTOA·Cl$_2$⊂1]**$^-$ at increasing CE voltages. The intensity was calculated as Intensity = I. Complex / (I. Complex + I. Fragments) x 100%.

The normalized integrated values of the ion peaks assigned to [**MTOA·Cl$_2$⊂1**]$^-$, [**Cl⊂1**]$^-$ and [**1**-H]$^-$ were plotted against the voltage applied, revealing the species distribution profile obtained for the CID experiment (**Figure 3.10**). We confirmed the dissociation of complex [**MTOA·Cl$_2$⊂1**]$^-$ to generate 1:1 complex [**Cl⊂1**]$^-$ to an 80% extent. This finding points out to the greater stability of the 1:1 complex in the gas-phase, which was still present at the final points of the CID experiments. Analogous

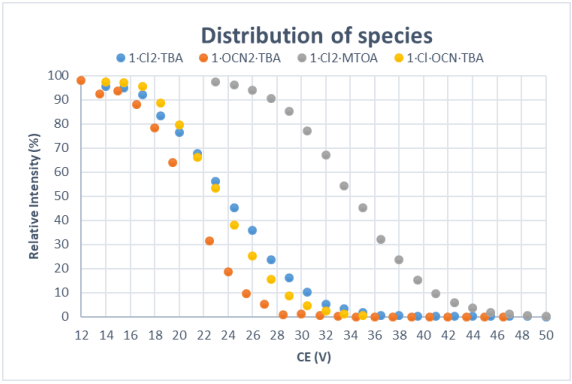

Figure 3.11. Relative intensity of the complexes obtained between receptor **1** and salts **2a-c** observed in the CID experiment at increasing CE voltages. The intensity was calculated as Intensity = I. Complex / (I. Complex + I. Fragments) x 100%.

results were obtained in the CID experiments performed with TBA·Cl and TBA·OCN (see Experimental Section). Interestingly, the disassembly of hetero-dimer [**TBA·Cl·OCN⊂1**]$^-$ was associated to the loss of TBA·Cl. This pointed out to a slightly increased stability of the complex formed with the cyanate anion.

Table 3.2. CE_{50} values obtained in the CID experiments of the complexes formed between receptor **1** and ion paris **2a-c**.

Complex	CE_{50} (V)
[TBA·Cl$_2$⊂1]$^-$	24
[MTOA·Cl$_2$⊂1]$^-$	34
[TBA·Cl·OCN⊂1]$^-$	23
[TBA·OCN$_2$⊂1]$^-$	21

The relative stabilities of the 2:1 complexes were investigated by direct comparison of the collision energies necessary to disassemble the complex in a 50% extent (CE_{50}) (**Figure 3.11**). As inferred from the values of CE_{50} obtained (**Table 3.2**), complex [**MTOA·Cl$_2$⊂1**]$^-$ presents a higher stability in the gas phase compared to the TBA

analogues. This is in agreement with the results obtained in the ^{1}H NMR and ITC experiments. We can rationalize these results by invoking again the better fit of the $MTOA^+$ cation in the electron rich aromatic cavity of receptor **1**. On the other hand, no significant differences were observed in the CE_{50} values obtained for the TBA^+ complexes, likewise to what was observed in the previous experiments in solution.

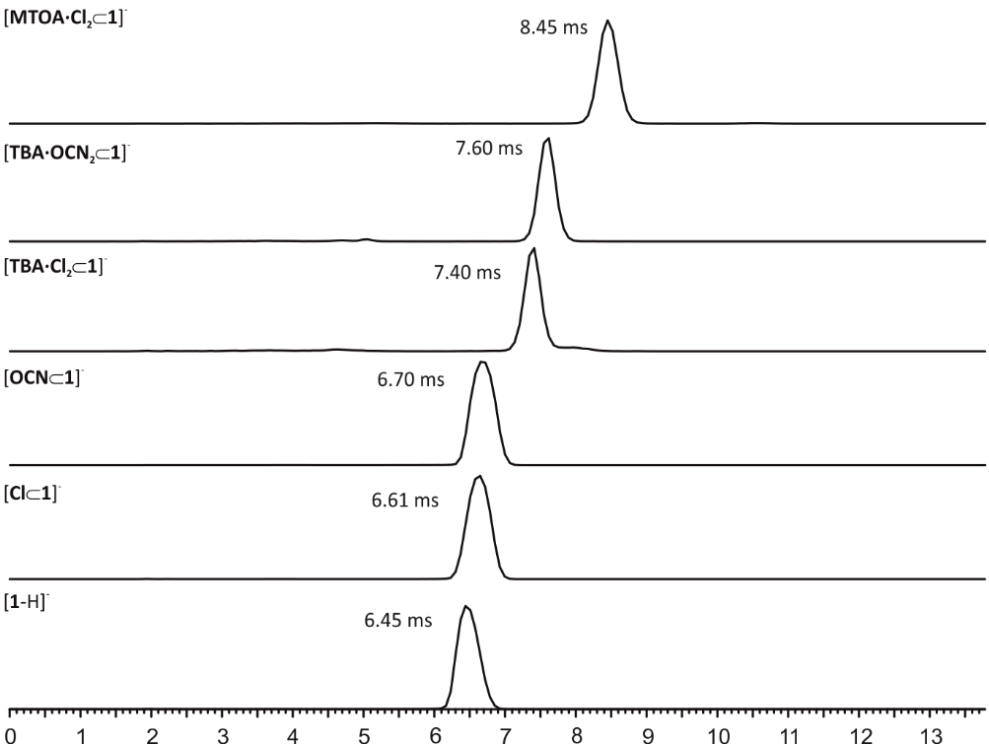

Figure 3.12. Arrival time distribution of most abundant ions obtained in the TW-IM-MS experiments of the different complexes formed between receptor **1** and ion pairs **2a-c**.

We also performed Ion Mobility Mass Spectrometry experiments (IMS) in order to confirm the differences in the relative size of the different complexes obtained (**Figure 3.12**). Accordingly, we observed a longer arrival time for the [**MTOA·Cl$_2$⊂1**]$^-$ complex due to the greater cross-section of the cation bound in the external area of the receptor. As expected, we obtained similar arrival times for the TBA^+ complexes. These results were rationalized in terms of the similar size of the bound anions inside the receptor, which do not alter dramatically the cross-section of the obtained complexes.

3.3. Conclusions

We have described the binding studies of BC4P receptor **1** towards tetraalkylammonium salts **2a-c**. The binding processes provide highly ordered assemblies with 1:1 and 2:1 stoichiometry. The 2:1 assemblies are thermodynamically and kinetically stable. In contrast, the kinetic stability on the chemical shift timescale of the intermediate 1:1 complexes are cation dependent. We report also the effects of the cation in the geometry of the 1:1 and 2:1 complexes, as well as the cooperativity in the binding processes of the ion pairs. The use of TBA salts, TBA·Cl **2b** and TBA·OCN **2c**, produced complexes featuring an included ion triplet with a cation sandwiched between the bound anions inside the receptor. The second cation was located in the C4P aromatic core displaying a receptor-separated binding geometry. The complex displayed no binding cooperativity. In contrast, the complex obtained with MTOA·Cl **2a** displayed two bound ion pairs featuring a receptor-separated binding geometries with a large negative cooperativity. We compared the binding affinities of the receptor with reference models **4** and **5** by ITC experiments. Interestingly, we obtained an increase in the stability of the complexes obtained with receptor **1**. We explained this behavior by invoking the preorganization of the covalently linked binding units in **1**. In contrast, the covalent connection of the binding units may also cause the difference in cooperativity levels measured in the binding of tetraalkylammonium ion-pair dimers. The stability of the complexes was also investigated in the gas phase by means of ESI-MS experiments in negative mode. The CE_{50} values obtained in the CID experiments for the molecular ions of the 2:1 complexes revealed a similar relative stability of the complexes as observed in ITC. Accordingly, the complex formed with MTOA·Cl proved to be more stable than those obtained with TBA salts.

3.4. Experimental section

3.4.1. General information and instruments

Reagents were obtained from commercial suppliers and used without further purification unless otherwise stated. All solvents were commercially obtained and used without further purification. Deuterated solvents were purchased from Sigma Aldrich. Dry solvents were taken from a solvent system MB SPS 800. DCM and DIPEA were dried, distilled and degassed by three freeze-pump-thaw cycles before used in the CuAAC reactions. Routine ^{1}H NMR and ^{13}C $\{^{1}H\}$ NMR spectra were recorded on a Bruker Avance 300 (300 MHz for ^{1}H NMR and 75 MHz for ^{13}C NMR), Bruker Avance

400 (400 MHz for ^{1}H NMR and 100 MHz for ^{13}C NMR), Bruker Avance 500 (500 MHz for ^{1}H NMR and 125 MHz for ^{13}C NMR) or Bruker Avance 500 with cryoprobe (500 MHz for ^{1}H NMR and 125 MHz for ^{13}C NMR). Deuterated solvents used are indicated in the characterization and chemical shifts are given in ppm. Residual solvent peaks were used as reference. All NMR J values are given in Hz. COSY, NOESY, ROESY, HMQC and HMBC experiments were recorded to help with the assignment of ^{1}H and ^{13}C signals. High-resolution mass spectra (HRMS) for determination of exact mass of compounds **4** and **5** were obtained on a Bruker HPLC-TOF (MicroTOF Focus) and Bruker HPLC-QqTOF (MaXis Impact) using the ionization mode indicated for each compound. IR spectra were recorded on a Bruker Optics FTIR Alpha spectrometer equipped with a DTGS detector, KBr beamsplitter at 4 cm^{-1} resolution using a one bounce ATR accessory with diamond windows. Melting points were measured on a MP70 Melting Point System Mettler Toledo. Column chromatography was performed with silica gel technical grade, pore size 60 Å, 230-400 mesh particle size, 40-63 µm particle size and thin layer chromatography (TLC) analysis on silica gel 60 F254. Ion mobility mass spectrometry and CID experiments were performed with Waters Synapt G2 Q-TOF mass spectrometer. Samples were prepared with 10-20 µM concentration in methanol solution with a 1:2 host–guest ratio. The modified Waters Synapt G2 was equipped with a linear drift cell filled with ~2 Torr nitrogen (298 K). Samples were ionized with a nanoESI ion source. In-house pulled capillary tips were used with inserted platinum wire for nanoESI. Parameters were optimized as follows: Capillary voltage 2.30 kV and source temperature 80 ºC. Data was analyzed using MassLynx v4.1 (Waters Corporation, USA) and Microsoft Excel 2016 (Microsoft, USA).

3.4.2. Synthesis and characterization data

Model receptor 4. Di-meso-4-azidephenylcalix[4]pyrrole (65 mg, 0.102 mmol, 1 equivalent), TBTA (27 mg, 0.051 mmol, 0.5 equivalent) and $Cu(CH_3CN)PF_6$ (19 mg, 0.05 mmol, 0.5 equivalent) were dissolved in 1.5 mL of dry and degassed dichloromethane. The mixture was sonicated for 1 min until a pale orange suspension was formed. Ethynylbenzene (45 µL, 0.41 mmol, 4 equivalent) and 0.14 mL of freshly distilled DIPEA were added. The reaction was stirred under Ar atmosphere for three hours. Afterwards 2.5 mL of dichloromethane and 5 mL of water were added. The organic phase was extracted and washed with 5 mL of water and 5 mL of brine. The organic phase was then dried with anhydrous sodium sulfate, filtered off and concentrated under reduced pressure to give 130 mg of a brown solid. The product was purified through silica column chromatography, using a

mixture of 1% tert-butyl methyl ether in dichloromethane as eluent (Rf = 0.4). The product was obtained as an orange solid (53 mg, 62%)

^{1}H NMR (500 MHz, $CDCl_3$, 298 K) δ 8.15 (s, 2H, Ha), 7.91 (d, 4H, J = 8.2 Hz, Hb), 7.65 (d, 4H, J = 8.8 Hz, Hf), 7.46 (dd, 4H, J1 = 7.5 Hz, J2 = 8.8 Hz, He), 7.37 (t, 2H, J = 7.5 Hz, Hd), 7.26 (br, 4H, NHs), 7.16 (d, 4H, J = 8.2 Hz, Hc), 5.97 (br, 4H, Hβ), 5.68 (br, 4H, Hβ), 1.94 (s, 6H, Hg), 1.66 (s, 6H, Hi), 1.57 (s, 6H, Hh), ^{13}C {^{1}H} NMR (125 MHz, $CDCl_3$, 298 K) δ149.0, 148.5, 136.8, 136.0, 135.5, 130.4, 129.1, 128.1, 128.6, 126.0, 119.9, 117.7, 106.4, 103.6, 44.7, 35.3, 30.2, 27.9, 27.8. FTIR (ATR): $\bar{\upsilon}_{max}$ (cm^{-1}) = 3404 (amine N-H stretching), 2968 (alkene C-H stretching), 1219 (amine C-N stretching), 1036 (alkene C=C bending), 766 (alkene C=C bending). HR-MS (ESI-TOF ES$^+$) m/z calculated for $C_{54}H_{51}N_{10}$ $[M+H]^+$ 839.4293, found 839.4314.

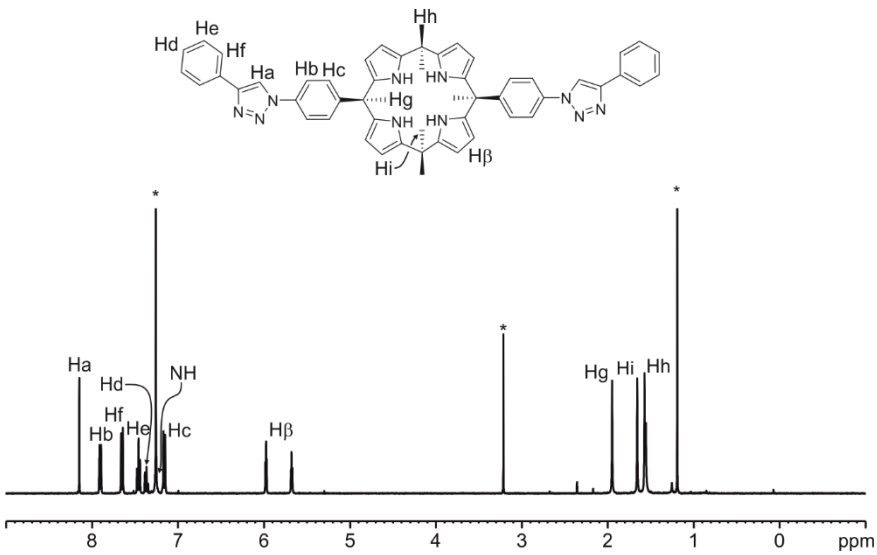

Figure 3.13. ^{1}H NMR (500 MHz, $CDCl_3$, 298 K) spectrum of model receptor **4** with proton assignments.*Solvent peaks.

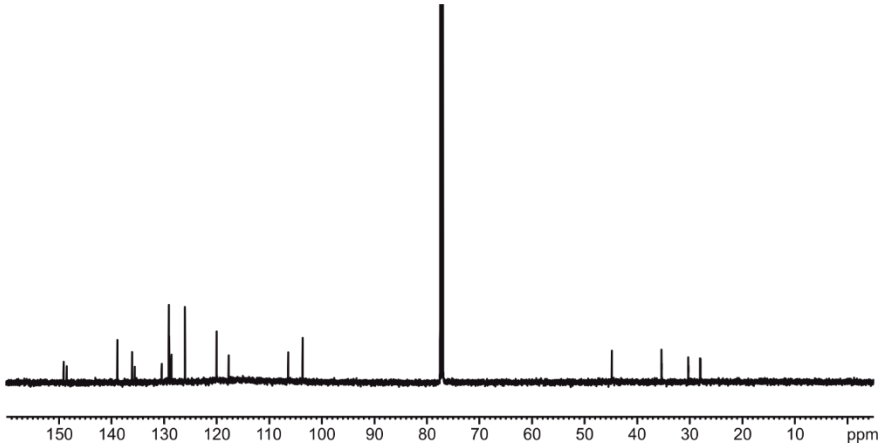

Figure 3.14. ^{13}C NMR (125 MHz, $CDCl_3$, 298 K) spectrum of model receptor **4**.

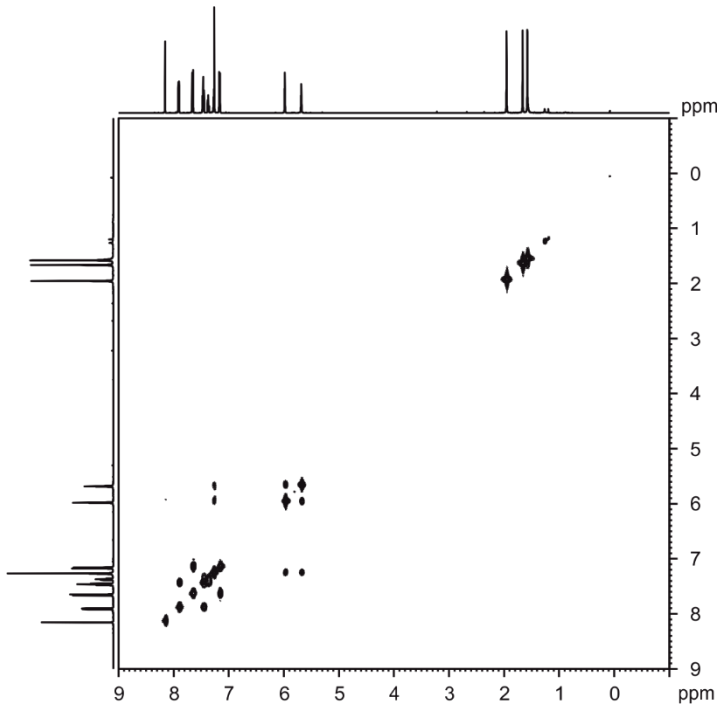

Figure 3.15. ^{1}H-^{1}H COSY (500 MHz, $CDCl_3$, 298 K) spectrum of model receptor **4**.

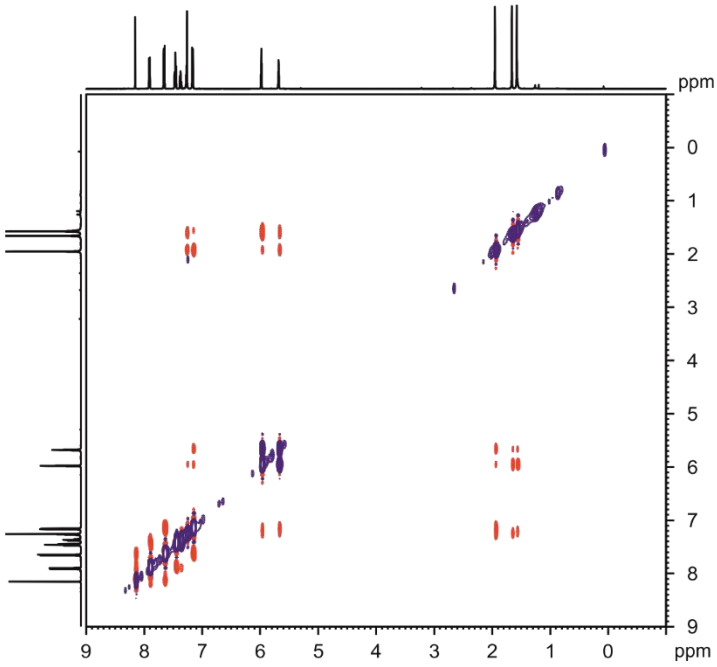

Figure 3.16. ^{1}H-^{1}H ROESY (500 MHz, $CDCl_3$, 298 K, spin-lock = 0.3 s) spectrum of model receptor **4**.

Model receptor 5. Di-meso-4-ethynylphenylcalix[4]pyrrole (65 mg, 0.108 mmol, 1 equivalent), TBTA (29 mg, 0.054 mmol, 0.5 equivalent) and $Cu(CH_3CN)PF_6$ (20 mg, 0.054 mmol, 0.5 equivalent) were dissolved in 1.5 mL of dry and degassed dichloromethane. The mixture was sonicated for 1 min until a pale brown suspension was formed. Azidobenzene (0.86 mL of a 0.5 M solution in tert-butyl methyl ether, 0.433 mmol, 4 equivalent) and 0.15 mL of freshly distilled DIPEA were added. The reaction was stirred under Ar atmosphere for three hours. Then, 2.5 mL of dichloromethane and 5 mL of water were added. The organic phase was extracted and washed with 5 mL of water and 5 mL of brine. The organic phase was then dried with anhydrous sodium sulfate, filtered off and concentrated under reduced pressure to give 125 mg of a brown solid. The product was purified through silica column chromatography, using a mixture of 1% tert-butyl methyl ether in dichloromethane as eluent (Rf = 0.4). The product was obtained as a yellow solid (40 mg, 40%).

^{1}H NMR (500 MHz, $CDCl_3$, 298 K) δ 8.16 (s, 2H, Ha), 7.78 (d, 4H, J = 8.4 Hz, Hb), 7.78 (t, 4H, J = 6.6 Hz, Hf), 7.55 (dt, 4H, J1 = 7.4 Hz, J2 = 6.6 Hz, He), 7.45 (t, 2H, J = 7.4 Hz, Hd), 7.26 (br, 4H, NHs), 7.08 (d, 4H, J = 8.4 Hz, Hc), 5.96 (br, 4H, Hβ), 5.69 (br, 4H, Hβ), 1.94 (s, 6H, Hg), 1.65 (s, 6H, Hi), 1.56 (s, 6H, Hh). ^{13}C {^{1}H} NMR (125 MHz, $CDCl_3$,

298 K) δ 148.4, 148.4, 138.7, 137.3, 136.5, 129.9, 128.9, 128.8, 128.5, 128.1, 125.4, 120.6, 117.6, 106.2, 103.5, 44.8, 35.3, 28.1, 27.9. FTIR (ATR): $\bar{\upsilon}_{max}$ (cm^{-1}) = 3419 (amine N-H stretching), 2970 (alkene C-H stretching), 1223 (amine C-N stretching), 1039 (alkene C=C bending), 759 (alkene C=C bending). HR-MS (ESI-TOF ES^+) m/z calculated for $C_{54}H_{51}N_{10}$ $[M+H]^+$ 839.4293, found 839.4318.

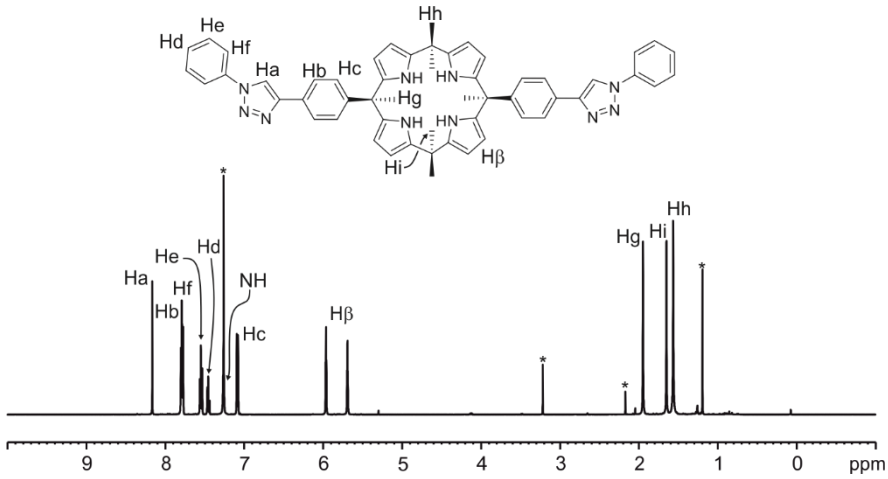

Figure 3.17. ^1H NMR (500 MHz, $CDCl_3$, 298 K) spectrum of model receptor **5** with proton assignments.*Solvent peaks.

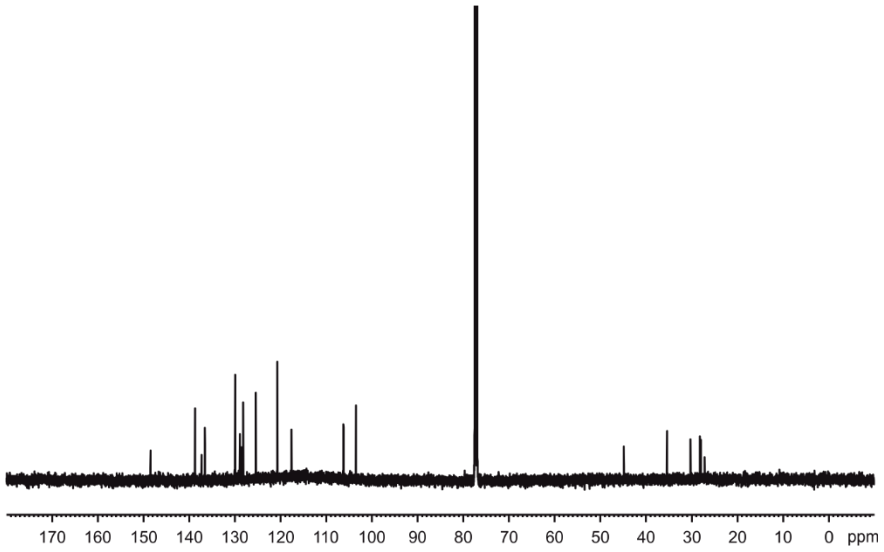

Figure 3.18. ^{13}C NMR (125 MHz, $CDCl_3$, 298 K) spectrum of model receptor **5**.

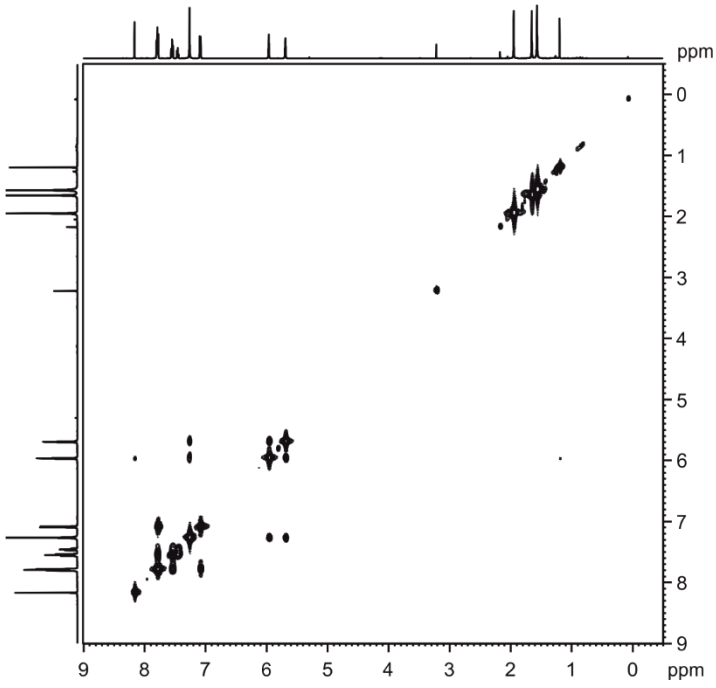

Figure 3.19. ^{1}H-^{1}H COSY (500 MHz, $CDCl_3$, 298 K) spectrum of model receptor **5**.

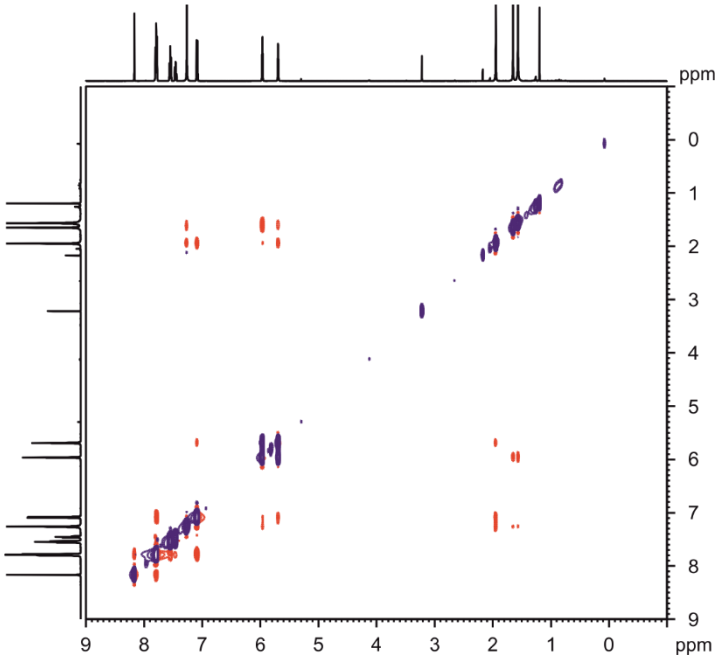

Figure 3.20. ^{1}H-^{1}H ROESY (500 MHz, $CDCl_3$, 298 K, spin-lock = 0.3 s) spectrum of model receptor **5**.

3.4.3. ^{1}H NMR titration experiments

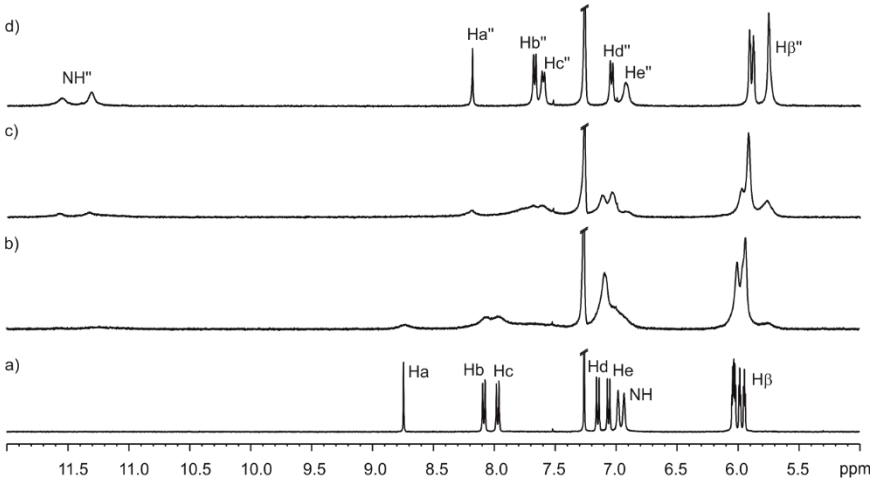

Figure 3.21. Selected region of the ^{1}H NMR spectra (400 MHz, $CDCl_3$, 298 K) of the titration experiment of a 2 mM solution of **1** (a) with 0.5 (b), 1.0 (c) and 2.0 equivalent (d) of TBA·OCN (**2c**).

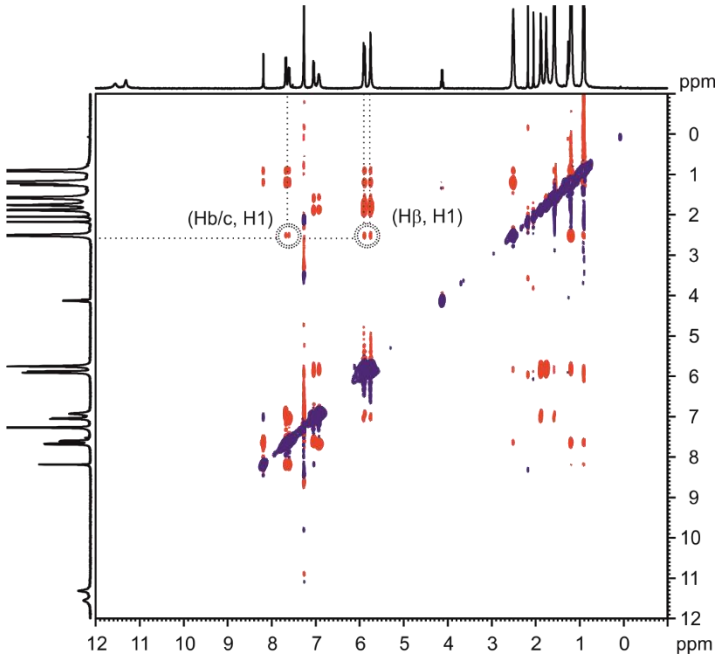

Figure 3.22. ^{1}H-^{1}H ROESY experiment (500 MHz, $CDCl_3$, 298 K, spin-lock = 0.3 s) of a1:2 mixture of receptor **1** and TBA·OCN (**2c**). Cross peaks between the β-pyrrole protons (Hβ) and the proton alpha to the nitrogen atom in the TBA^+ cation (H1) are marked.

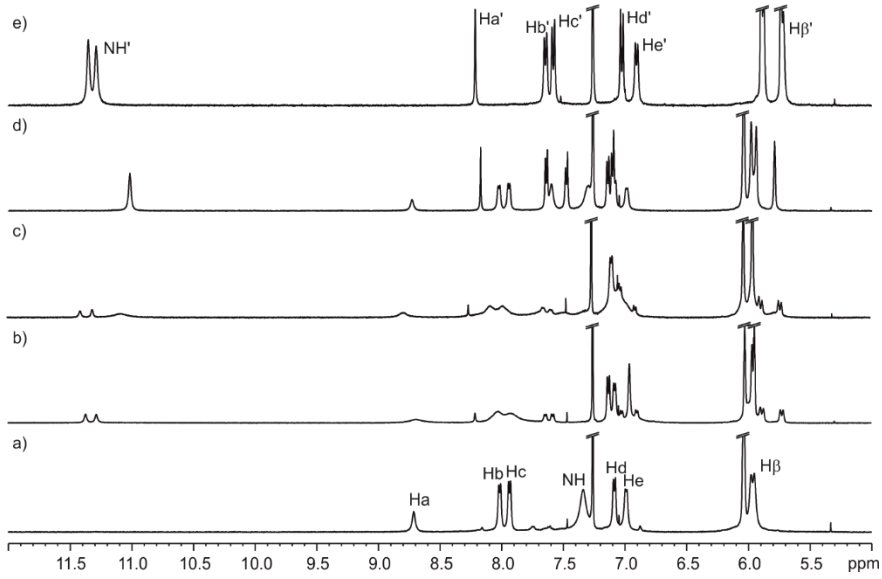

Figure 3.23. Variable temperature ^{1}H NMR experiment (500 MHz, $CDCl_3$) of a 2 mM solution of receptor **1** with 0.5 equivalent of TBA·Cl **2b** at 298 K (b), 263 K (c), 213 K (d). For comparison the ^{1}H NMR spectra of free **1** at 213 K (a) and of a 1:2 mixture of **2b** and **1** at 298 K (e) are shown.

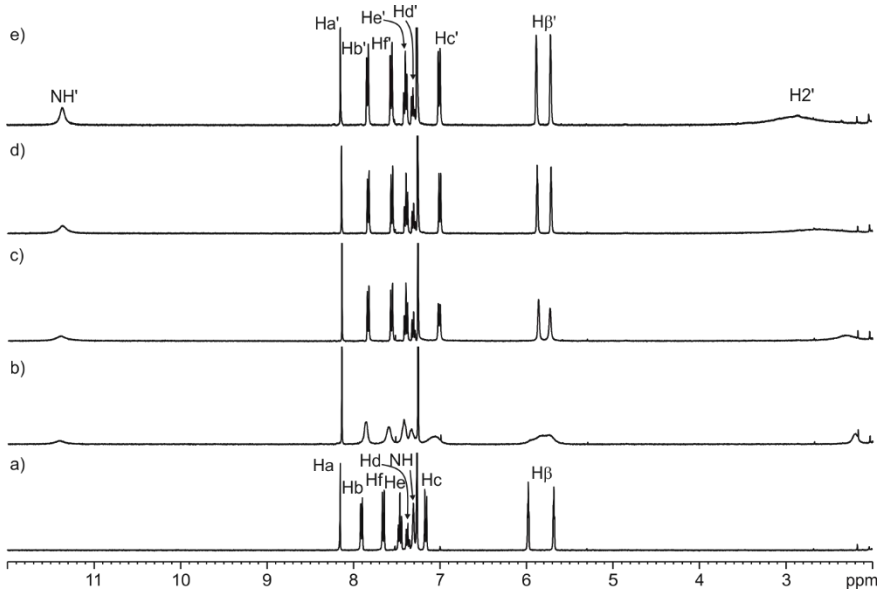

Figure 3.24. Selected region of the ^{1}H NMR spectra (400 MHz, $CDCl_3$, 298 K) of the titration experiment of a 2 mM solution of **4** (a) with 0.5 (b), 1.0 (c), 1.5 (d) and 2.0 equivalent (e) of MTOA·Cl (**2a**). See Figure 3.13 for proton assignments.

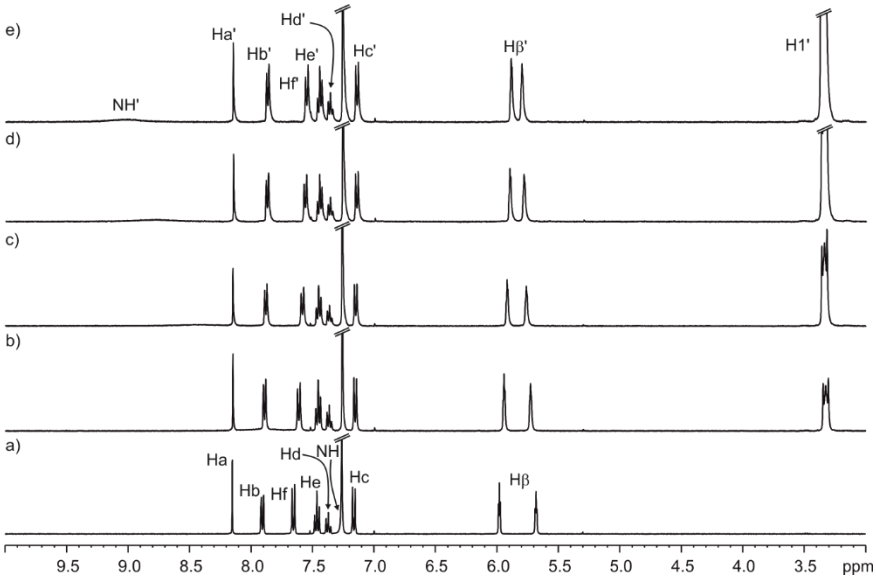

Figure 3.25. Selected region of the ^{1}H NMR spectra (400 MHz, $CDCl_3$, 298 K) of the titration experiment of a 2 mM solution of **4** (a) with 1.0 (b), 2.0 (c), 3.0 (d) and 4.0 equivalent (e) of TBA·Cl (**2b**). See Figure 3.13 for proton assignments.

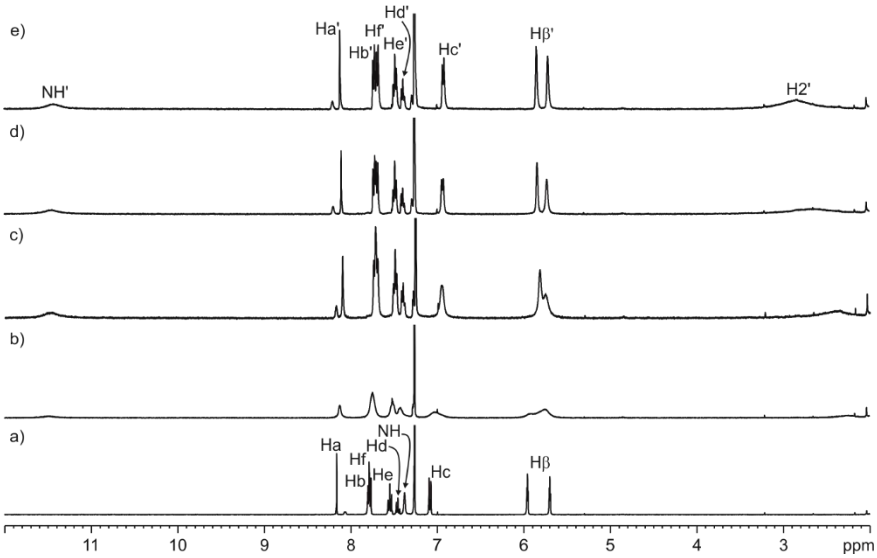

Figure 3.26. Selected region of the ^{1}H NMR spectra (400 MHz, $CDCl_3$, 298 K) of the titration experiment of a 2 mM solution of **5** (a) with 0.5 (b), 1.0 (c), 1.5 (d) and 2.0 equivalent (e) of MTOA·Cl (**2a**). See Figure 3.17 for proton assignments.

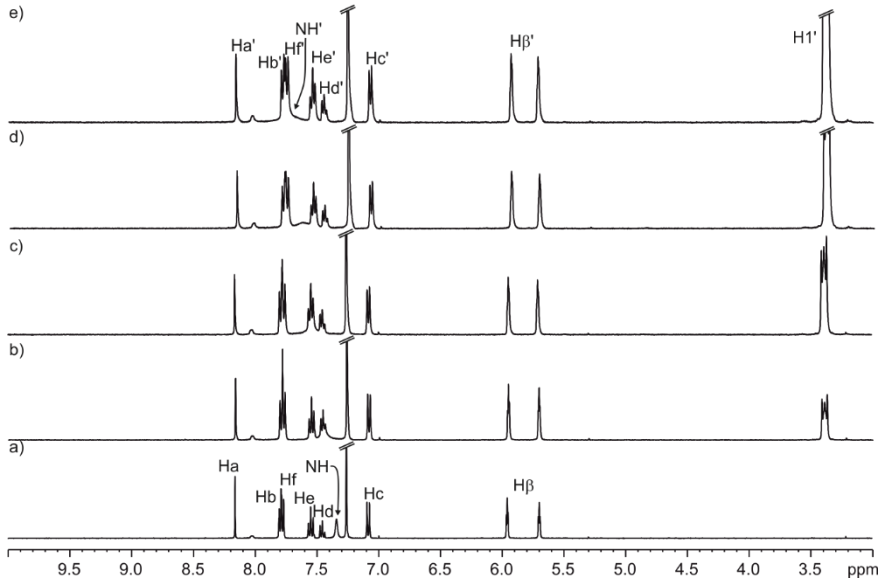

Figure 3.27. Selected region of the ^{1}H NMR spectra (400 MHz, $CDCl_3$, 298 K) of the titration experiment of a 2 mM solution of **5** (a) with 1.0 (b), 2.0 (c), 3.0 (d) and 4.0 equivalent (e) of TBA·Cl (**2b**). See Figure 3.17 for proton assignments.

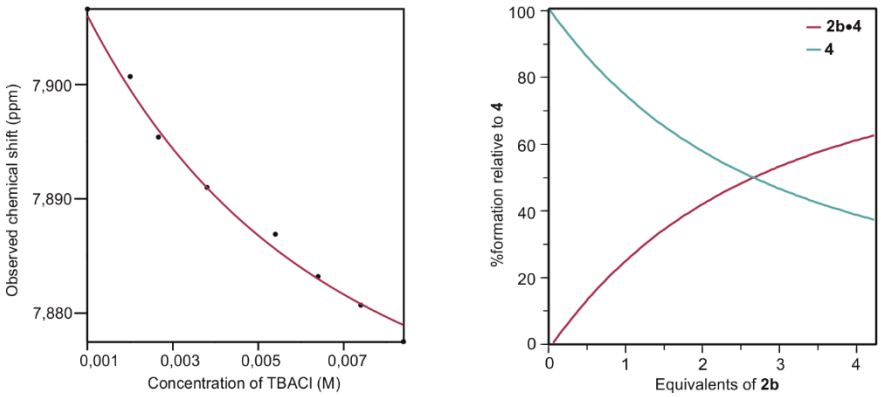

Figure 3.28. Left – Fit of the chemical shift changes, experienced by Hb proton of **4** during the titration with **2b**, using a 1:1 binding model (line) implemented in the HypNMR2008 software. Right - Speciation profile of the addition of increasing amounts of **2b** (up to 4 equivalent) over a 2 mM solution of receptor **4** considering the value for the binding constant obtained in the mathematical adjustment (K[**2b**⊂**4**] =10^2 M^{-1}).

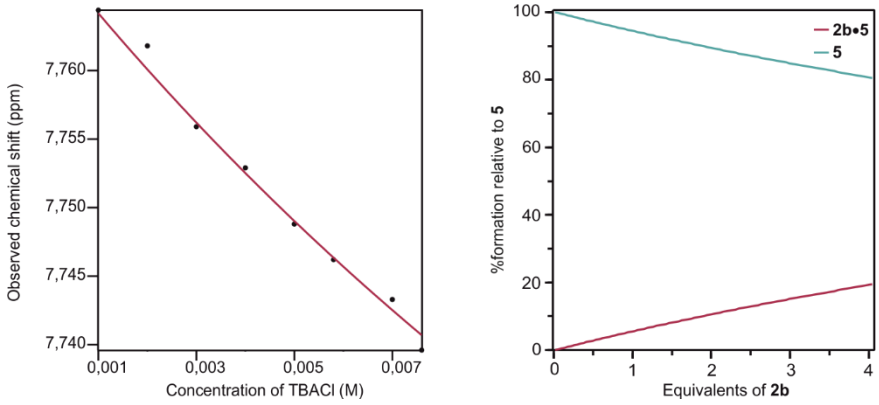

Figure 3.29. Left – Fit of the chemical shift changes, experienced by Hb protons of **5** during the titration with **2b**, using a 1:1 binding model (line) implemented in the HypNMR2008 software. Right - Speciation profile of the addition of increasing amounts of **2b** (up to 4 equivalent) over a 2 mM solution of receptor **5** considering the value for the binding constant obtained in the mathematical adjustment (K[**2b**⊂**5**] =10 M^{-1}).

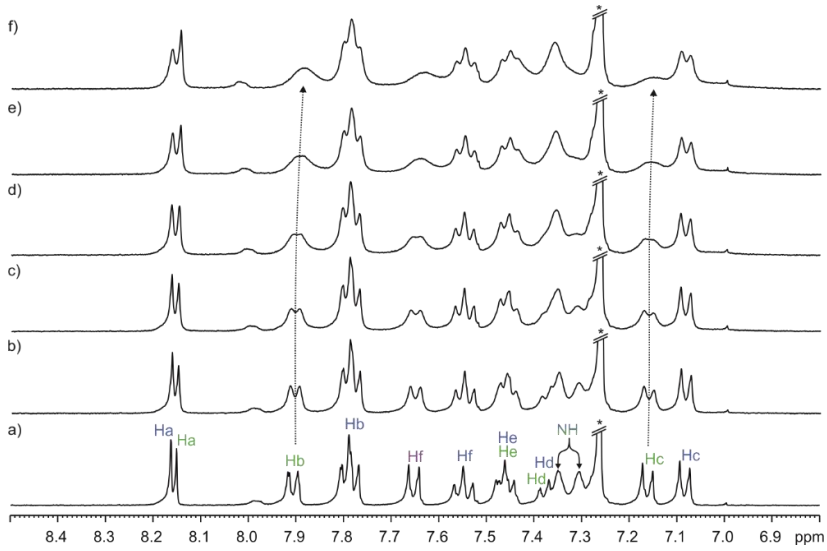

Figure 3.30. Selected downfield region of the ^{1}H NMR spectra (400 MHz, $CDCl_3$, 298 K) of the competitive titration experiment of a 2 mM 1:1 mixture of calix[4]pyrrole **4** (green letters) and **5** (blue letters) (a) with 0.1 (b), 0.2 (c), 0.3 (d), 0.4 (e) and 0.5 equivalent (f) of MTOA·Cl (**2a**). *Solvent peaks. See Figures 3.13 and 3.17 for proton assignments.

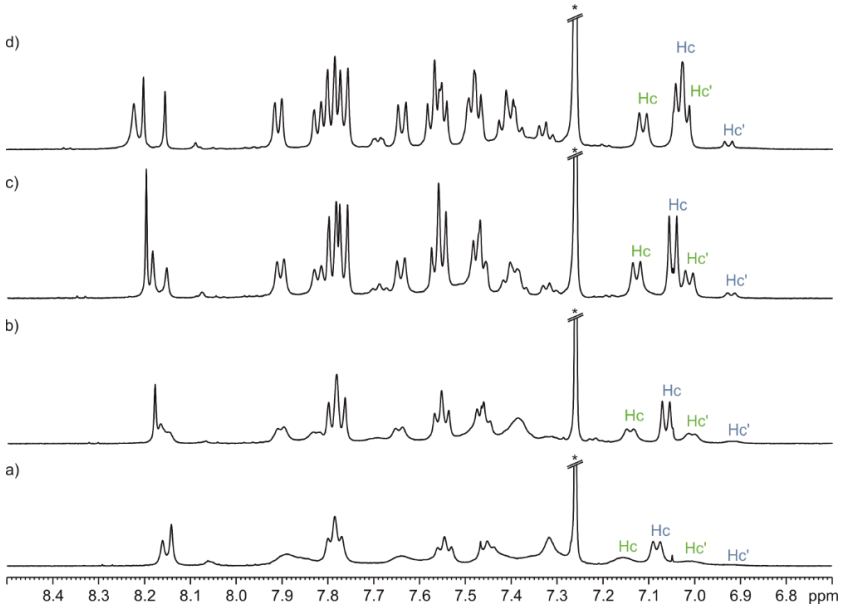

Figure 3.31. Variable temperature ^{1}H NMR experiment ($CDCl_3$) of a 1:1:0.5 mixture of **4** (green letters), **5** (blue letters) and tetraalkylammonium salt **2a**, respectively, at 298 K (a), 273 K (b), 253 K (c) and 233 K (d). Primed letters correspond to the signals attributed to the 1:1 complexes formed between receptor **4** or **5** and **2a**. The integrals of the signals marked were used to estimate the ratio between **2a**⊂**4** and **2a**⊂**5** binding constants, *K*[**2a**⊂**4**] / *K*[**2a**⊂**5**] ≈ 4. See Figures 3.13 and 3.17 for proton assignments.

3.4.4. ITC experiments

Isothermal titration calorimetry experiments were performed using a Microcal VP-ITC Microcalorimeter. All the titrations were carried out in chloroform solution at 298 K. Titrations were carried out by adding small aliquots (7 µL, 10 s) of a chloroform solution of the host into a solution of the guest in the same solvent. The concentration of host solution was approximately seven to ten times more concentrated than guest solutions (see corresponding figures for details). Reverse titrations (guest over host) were also performed and yielded similar results. The association constants and the thermodynamic parameters were obtained from the fit of the titration data to either a simple one set of sites binding model for tetrabutylammonium ion-pair or sequential binding sites model for methyltrioctylammonium chloride by using the Microcal ITC Data Analysis module. The association constant (Ka), TΔS and ΔH values for the binding process were determined by averaging the values from two titrations.

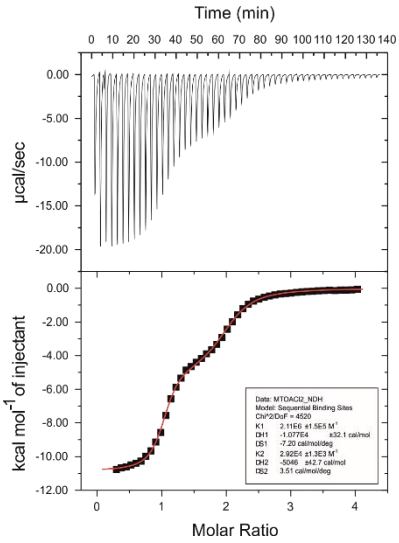

Figure 3.32. Top – Traces of the raw data (heat vs time) of the titration experiment of a $6 \cdot 10^{-4}$ M solution of receptor **1**, with a $1.5 \cdot 10^{-3}$ M solution of **2a** (MTOA·Cl) in chloroform. Bottom – Binding isotherms of the calorimetric titration shown on top. To determine the values of the thermodynamic variables the ITC data were fit to a sequential binding sites model (red line).

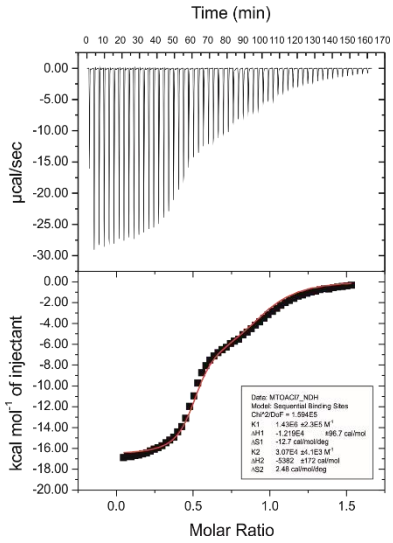

Figure 3.33. Top – Traces of the raw data (heat vs time) of the titration experiment of a $0.9 \cdot 10^{-3}$ M solution of **2a** (MTOA·Cl), with a $8 \cdot 10^{-3}$ M solution of receptor **1** in chloroform. Bottom – Binding isotherms of the calorimetric titration shown on top. To determine the values of the thermodynamic variables the ITC data were fit to a sequential binding sites model (red line).

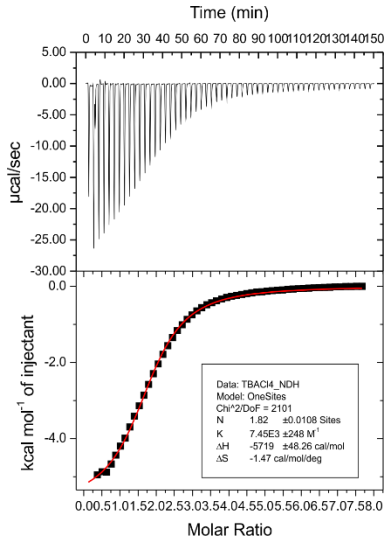

Figure 3.34. Top – Traces of the raw data (heat vs time) of the titration experiment of a $7 \cdot 10^{-4}$ M solution of receptor **1**, with a $2.5 \cdot 10^{-3}$ M solution of **2b** (TBA·Cl) in chloroform. Bottom – Binding isotherms of the calorimetric titration shown on top. To determine the values of the thermodynamic variables the ITC data were fit to a one set of sites binding model (red line).

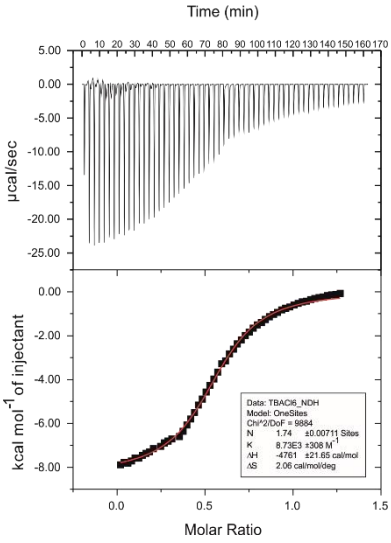

Figure 3.35. Top – Traces of the raw data (heat vs time) of the titration experiment of a $2 \cdot 10^{-3}$ M solution of **2b** (TBA·Cl), with a $11 \cdot 10^{-3}$ M solution of receptor **1** in chloroform. Bottom – Binding isotherms of the calorimetric titration shown on top. To determine the values of the thermodynamic variables the ITC data were fit to a one set of sites binding model (red line).

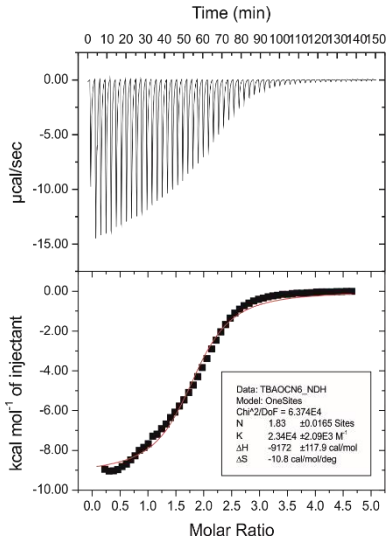

Figure 3.36. Top – Traces of the raw data (heat vs time) of the titration experiment of a $6 \cdot 10^{-4}$ M solution of receptor **1**, with a $1.3 \cdot 10^{-3}$ M solution of **2c** (TBA·OCN) in chloroform. Bottom – Binding isotherms of the calorimetric titration shown on top. To determine the values of the thermodynamic variables the ITC data were fit to a one set of sites binding model (red line).

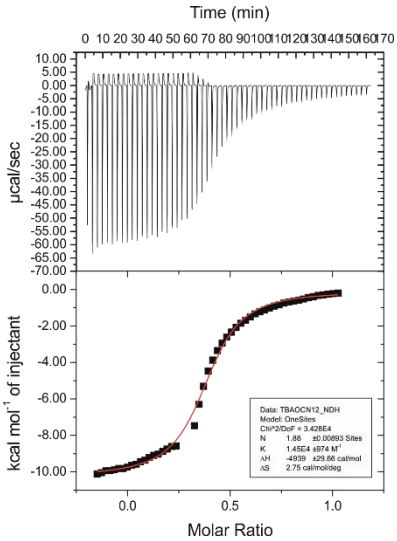

Figure 3.37. Top – Traces of the raw data (heat vs time) of the titration experiment of a $2.6 \cdot 10^{-3}$ M solution of **2c** (TBA·OCN), with a $18 \cdot 10^{-3}$ M solution of receptor **1** in chloroform. Bottom – Binding isotherms of the calorimetric titration shown on top. To determine the values of the thermodynamic variables the ITC data were fit to a one set of sites binding model (red line).

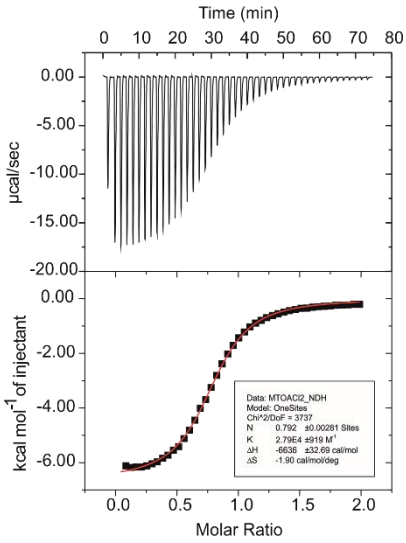

Figure 3.38. Top – Traces of the raw data (heat vs time) of the titration experiment of a $9 \cdot 10^{-4}$ M solution of receptor **4**, with a $1.2 \cdot 10^{-3}$ M solution of **2a** (MTOA·Cl) in chloroform. Bottom – Binding isotherms of the calorimetric titration shown on top. To determine the values of the thermodynamic variables the ITC data were fit to a one set of sites model (red line).

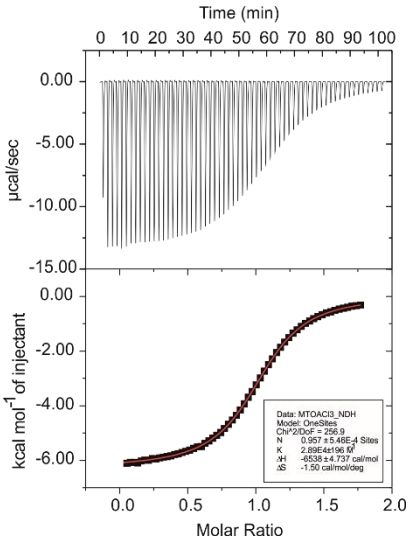

Figure 3.39. Top – Traces of the raw data (heat vs time) of the titration experiment of a $1 \cdot 10^{-3}$ M solution of **2a** (MTOA·Cl), with a $10 \cdot 10^{-3}$ M solution of receptor **4** in chloroform. Bottom – Binding isotherms of the calorimetric titration shown on top. To determine the values of the thermodynamic variables the ITC data were fit to a one set of sites model (red line).

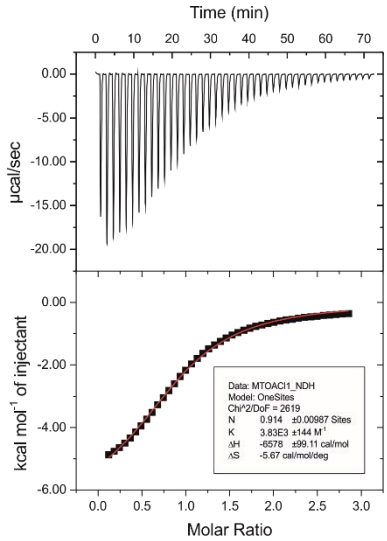

Figure 3.40. Top – Traces of the raw data (heat vs time) of the titration experiment of a $1 \cdot 10^{-3}$ M solution of receptor **5**, with a $12 \cdot 10^{-3}$ M solution of **2a** (MTOA·Cl) in chloroform. Bottom – Binding isotherms of the calorimetric titration shown on top. To determine the values of the thermodynamic variables the ITC data were fit to a one set of sites model (red line).

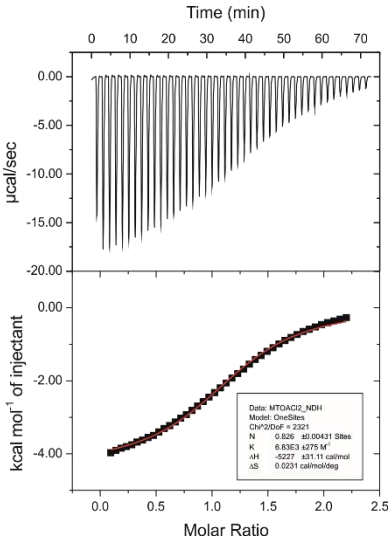

Figure 3.41. Top – Traces of the raw data (heat vs time) of the titration experiment of a $1 \cdot 10^{-3}$ M solution of **2a** (MTOA·Cl), with a $12 \cdot 10^{-3}$ M solution of receptor **5** in chloroform. Bottom – Binding isotherms of the calorimetric titration shown on top. To determine the values of the thermodynamic variables the ITC data were fit to a one set of sites model (red line).

3.4.5. Molecular electrostatic potential MEP

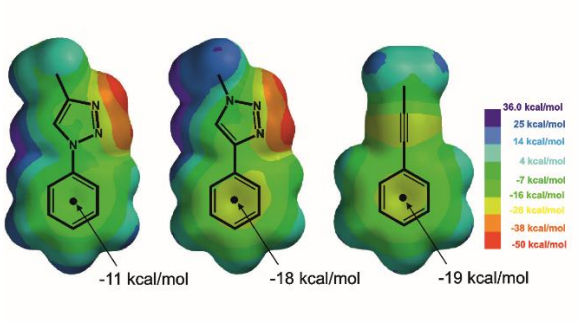

Figure 3.42. Representation of the molecular electrostatic potential on the Van der Waals surface corresponding to 4-methyl-1-*N*-phenyl-1,2,3-triazole (left), 1-methyl-4-*C*-phenyl-1,2,3-triazole (center), and 1-propyn-1-yl-benzene (right). Structures were energy-minimized at the B3LYP 6-31G* level of theory using the Spartan'02 (Wavefuntion, Inc., Irvine, CA, USA) software. MEPs were computed at the same level of theory and plotted on the 0.002 isodensity surface corresponding to the van der Waals surface.

3.4.6. ESI-MS experiments

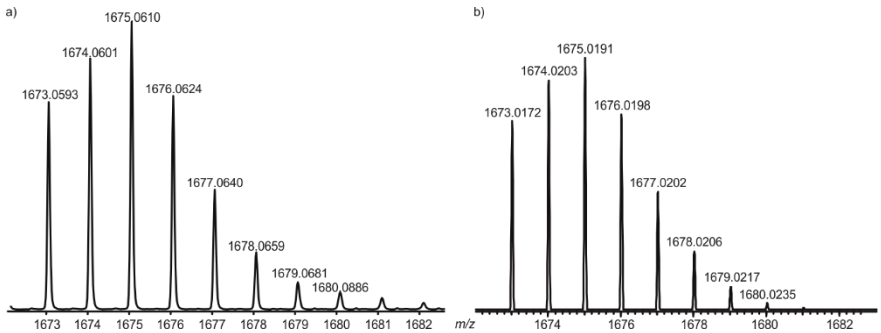

Figure 3.43. Experimental a) and calculated b) isotopic distribution of complex [**MTOA·Cl$_2$⊂1**]$^-$.

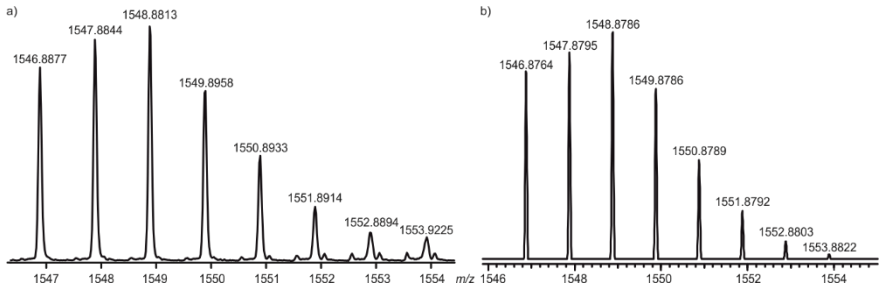

Figure 3.44. Experimental a) and calculated b) isotopic distribution of complex [**TBA·Cl$_2$⊂1**]$^-$.

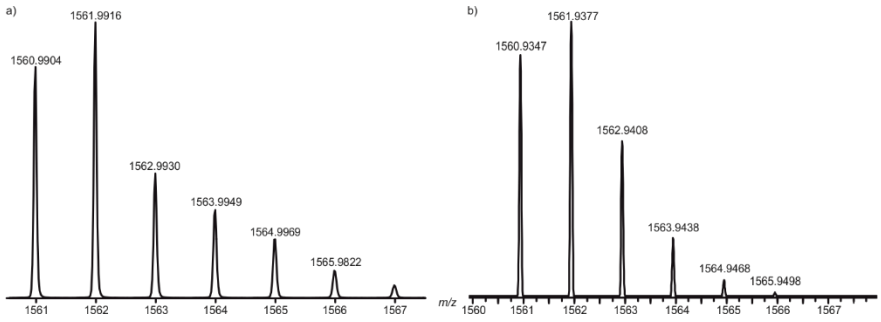

Figure 3.45. Experimental a) and calculated b) isotopic distribution of complex [**TBA·OCN$_2$⊂1**]$^-$.

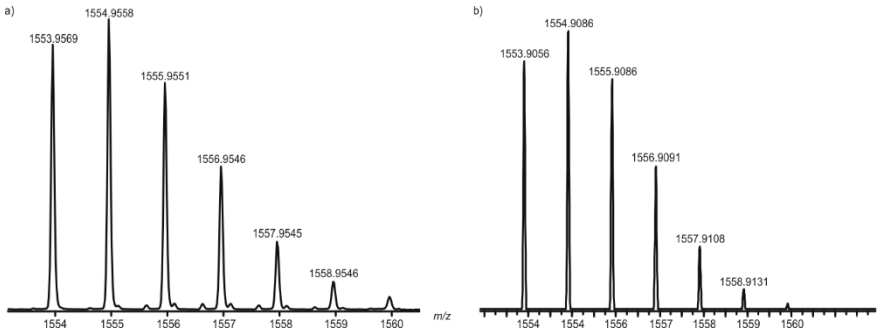

Figure 3.46. Experimental a) and calculated b) isotopic distribution of complex [**TBA·Cl·OCN⊂1**]$^-$.

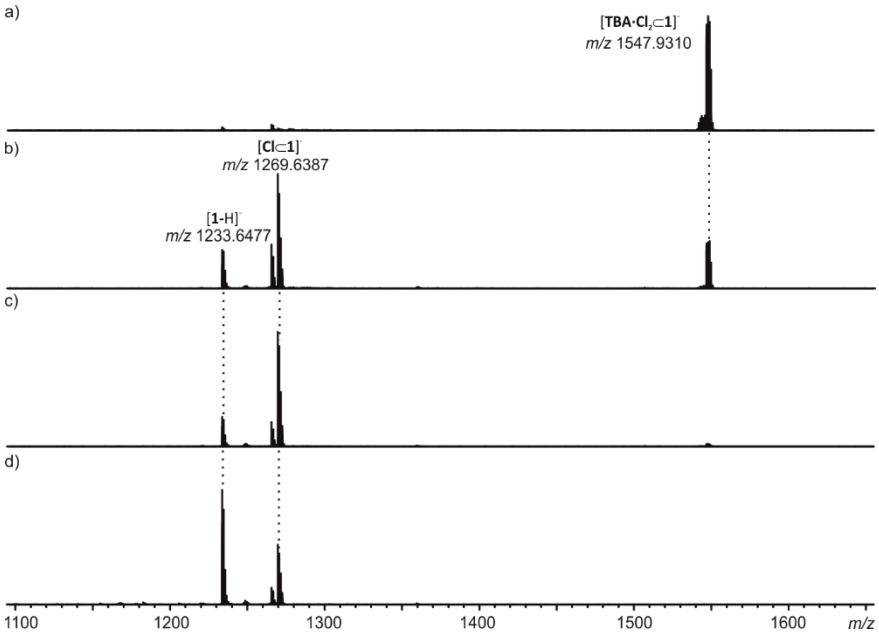

Figure 3.47. CID experiment performed with mass-selected ion [**TBA·Cl$_2$⊂1**]$^-$ a) with CE of 25 V b), 50 V c) and 60 V d).

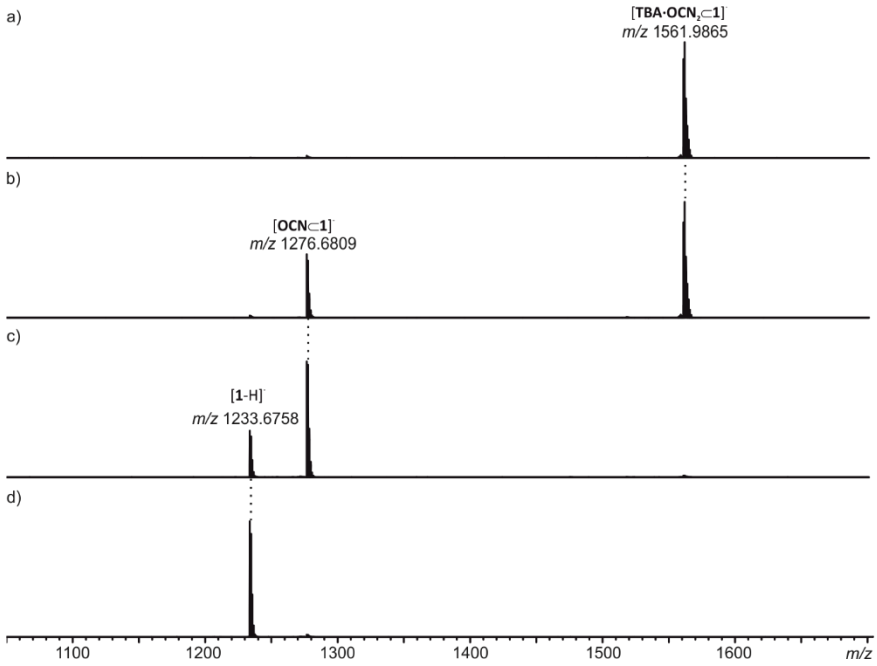

Figure 3.48. CID experiment performed with mass-selected ion [**TBA·OCN$_2$⊂1**]$^-$ a) with CE of 19 V b), 30 V c) and 43 V d).

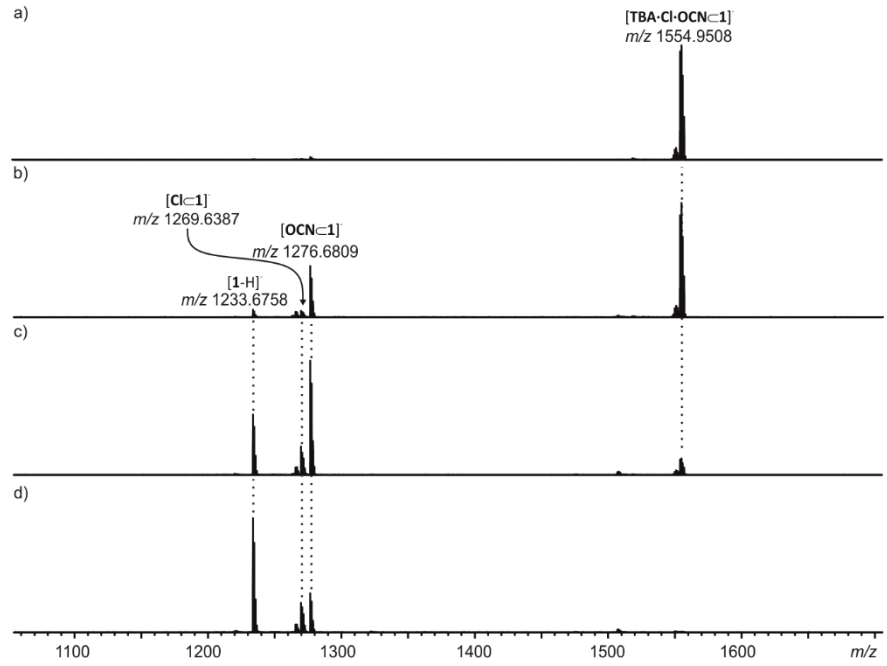

Figure 3.49. CID experiment performed with mass-selected ion [**TBA·Cl·OCN⊂1**]$^-$ a) with CE of 21 V b), 29 V c) and 35 V d).

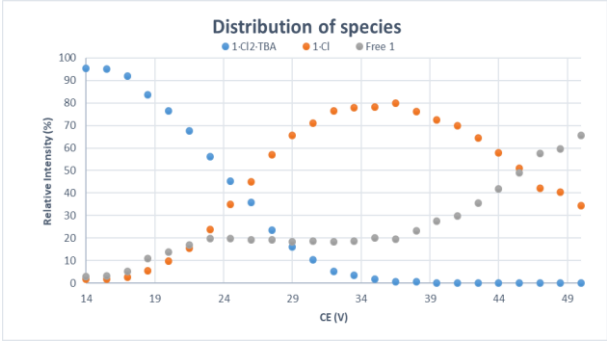

Figure 3.50. Relative intensity of the fragments observed in the CID experiment of complex **[TBA·Cl_2⊂1]**$^-$ at increasing CE voltages. The intensity was calculated as Intensity = I. Complex / (I. Complex + I. Fragments) x 100%.

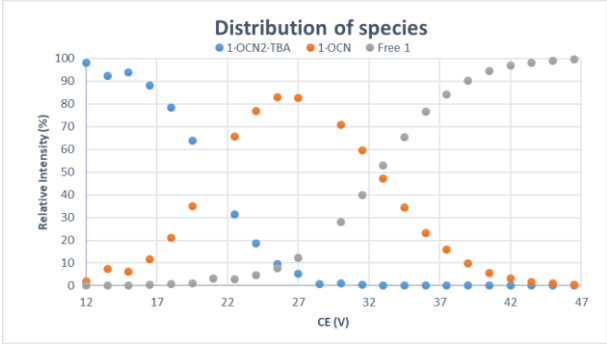

Figure 3.51. Relative intensity of the fragments observed in the CID experiment of complex **[TBA·OCN_2⊂1]**$^-$ at increasing CE voltages. The intensity was calculated as Intensity = I. Complex / (I. Complex + I. Fragments) x 100%.

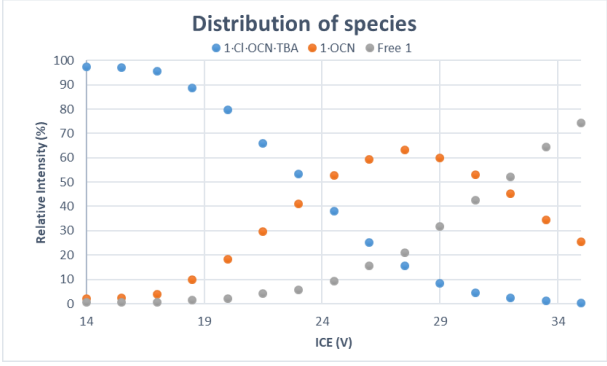

Figure 3.52. Relative intensity of the fragments observed in the CID experiment of complex **[TBA·Cl·OCN⊂1]**$^-$ at increasing CE voltages. The intensity was calculated as Intensity = I. Complex / (I. Complex + I. Fragments) x 100%.

3.4.7. Energy-minimized structures

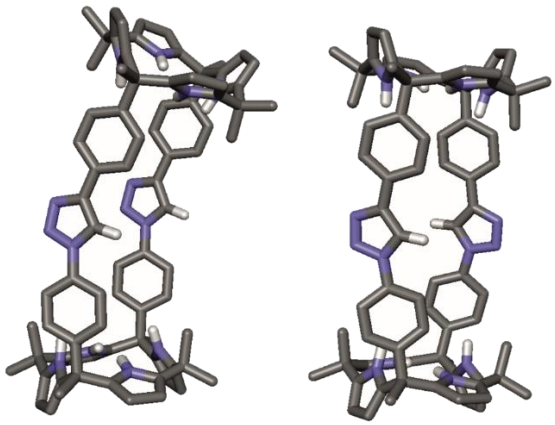

Figure 3.53. Energy-minimized structure (MM3) of the cis (left) and trans (right) isomers of receptor **1**.

3.5 References and notes

[1] Lehn, J. M., Supramolecular chemistry - Scope and perspectives molecules, supermolecules, and molecular devices. *Angew. Chem., Int. Ed.* **1988,** *27* (1), 89-112.
[2] Bianchi, A.; Bowman-James, K.; Garcia-España, E., *Supramolecular chemistry of anions*. Wiley-VCH: New York, 1997.
[3] Reetz, M. T.; Niemeyer, C. M.; Harms, K., Crown Ethers with a Lewis Acidic Center: A New Class of Heterotopic Host Molecules. *Angew. Chem. Int. Ed.* **1991,** *30* (11), 1472-1474.
[4] Bowman-James, K.; Bianchi, A.; Garcia-España, E., *Anion Coordination Chemistry*. Wiley-VCH: New York, 2011; p XI-XII.
[5] Gale, P. A.; Howe, E. N. W.; Wu, X.; Spooner, M. J., Anion receptor chemistry: Highlights from 2016. *Coord. Chem. Rev.* **2018,** *375*, 333-372.
[6] Chen, L.; Berry, S. N.; Wu, X.; Howe, E. N. W.; Gale, P. A., Advances in Anion Receptor Chemistry. *Chem* **2020,** *6* (1), 61-141.
[7] Kim, S. K.; Sessler, J. L., Ion pair receptors. *Chem. Soc. Rev.* **2010,** *39* (10), 3784-3809.
[8] McConnell, A. J.; Beer, P. D., Heteroditopic Receptors for Ion-Pair Recognition. *Angew. Chem., Int. Ed.* **2012,** *51* (21), 5052-5061.
[9] He, Q.; Vargas-Zúñiga, G. I.; Kim, S. H.; Kim, S. K.; Sessler, J. L., Macrocycles as Ion Pair Receptors. *Chem. Rev.* **2019,** *119* (17), 9753-9835.
[10] von Krbek, L. K. S.; Schalley, C. A.; Thordarson, P., Assessing cooperativity in supramolecular systems. *Chem. Soc. Rev.* **2017,** *46* (9), 2622-2637.
[11] Moerkerke, S.; Malytskyi, V.; Marcelis, L.; Wouters, J.; Jabin, I., Selective recognition of quaternary ammonium ions and zwitterions by using a biomimetic bis-calix[6]arene-based receptor. *Org. Biomol. Chem.* **2017,** *15* (42), 8967-8974.
[12] Tepper, R.; Schulze, B.; Bellstedt, P.; Heidler, J.; Gorls, H.; Jager, M.; Schubert, U. S., Halogen-bond-based cooperative ion-pair recognition by a crown-ether-embedded 5-iodo-1,2,3-triazole. *Chem. Commun.* **2017,** *53* (14), 2260-2263.
[13] Fatila, E. M.; Twum, E. B.; Sengupta, A.; Pink, M.; Karty, J. A.; Raghavachari, K.; Flood, A. H., Anions Stabilize Each Other inside Macrocyclic Hosts. *Angew. Chem., Int. Ed.* **2016,** *55* (45), 14057-14062.
[14] He, Q.; Kelliher, M.; Bähring, S.; Lynch, V. M.; Sessler, J. L., A Bis-calix[4]pyrrole Enzyme Mimic That Constrains Two Oxoanions in Close Proximity. *J. Am. Chem. Soc.* **2017,** *139* (21), 7140-7143.
[15] Kim, S. K.; Sessler, J. L., Calix[4]pyrrole-Based Ion Pair Receptors. *Acc. Chem. Res.* **2014,** *47* (8), 2525-2536.
[16] Rather, I. A.; Wagay, S. A.; Hasnain, M. S.; Ali, R., New dimensions in calix[4]pyrrole: the land of opportunity in supramolecular chemistry. *RSC Adv.* **2019,** *9* (66), 38309-38344.
[17] Wagay, S. A.; Rather, I. A.; Ali, R., Functionalized calix[4]pyrroles: Emerging class of ion-pair receptors in supramolecular chemistry. *Materials Today: Proceedings* **2020**.
[18] Kim, D. S.; Sessler, J. L., Calix[4]pyrroles: versatile molecular containers with ion transport, recognition, and molecular switching functions. *Chem. Soc. Rev.* **2015,** *44* (2), 532-546.
[19] Gross, D. E.; Schmidtchen, F. P.; Antonius, W.; Gale, P. A.; Lynch, V. M.; Sessler, J. L., Cooperative Binding of Calix[4]pyrrole–Anion Complexes and Alkylammonium Cations in Halogenated Solvents. *Chem.--Eur. J.* **2008,** *14* (26), 7822-7827.

[20] Custelcean, R.; Delmau, L. H.; Moyer, B. A.; Sessler, J. L.; Cho, W.-S.; Gross, D.; Bates, G. W.; Brooks, S. J.; Light, M. E.; Gale, P. A., Calix[4]pyrrole: An Old yet New Ion-Pair Receptor. *Angew. Chem. Int. Ed.* **2005,** *44* (17), 2537-2542.

[21] Xiong, S.; Chen, F.; Zhao, T.; Li, A.; Xu, G.; Sessler, J. L.; He, Q., Selective Inclusion of Fluoride within the Cavity of a Two-Wall Bis-calix[4]pyrrole. *Org. Lett.* **2020,** *22* (11), 4451-4455.

[22] Saha, I.; Lee, J. H.; Hwang, H.; Kim, T. S.; Lee, C.-H., Remarkably selective, non-linear allosteric regulation of anion binding by a tetracationic calix[4]pyrrole homodimer. *Chem. Commun.* **2015,** *51* (26), 5679-5682.

[23] Valderrey, V.; Escudero-Adán, E. C.; Ballester, P., Polyatomic Anion Assistance in the Assembly of [2]Pseudorotaxanes. *J. Am. Chem. Soc.* **2012,** *134* (26), 10733-10736.

[24] Valderrey, V.; Escudero-Adán, E. C.; Ballester, P., Highly Cooperative Binding of Ion-Pair Dimers and Ion Quartets by a Bis(calix[4]pyrrole) Macrotricyclic Receptor. *Angew. Chem., Int. Ed.* **2013,** *52* (27), 6898-6902.

[25] Sessler, J. L.; Gross, D. E.; Cho, W.-S.; Lynch, V. M.; Schmidtchen, F. P.; Bates, G. W.; Light, M. E.; Gale, P. A., Calix[4]pyrrole as a Chloride Anion Receptor: Solvent and Countercation Effects. *J. Am. Chem. Soc.* **2006,** *128* (37), 12281-12288.

[26] Weinhold, F., Polyion Covalency: Exotic Species from the Unexplored World of Electrostatically Shielded Molecular Ion Chemistry. *Angew. Chem., Int. Ed.* **2017,** *56* (46), 14577-14581.

[27] Romero, J. R.; Aragay, G.; Ballester, P., Ion-pair recognition by a neutral [2]rotaxane based on a bis-calix[4]pyrrole cyclic component. *Chem. Sci.* **2017,** *8* (1), 491-498.

[28] X-ray crystallographic data of (**2a**)$_2$⊂**1** and (**2b**)$_2$⊂**1** are deposited in the Cambridge Crystallographic Data Center with the numbers CCDC 1868846 and 1868847, respectively.

[29] We tried to determine the binding constant values for TBA·Cl by fitting the ^{1}H NMR spectroscopic titration data using the HypNMR software. The fit returned K_a values of the order of 10 and 10^2 M^{-1} for **5** and **4**, respectively. The reduced concentration of complexes achieved in the titrations (<20%) makes these values unreliable (see Experimental Section)

[30] Gil-Ramírez, G.; Escudero-Adán, E. C.; Benet-Buchholz, J.; Ballester, P., Quantitative Evaluation of Anion–π Interactions in Solution. *Angew. Chem. Int. Ed.* **2008,** *47* (22), 4114-4118.

[31] Frontera, A.; Gamez, P.; Mascal, M.; Mooibroek, T. J.; Reedijk, J., Putting Anion–π Interactions Into Perspective. *Angew. Chem. Int. Ed.* **2011,** *50* (41), 9564-9583.

[32] Reverse ITC experiments gave consistent thermodynamic values.

[33] The values of ΔS obtained for complexes *K*[**2a**⊂**4**] and *K*[**2a**⊂**1**]were of -1.5 and -12.0 Kcal·mol^{-1}·K^{-1}, respectively.

[34] The binding of a receptor having two almost identical sites defines a single-sigmoidal binding isotherm. The fit of the data to a two sequential sites theoretical model requires the optimization of six parameters. Multiple combinations of the six parameters result in similar theoretical curves making the fitting process not suitable for obtaining reliable results.

[35] The molar conductivity values measured for 2 mM chloroform solutions of TBA·Cl, **2b**, and TBA·OCN, **2c**, are not significantly different to support that the higher thermodynamic stability of TBA·OCN complex relates to its superior dissociation (λm (S·cm^2/mol) = 3.49 ± 0.08 and 3.70 ± 0.08 for TBA·Cl, **2b**, and TBA·OCN, **2c**, respectively).

[36] The energy-minimized structure was obtained using the software package Fujitsu Scigress Version 2.2.0. The structure was optimized by performing a geometry calculation using the implemented molecular mechanics force field with augmented MM3 parameters.

[37] Cera, L.; Schalley, C. A., Supramolecular reactivity in the gas phase: investigating the intrinsic properties of non-covalent complexes. *Chem. Soc. Rev.* **2014,** *43* (6), 1800-1812.

UNIVERSITAT ROVIRA I VIRGILI
Calix[4]pyrrole Based Receptors for the Recognition of Ion Pairs
Ricardo Molina Muriel

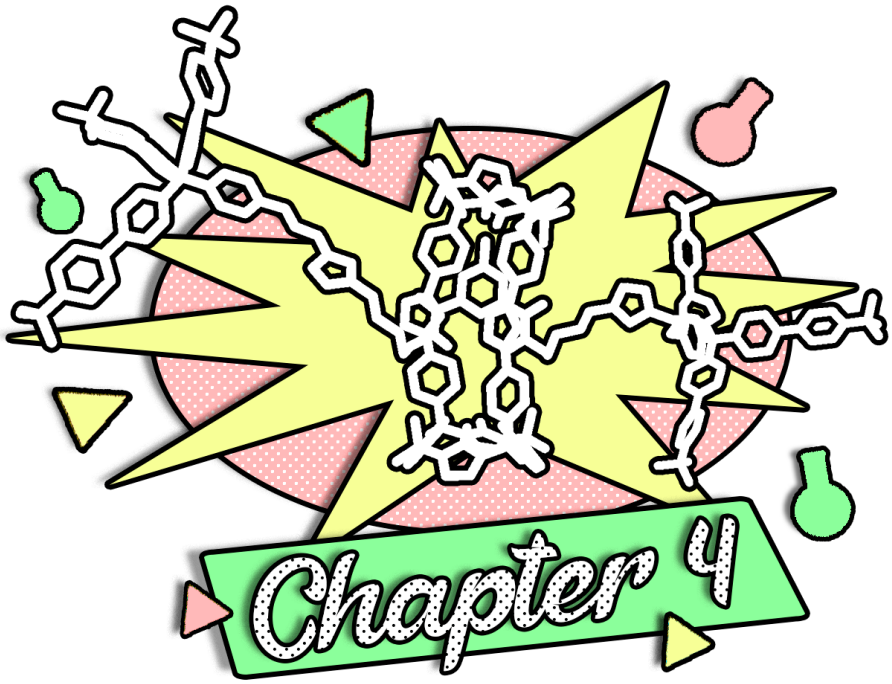

Anion templated assembly of pseudorotaxane complexes
Synthesis and binding studies of a [2]rotaxane receptor

Unpublished results

UNIVERSITAT ROVIRA I VIRGILI
Calix[4]pyrrole Based Receptors for the Recognition of Ion Pairs
Ricardo Molina Muriel

4.1. Introduction

In the field of supramolecular chemistry, architectures with rotaxane topology have gained significant attention in the recent decades owing to its applications as synthetic receptors and molecular machines.[1,2,3,4,5] The superior properties of rotaxanes as synthetic receptors are due to the three-dimensional cavities generated between the macrocycle and lineal component, resembling the binding sites of naturally occurring molecules. Nowadays, the synthesis of rotaxane architectures is achieved through the formation of a key intermediate: pseudorotaxanes (**Figure 4.1**).[6,7,8,9] Pseudorotaxane assemblies are complexes formed by the establishment of reversible interactions between an axle and a macrocycle or between both components and a suitable template. Plenty of examples can be found in the literature of pseudorotaxanes based on hydrogen bonding[10,11,12] and π-π interactions,[13,14,15,16] on metal coordination[17,18] or on exploiting the hydrophobic effect.[19,20] In some cases, an anion serves to coordinate orthogonally both components.[21] Once the pseudorotaxane assembly is obtained, the attention is then shifted on finding a suitable closing reaction able to generate the interlocked architecture. For this purpose, robust synthetic methodologies such as the Copper(I)-catalyzed azide-alkyne cycloaddition (CuAAC) reaction have been extensively used to generate rotaxane receptors.[22]

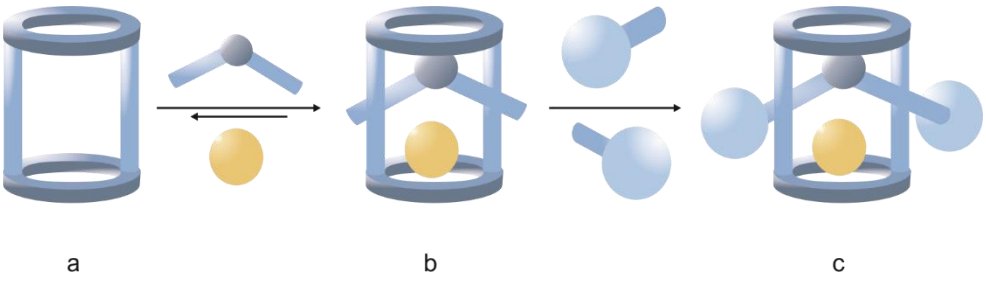

Figure 4.1. Schematic representation of the templated synthesis of a [2]rotaxane. a) Macrocyclic component, b) assembly of pseudorotaxane complex and c) formation of [2]rotaxane by stoppering procedure.

In this chapter, we report the construction of anion-templated pseudorotaxane assemblies based on bis(calix[4]pyrrole) macrocycle **1** (**Figure 4.2**). In the previous chapter, we have demonstrated the properties of receptor **1** to bind tetraalkylammonium salts **2a-c** in a non-competitive solvent. Now, the anion will be recognized by the supramolecular complex formed by lineal component **3**, a heteroditopic amide-functionalized *N*-oxide, coordinated in the C4P units of

macrocycle **1**. The pseudorotaxane complex **3⊂1** generates a binding site for anions where up to six hydrogen bond donors converge. The countercation will bind externally in the aromatic rim of the C4P in cone conformation opposed to the bound anion. Later in the chapter, we will disclose the synthesis of [2]rotaxane **4** obtained by the CuAAC stoppering reaction of the pseudorotaxane assembly with bulky stoppers **5**. We will discuss the effect that the use of an anion template has in the synthesis of the interlocked molecule. In addition, we will investigate the binding properties of the receptor towards tetraalkylammonium ion pairs (**2a-c**). The stability of the complexes will be investigated by ^{1}H NMR, ITC experiments and MS-ESI analysis in the gas phase.

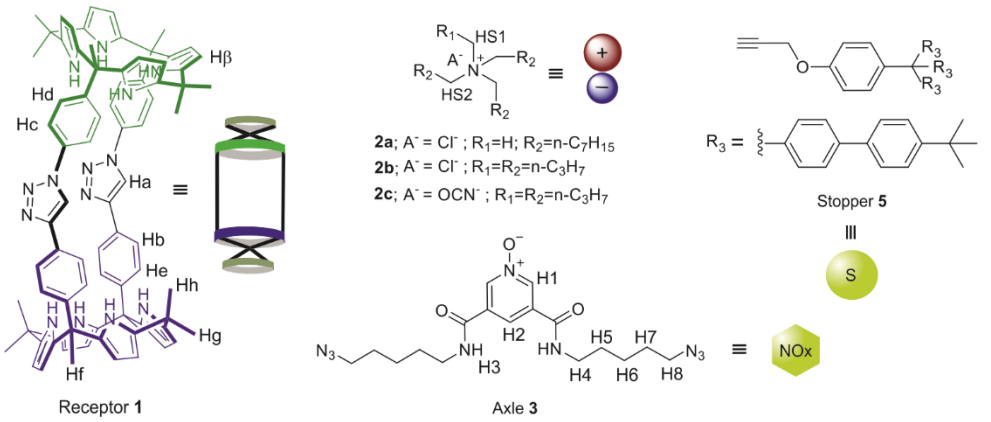

Figure 4.2. Line-drawing structures of BC4P macrocycle **1**, tetraalkylammonium salts **2a-c**, axle **3**, stopper **5** and their cartoon representations.

Recently, our group introduced the synthesis of [2]rotaxane receptor **6** based on the bis-alkynyl analogue of macrocycle **1** (**Figure 4.3**).[23] [2]Rotaxane **6** formed kinetically and thermodynamically stable 1:1 complexes with the TBA salts of Cl^-, OCN^- and NO_3^- anions, as well as MTOA·Cl. The determined binding affinity constants for the 1:1 complexes were in the range of 10^4 – 10^7 M^{-1}. Interestingly, we observed the formation of a 2:1 complex with MTOA·Cl after the addition of more than 1 equivalent of the ion pair. Most likely, in the complex the *N*-oxide knob of the axle was slightly displaced due to the coordination of a second Cl^- anion in the C4P core of the macrocycle. An increase of one order of magnitude was observed in the binding affinity constant towards the OCN^- salt of TBA^+ compared with its Cl^- counterpart, owing to the better fit of the cylindrical polyatomic anion in the cavity of the receptor. In the energy-minimized structure of the [2]rotaxane receptor **4**, we measured a N-H···H-N distance between axle and macrocycle of *ca.* 4.37 Å (**Figure**

4.4). This is in contrast with the longer N-H···H-N distance measured for the [2]rotaxane receptor **6**, of *ca.* 6.68 Å. [2]Rotaxane **4** features two different binding sites owing to the 1,3-triazole spacer. Considering these structural differences, we surmised that [2]rotaxane **4** will display different binding properties towards ion pairs **2a-c** compared to receptor **6**.

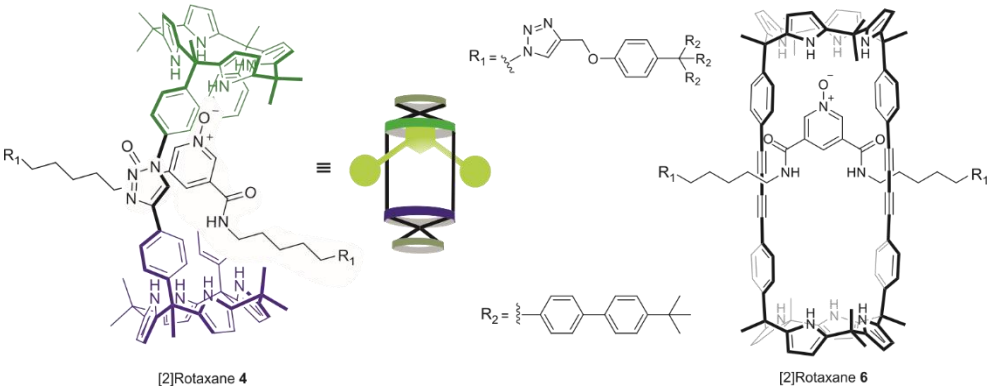

Figure 4.3. Line-drawing structures of [2]rotaxane **4** and bis-alkynyl analogue **6**.

4.2. Results and discussion

4.2.1. Formation of pseudorotaxane assemblies with ion pairs **2a-c**

We investigated the binding selectivity of axle **3** towards the two different binding sites of macrocycle **1**. To this end, we performed ^{1}H NMR titration experiments at millimolar concentrations of model receptors **7** (*N*-substituted C4P) and **8** (*C*-substituted C4P) with *N*-oxide **3** (**Figure 4.5**). The incremental addition of axle **3** to separate $CDCl_3$ solutions of **7** and **8** produced reduced changes in the ^{1}H NMR spectra of the free receptors (see Experimental Section). In particular, a reduced shift of the signals assigned to the aromatic protons Ha, Hb and Hf of **7** and **8** was observed. The downfield shift experienced by the NH protons of **7** and **8** after addition of more than 3 equivalent of the axle ($\Delta\delta$ = ~1.0 ppm) suggested the coordination of axle **3** through hydrogen bonding interactions with the oxygen atom.

The titration data were mathematically analyzed using HypNMR 2008 software Version 4.0.66. The fit of the chemical shift changes of the proton signals Ha and Hb to a binding model considering the formation of a 1:1 complex was good. We calculated the binding constant values as K[**3**⊂**7**] = 2.6 ± 0.2 x 10^2 M^{-1} and K[**3**⊂**8**] =

$5.4 \pm 0.4 \times 10^2\ M^{-1}$ (see Experimental Section). The difference between the calculated free energies of binding is $\Delta\Delta G = 0.36$ Kcal·mol^{-1}.

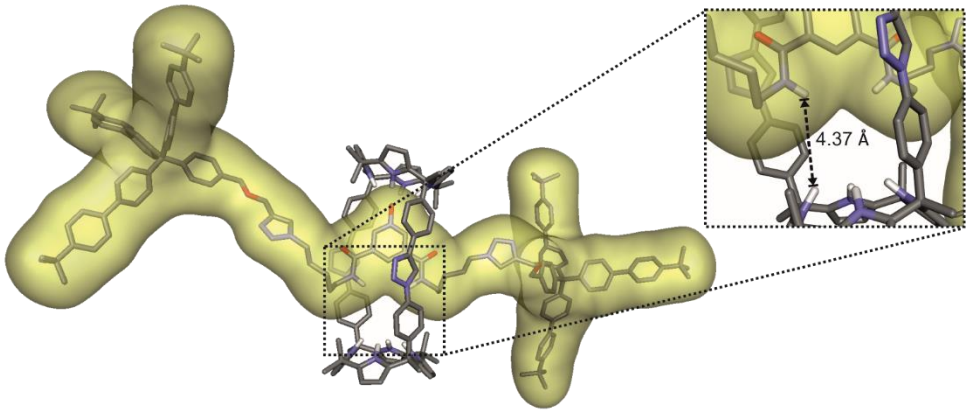

Figure 4.4. Energy-minimized structure (MM3) of [2]rotaxane **4**. Lineal component is depicted with a van der Waals surface. Non-polar hydrogens were removed for clarity. N-H···H-N distance between axle and macrocycle (inset).[24]

Taken together, these results suggest that axle **3** is expected to bind *C*-substituted hemisphere of **1** with a minor preference over the *N*-substituted.

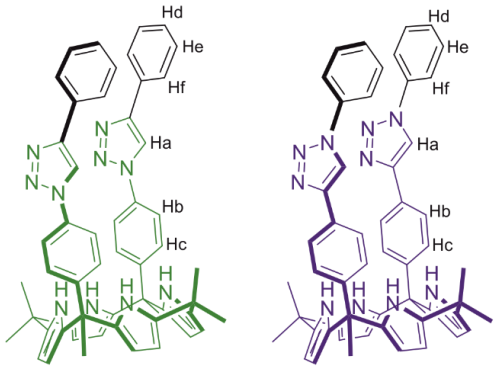

Figure 4.5. Schematic representation of model calix[4]pyrroles **7** and **8**.

We then performed ^{1}H NMR titrations experiments of receptor **1**, in $CDCl_3$ solution and at millimolar concentration, by adding incremental amounts of axle **3**. The addition of 0.5 equivalent of **3** into a solution of macrocycle **1** produced chemical shift changes for the signals of the Ha, Hb and Hc protons of the receptor (**Figure 4.6**). The proton signal assigned to the pyrrole NHs broadened beyond detection.

We also observed a new set of signals resonating at 8.4, 7.3 and 3.3 ppm. These signals were assigned to protons H1, H3 and H4-8, of axle **3**. The addition of up to 1 equivalent of the *N*-oxide axle **3** induced similar chemical shift changes in the proton signals of receptor **1** and axle **3**.

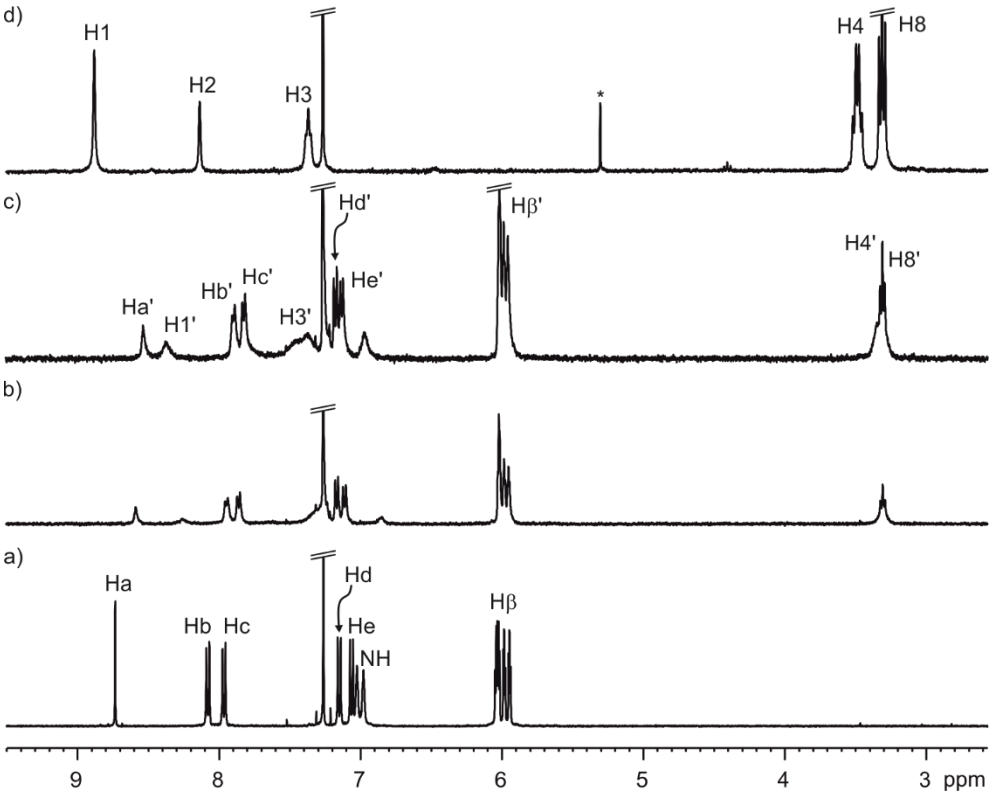

Figure 4.6. Selected region of the ^{1}H NMR spectra (400 MHz, 298 K, $CDCl_3$) acquired during the titration experiment of receptor **1** (a) with incremental additions of axle **3** (d): 0.5 equivalent (b) and 1.0 equivalent (c). Primed letters correspond to complex **3**⊂**1**. See Figure 4.2 for proton assignments. *Residual solvent signal.

Taken together, these results support the formation of a complex between receptor **1** and axle **3**. The binding equilibrium displayed exchange dynamics that were fast/intermediate for the proton signals of both binding partners i.e. fast for Ha-c and H1 and intermediate for NH. We hypothesized that in the formed complex, axle **3** threads macrocycle **1** forming four simultaneous hydrogen bonding interactions between the oxygen atom of the *N*-oxide group and the pyrrole NHs of one of the C4P binding site. In the complex, the bound axle can experience a pirouetting

motion inside the receptors cavity. This motion will led to an alternative binding of the two different C4P binding sites of receptor **1**. The change in the binding position of the axle in the complex can also be produced by its dissociation and re-assembly. The existence of chemical exchange processes in the binding equilibrium that are intermediate on the chemical shift timescale is supported by the broadening experienced by the NH signal of receptor **1**. The obtained results do not provide evidence for the binding selectivity of the *N*-oxide axle **3** for any of the two C4P sites of receptor **1**. We anticipated above that both binding sites in **1** are expected to have very similar affinity for axle **3**.

In this regard, we performed variable temperature ^{1}H NMR experiments using a mM $CDCl_3$ solution containing a 1:0.5 molar ratio of receptor **1** and *N*-oxide **3** (**Figure 4.7**). The ^{1}H NMR spectrum of the mixture recorded at 213 K displayed several set of signals for some of the protons of receptor **1**. One set of signals was easily assigned to the free receptor **1** by direct comparison with its ^{1}H NMR spectrum also acquired at 213 K. The remaining set of signals should correspond to protons of the bound receptor. For example, we observed two separate signals for the bound pyrrole NHs resonating at δ = 9.7 ppm (singlet) and δ = 9.6 ppm (broad singlet) while the free pyrrole NHs appeared at δ = 7.3 ppm. The existence of a duplicity of signals for some protons of the bound receptor suggested the presence of two binding geometries for the complex in solution. Moreover, the ratio of the integral values of the proton signals assigned to the free and bound receptor was close to 1:1. This result was indicative of a complexation of the receptor in 50% extent. We did not detect proton signals that could be assigned to the free axle **3**. Instead, each one of the two downfield shifted methylene groups, H4 and H8, of axle **3** appeared shifted and resonating as two separate signals of similar intensity.

In short, we propose the formation of a 1:1 complex, **3**⊂**1**, with pseudorotaxane topology. To further support this conclusion, the titration data were mathematically analyzed using HypNMR 2008 software Version 4.0.66. The fit of the chemical shift values of the Ha proton to a 1:1 binding model was good and returned a binding constant value of K[**3**⊂**1**] = 1.58 ± 0.04 x 10^3 M^{-1} (see Experimental Section). This value is one order of magnitude larger than the ones obtained for the model complexes **3**⊂**7** and **3**⊂**8**. We attribute this result to the preorganization of the calix[4]pyrrole binding sites when incorporated into the macrocyclic scaffold of receptor **1** compared to the more conformationally flexible structures of **7** and **8**. In the 1:1 complex, the pyridyl-*N*-oxide group of the axle binds at any of the two

different binding sites of the macrocycle **1**. At 213 K, the chemical exchange process between the free and bound components of the **3⊂1** complex is slow on the ^{1}H NMR chemical shift timescale. Likewise, the pirouetting motion of the axle inside the receptor also becomes slow on the ^{1}H NMR chemical shift timescale. The fact that the two binding geometries of the **3⊂1** complex are isoenergentic is in agreement with the results obtained in the titrations of the model C4P receptors **7** and **8** with axle **3**, where only a minor preference for the *C*-substituted hemisphere was observed. We did not detect any significant binding selectivity for axle **3**.

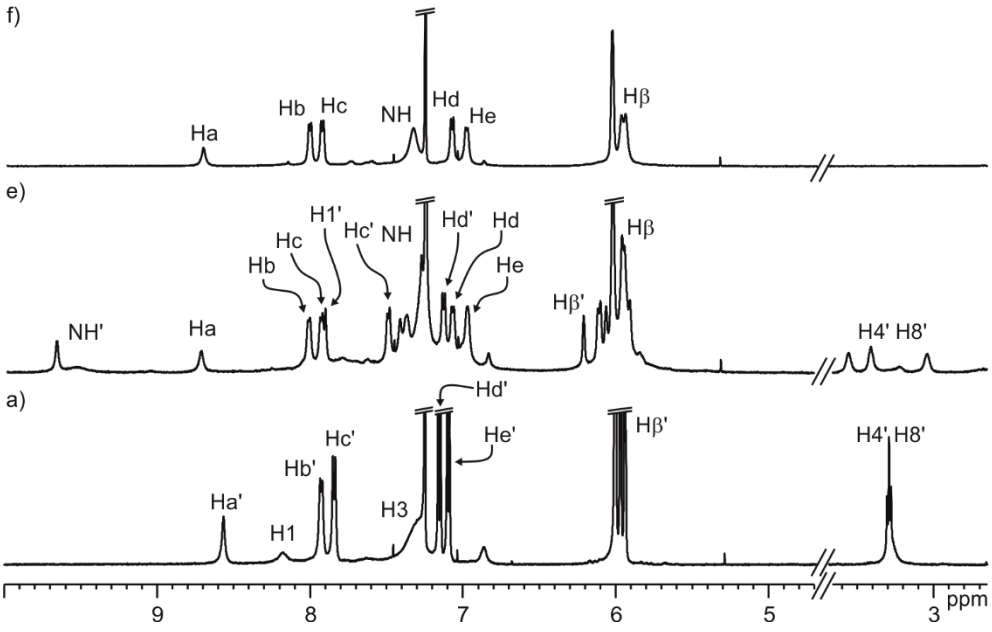

Figure 4.7. Selected region of the ^{1}H NMR spectra (500 MHz, $CDCl_3$) of a solution containing a 1:0.5 molar ratio of macrocycle **1** and axle **3** at 298 K (a) and 213 K (b). The corresponding region of the spectrum of the free macrocycle **1** at 213 K is depicted for comparison (c). Primed letter correspond to bound receptor **1**. See Figure 4.2 for proton assignments.

<u>^{1}H NMR characterization of the pseudorotaxane topology of the **3⊂1** complex assisted by coordination to tetraalkyammonium ion-pairs **2a-c**</u>

Using ^{1}H NMR titration experiments, we probed the interaction of the assembled **3⊂1** complex with a series of tetraalkylammonium halide ion-pairs **2a-c**. The resulting four particle aggregates are expected to feature pseudorotaxane topology. In chapter 3, we disclosed the binding properties of **1** towards the same series of tetraalkylammonium halide salts. We observed that the ion-pairs interacted with

macrocycle **1** producing 1:1 and 2:1 complexes. In addition, for the **2a**⊂**1** complex we demonstrated the preferential binding of MTOA·Cl (**2a**) in the *N*-substituted C4P binding site of the macrocyclic receptor **1**. We surmised that the lack of binding selectivity displayed by the axle **3** towards the two C4P binding sites of **1** will generate two isomeric binding geometries for the four particle [2]pseudorotaxane complexes produced with the assistance of the ion-pair.

The ^{1}H NMR spectrum of a 1 mM equimolar $CDCl_3$ solution of receptor **1** and axle **3** displayed sharp and well-resolved signals for most of the hydrogen atoms (**Figure 4.8a**). Under these conditions, the **3**⊂**1** complex is not quantitatively assembled but the chemical exchange between its free and bound components is fast on the chemical shift timescale. The addition of 1 equivalent of TBA·Cl **2b** to the above solution produced

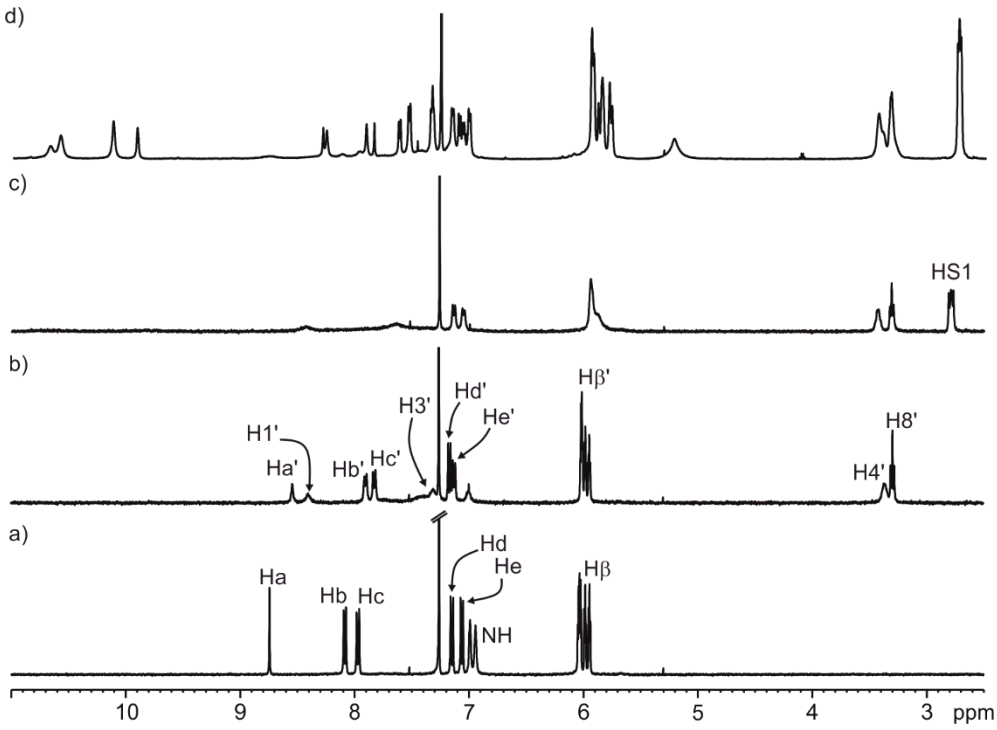

Figure 4.8. Selected region of the ^{1}H NMR titration experiment (400 MHz, $CDCl_3$) of free receptor **1** (a), equimolar mixture of **1** and **3** (b) and a 1:1:1 mixture of receptor **1**, axle **3** and TBA·Cl **2b** at 298 K (c) and 253 K (d). Primed letter correspond to complex **3**⊂**1**. See Figure 4.2 for proton assignments.

a dramatic broadening for most proton signals of the macrocyle **1** and axle **3**. We attributed this observation to the existence of chemical exchange processes between the different species in solution displaying intermediate dynamics on the

^{1}H NMR chemical shift timescale. Remarkably, the methylene group *alpha* to the nitrogen atom in the TBA$^+$ cation HS1 resonated as a well-defined signal at δ = 2.9 ppm. The upfield shift experienced by the methylene proton signal with respect to its value for the free TBA$^+$ cation ($\Delta\delta$ = -0.6 ppm) was indicative of its involvement in the binding event.

We performed variable temperature ^{1}H NMR experiments using the equimolar $CDCl_3$ solution of the macrocycle **1**, axle **3** and TBA·Cl **2a**. The ^{1}H NMR spectrum recorded at 253 K shows sharp and well-defined signals for all the protons of the three species (**Figure 4.8d**). In particular, we observed four singlets resonating between 10.7 - 9.8 ppm that were assigned to the NHs of bound **1**. We also detected two sharp singlets around δ = 8.3 ppm that were assigned to hydrogen atoms attached to the *sp*^{3} carbon of the triazole spacer. The aromatic protons of bound **1** resonated between 7.0 and 8.0 ppm (Hb, Hc, Hd and He) as two set of signals for each proton.

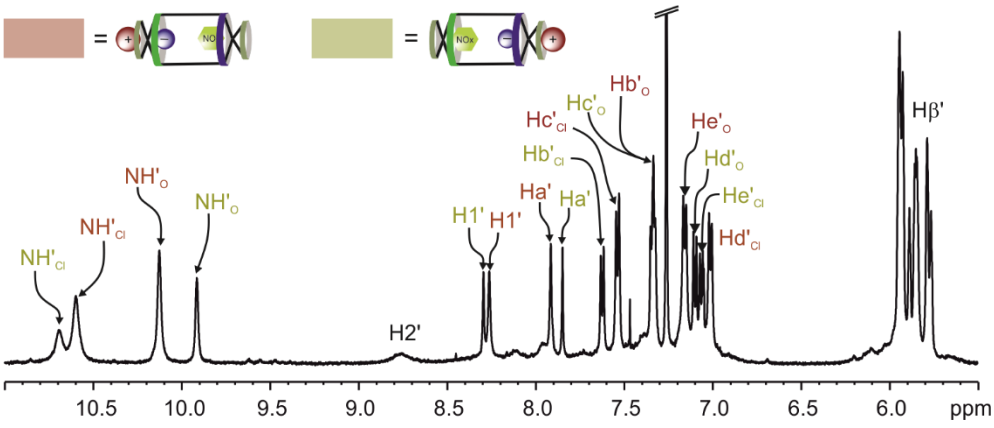

Figure 4.9. Selected region of the ^{1}H NMR spectrum (500 MHz, 253 K, $CDCl_3$) of the 1:1:1 mixture of receptor **1**, axle **3** and TBA·Cl **2b**. Primed letter correspond to the proton atoms in the complex **2b·3⊂1**. Proton signals highlighted in red correspond to the binding isomer of the complex **2b·3⊂1** in which the chloride is bound in the *N*-substituted binding site of **1**. Proton signals highlighted in yellow are assigned to the other binding isomer locating the chloride in the *C*-substituted C4P binding site of **1**. Suffix *O* and *Cl* for proton signals assigned to receptor **1** indicate binding to axle **3** and the Cl^- anion, respectively. See Figure 4.2 for proton assignments.

These observations provide strong support for the quantitative assembly of the **2b·3⊂1** complex. The complex is present in solution as a mixture of two geometrical isomers (**Figure 4.9**). The two isomers are involved in a chemical exchange process displaying slow dynamics on the proton chemical shift timescale at 253 K. In any of the two binding geometries of the **2b·3⊂1** complex, the Cl^- anion is stabilized by the

establishment of 6 simultaneous hydrogen bonding interactions between the 4 NH of one of the C4P binding sites of receptor **1** and the 2 amide protons of axle **3**. The involvement of the pyrrole NHs in the hydrogen-bonding interactions is inferred from the experienced downfield shift ($\Delta\delta$ = - 3.3 ppm). The TBA^+ cation is coordinated to the electron rich cavity of the C4P's cone conformation, opposite to the bound anion. The location of the cation derives from the upfield shift experienced by the signal of the methylene protons alpha to the nitrogen atom HS1.

Owing to the quantitative formation of the **2b·3⊂1** complex at mM concentration of its components, we estimated its stability constant as K[**2b·3⊂1**] > 10^8 M^{-2}.

The full assignation of the proton signals of the two isomers of **2b·3⊂1** and further details regarding their binding geometries was possible by performing ^{1}H-^{1}H ROESY and NOESY experiments using a solution of an equimolar mixture of the three components at 253 K (**Figure 4.10**). In the recorded spectra, we observed selective cross-peaks, related to space proximity, between the signals assigned to H1 of the axle in the two binding modes of the complex and the NH signals resonating at 10.1 and 9.9 ppm. In particular, the more downfield shifted signal of the H1 proton showed a NOESY/ROESY cross peak with the more upfield shifted NH signal. Based on these cross peaks and the preferential binding of Cl^- on the *N*-substituted binding site of **1**, we assigned the two NH signals to the pyrrole protons of **1** binding the oxygen atom of the pyridyl-*N*-oxide group of **3** in the two isomeric **2b·3⊂1** complexes.

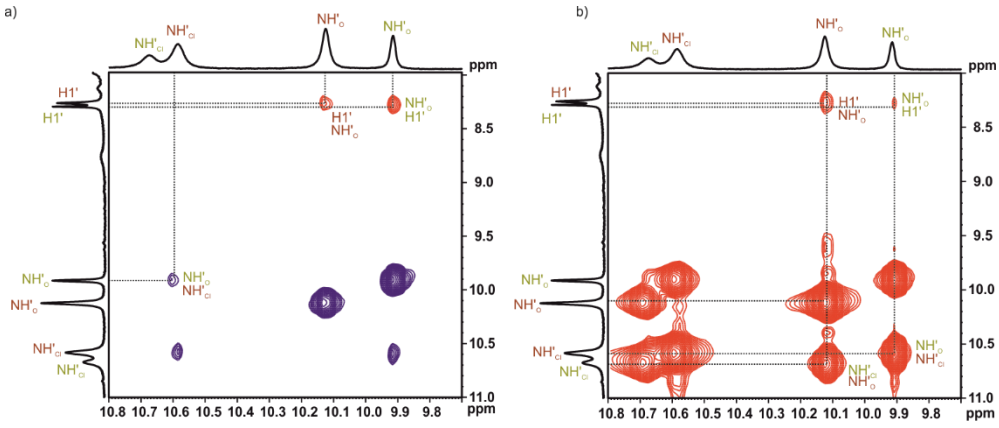

Figure 4.10. ^{1}H-^{1}H ROESY (a) and ^{1}H-^{1}H NOESY (b) (500 MHz, $CDCl_3$, 253 K, mixing time and spin-lock = 0.3 s) spectrum of the 1:1:1 mixture of macrocycle **1**, axle **3** and TBA·Cl **2b**.

Consequently, the two other signals resonating at 10.7 and 10.6 ppm must be assigned to the pyrrole NHs of **1** binding the Cl^- anion in the two binding geometries of the same complex. In the ^1H-^1H NOESY spectrum, we observed strong cross-peaks indicative of chemical exchange (positive sign in the ROESY spectrum) between pairs of pyrrole NHs assigned to the binding of chloride and the oxygen atom of the *N*-oxide in the two isomeric complexes. The chemical exchange between NH pairs binding the same nuclei (chloride or oxygen) in the two isomeric complexes is physically not feasible.

Multiple mechanisms might contribute to the observed chemical exchange process. For example, the dissociation/reassembly of the axle or the anion of one isomeric complex. Most likely, the dissociation of the axle occurs first as is the energetically more favored process. It requires the breaking of only three hydrogen bonds compared to six for the analogous chloride dissociation. The dissociation/reassembly of the cyclic component or its pirouetting motion around a preassembled **2b⊂3** complex could also explain the observed chemical exchange. However, this process requires the rupture of eight hydrogen bonds.

The integral values of the two pyrrole NH signals associated with each of the two isomers of the **2b·3⊂1** complex was used to calculate an isomeric distribution of *ca.* 0.65:0.35 (**Figure 4.11**). Based on the binding selectivity displayed by macrocycle **1** for the complexation of MTOA·Cl in the C4P binding site having *N*-substituted *meso*-

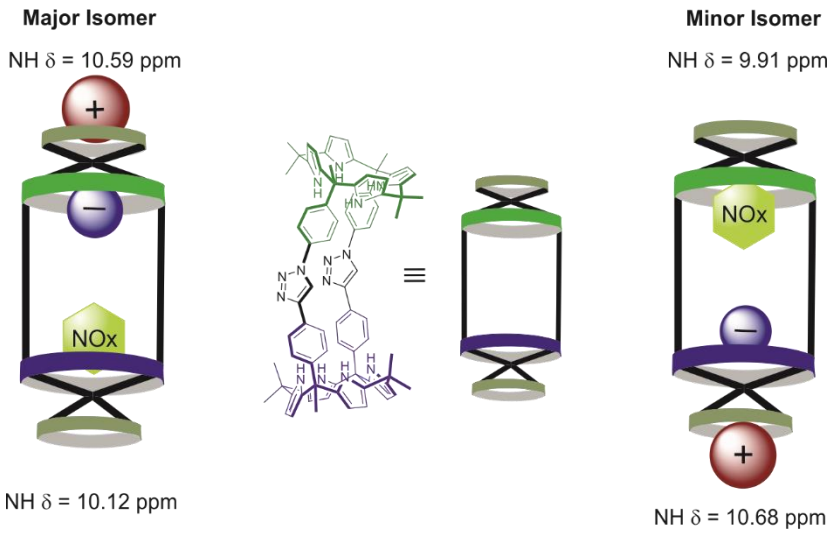

Figure 4.11. Cartoon representation of the two binding geometries of complex **2b·3⊂1**. Chemical shift of the C4P NH in the complexes is also depicted

phenyl rings, we hypothesized that the more abundant isomer of the **2b·3⊂1** complex contains the chloride anion in the identical C4P binding site (**Figure 4.12**).

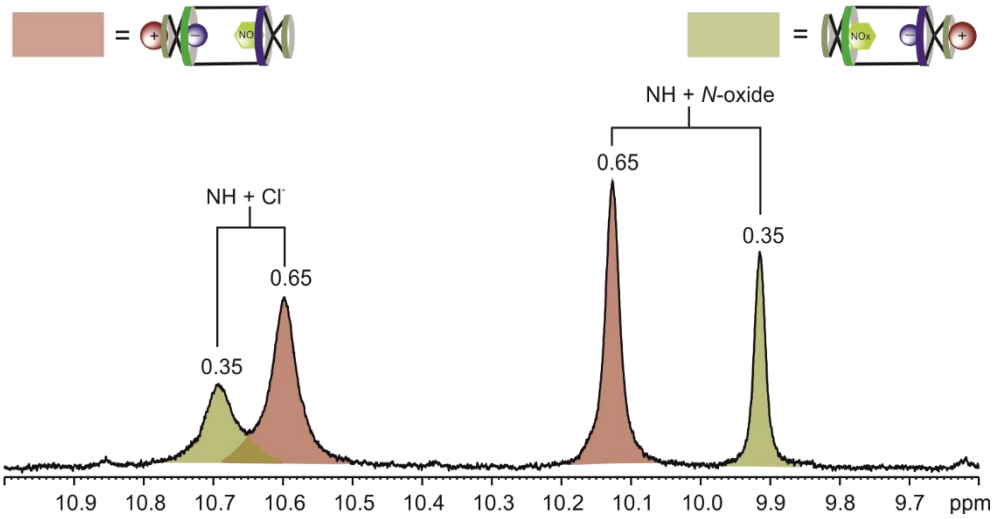

Figure 4.12. Selected region of the ^{1}H NMR spectrum (500 MHz, 253 K, $CDCl_3$) of a 1:1:1 mixture of receptor **1**, axle **3** and TBA·Cl **2b**. Proton signals highlighted in red correspond to the binding isomer of the complex **2b·3⊂1** in which the chloride is bound in the *N*-substituted binding site of **1**. Proton signals highlighted in yellow are assigned to the other binding isomer locating the chloride in the *C*-substituted C4P binding site of **1**. Suffix *O* and *Cl* for proton signals assigned to the NH protons of receptor **1** indicate binding to axle **3** and the Cl^- anion, respectively. Relative integral value of the signals are indicated.

Similar results were obtained in the ^{1}H NMR titration experiments of equimolar mixtures of **1** and **3** with incremental amounts of MTOA·Cl **2a** and TBA·OCN **2c** (see Experimental Section). Interestingly, for the majority of the protons signals, the exchange dynamics between the two isomers of the **2a·3⊂1** and **2c·3⊂1** complexes was slow on the chemical shift timescale even at 298 K. These findings were rationalized in terms of greater thermodynamic and kinetic stabilities displayed by the later complexes compared to **2b·3⊂1** (*vide infra*). The isomeric distribution observed for the TBA·OCN complex, **2c·3⊂1,** was identical to the one obtained for the TBA·Cl complex, **2b·3⊂1**. However, we obtained a 50:50 distribution ratio between the two binding isomers of the **2a·3⊂1** complex.[25] This result indicated that both isomers of complex **2a·3⊂1** are isoenergetic. We rationalize this result by invoking the binding selectivity displayed by MTOA·Cl **2a** towards the *N*-substituted binding site of receptor **1**, which ultimately erases the minimal binding selectivity of the *N*-oxide group of **3** for the *C*-substituted C4P binding site of **1**.

Thermodynamic characterization of the binding of the self-assembled pseudorotaxane complex **3⊂1** with tetraalkyammonium ion-pairs **2a-c**.

We performed ITC experiments at millimolar concentrations in $CHCl_3$ solution in order to quantify the binding affinity constant of the self-assembled pseudorotaxane complex **3⊂1** with a series of tetraakylammonium ion-pairs. The sequential injection of a solution of axle **3** into a solution containing an equimolar mixture of **1** and **2b** produced the gradual release of heat due to an exothermic binding process (**Figure 4.13**). The normalized integrated heat data displayed a sigmoidal binding isotherm with an inflection point centered at a **3/1** molar ratio of 1. The analysis of the titration data was performed using HypΔH software version 1.1.0. The data was analyzed assuming a binding model that considered the formation of complexes **2b⊂1**, **2b$_2$⊂1**, **3⊂1** and pseudorotaxane **2b·3⊂1**.[26] The values for the binding affinity constants and enthalpic contributions of complexes **2b⊂1**, **2b$_2$⊂1** and **3⊂1** were previously calculated (see Experimental Section) and were fixed during the mathematical analysis of the titration data. It is worth mentioning that the values estimated for the binding constant using this mathematical model will correspond to the apparent binding constant for the formation of the overall complex. An accurate calculation of the binding constant *K*[**3⊂1** ↔ **2b·3⊂1**] in a direct titration of **3⊂1** with **2b** is not feasible due to the competitive formation of 2:1 complexes between receptor **1** and **2b**. The best fit of

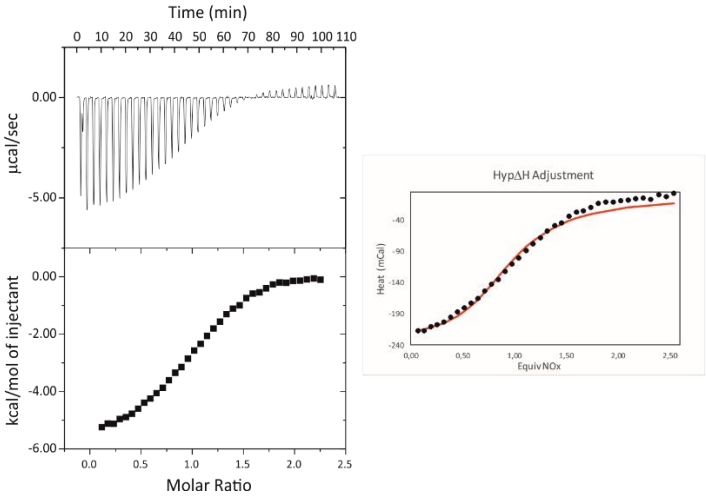

Figure 4.13. (Left) Top – Traces of the raw data (heat vs time) of the titration experiment of a $5 \cdot 10^{-4}$ M solution of receptor **1** and TBA·Cl **2b**, with a $7.5 \cdot 10^{-3}$ M solution of **3** in chloroform. Bottom – Binding isotherms of the calorimetric titration shown on top. (Right) Data adjustment (red line) performed with HypΔH software.

the experimental ITC data to the aforementioned mathematical model reported the thermodynamic values K[**2b·3⊂1**] = 4.3 ± 0.5 x 10^8 M^{-2} and ΔH = -10.8 ± 0.3 kcal·mol^{-1}.

The simulated speciation titration profile obtained with the calculated stability constant supports the quantitative formation of the pseudorotaxane complex **2b·3⊂1** with the working concentrations at the end of the titration (see Experimental Section).

Analogue results were obtained in the ITC experiments performed with ion pairs **2a** and **2c** (see Experimental Section). The calculated value for the stability constant of complex **2c·3⊂1** was one order of magnitude higher than that of the **2b·3⊂1** counterpart (K[**2c·3⊂1**] = 3.1 ± 0.5 x 10^9 M^{-2}) (**Table 4.1**). Despite the reduced cavity of the **3⊂1** complex compared to its bis-alkynyl analogue, it also displays a higher binding selectivity for TBA·OCN compared to TBA·Cl. We propose a better fit of the cylindrical anion in the three-dimensional polar cavity. We also observed an increase in the binding stability of 2 orders of magnitude for the **2a·3⊂1** complex (K[**2a·3⊂1**] = 6.0 ± 0.6 x 10^{10} M^{-2}) compared to its TBA^+ analogue. We rationalize this result invoking the superior fit of the methyl group of the $MTOA^+$ cation in the shallow aromatic cavity of the C4P core in cone conformation.

Table 4.1. Association constant values (M^{-2}) for the 1:1:1 complexes of macrocycle **1**, tetraalkylammonium salts **2a–c** and axle **3** measured in chloroform solution using HypΔH.

Ion pair	Ka x 10^{-8} (M^{-2})	ΔH (kcal/mol)
MTOA·Cl **2a**	4.3 ± 0.5	-10.8 ± 0.3
TBA·Cl **2b**	31 ± 5	-15.7 ± 0.1
TBA·OCN **2c**	600 ± 60	-14.9 ± 0.5

4.2.2. Synthesis and binding studies of [2]rotaxane **4**

Synthesis of **4**

[2]Rotaxane **4** was synthetized following the conditions previously developed by our group for the synthesis of the analogous [2]rotaxane receptor **6** (**Scheme 4.1**).[23] We prepared an 8 mM solution in DCM containing a mixture of receptor **1**, axle **3** and alkyne-functionalized stopper **5** using a strict stoichiometric molar ratio of 1:2:4. Next, we added 8 equivalent of DIPEA as base, 0.5 equivalent of TBTA ligand and 0.5 equivalent of $[Cu(CH_3CN)_4]PF_6$ as catalyst. The resulting yellow solution was left stirring at r.t. for 4 h. The reaction was then quenched and worked-up. [2]Rotaxane **4** was isolated as a brown solid in an 8 % yield after purification of the crude by silica

column chromatography using a gradient of solvents from pure DCM to 30% AcOEt in DCM.

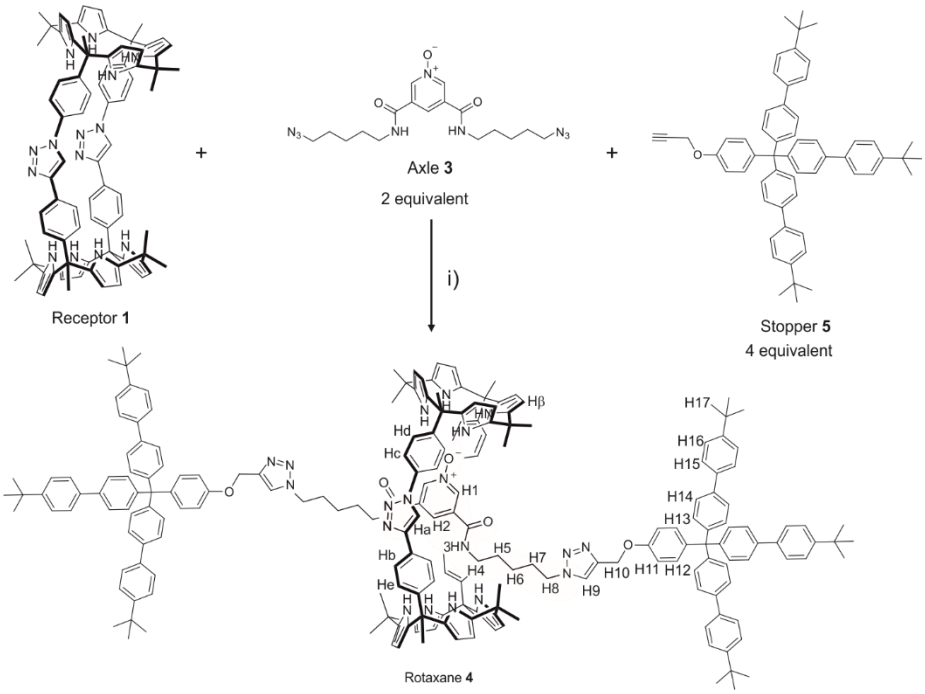

Scheme 4.1. Synthetic scheme of [2]rotaxane **4**. i) Reaction conditions: 0.5 equivalent of $[Cu(CH_3CN)_4PF_6]$, 0.5 equivalent TBTA and 8 equivalent of DIPEA in DCM. See Experimental Section for further details.

[2]Rotaxane **4** was fully characterized by a set of high-resolution spectra (1D and 2D NMR experiments as well as ESI-HRMS). The ^{1}H NMR spectrum of **4** in $CDCl_3$ solution showed sharp and well-resolved proton signals (**Figure 4.14**). We observed a broad signal at 9.2 ppm that was assigned to the NH protons of the macrocycle. The signal is downfield shifted in comparison to the NHs of free macrocycle **1** ($\Delta\delta$ = 2.2 ppm). We rationalize this observation by the existence of hydrogen bonding interactions between the NH protons and the oxygen atom of the pyridyl-*N*-oxide group in the lineal component. Taking into account the two different C4P binding sites presents in the macrocyclic component of **4**, we hypothesize that the lineal component is involved in a dynamic exchange binding process between the two C4P units of **4**. This process displays intermediate to fast dynamics on the ^{1}H NMR chemical shift timescale causing the broadening of some proton signals. Likewise, fast exchange dynamic is observed for other proton signals i.e. Ha-e assigned to the aromatic walls

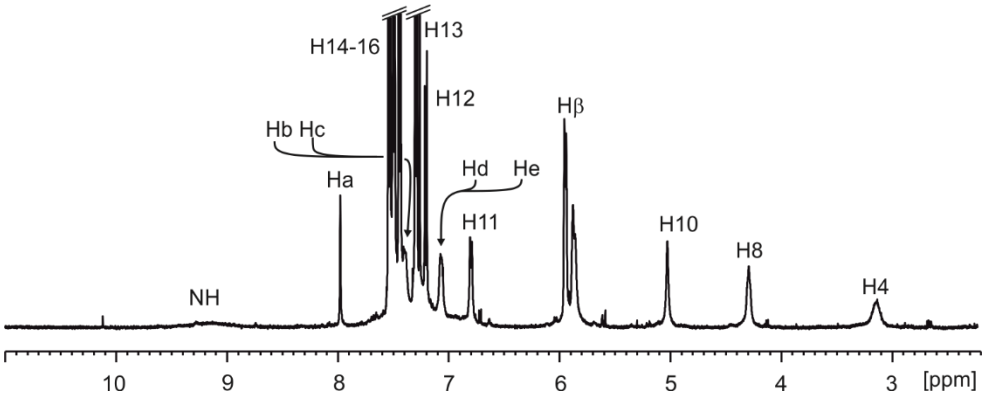

Figure 4.14. Selected region of the ^{1}H NMR spectrum (500 MHz, 298 K, $CDCl_3$) of [2]rotaxane **4**. See Scheme 4.1 for proton assignments.

of the macrocyclic component and protons H4, H8 and H10 attributed to the lineal component.

To further confirm the formation of [2]rotaxane **4**, we performed ^{1}H DOSY NMR experiments in $CDCl_3$ solution (**Figure 4.15**). The ^{1}H DOSY experiment assigned similar diffusion constant values using the decays of proton signals of either the macrocycle or the axle components ($D = 3.38 \pm 0.1 \times 10^{-10}$ $m^2 \cdot s$). Taking into account

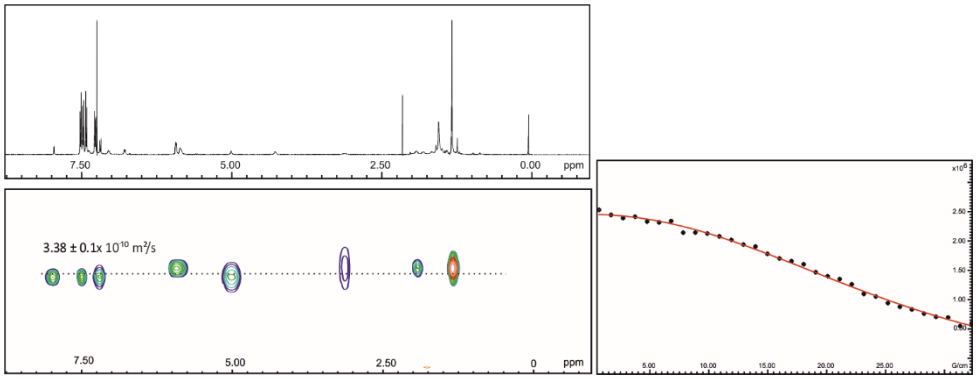

Figure 4.15. (left) ^{1}H pseudo 2D plot of DOSY (500 MHz, 298K, $CDCl_3$) of [2]rotaxane **4** (D20 = 0.15 s, P30 = 1 ms). (right) Fit of the decay of the signal of proton Ha to a mono-exponential function using Dynamics Center software from Bruker. Error is indicated as standard deviation.

the difference in sizes for the macrocycle and the axle, this result advocates for the formation of the interlocked molecule. We also performed ^{1}H-^{1}H ROESY experiments using a $CDCl_3$ solution of **4** (see Experimental Section). We observed cross-peaks related to spatial proximity between protons Hb and Hc of the aromatic

walls of the macrocyclic component and the protons H10 and H8 of the stoppered axle. This finding also supported the formation of the interwoven receptor **4**.

Taking into consideration the binding affinity constant of axle **3** towards receptor **1** (K[**3**⊂**1**] = 1.58 ± 0.04 x 10^3 M^{-1}) we expected that at the working concentrations a majority of the **3**⊂**1** complex would be formed in solution, favoring the subsequent formation of [2]rotaxane **4**. Indeed, the simulated speciation profile of the millimolar solution containing macrocycle **1** and axle **3** indicated the quantitative formation of **3**⊂**1** under the reaction conditions, i.e. a 1:2 ratio between macrocycle and axle (see Experimental section). On the other hand, we have shown that the **3**⊂**1** complex is involved in a binding equilibrium between free and bound components displaying intermediate to fast dynamic on the ^{1}H NMR chemical shift timescale (*vide supra*). This dynamic exchange may serve to explain the low yields of **4** (8%) obtained in the CuAAC reaction and the isolation of significant amounts of the free dumbbell axle. For this reason, we evaluated the template effect, if any, imposed by the binding of TBA·OCN **2c** by the **3**⊂**1** complex in the synthesis of [2]rotaxane **4**. Our expectations were that formation in solution of the complex **2c·3**⊂**1** would increase the thermodynamic stability of the pseudorotaxane structure.

We prepared a solution in deuterated DCM-d_2 containing a mixture of receptor **1**, axle **3**, TBA·OCN **2c** and alkyne-functionalized stopper **5** under strict 1:1:1:2 molar ratio and at 8 mM concentration with respect to **1**. We performed a ^{1}H NMR analysis of an aliquot withdrawn from the reaction mixture. The ^{1}H NMR spectrum of the mixture evidenced the quantitative formation of the pseudorotaxane assembly **2c·3**⊂**1** (**Figure 4.16a**). After the addition of the base and the catalytic system, the reaction was stirred at r.t. for 4 h. After that, the reaction was quenched and worked-up. The ^{1}H NMR spectrum of the reaction crude showed the presence of some of diagnostic signals attributed to the complex of the [2]rotaxane **4** with TBA·OCN (**Figure 4.16b**). We detected four proton signals in the low-field region of the spectrum that were assigned to the NHs of the macrocyclic component involved in hydrogen bonding interactions with the oxygen atom of *N*-oxide **3** (δ = 9.5 and 9.4 ppm) and the bound OCN^- (δ = 10.3 and 10.1 ppm). These signals are reminiscent to those observed for the two isomers of the **2c·3**⊂**1** pseudorotaxane complex. We also observed a sharp singlet resonating at 7.9 ppm that was assigned to the proton H9 attached to the sp^3 carbon of the triazole rings formed during the stoppering reaction. This proton signal is indicative of the covalent connection between the axle

and the stoppers. Interestingly, this proton signal was not detected in the ^{1}H NMR spectrum of the free [2]rotaxane due to the fast exchange dynamics of the lineal component (*vide supra*). Most likely, the pirouetting motions of the axle and the macrocycle become slower on the ^{1}H NMR chemical shift timescale when [2]rotaxane **4** binds the cyanate anion. Slow exchange dynamics were also observed between the two isomers of the **2c·3⊂1** complex.

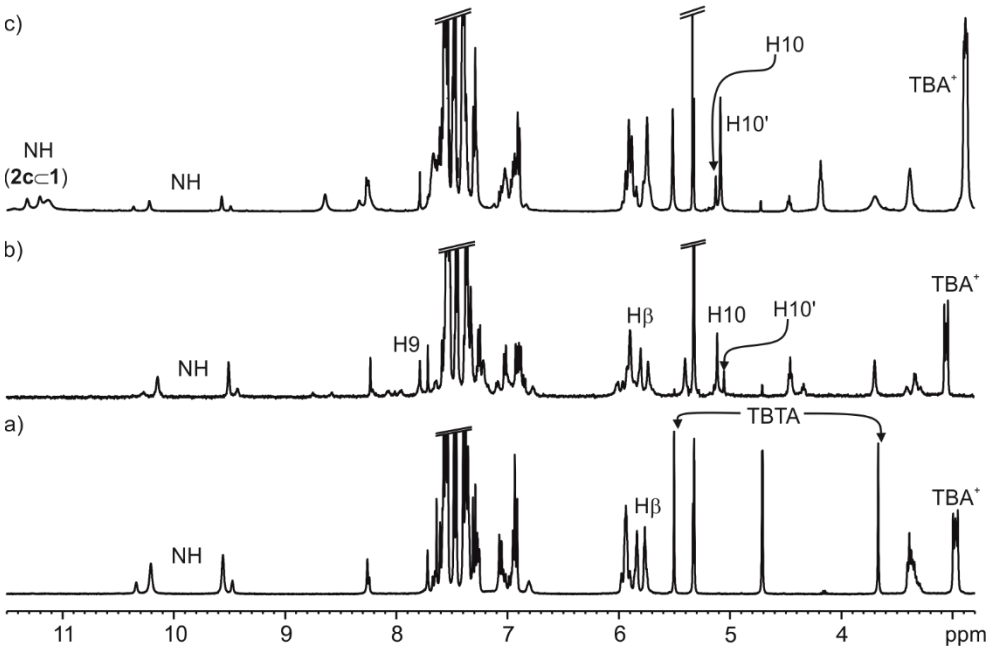

Figure 4.16. Selected region of the ^{1}H NMR spectra (400 MHz, 298K, DCM-d_2) of the TBA·OCN template synthesis of [2]rotaxane **4**: a) aliquot taken before the addition of the catalyst and b) reaction crude obtained. Spectrum c) shows the reaction crude obtained on the control experiment in which TBA·OCN **2c** was added only after the reaction was completed. Proton signal H10 is assigned to the interlocked lineal component while H10′ is assigned to free lineal component. See Scheme 4.1 for proton assignments.

We evaluated the extent to which [2]rotaxane **4** was formed under the used reaction conditions. To this end, we compared the integral values of the proton signals resonating at 5.1 and 5.0 ppm assigned to proton H10 in the interlocked and in the free-stoppered lineal component, respectively. We estimated that *ca.* 80% of the dumbbell axle was involved in the interlocked molecule **4** and only 20% remained free in solution. Then, we performed a control experiment under the same CuAAC reaction conditions in the absence of template cyanate salt. After the reaction was quenched and worked-up, we added 1 equivalent of TBA·OCN salt to the reaction crude with respect to the total amount of used macrocycle **1**. The ^{1}H

NMR spectrum of the resulting crude showed the diagnostic signals attributed to the bound [2]rotaxane **4** to TBA·OCN (**Figure 4.16c**). In addition, we observed a set of signals in the low field region of the spectrum that were assigned to the NH protons of **1** binding TBA·OCN. This finding was indicative of the presence of free macrocycle to a high extent in the reaction crude. By comparison of the integral values of the proton signals H10 in the free and interlocked dumbbell lineal component, we estimated that only 25% percent was involved in the [2]rotaxane **4**.

Taken together, the obtained results are indicative of the almost quantitative formation of the [2]rotaxane **4** in the template reaction mediated by TBA·OCN **2c**. The superior properties of TBA·OCN to template the formation of rotaxane **4** are rationalized by the increase in the thermodynamic and kinetic stability of the intermediate pseudorotaxane assembly **2c·3⊂1** compared to the **3⊂1** counterpart. Unfortunately, for the moment we have not been able to remove the ion-pair bound to the [2]rotaxane receptor **4**. We performed several purification attempts using normal- and reverse-phase column chromatography, aqueous extractions and anion-exchange resins. For this reason, we focused on the synthesis of **4** by the low-yield and capricious reaction methodology that does not involve the use of TBA·OCN **2c**.

Binding studies of [2]rotaxane **4** with ion pairs **2a-c**

The binding properties of [2]rotaxane **4** towards ion pairs **2a-c** were investigated in chloroform solution by means of ^{1}H NMR titration experiments.

The addition of 0.5 equivalent of TBA·OCN **2c** to a 2 mM solution of receptor **4** produced the appearance of a new set of sharp signals that were assigned to the bound receptor. The new set of signals clearly resemble those observed in the formation of the [2]pseudorotaxane complex **2c·3⊂1** (*vide supra*) (**Figure 4.17**). Along the course of the titration, the proton signals associated with bound **4** grew in intensity to the expenses of those of the free receptor. When 1 equivalent of the ion pair **2c** was added, we only detected the proton signals attributed to the bound receptor. This result indicates the formation of a 1:1 complex, **2c⊂4**, as a mixture of two isomers for which we can estimate a binding affinity constant larger than 10^4 M^{-1}. The four singlets resonating between 10.5 and 9.4 ppm are attributed to the pyrrole NH protons of bound **4** in the two isomeric complexes. The H1 proton corresponding to the triazole rings of the axle was broadened beyond detection in the ^{1}H NMR spectrum of free **4**. In contrast, it resonates as two sharp singlets at 8.3

ppm in the spectrum of the **2c⊂4** complex. The proton signals associated to the aromatic walls of the macrocyclic component in the **2c⊂4** complex appeared as 8 different doublets between 6.9 and 7.6 ppm. Moreover, in the initial phases of the titration, the signal attributed to the methylene proton *alpha* to the nitrogen atom in the TBA^+ cation (HS1), experienced a dramatic upfield shift compared to its free form ($\Delta\delta$ = -0.5 ppm). Addition of more than 1 equivalent of **2c** produced a gradual downfield shift of this signal, towards the chemical shift value of the free salt.

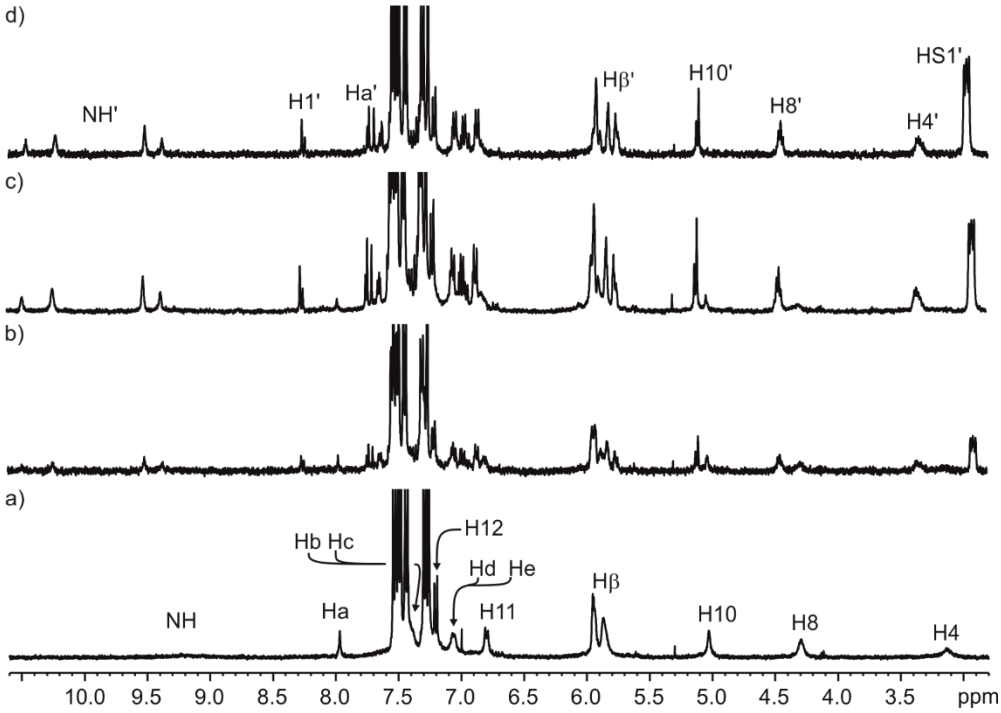

Figure 4.17. Selected region of the ^1H NMR spectra (400 MHz, 298 K, $CDCl_3$) acquired during the titration of [2]rotaxane **4** (a) with incremental additions of **2c**: 0.5 equivalent (b), 1.0 (b) and 1.5 (d) equivalent. Primed letter correspond to protons in the complex **2c⊂4**. See Scheme 4.1 for proton assignments.

In short, [2]rotaxane **4** acts as a heteroditopic receptor capable of coordinating TBA·OCN **2c**. Complex **2c⊂4** displays a macrocycle-separated binding mode with the OCN^- anion bound in the receptors inner cavity. The TBA^+ cation is located in the shallow and electron rich aromatic cavity generated by the C4P's cone conformation, opposite to the bound anion. The 1:1 complex **2c⊂4** exists in solution as two isomeric forms that are involved in a slow chemical exchange process on the ^1H NMR chemical shift timescale between. The isomeric ratio is 65:35 as observed in the pseudorotaxane analogue complex **2c·3⊂1** (**Figure 4.18**).

We performed ^{1}H-^{1}H ROESY and NOESY experiments using an equimolar solution mixture of **4** and **2c**. The observed cross peaks were in agreement with the results obtained for the pseudorotaxane assembly **2c·3⊂1** (see Experimental Section).

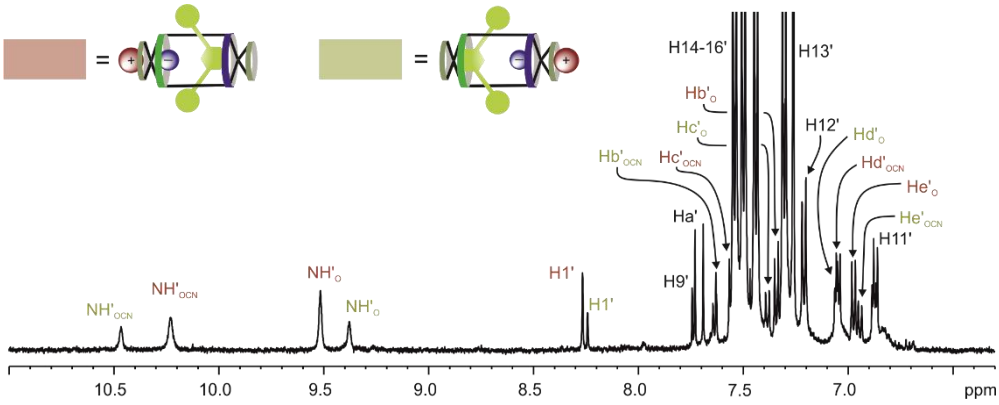

Figure 4.18. Selected region of the ^{1}H NMR spectrum (500 MHz, 298 K, $CDCl_3$) of a 1:1.5 mixture of [2]rotaxane **4** and TBA·OCN **2c**. Primed letters correspond to proton signals of complex **2c⊂4**. Proton signals highlighted in red correspond to the binding isomer of the complex **2c⊂4** in which the cyanate is bound in the *N*-substituted binding site of **4**. Proton signals highlighted in yellow are assigned to the other binding isomer locating the cyanate in the *C*-substituted C4P binding site of **4**. Suffix *O* and *OCN* for proton signals assigned to the protons of receptor **4** indicate binding to lineal component and the OCN^- anion, respectively. See Scheme 4.1 for proton assignments.

In general, the ^{1}H NMR titration experiment of receptor **4** with MTOA·Cl **2a** showed similar spectroscopic changes than those described for the binding of the cyanate salt (**Figure 4.19**). Surprisingly to us, a set of four proton signals resonating between 9.7 and 9.3 ppm emerged after the initial additions of the salt (0-0.5 equivalent). The intensity of this set of proton signals remained unchanged throughout the course of the titration. In contrast, the proton signals of the pyrrole NHs assigned to the two isomers of the **2a⊂4** complex grew in intensity with the incremental addition of the salt. The isomeric ratio was close to 50:50 as observed for the **2a·3⊂1** pseudorotaxane counterpart (**Figure 4.20**). We were also surprised to observe proton signals of the free receptor **4** (e.g. H8 and H10) in the presence of more than 1.5 equivalent of the ion pair. This result is also striking when compared to the quantitative formation of the **2c⊂4** and the **2a·3⊂1** complexes, in the presence of just 1 equivalent of the salts. The proton signal associated to the methylene group *alpha* to the nitrogen atom in the $MTOA^+$ cation appeared upfield shifted with respect to its free form ($\Delta\delta$ = - 0.6 ppm) and quite broad. While the first observation is indicative of the inclusion of the MTOA cation in the shallow and electron rich aromatic cavity generated by the C4P units of **4**, the second suggest its involvement

in other binding processes than the complexation with **4**. We speculate that the used sample of the [2]rotaxane **4** might contained some impurities that led to the appearance of the unexpected set of proton signals. At the moment, we do not have any plausible explanation for these results and producing additional batches of pure **4** rotaxane has proven to be very troublesome.

Titration experiments carried out with of TBA·Cl **2b** gave analogue results to the ones obtained with MTOA·Cl **2a** (see Experimental Section).

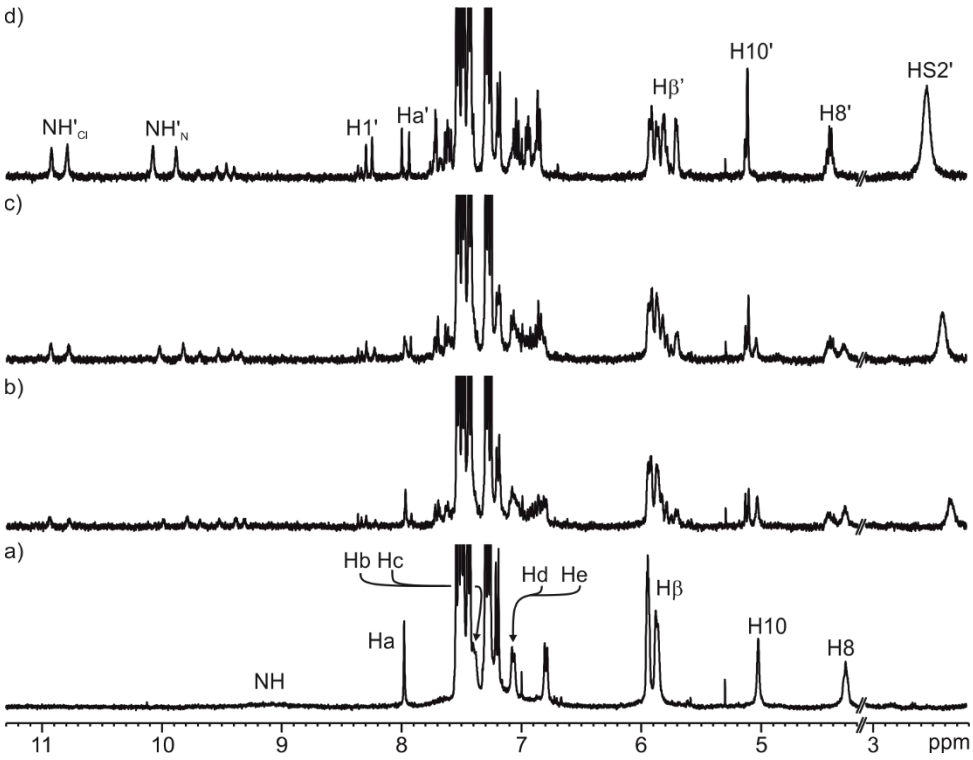

Figure 4.19. Selected region of the ^{1}H NMR spectra (400 MHz, 298 K, $CDCl_3$) acquired during the titration experiment of [2]rotaxane **4** (a) with incremental additions of MTOACl **2a**: 1.0 (b), 1.5 (b) and 2.0 (d) equivalent. Primed letter correspond to complex **2a**⊂**4**. See Scheme 4.1 for proton assignments.

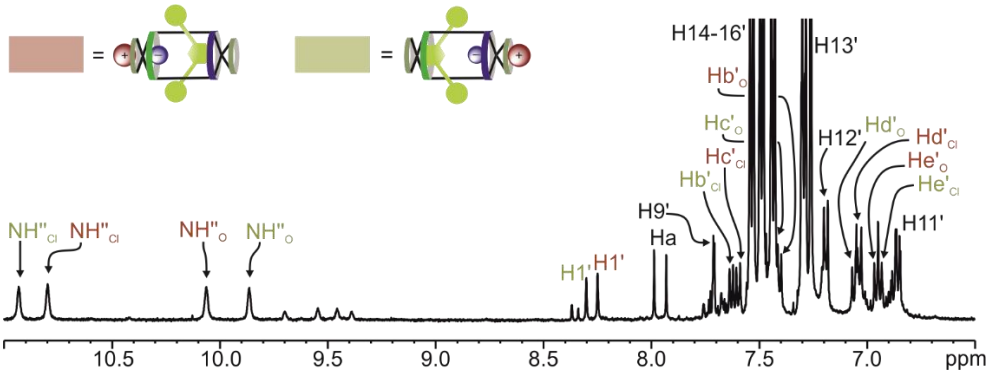

Figure 4.20. Selected region of the ^{1}H NMR spectrum (500 MHz, 298 K, $CDCl_3$) of a 1:2 mixture of [2]rotaxane **4** and MTOA·Cl **2a**. Primed letters correspond to proton signals of complex **2a**⊂**4**. Proton signals highlighted in red correspond to the binding isomer of the complex **2a**⊂**4** in which the chloride is bound in the *N*-substituted binding site of **4**. Proton signals highlighted in yellow are assigned to the other binding isomer locating the chloride in the *C*-substituted C4P binding site of **4**. Suffix *O* and *Cl* for proton signals assigned to the protons of receptor **4** indicate binding to lineal component and the Cl^- anion, respectively. See Scheme 4.1 for proton assignments.

4.2.3. Gas phase characterization

All the complexes previously discussed were characterized by means of ESI-MS and IMS-TW experiments. Likewise, we investigated the relative stability of the pseudorotaxane and [2]rotaxane complexes by CID experiments.

Gas phase characterization of pseudorotaxane assemblies

We performed an ESI-MS analysis of an equimolar mixture of **1**, **3** and **2c** in methanol at μM concentrations. In the chromatogram we observed the presence of an ion peak with m/z = 1680.9043 (**Figure 4.21**). We attributed this ion peak to complex [**OCN**·**3**⊂**1**]$^-$. The experimental isotopic pattern of the molecular ion matched the theoretical one (see Experimental Section). Similar results were obtained in an analogue experiment using TBA·Cl **2b** in which we detected the ion peak of molecular ion [**Cl**·**3**⊂**1**]$^-$ (see Experimental Section). From these results we concluded that the transition of the complexes from solution to the gas-phase implied the loss of the weakly coordinated cation, generating negatively charged complexes.[27]

The stability of the pseudorotaxane complexes was investigated by CID experiments. Gradual increase of the voltage applied at the entrance of the hexapole produced the fragmentation of the mass-selected molecular ion [**OCN**·**3**⊂**1**]$^-$ (**Figure 4.21**). We observed the appearance of two ion peaks of m/z = 1276.6809 and 445.2153 at high voltage values (34 V) that were assigned to

complexes [**OCN⊂1**]$^-$ and [**OCN⊂3**]$^-$, respectively. Further increase of the voltage values produced the total disassembly of the pseudorotaxane to regenerate the free macrocyclic component, as inferred by the presence of an ion peak with m/z = 1233.6758 attributed to the [**1**-H]$^-$ ion. These results point out to the disassembly of complex [**OCN·3⊂1**]$^-$ by two simultaneous mechanisms (**Figure 4.22**). We hypothesize that a first process consists on the dethreading of neutral axle **3** to generate charged complex [**OCN⊂1**]$^-$. Further increase of the voltage applied produces the dissociation of the cyanate anion, lost as H·OCN to regenerate the free

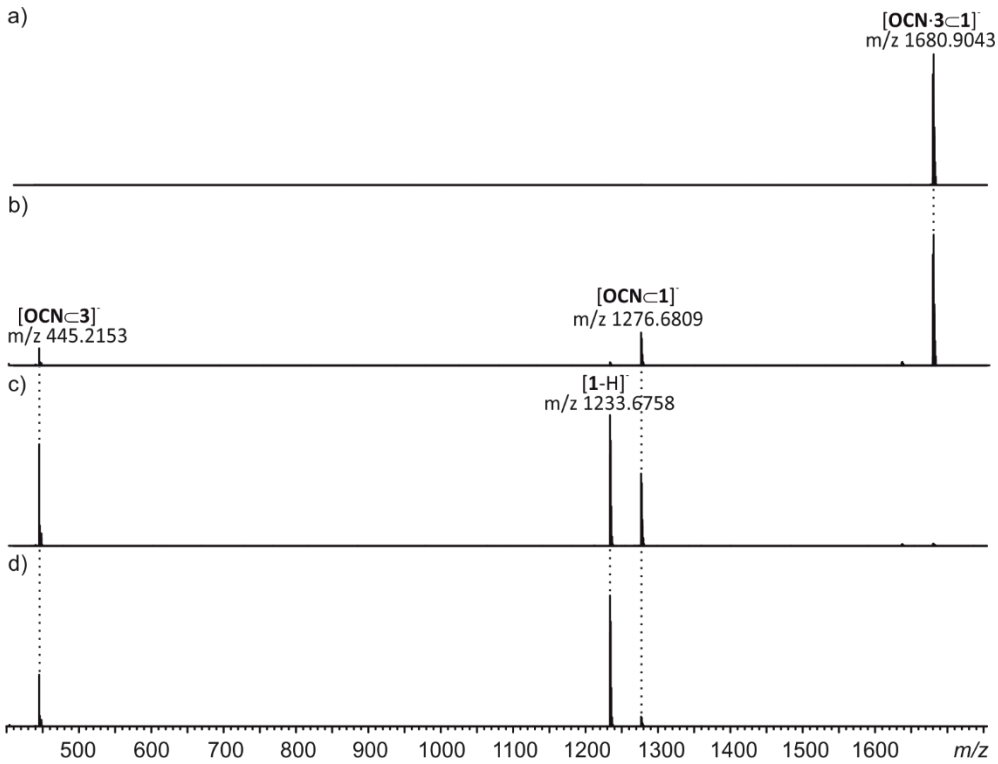

Figure 4.21. CID experiment performed with mass-selected ion [**OCN·3⊂1**]$^-$ a) with CE of 22 V b), 34 V c) and 40 V d).

macrocycle [**1**-H]$^-$. The second process for the disassembly of [**OCN·3⊂1**]$^-$ implies the concomitant dissociation of the cyanate anion and the axle in the form of [**OCN⊂3**]$^-$. This produces the recovery of neutral macrocycle **1**, which is not detected in the ESI-MS chromatogram. Attending to the relative intensity of the ion peaks of the complexes aforementioned, the preferred mechanism for the disassembly of [**OCN·3⊂1**]$^-$ involves the dissociation of axle **3**. This is most likely due to the greater affinity of the cyanate anion towards the C4P core of macrocycle **1** than for the

amide NH of axle **3**. Indeed, the binding affinity constant calculated in chloroform for complex **OCN⊂3** was K[**2c⊂3**] = 3.2 ± 0.7 x 10^3 M^{-1}, one order of magnitude lower than the one obtained for macrocycle **1** (see Experimental Section).

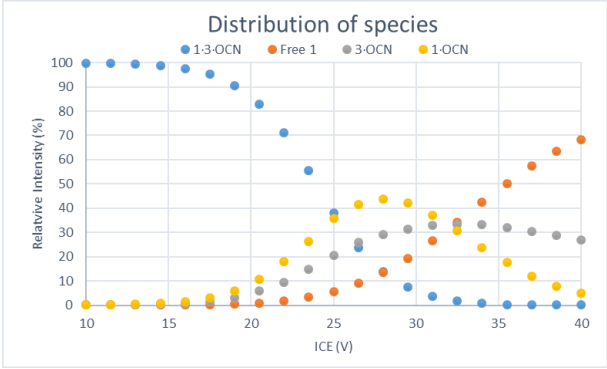

Figure 4.22. Relative intensity of the fragments observed in the CID experiment of complex [**OCN·3⊂1**]$^-$ at increasing CE voltages. The intensity was calculated as Intensity = I. Complex / (I. Complex + I. Fragments) x 100%.

In the CID experiments carried out with TBA·Cl **2b** we obtained analogue results (see Experimental Section). Likewise, disassembly of complex [**Cl·3⊂1**]$^-$ was confirmed by the appearance of molecular ions [**Cl⊂3**]$^-$ and [**Cl⊂1**]$^-$. Interestingly, the relative intensity of the ion peaks of these two complexes revealed that the disassembly of complex [**Cl·3⊂1**]$^-$ takes place mainly by the dissociation of [**Cl⊂3**]$^-$. This is in striking

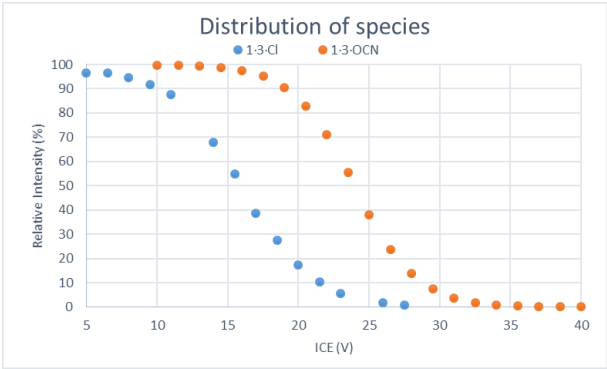

Figure 4.23. Relative intensity of molecular ions [**OCN·3⊂1**]$^-$ and [**Cl·3⊂1**]$^-$ observed in the CID experiment at increasing CE voltages. The intensity was calculated as Intensity = I. Complex / (I. Complex + I. Fragments) x 100%.

contrast to what we observed for complex [**OCN·3⊂1**]$^-$. These findings were rationalized in terms of the greater affinity of the Cl$^-$ anion towards axle **3**. The value for the binding affinity constant calculated in chloroform for complex [**Cl⊂3**]$^-$ was K[**2b⊂3**] = 1.3 ± 0.4 x 10^4 M^{-1}, almost one order of magnitude higher than the one obtained for receptor **1** (see Experimental Section).

Table 4.2. CE_{50} values obtained in the CID experiments of the complexes formed between receptor **1**, axle **3** and ion paris **2b-c**.

Complex	CE_{50} (V)
[OCN·3⊂1]$^-$	24
[Cl·3⊂1]$^-$	16

The relative stability of the 2:1 assemblies was investigated by direct comparison of the collision energy necessary to disassemble the complex to a 50% extent (CE_{50}) (**Figure 4.23**). The results obtained advocate for the greater stability of complex [**OCN·3⊂1**]$^-$ (**Table 4.2**). This is in agreement with the results obtained in the ^{1}H NMR and ITC titration experiments carried out in chloroform solution. We rationalize these results by invoking the greater compatibility in size and shape of the cylindrical polyatomic anion with the binding site generated between axle **3** and macrocycle **1**.

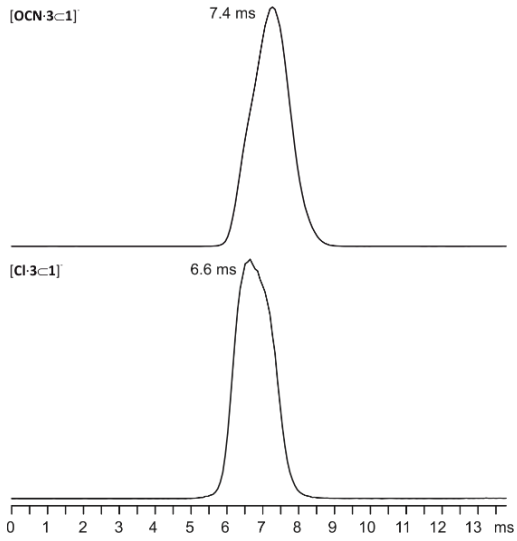

Figure 4.24. Arrival time distribution of molecular ions [**OCN·3⊂1**]$^-$ and [**Cl·3⊂1**]$^-$.

Finally, we ran IMS-TW experiments in order to investigate the effect of the isomeric forms of the complexes (**Figure 4.24**). However, we were not able to separate the isomeric forms of complexes [**OCN**·**3**⊂**1**]$^-$ and [**Cl**·**3**⊂**1**]$^-$ most likely due to the similar cross-section of the two species. In addition, we obtained similar arrival times for the two complexes owing to the similar sizes of the bound anions.

Gas phase characterization of [2]rotaxane complexes

We performed ESI-MS experiments to a methanol solution containing an equimolar

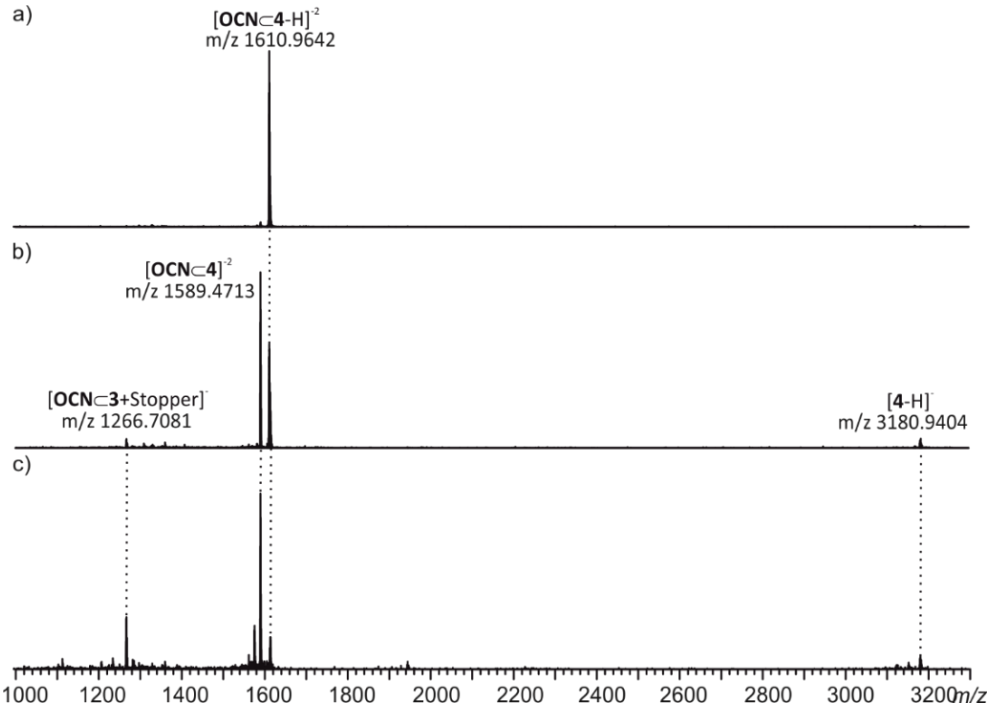

Figure 4.25. CID experiment performed with mass-selected ion [**OCN**⊂**4**-H]$^{-2}$ a) with CE of 22 V b) and 44 V c).

mixture of **4** and **2c** at μM concentrations (**Figure 4.25**). The obtained chromatogram revealed the presence of an ion peak with m/z = 1610.9642. We attributed this ion peak to the molecular ion [**OCN**⊂**4**-H]$^{-2}$. The observed isotopic pattern was similar to the theoretical one, confirming the presence of the doubly-charged ion (see Experimental Section).

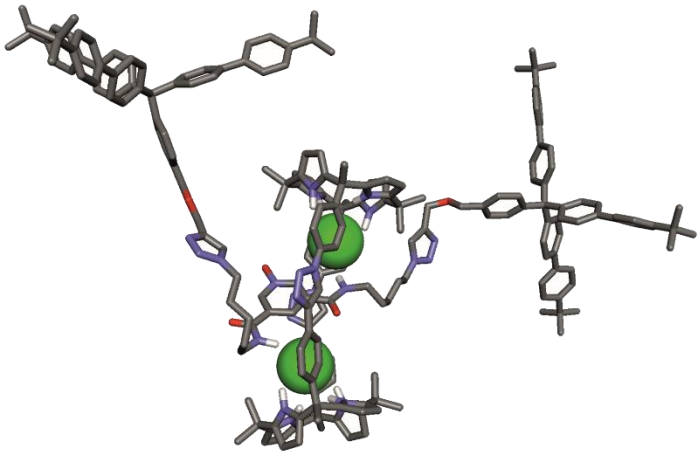

Figure 4.26. Energy-minimized structure (MM3) of complex (**Cl**)$_2$⊂**4**. Non-polar hydrogens were removed for clarity. [24]

We performed an analogue experiment with TBA·Cl **2b** where we observed the presence of molecular ion [**Cl**⊂**4**-H]$^{-2}$ (see Experimental Section).[28] Interestingly, we also detected an ion peak with m/z = 1624.3500 that was attributed to the doubly-charged ion [(**Cl**)$_2$⊂**4**]$^{-2}$. Most likely, this complex features two chloride anions bound to each of the C4P units of the macrocyclic component. In this complex, the axle is located slightly displaced from the interior cavity of the macrocycle, as depicted in the energy minimize structure (**Figure 4.26**). This species was not observed in the ^{1}H NMR experiments carried out in chloroform solution. However, formation of 2:1 complexes was already described in our previous work with bis-alkynyl analogue **6**.[23]

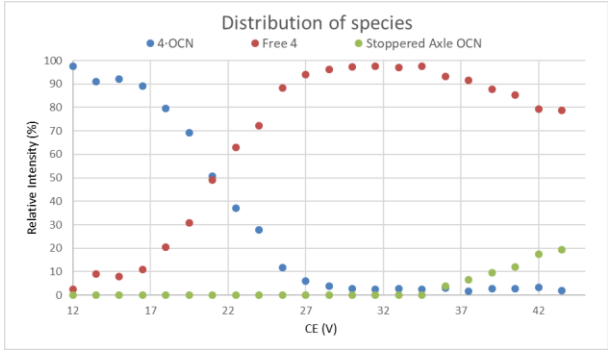

Figure 4.27. Relative intensity of the fragments observed in the CID experiment of complex **[OCN⊂4-H]$^{-2}$** at increasing CE voltages. The intensity was calculated as Intensity = I. Complex / (I. Complex + I. Fragments) x 100%.

We investigated the stability of the complex formed with **2c** by means of MS-CID experiments (**Figure 4.25**). The gradual increase of voltage applied at the entrance of the hexapole produced the fragmentation of the mass-selected ion [**OCN**⊂**4**-H]$^{-2}$. We detected an ion peak with m/z = 1589.4713 that grew in intensity as the voltage applied increased. We assigned this ion peak to complex [**4**-2H]$^{-2}$ generated by the dissociation of cyanate in the form of H·OCN. At higher values of applied voltage, we also observed an ion peak with m/z = 1266.7081 that was attributed to the mono-stoppered axle bound to the cyanate anion.

The results obtained suggest that complex [**OCN**⊂**4**-H]$^{-2}$ disassembles in the gas phase mainly through the loss of H·OCN, recovering the doubly-deprotonated [2]rotaxane [**4**-2H]$^{-2}$. The previous mechanism observed for the pseudorotaxane assemblies consisting on the dissociation of the axle is now energetically demanding. For this to occur, the cleavage of a covalent bond has to take place. This is observed at higher values of applied voltage as evidenced by the presence of the mono-stoppered axle (**Figure 4.27**).

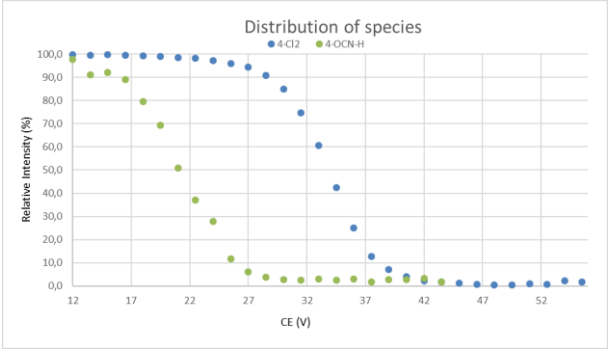

Figure 4.28. Relative intensity of molecular ions [**OCN**⊂**4**-H]$^{-2}$ and [(**Cl**)$_2$⊂**4**]$^{-2}$ observed in the CID experiment at increasing CE voltages. The intensity was calculated as Intensity = I. Complex / (I. Complex + I. Fragments) x 100%.

We also performed MS-CID experiments to the complexes obtained with TBA·Cl [**Cl**⊂**4**-H]$^{-2}$ and [(**Cl**)$_2$⊂**4**]$^{-2}$. We observed similar dissociation mechanisms as in the complexes obtained with the cyanate anion (see Experimental Section). Interestingly, we needed to apply a voltage of approximately 45 V to produce the total disassembly of molecular ion [(**Cl**)$_2$⊂**4**]$^{-2}$, pointing out to the greater stability of the 2:1 complex.

Table 4.3. CE_{50} values obtained in the CID experiments of the complexes formed between [2]rotaxane **4** and ion pairs **2b-c**.

Complex	CE_{50} (V)
[OCN⊂4-H]$^{-2}$	21
[(Cl)$_2$⊂4]$^{-2}$	33

The higher value of CE_{50} calculated for complex [(**Cl**)$_2$⊂**4**]$^{-2}$ when compared with the one obtained for [**OCN**⊂**4**-H]$^{-2}$ points out to the higher stability of the 2:1 complex (**Table 4.3**)(**Figure 4.28**).[29] This was expected, as the hydrogen-bonding interaction established with the NH can be stronger with the bound chloride anion due to the more concentrated charge.

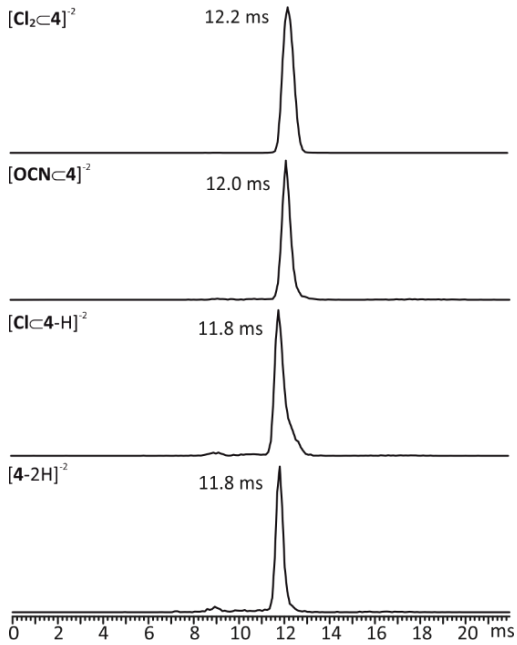

Figure 4.29. Arrival time distribution of the species observed in the CID experiments of [2]rotaxane **4** and ion pairs **2b-c**.

We also performed IMS-TW experiments to separated solutions containing 1:1 mixtures of **4** with **2b** and **2c**. We obtained similar arrival times distribution for all the complexes. Most likely, the similar size of the bound anions does not significantly alter the cross-section of the complex, even in the case of the 2:1 complex [(**Cl**)$_2$⊂**4**]$^{-2}$. Similar to what we obtained in the experiments performed to

the pseudorotaxane complexes, we were not able to separate the isomeric forms of the [2]rotaxane complexes.

4.3. Conclusions

In this chapter, we investigated the formation of pseudorotaxane complexes between macrocycle **1** and axle **3**. The assembly of the pseudorotaxane complexes was templated by tetraalkylammonium ion pairs **2a-c**. We proved the formation of thermodynamically and kinetically stable complexes with all the salts studied by ^{1}H NMR and ITC experiments. In the complexes, the axle was coordinated to receptor **1** by the establishment of hydrogen bonding interactions between the oxygen atom of the *N*-oxide knob of **3** and the NH protons of the C4P of **1**. Simultaneously, the bound anion was located in the polar cavity generated between macrocycle **1** and bound axle **3.** The anion was stabilized by the establishment of up to six hydrogen bonding interactions: four with the C4P unit of **1** and two with the amide protons of axle **3**. We observed that the pseudorotaxane complexes existed in solution as two isomeric forms depending on the binding of the anion and the axle in each of the two inequivalent hemispheres of receptor **1**. We observed that for the complexes obtained with TBA·Cl and TBA·OCN the isomeric distribution was of 0.65 to 0.35. Binding of the anion in the *N*-substituted hemisphere was energetically more favorable, owing to the less repulsive interactions between the bound anion and the aromatic panels of the macrocycle. In the case of MTOA·Cl, the two isomeric forms obtained were isoenergetic. We explained these results by the difference in selectivity displayed by the ion pair towards the *N*-substituted hemisphere when compared with **2b** and **2c**. We estimated values for the binding constant for the three complexes in the order of $10^{8} – 10^{10}$ M^{-2}. The greater stability observed for complex **2a**·**3**⊂**1** was explained by the better fit of the methyl group of the $MTOA^{+}$ cation into the shallow and electron rich cavity generated in the receptor's cone conformation. At the same time, the higher value for the binding affinity constant obtained for TBA·OCN over TBA·Cl was rationalized by invoking the better fit of the cylindrical anion inside the cavity generated in **3**⊂**1**. Analogue results in the stability of the pseudorotaxane assemblies were obtained in the gas-phase experiments performed by ESI-MS.

We also described in this chapter the synthesis of [2]rotaxane **4** by the CuAAC reaction of axle **3** with alkyne functionalized stoppers **5**. The low yield obtained in the reaction (8%) prompted us to use TBA·OCN as a template to favor the formation of the interlocked molecule. In the presence of 1 equivalent of TBA·OCN we

observed the almost quantitative formation of [2]rotaxane in the ^{1}H NMR analysis of the crude obtained. However, we were not able to dissociate the bound anion from the receptor's cavity after purification. We also investigated the properties of [2]rotaxane **4** to bind tetraalkylammonium salts **2a-c** by ^{1}H NMR titration experiments. We obtained thermodynamically and kinetically stable complexes with all the ion pairs studied. As observed in the pseudorotaxane assemblies, the obtained complexes exist in solution as a mixture of two isomeric forms according to the coordination of the anion in each of the C4P units. Similar isomeric distributions were observed as for the case of pseudorotaxane complexes. The experiments carried out in the gas phase also revealed the formation of a 2:1 complex with chloride that proved to be more stable than the 1:1 complex obtained with the cyanate salt.

4.4. Experimental section

4.4.1. General information and instruments

Reagents were obtained from commercial suppliers and used without further purification unless otherwise stated. All solvents were commercially obtained and used without further purification. Dry solvents were taken from a solvent system MB SPS 800. DCM was degassed by three freeze-pump-thaw cycles before used in the CuAAC reaction. Routine ^{1}H NMR and ^{13}C {^{1}H} NMR spectra were recorded on a Bruker Avance 300 (300 MHz for ^{1}H NMR and 75 MHz for ^{13}C NMR), Bruker Avance 400 (400 MHz for ^{1}H NMR and 100 MHz for ^{13}C NMR), Bruker Avance 500 (500 MHz for ^{1}H NMR and 125 MHz for ^{13}C NMR) or Bruker Avance 500 with cryoprobe (500 MHz for ^{1}H NMR and 125 MHz for ^{13}C NMR). Deuterated solvents were purchase from Sigma Aldrich. Chemical shifts are reported in ppm using residual solvent peaks as reference. Coupling constant values J are given in Hz. COSY, NOESY, ROESY, HMQC and HMBC experiments were recorded to help with the assignment of ^{1}H and ^{13}C signals. High-resolution mass spectra (HRMS) were obtained on a Bruker HPLC-TOF (MicroTOF Focus) and Bruker HPLC-QqTOF (MaXis Impact) using the ionization mode indicated for each compound. IR spectra were recorded on a Bruker Optics FTIR Alpha spectrometer equipped with a DTGS detector, KBr beamsplitter at 4 cm^{-1} resolution using a one bounce ATR accessory with diamond windows. Melting points were measured on a MP70 Melting Point System Mettler Toledo. Column chromatography was performed with silica gel technical grade, pore size 60 Å, 230-400 mesh particle size, 40-63 µm particle size and thin layer chromatography (TLC) analysis on silica gel 60 F254. Ion mobility mass spectrometry and CID experiments

were performed with Waters Synapt G2 Q-TOF mass spectrometer. Samples were prepared with 10-20 μM concentration in methanol solution. The modified Waters Synapt G2 was equipped with a linear drift cell filled with ~2 Torr nitrogen (298 K). Samples were ionized with a nanoESI ion source. In-house pulled capillary tips were used with inserted platinum wire for nanoESI. Parameters were optimized as follows: Capillary voltage 2.30 kV and source temperature 80 ºC. Data was analyzed using MassLynx v4.1 (Waters Corporation, USA) and Microsoft Excel 2016 (Microsoft, USA).

4.4.2. Synthesis and characterization data

[2]Rotaxane 4. Macrocycle **1** (80 mg, 65 μmol, 1 equiv), axle **3** (52 mg, 130 μmol, 2 equiv) and stoppers **5** (200 mg, 260 μmol, 4 equiv) were dissolved in 10 mL of dry and degassed DCM. $[Cu(CH_3CN)_4]PF_6$ (12 mg, 30 μmol, 0.5 equiv), TBTA (17 mg, 32 μmol, 0.5 equiv), and 0.5 mL of freshly distilled DIPEA were added. The reaction was stirred at room temperature for 4 h. After that, 50 mL of dichloromethane were added to the reaction crude. The organic phase was washed three times with 10 mL of water and later dried with anhydrous Na_2SO_4, filtered, and concentrated under reduced pressure to give a dark brown solid. Purification of the crude by silica column chromatography using a gradient of solvents from pure DCM to 30% AcOEt (Rf = 0.4) afforded **4** as a brown solid (18 mg, 8% yield). ^{1}H NMR (500 MHz, $CDCl_3$, 298 K) δ 9.15 (br, 8H, NH), 7.98 (s, 2H, Ha), 7.53 (d, 12H, J = 8.5 Hz, H15), 7.49 (d, 12H, J = 8.5 Hz, H16), 7.44 (d, 12H, J = 8.5 Hz, H14), 7.39 (br, 8H, Hb-c), 7.29 (d, 12H, J = 8.5 Hz, H13), 7.20 (d, 4H, J = 9.0 Hz, H12), 7.07 (br, 8H, Hd-e), 6.80 (d, 4H, J = 9.0 Hz, H11), 5.91 (m, 16H, Hβ), 5.02 (br, 4H, H10), 4.29 (br, 4H, H8), 3.14 (br, 4H, H4), 1.94 (br, 4H, H7), 1.60 (br, 4H, H5) 1.43 (br, 4H, H6), 1.34 (s, 54 H, H17) .^{13}C {^{1}H} NMR (125 MHz, $CDCl_3$, 298 K) δ 156.1, 150.2, 145.7, 138.4, 137.6, 137.5, 132.3, 132.1, 132.0, 131.41, 128.6, 114.3, 113.4, 67.1, 63.6, 53.5, 29.7, 29.4, 25.3, 22.3, 19.8, 14.1, 13.5, 13.4. FTIR (ATR): $\bar{\upsilon}_{max}$ (cm^{-1}) = 3443 (amine N–H stretching), 2965 (alkene C–H stretching), 1676 (triazole C=N stretching), 1508 (N-O stretching), 1220 (amine C–N stretching), 1039 (alkene C═C bending), 829 (alkene C=C bending) and 768 (alkene C═C bending). HR-MS (ESI-TOF-MS) m/z calculated for $C_{213}H_{219}N_{23}O_5$ $[M - 2H]^{-2}$ 1588.3721, found 1588.3784. mp > 190 °C (decomp).

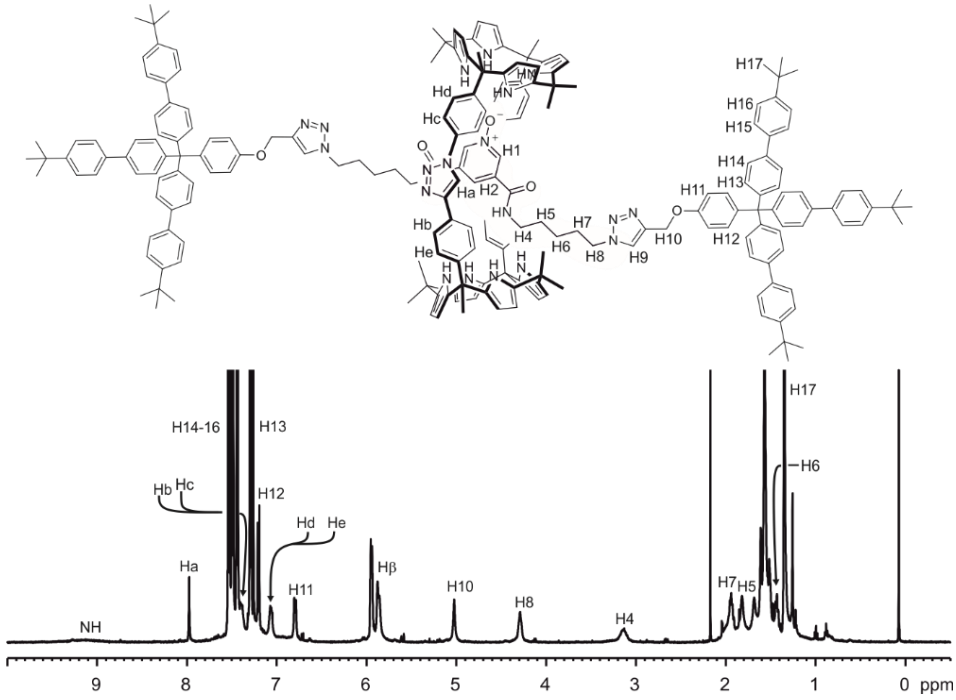

Figure 4.30. ^{1}H NMR spectrum (500 MHz, 298 K, $CDCl_3$) of [2]rotaxane **4**.

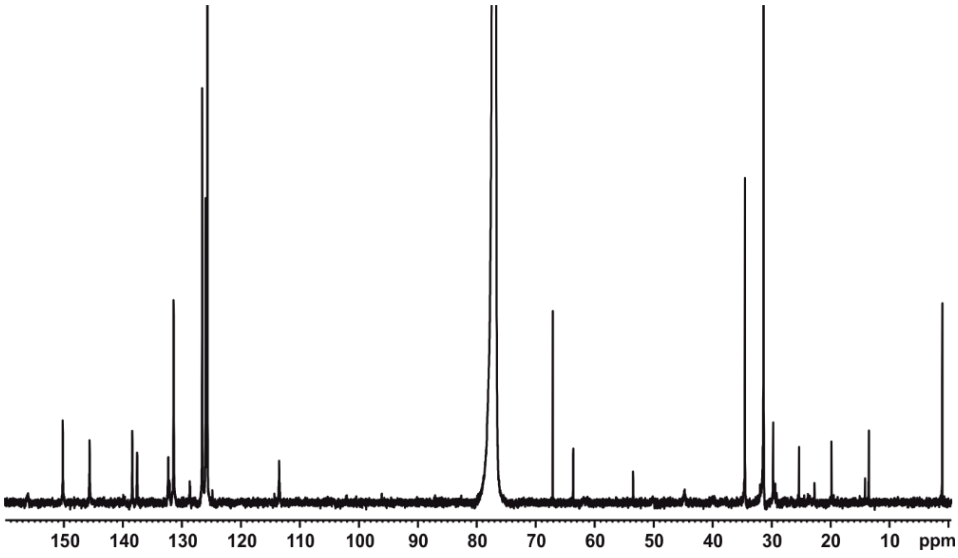

Figure 4.31. ^{13}C {^{1}H} NMR spectrum (125 MHz with cryoprobe, 298 K, $CDCl_3$) of [2]rotaxane **4**.

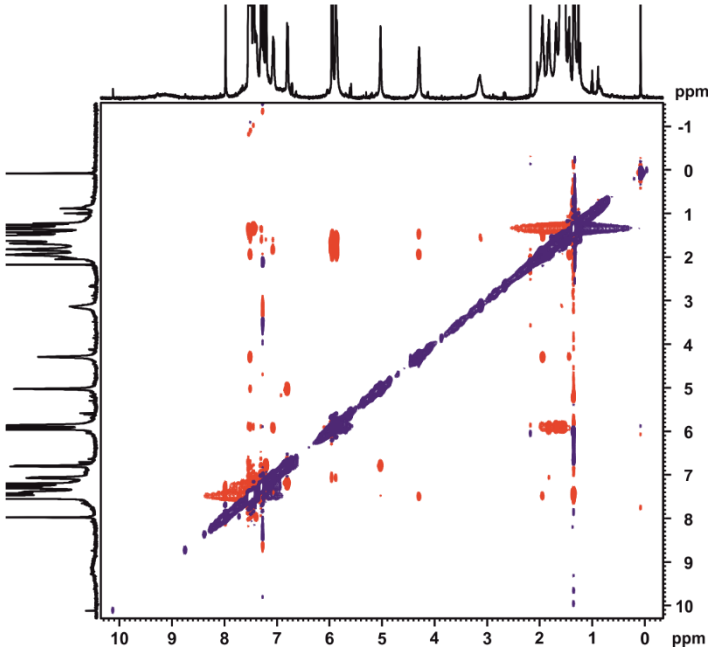

Figure 4.32. ^{1}H-^{1}H ROESY (500 MHz, $CDCl_3$, 298 K, spin-lock = 0.3 s) spectrum of [2]rotaxane **4**.

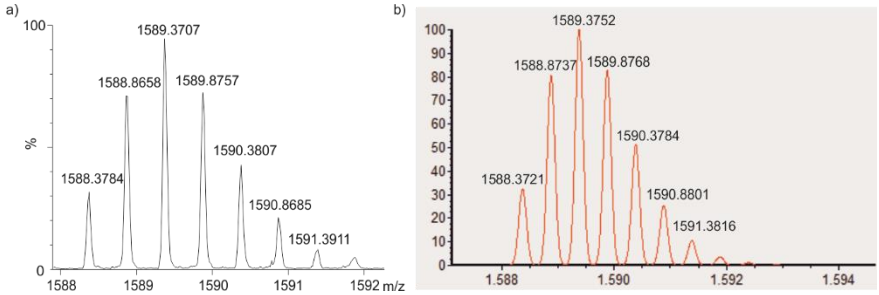

Figure 4.33. Experimental (a) and theoretical (b) isotopic distribution for [**4**-2H]$^{-2}$.

4.4.3. ^{1}H NMR titration experiments

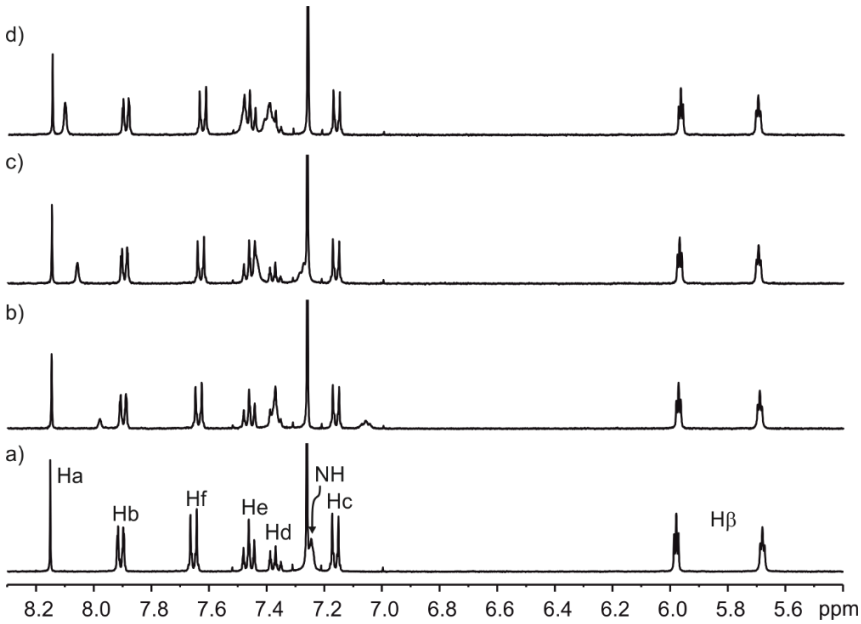

Figure 4.34. Selected region of the ^{1}H NMR titration experiment (400 MHz, 298K, $CDCl_3$) of receptor **7** (a), with 1 (b), 2 (c) and 3 (c) equivalent of axle **3**. See Figure 4.4 for proton assignments.

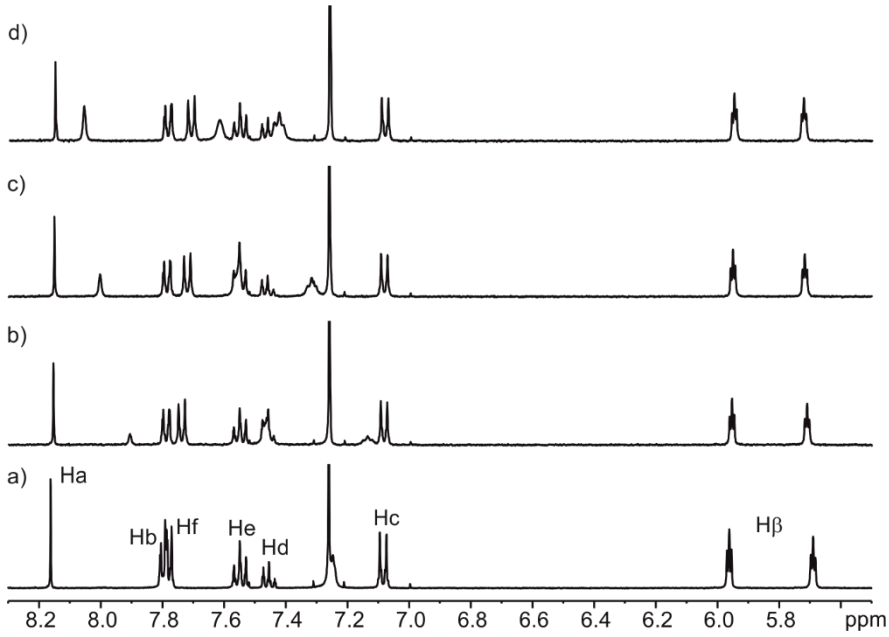

Figure 4.35. Selected region of the ^{1}H NMR titration experiment (400 MHz, 298K, $CDCl_3$) of receptor **8** (a), with 1 (b), 2 (c) and 3 (c) equivalent of axle **3**. See Figure 4.4 for proton assignments.

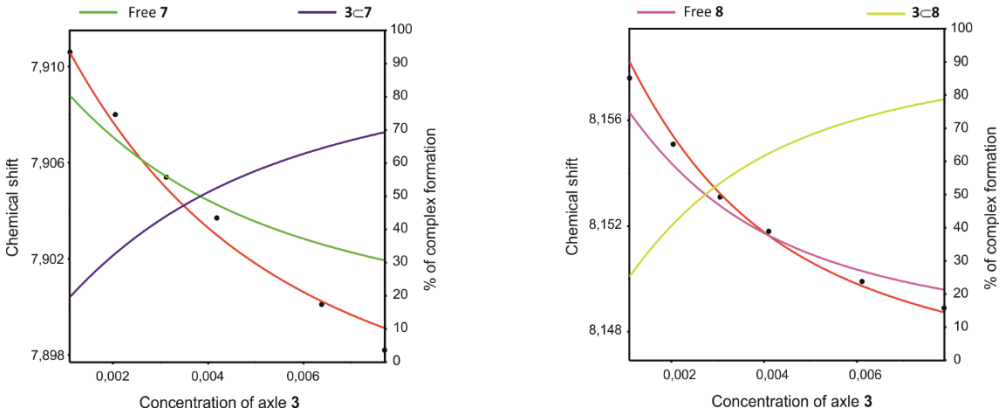

Figure 4.36. Simulated speciation profile and fit (red line) of the chemical shift changes experienced by proton Hb of **7** (left) and proton Ha of **8** (right) during the titration with **3**. Fit of the data was performed using a theoretical binding model in HypNMR2008 software that considers the formation of 1:1 complexes **3**⊂**7** and **3**⊂**8** and the presence of dimerization complex $(\mathbf{3})_2$ (K_{dim} =35.5 M^{-1}).

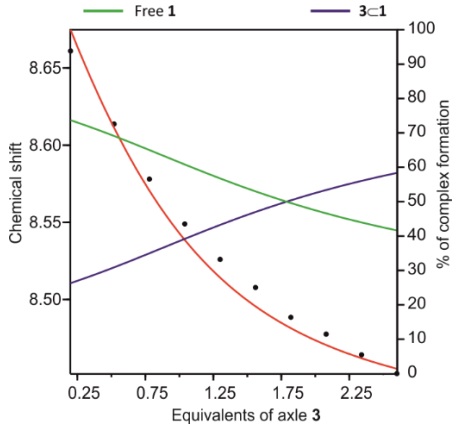

Figure 4.37. Simulated speciation profile and fit (red line) of the chemical shift changes experienced by proton Ha of **1** during the titration with **3**. Fit of the data was performed using a theoretical binding model in HypNMR2008 software that considers the formation of 1:1 complex **3**⊂**1**.

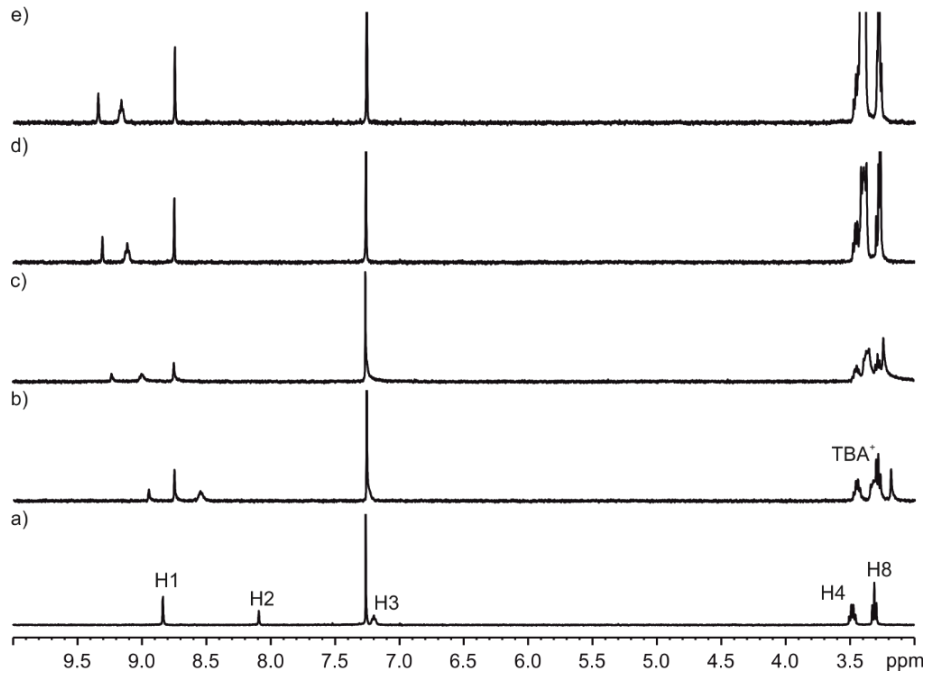

Figure 4.38. Selected region of the ^{1}H NMR titration experiment (400 MHz, 298K, $CDCl_3$) of axle **3** (a), with 1 (b), 2 (c), 3 (c) and 4 equivalent of MTOA·Cl **2a**. See Figure 4.2 for proton assignments.

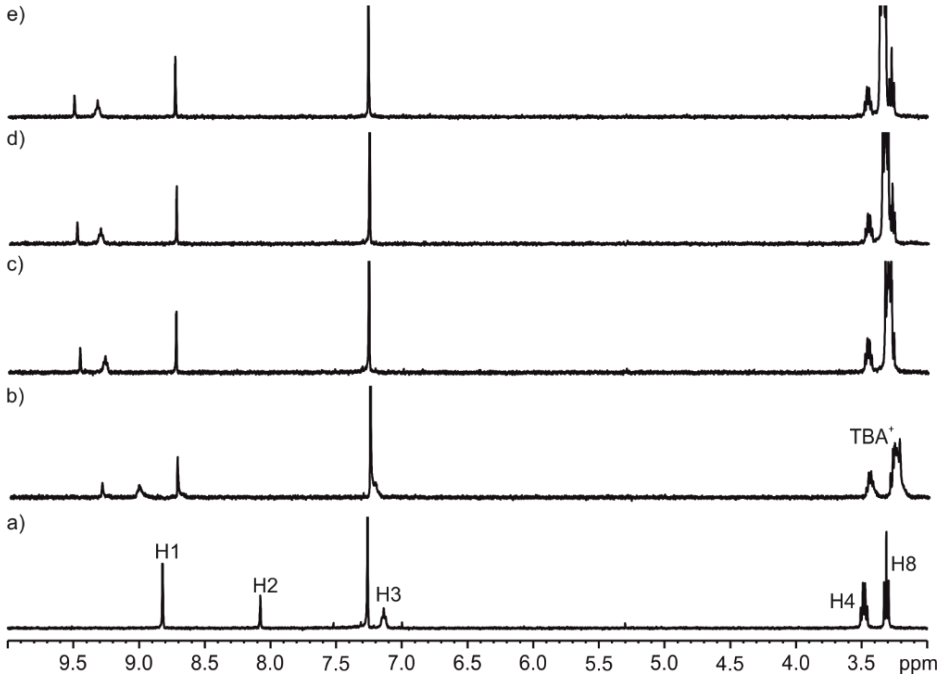

Figure 4.39. Selected region of the ^{1}H NMR titration experiment (400 MHz, 298K, $CDCl_3$) of axle **3** (a), with 1 (b), 2 (c), 3 (c) and 4 equivalent of TBA·Cl **2b**. See Figure 4.2 for proton assignments.

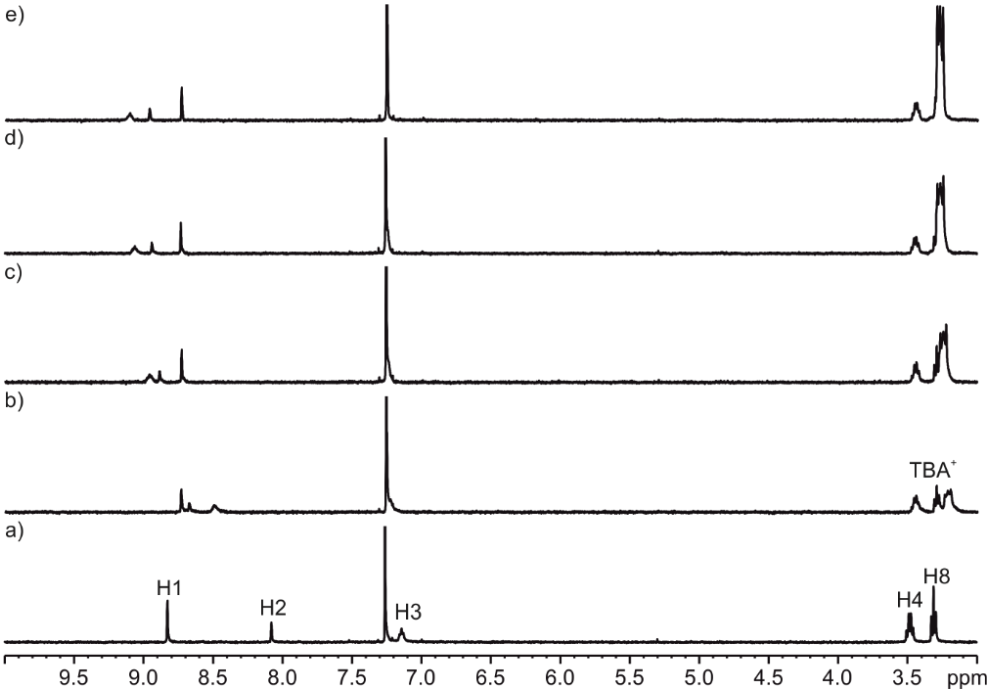

Figure 4.40. Selected region of the ^{1}H NMR titration experiment (400 MHz, 298K, $CDCl_3$) of axle **3** (a), with 1 (b), 2 (c), 3 (c) and 4 equivalent of TBA·OCN **2c**. See Figure 4.2 for proton assignments.

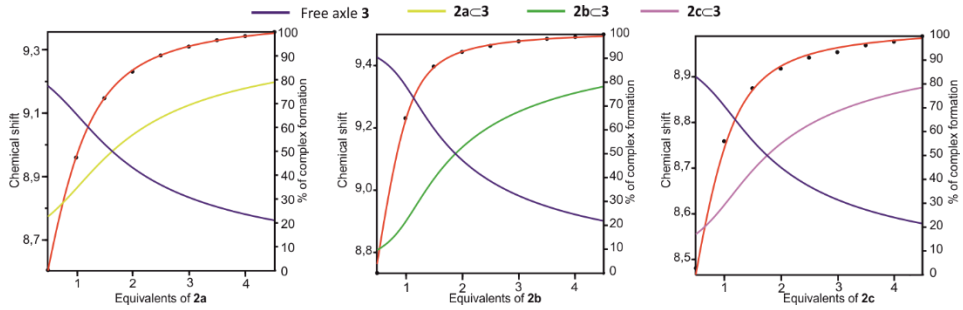

Figure 4.41. Simulated speciation profile and fit of the chemical shift changes experienced by proton H2 of **3** during the titration with **2a** (left), **2b** (middle) and **2c** (right). Data adjustment performed using a 1:1 binding model (red line) implemented in the HypNMR2008 software. The calculated values were: K[**2a**⊂**3**] = 2.1 ± 0.1 x 10^3 M^{-1}, K[**2b**⊂**3**] = 1.3 ± 0.4 x 10^4 M^{-1} and K[**2c**⊂**3**] = 3.2 ± 0.7 x 10^3 M^{-1}.

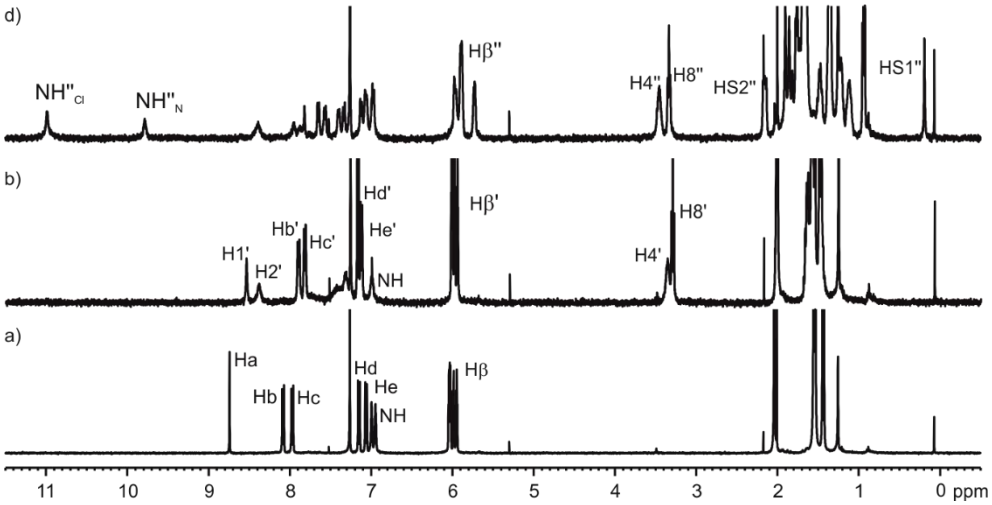

Figure 4.42. ^{1}H NMR titration experiment (400 MHz, 298K, $CDCl_3$) of free receptor **1** (a), 1:1 complex **3**⊂**1** (b) and a 1:1:1 mixture of receptor **1**, axle **3** and MTOA·Cl **2a**. Primed letter correspond to complex **3**⊂**1**. Doubled primed letters correspond to complex **2a**·**3**⊂**1**. See Figure 4.2 for proton assignments.

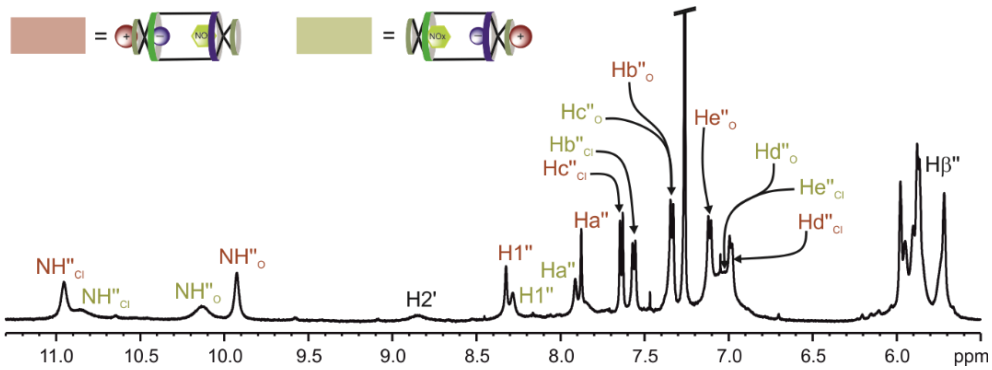

Figure 4.43. Selected region of the ^{1}H NMR spectrum (500 MHz, 213 K, $CDCl_3$) of a 1:1:1 mixture of receptor **1**, axle **3** and MTOA·Cl **2a**. Primed letter correspond to complex **2a**·**3**⊂**1**. Proton signals highlighted in red correspond to the binding isomer of the complex **2a**·**3**⊂**1** in which the chloride is bound in the *N*-substituted binding site of **1**. Proton signals highlighted in yellow are assigned to the other binding isomer locating the chloride in the *C*-substituted C4P binding site of **1**. Suffix *O* and *Cl* for proton signals assigned to the NH protons of receptor **1** indicate binding to axle **3** and the Cl^- anion, respectively. See Figure 4.2 for proton assignments.

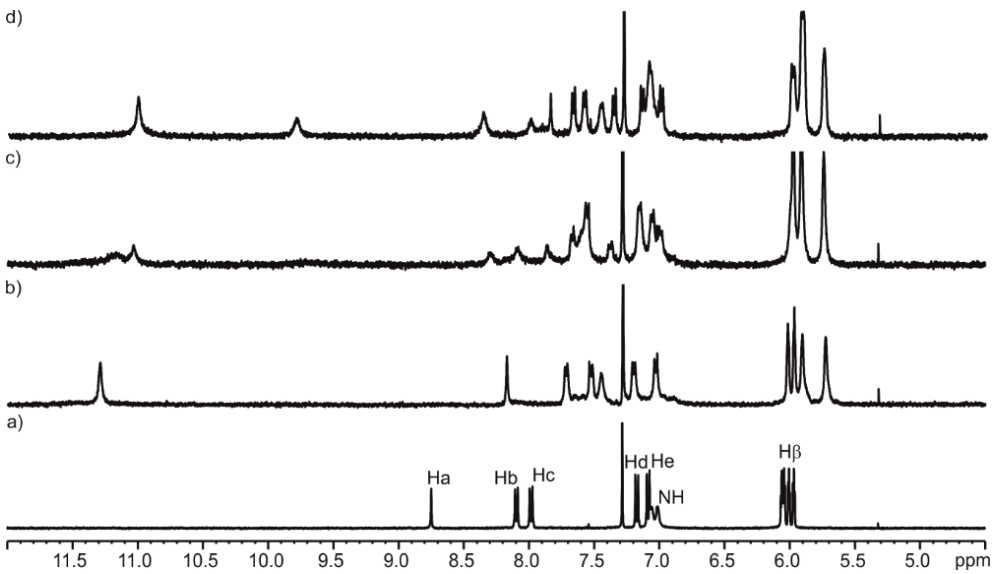

Figure 4.44. Selected region of the inverse ^{1}H NMR titration experiment (400 MHz, 298K, $CDCl_3$) of free receptor **1** (a). Addition of 1 equivalent of **2a** (b) is followed by the addition of 0.5 (c) and 1.0 (d) equivalent of axle **3** (d). See Figure 4.2 for proton assignments.

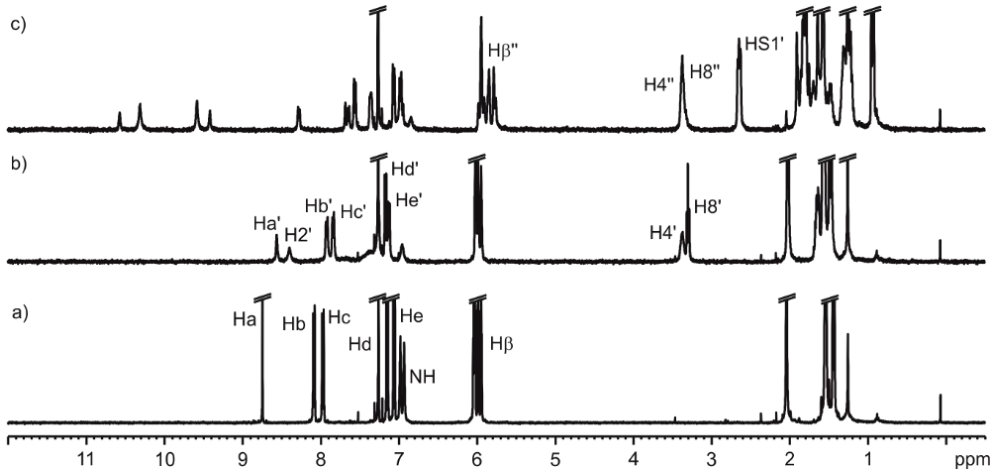

Figure 4.45. ^{1}H NMR titration experiment (400 MHz, 298K, $CDCl_3$) of free receptor **1** (a), 1:1 complex **3**⊂**1** (b) and a 1:1:1 mixture of receptor **1**, axle **3** and TBA·OCN **2c**. Primed letter correspond to complex **3**⊂**1**. Doubled primed letters correspond to complex **2c**·**3**⊂**1**. See Figure 4.2 for proton assignments.

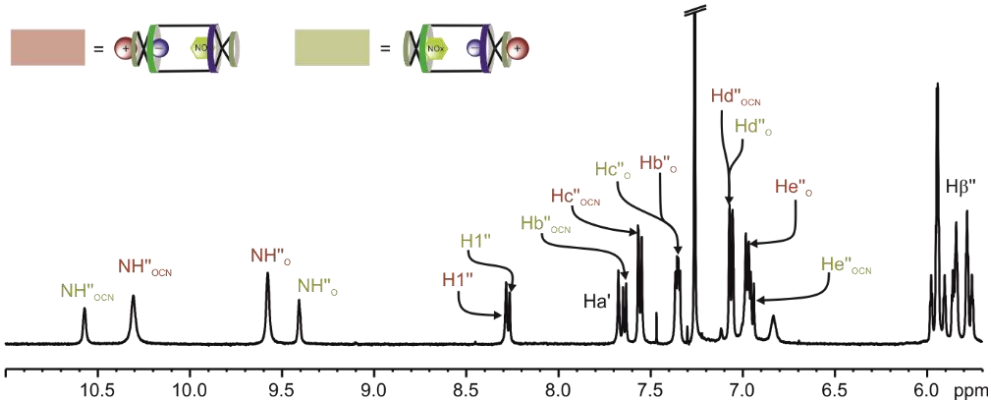

Figure 4.46. Selected region of the ^{1}H NMR spectrum (500 MHz, 298 K, $CDCl_3$) of a 1:1:1 mixture of receptor **1**, axle **3** and TBA·OCN **2c**. Primed letter correspond to complex **2c·3⊂1**. Proton signals highlighted in red correspond to the binding isomer of the complex **2b·3⊂1** in which the cyanate is bound in the *N*-substituted binding site of **1**. Proton signals highlighted in yellow are assigned to the other binding isomer locating the cyanate in the *C*-substituted C4P binding site of **1**. Suffix *O* and *OCN* for proton signals assigned to the NH protons of receptor **1** indicate binding to axle **3** and the OCN^- anion, respectively. See Figure 4.2 for proton assignments.

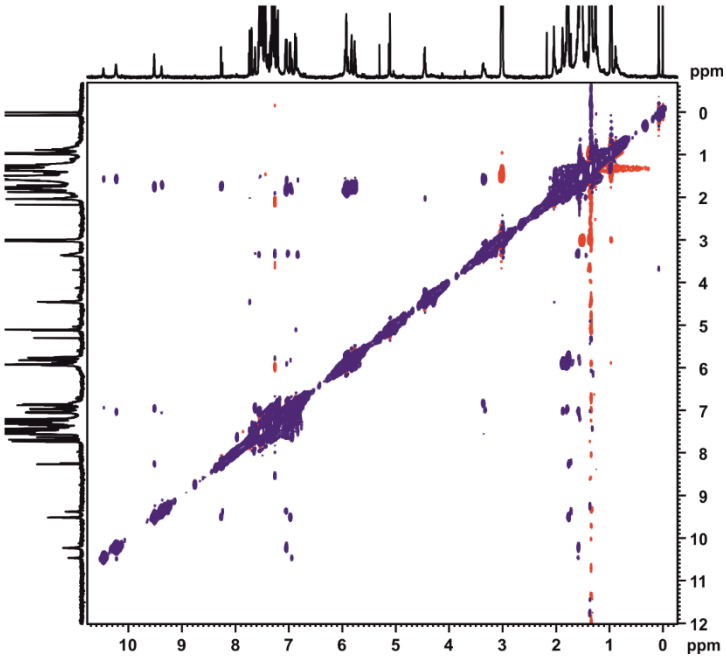

Figure 4.47. ^{1}H-^{1}H NOESY (500 MHz, $CDCl_3$, 298 K, mixing time = 0.3 s) spectrum of the 1:1 mixture of [2]rotaxane **4** and TBA·OCN **2c**.

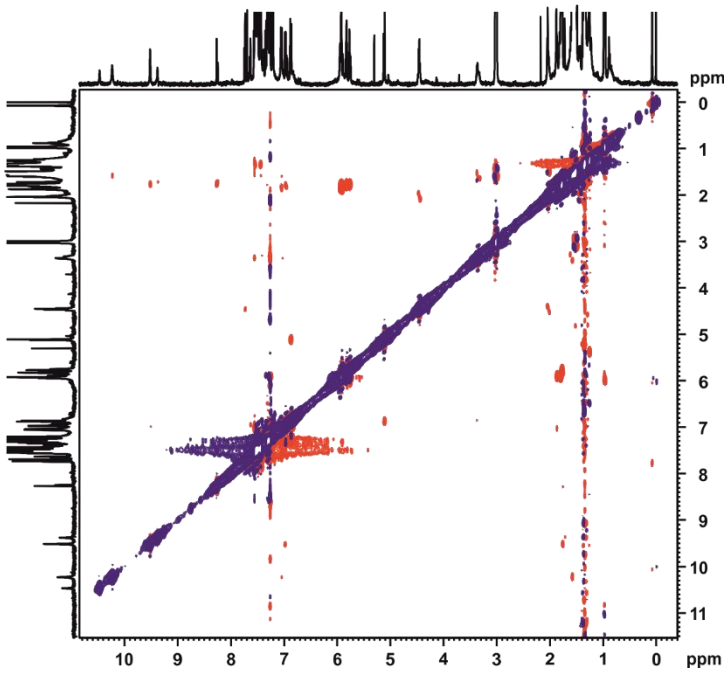

Figure 4.48. ^{1}H-^{1}H ROESY (500 MHz, $CDCl_3$, 298 K, spin-lock = 0.3 s) spectrum of the 1:1 mixture of [2]rotaxane **4** and TBA·OCN **2c**.

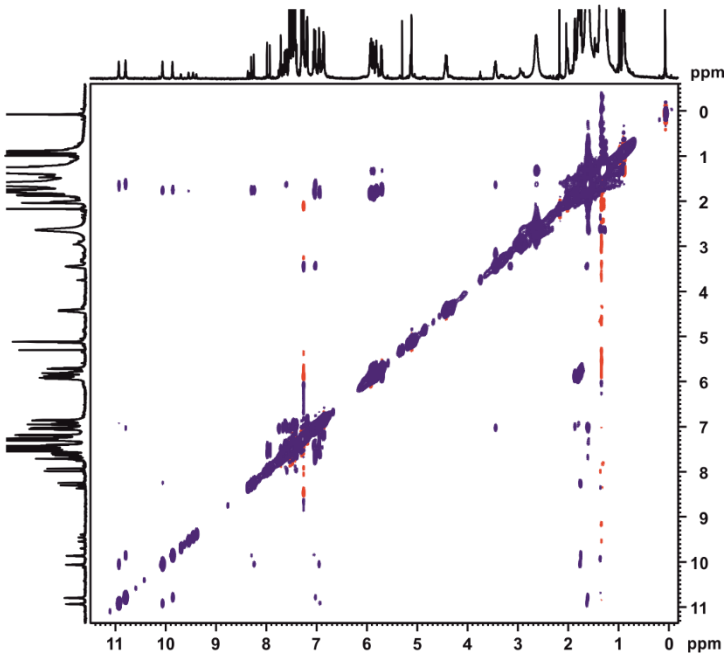

Figure 4.49. ^{1}H-^{1}H NOESY (500 MHz, $CDCl_3$, 298 K, mixing time = 0.3 s)) spectrum of the 1:1 mixture of [2]rotaxane **4** and MTOA·Cl **2a**.

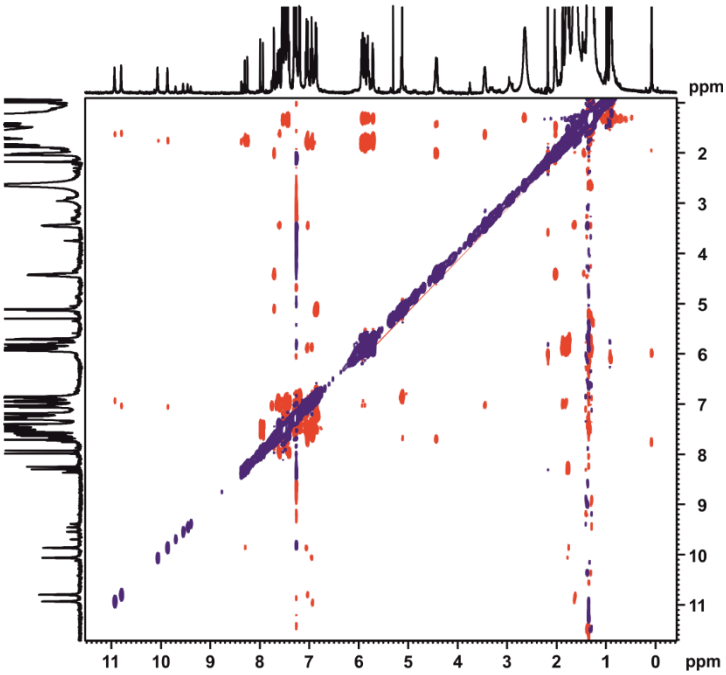

Figure 4.50. ^{1}H-^{1}H ROESY (500 MHz, $CDCl_3$, 298 K, spin-lock = 0.3 s) spectrum of the 1:1 mixture of [2]rotaxane **4** and MTOA·Cl **2a**.

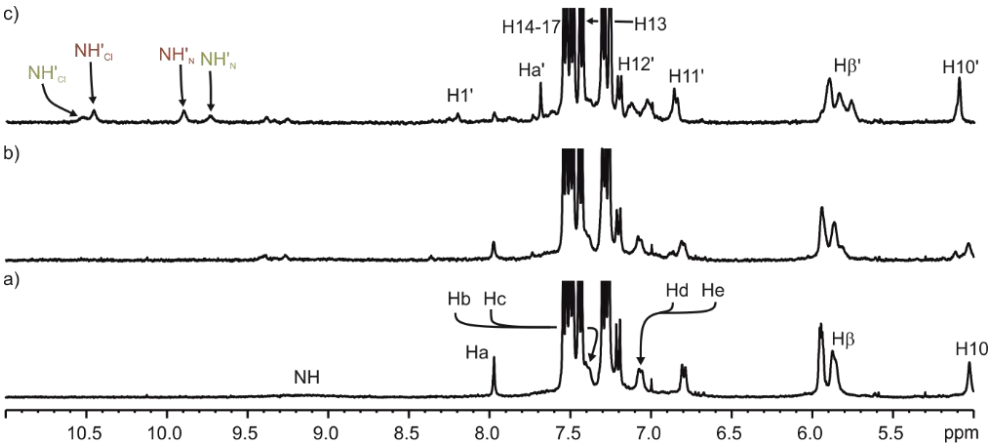

Figure 4.51. Selected region of the ^{1}H NMR spectra (400 MHz, 298 K, $CDCl_3$) acquired during the titration experiment of [2]rotaxane **4** (a) with incremental additions of **2b**: 1.0 equivalent (b) and 2.0 (c) equivalent. Proton signals highlighted in red correspond to the binding isomer of the complex **2b**⊂**4** in which the chloride is bound in the *N*-substituted binding site of **4**. Proton signals highlighted in yellow are assigned to the other binding isomer locating the chloride in the *C*-substituted C4P binding site of **4**. Suffix *O* and *Cl* for proton signals assigned to the NH protons of receptor **4** indicate binding to lineal component and the Cl^- anion, respectively. See Figure 4.3 for proton assignments.

4.4.4. Speciation profiles

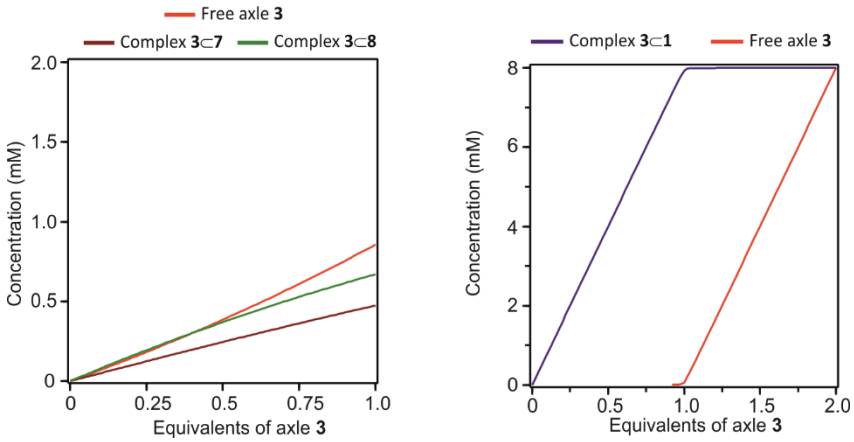

Figure 4.52. (Left) Speciation profile of the simulated titration of a 2 mM solution of receptors **7** and **8** with axle **3**. (Right) Speciation profile of the simulated titration of 8 mM solution of receptor **1** with axle **3** used to confirm the formation of the 1:1 complex in the conditions used in the [2]rotaxane synthesis.

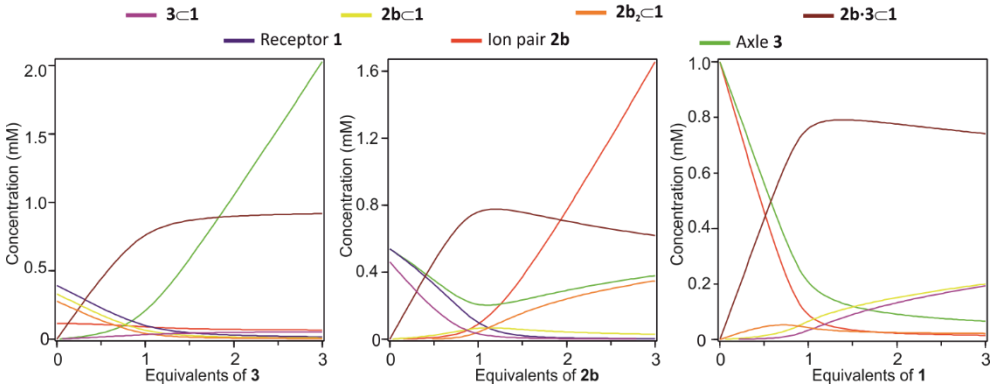

Figure 4.53. Speciation profile of the simulated titration of 1 mM solutions of: (left) Receptor **1** and TBA·Cl **2b** with axle **3**; (middle) receptor **1** and axle **3** with TBA·Cl **2b** and (right) axle **3** and TBA·Cl **2b** with receptor **1**.

4.4.5. ITC Experiments

Isothermal titration calorimetry experiments were performed using a Microcal VP-ITC Microcalorimeter. All the titrations were carried out in chloroform solution at 298 K. Titrations were carried out by adding small aliquots (7 µL, 10 s) of a chloroform solution of axle **3** into a solution containing a 1:1 mixture of **1** and **2a-c** in the same solvent. The concentration of **3** was approximately seven to ten times more concentrated than the solution containing **1** and **2a-c** (see corresponding figures for details). Reverse titrations (guest over host) were also performed and

yielded similar results. The association constants and the thermodynamic parameters were obtained from the fit of the titration data using HypΔH software version 1.1.0. The association constant (Ka), TΔS and ΔH values for the binding process were determined by averaging the values from two titrations.

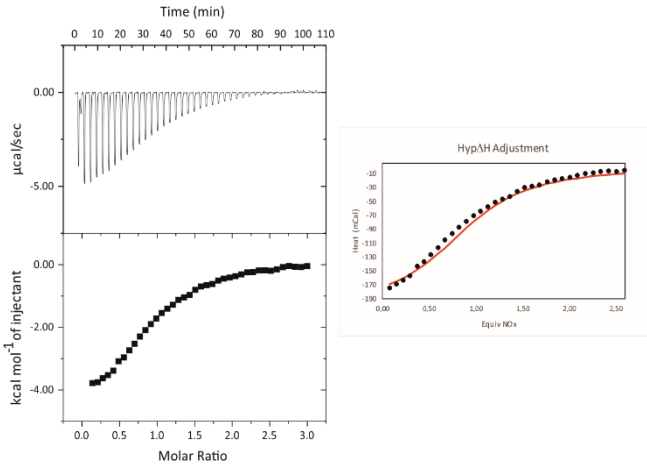

Figure 4.54. (Left) Top – Traces of the raw data (heat vs time) of the titration experiment of a $9 \cdot 10^{-4}$ M solution of receptor **1** and MTOA·Cl **2a**, with a $7 \cdot 10^{-3}$ M solution of **3** in chloroform. Bottom – Binding isotherms of the calorimetric titration shown on top. (Right) Data adjustment (red line) performed with hypΔH software.

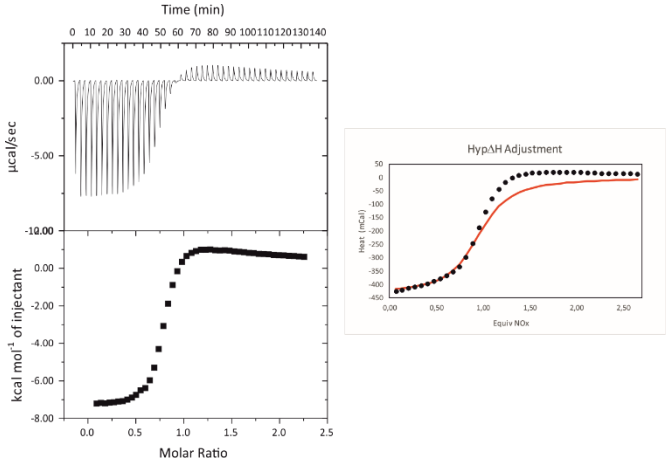

Figure 4.55. (Left) Top – Traces of the raw data (heat vs time) of the titration experiment of a $1.5 \cdot 10^{-3}$ M solution of receptor **1** and TBA·OCN **2c**, with a $11 \cdot 10^{-3}$ M solution of **3** in chloroform. Bottom – Binding isotherms of the calorimetric titration shown on top. (Right) Data adjustment (red line) performed with hypΔH software.

4.4.6. ESI-MS experiments

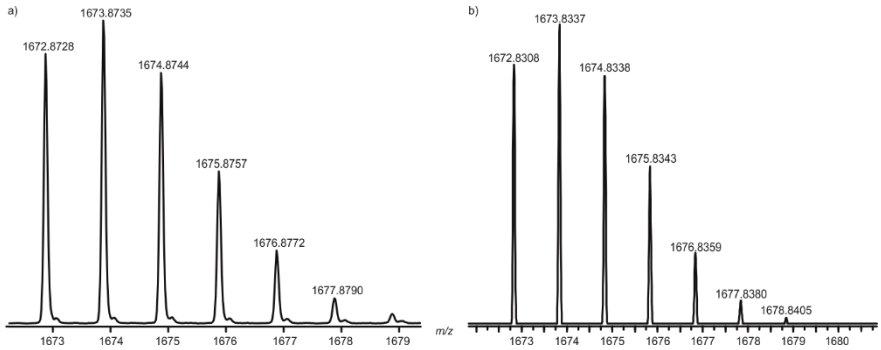

Figure 4.56. Experimental a) and calculated b) isotopic distribution of complex [**Cl·3⊂1**]$^-$.

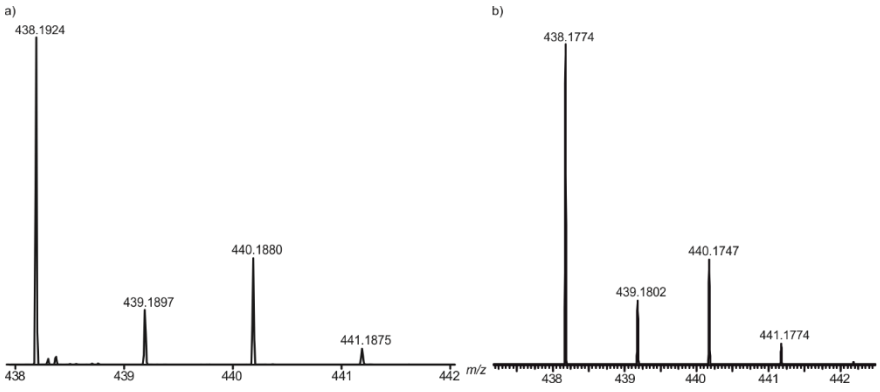

Figure 4.57. Experimental a) and calculated b) isotopic distribution of complex [**Cl⊂3**]$^-$.

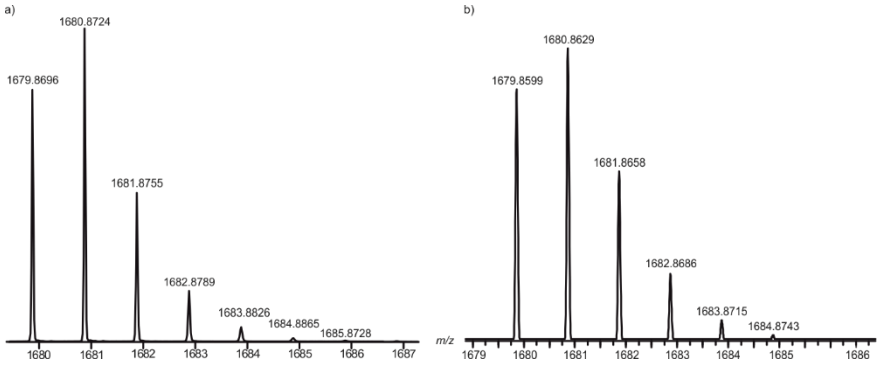

Figure 4.58. Experimental a) and calculated b) isotopic distribution of complex [**OCN·3⊂1**]$^-$.

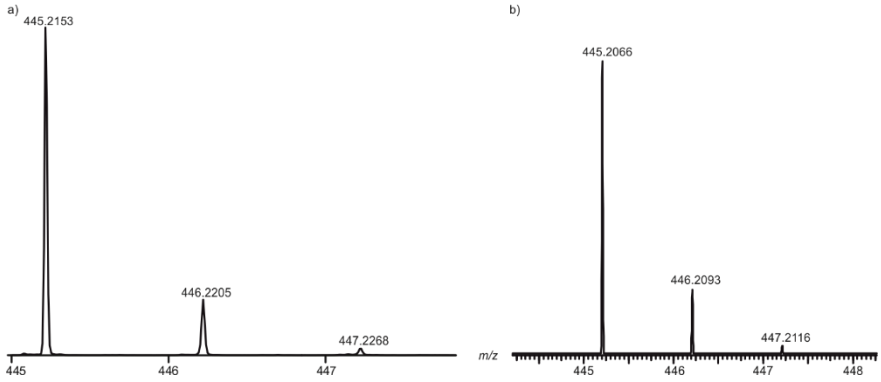

Figure 4.59. Experimental a) and calculated b) isotopic distribution of complex [**OCN⊂3**]$^-$.

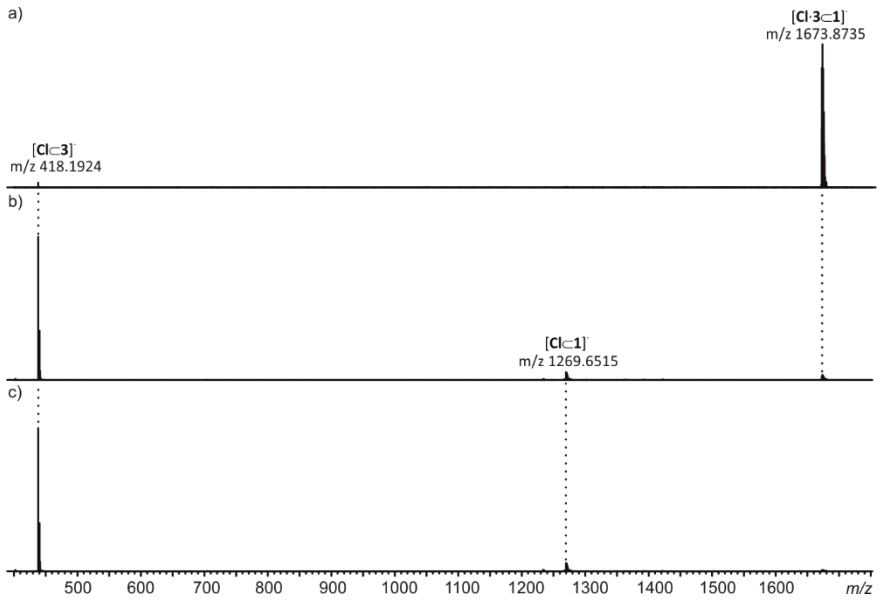

Figure 4.60. CID experiment performed with mass-selected ion [**Cl·3⊂1**]$^-$ a) with CE of 5 V b), 25 V c) and 28 V d).

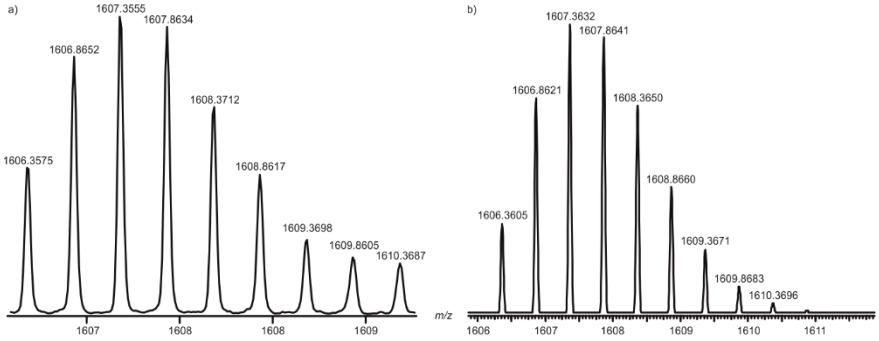

Figure 4.61. Experimental a) and calculated b) isotopic distribution of complex [**Cl**⊂**4**-H]$^{-2}$.

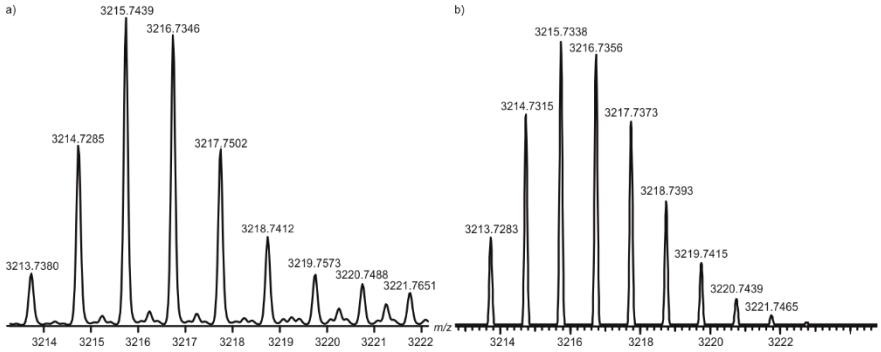

Figure 4.62. Experimental a) and calculated b) isotopic distribution of complex [**Cl**⊂**4**]$^{-}$.

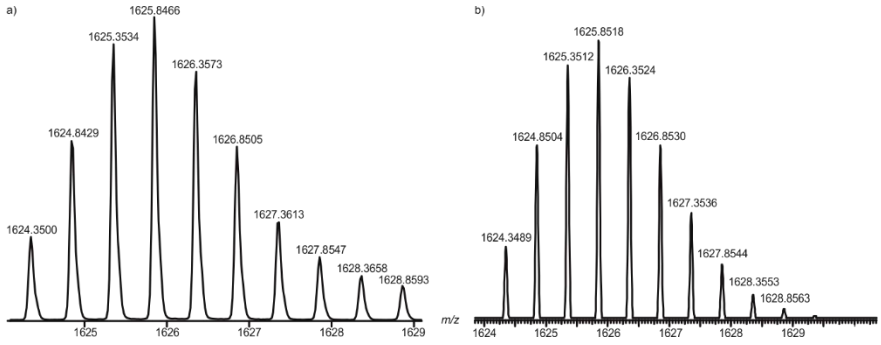

Figure 4.63. Experimental a) and calculated b) isotopic distribution of complex [(**Cl**)$_2$⊂**4**]$^{-2}$.

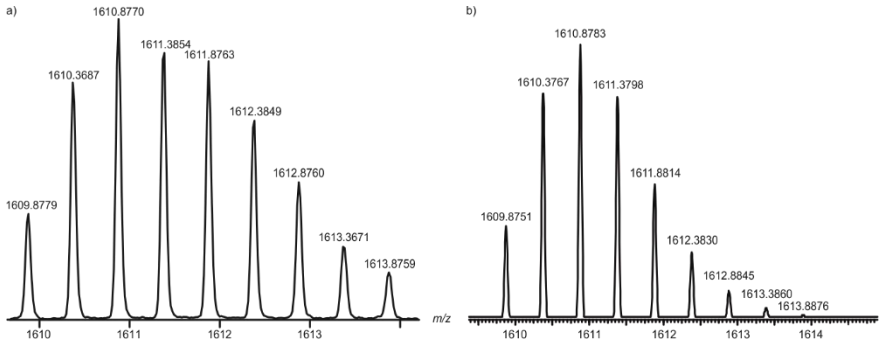

Figure 4.64. Experimental a) and calculated b) isotopic distribution of complex [**OCN**⊂**4**-H]$^{-2}$.

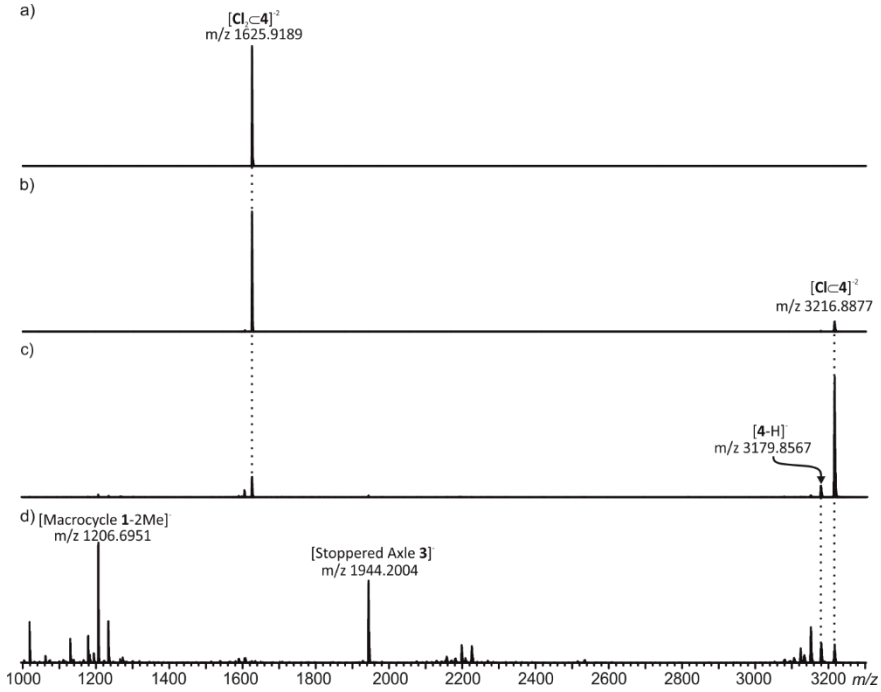

Figure 4.65. CID experiment performed with mass-selected ion [(**Cl**)$_2$⊂**4**]$^{-2}$ a) with CE of 28 V b), 38 V c) and 55 V d).

4.5 References and notes

[1] Langton, M. J.; Beer, P. D., Rotaxane and Catenane Host Structures for Sensing Charged Guest Species. *Acc. Chem. Res.* **2014,** *47* (7), 1935-1949.
[2] Erbas-Cakmak, S.; Leigh, D. A.; McTernan, C. T.; Nussbaumer, A. L., Artificial Molecular Machines. *Chem. Rev.* **2015,** *115* (18), 10081-10206.
[3] Kassem, S.; van Leeuwen, T.; Lubbe, A. S.; Wilson, M. R.; Feringa, B. L.; Leigh, D. A., Artificial molecular motors. *Chem. Soc. Rev.* **2017,** *46* (9), 2592-2621.
[4] Mena-Hernando, S.; Pérez, E. M., Mechanically interlocked materials. Rotaxanes and catenanes beyond the small molecule. *Chem. Soc. Rev.* **2019,** *48* (19), 5016-5032.
[5] Langton, M. J.; Serpell, C. J.; Beer, P. D., Anion Recognition in Water: Recent Advances from a Supramolecular and Macromolecular Perspective. *Angew. Chem. Int. Ed.* **2016,** *55* (6), 1974-1987.
[6] Han, X.; Liu, G.; Liu, S. H.; Yin, J., Synthesis of rotaxanes and catenanes using an imine clipping reaction. *Org. Biomol. Chem.* **2016,** *14* (44), 10331-10351.
[7] Xue, M.; Yang, Y.; Chi, X.; Yan, X.; Huang, F., Development of Pseudorotaxanes and Rotaxanes: From Synthesis to Stimuli-Responsive Motions to Applications. *Chem. Rev.* **2015,** *115* (15), 7398-7501.
[8] Qu, D.-H.; Tian, H., Novel and efficient templates for assembly of rotaxanes and catenanes. *Chem. Sci.* **2011,** *2* (6), 1011-1015.
[9] Barin, G.; Coskun, A.; Fouda, M. M. G.; Stoddart, J. F., Mechanically Interlocked Molecules Assembled by π–π Recognition. *ChemPlusChem* **2012,** *77* (3), 159-185.
[10] Schalley, C. A.; Weilandt, T.; Brüggemann, J.; Vögtle, F., Hydrogen-Bond-Mediated Template Synthesis of Rotaxanes, Catenanes, and Knotanes. In *Templates in Chemistry I*, Schalley, C. A.; Vögtle, F.; Dötz, K. H., Eds. Springer Berlin Heidelberg: Berlin, Heidelberg, 2004; pp 141-200.
[11] Fletcher, B. E.; Peach, M. J. G.; Evans, N. H., Rapidly accessible "click" rotaxanes utilizing a single amide hydrogen bond templating motif. *Org. Biomol. Chem.* **2017,** *15* (13), 2797-2803.
[12] Evans, N. H., Recent Advances in the Synthesis and Application of Hydrogen Bond Templated Rotaxanes and Catenanes. *Eur. J. Org. Chem.* **2019,** *2019* (21), 3320-3343.
[13] Anelli, P. L.; Spencer, N.; Stoddart, J. F., A molecular shuttle. *J. Am. Chem. Soc.* **1991,** *113* (13), 5131-5133.
[14] Klivansky, L. M.; Koshkakaryan, G.; Cao, D.; Liu, Y., Linear π-Acceptor-Templated Dynamic Clipping to Macrobicycles and [2]Rotaxanes. *Angew. Chem. Int. Ed.* **2009,** *48* (23), 4185-4189.
[15] Wang, Y.; Cheng, T.; Sun, J.; Liu, Z.; Frasconi, M.; Goddard, W. A.; Stoddart, J. F., Neighboring Component Effect in a Tri-stable [2]Rotaxane. *J. Am. Chem. Soc.* **2018,** *140* (42), 13827-13834.
[16] David, A. H. G.; García-Cerezo, P.; Campaña, A. G.; Santoyo-González, F.; Blanco, V., [2]Rotaxane End-Capping Synthesis by Click Michael-Type Addition to the Vinyl Sulfonyl Group. *Chem.--Eur. J.* **2019,** *25* (24), 6170-6179.
[17] Wu, K.-D.; Lin, Y.-H.; Lai, C.-C.; Chiu, S.-H., Na+ Ion Templated Threading of Oligo(ethylene glycol) Chains through BPX26C6 Allows Synthesis of [2]Rotaxanes under Solvent-Free Conditions. *Org. Lett.* **2014,** *16* (4), 1068-1071.

[18] Echavarren, J.; Gall, M. A. Y.; Haertsch, A.; Leigh, D. A.; Marcos, V.; Tetlow, D. J., Active template rotaxane synthesis through the Ni-catalyzed cross-coupling of alkylzinc reagents with redox-active esters. *Chem. Sci.* **2019,** *10* (30), 7269-7273.

[19] Wyman, I. W.; Macartney, D. H., Host–Guest Complexes and Pseudorotaxanes of Cucurbit[7]uril with Acetylcholinesterase Inhibitors. *J. Org. Chem.* **2009,** *74* (21), 8031-8038.

[20] Ramalingam, V.; Urbach, A. R., Cucurbit[8]uril Rotaxanes. *Org. Lett.* **2011,** *13* (18), 4898-4901.

[21] Vickers, M. S.; Beer, P. D., Anion templated assembly of mechanically interlocked structures. *Chem. Soc. Rev.* **2007,** *36* (2), 211-225.

[22] Hänni, K. D.; Leigh, D. A., The application of CuAAC 'click' chemistry to catenane and rotaxane synthesis. *Chem. Soc. Rev.* **2010,** *39* (4), 1240-1251.

[23] Romero, J. R.; Aragay, G.; Ballester, P., Ion-pair recognition by a neutral [2]rotaxane based on a bis-calix[4]pyrrole cyclic component. *Chem. Sci.* **2017,** *8* (1), 491-498.

[24] The energy-minimized structure was obtained using the software package Fujitsu Scigress Version 2.2.0. The structure was optimized by performing a geometry calculation using the implemented molecular mechanics force field with augmented MM3 parameters.

[25] Similar results were obtained in the inverse titration experiments of complex **2a**⊂**1** with *N*-oxide **3** (See Experimental Section).

[26] Considering the formation of dimeric complex $\mathbf{3_2}$ and 1:1 complex **2b**⊂**3** produced no significant changes in the values calculated for the thermodynamic parameters. The two complexes were present at a negligible extent in the working conditions. This was inferred from the analysis of the speciation profiles obtained assuming formation of these two complexes.

[27] The negatively charged complexes obtained with ion pair MTOA·Cl **2a** were identical as those obtained with TBA·Cl **2b** due to the loss of the cation.

[28] The mono-charged complex [**Cl**⊂**4**]$^-$ was also detected. We were not able to perform CID experiments due to the low intensity of the ion peak.

[29] We could not obtain a reliable CE_{50} value for complex [**Cl**⊂**4**-H]$^{-2}$ due to the disassembly of the system via multiple covalent bond leakage processes.

Synthesis and binding studies of a strapped calix[4]pyrrole receptor

Unpublished results

UNIVERSITAT ROVIRA I VIRGILI
Calix[4]pyrrole Based Receptors for the Recognition of Ion Pairs
Ricardo Molina Muriel

5.1. Introduction

Strapped calix[4]pyrrole (C4P) receptors are a special class of *meso* functionalized C4P.[1,2,3,4] In these receptors, two *meso* substituents are connected forming a macrocycle. The connection between the two *meso*-substituents is referred as the strap. In turn, the strap can be decorated with polar groups able to engage in recognition processes. These groups can assist the binding of neutral and charged molecules to the C4P core. These structural modifications of the C4P scaffold generate conformationally more rigid multitopic receptors able to coordinate ion pair dimers in a close-contact binding geometry.[5,6] The close proximity of the two different binding sites (strap and C4P) can also induce allosteric cooperativity effects in the binding of ion pairs.[7] In other cases, the use of a chromophore as strapping unit to covalently connect the two *meso*-arms produces optical molecular sensors.[8] Hence, the binding affinity and selectivity of strapped C4P receptors is modulated according to the size and shape of the strap. [9,10,11]

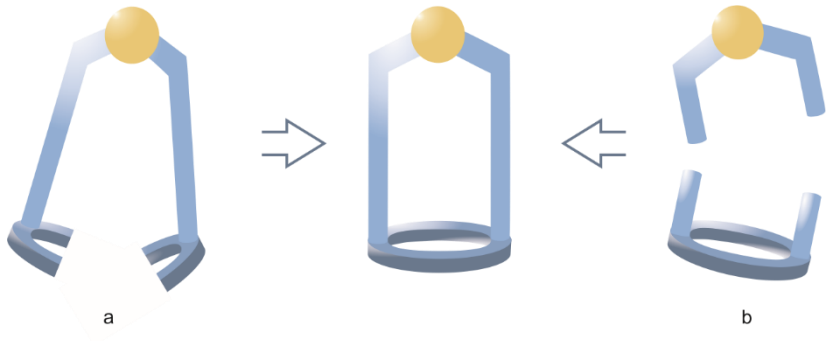

Figure 5.1. Schematic representation of the synthesis of a strapped 2W-C4P by a) condensation of bis(dipyrromethane)-functionalized strap and b) intermolecular coupling reaction of the strap and C4P.

We have already discussed in previous chapters the synthesis of a strapped C4P receptor featuring a C4P unit also as the strap. The synthesis of this receptor was based on the intermolecular copper(I)-catalyzed azide-alkyne cycloaddition (CuAAC) coupling reaction between two C4P units. The synthesis of the macrocyclic receptor was assisted by the use of a template that reduced the formation of polymeric products to a minor extent. However, the synthesis of strapped C4P receptors is commonly based on the synthetic approach introduced by Lee and co-workers.[12] This methodology consists on the derivatization of the strap unit in order to obtain a bis(di-pyrromethane), which will be the precursor of the C4P core (**Figure 5.1**). The acid-catalyzed condensation of the bis-(di-pyrromethane) components in the

presence of an excess of acetone would yield the strapped C4P. This methodology does not require the use of any template molecule. However, the use of a suitable strap that locates both di-pyrromethane reacting units in close proximity is mandatory in order to minimize the formation of polymeric products.

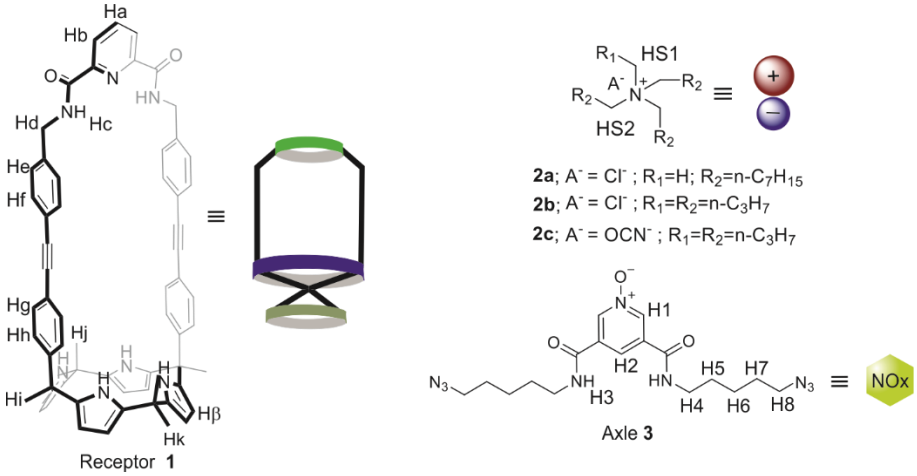

Figure 5.2. Line-drawing structures of strapped macrocycle **1**, tetraalkylammonium salts **2a-c**, axle **3** and their cartoon representations.

In this chapter, we describe the synthesis of strapped C4P receptor **1** (**Figure 5.2**). Receptor **1** consists on a two-wall super aryl-extended C4P (2W-SAE-C4P) featuring a 2,6-pyridinedicarboxamide as strap. Macrocycle **1** features two distal binding sites with polar groups able to engage in hydrogen bonding interactions: four NH in the C4P core and two amide NH in the strap. In addition, the C4P unit is able to coordinate cationic species in its electron rich aromatic cup generated by the pyrrole rings in the cone conformation. It is worth mentioning that receptor **1** does not display a lineal arrangement of the two polar binding sites. The strap unit tilts out of the plane defined by two *meso*-aryl substituents. This molecular conformation can be observed in the energy-minimized structure (MM3) of the receptor (**Figure 5.3**). Indeed, the 2,6-pyridinedicarboxamide strap displays a tilted geometry of *ca.* 45˚ with respect to the plane defined by the rigid aromatic walls.

In this chapter, we also evaluated the properties of receptor **1** towards the binding of ion pairs **2a-c** in chloroform solution. We envisaged that the spatial proximity of the two different anionic binding sites would favor the binding of close-contact ion triplets displaying an anion-cation-anion binding geometry. In addition, we studied the formation of pseudorotaxane assemblies with axle **3** assisted by Cl^- and OCN^-

anions. We studied the preference of the anion and the axle for binding in the two different polar binding sites of receptor **1**. The formation of ion pair quartet complexes with **2a-c**, as well as pseudorotaxane assemblies in the presence of equimolar amounts of axle **3**, were studied by means of ^{1}H NMR titration experiments. The formed complexes were also characterized in the gas phase by ESI-MS techniques.

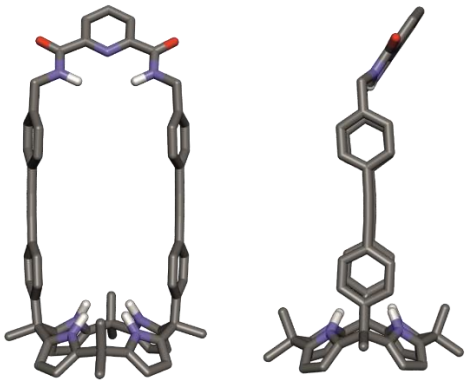

Figure 5.3. Two different views of the energy-minimized structure (MM3) of receptor **1**. Non-polar hydrogens were removed for clarity.[13]

5.2. Results and discussion

5.2.1. Design and synthesis of receptor **1**

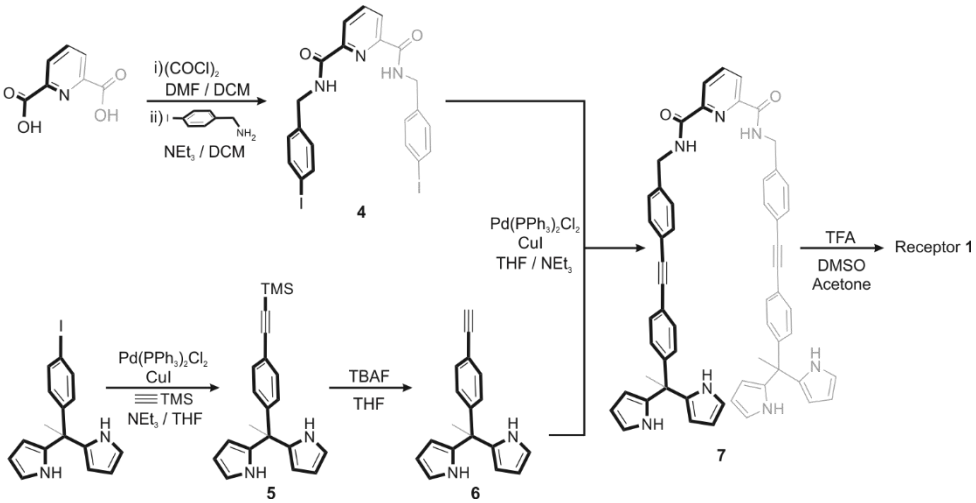

Scheme 5.1. Schematic representation of the synthetic route of receptor **1**.

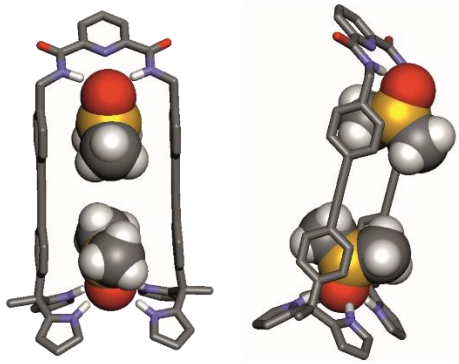

Figure 5.4. Two different views of the energy-minimized structure (MM3) of the putative complex formed between bis(di-pyrromethane) **7** and DMSO in the synthesis of receptor **1**. Non-polar hydrogens were removed for clarity.

Strapped C4P receptor **1** was prepared following the synthetic procedure depicted in **Scheme 5.1**. The macrocyclization reaction was based on the acid catalyzed condensation of bis(di-pyrromethane) **7** performed in a solution mixture of acetone containing 5% of DMSO. We envisaged that the coordination of a DMSO molecule with the two NH protons of the dicarboxamide strap would favor the arrangement of both amide groups in *cis* conformation. In addition, the formation of CH-π interactions with bound DMSO molecule could produce a favorable arrangement of the two di-pyrromethane units favoring the transition state geometry of the macrocyclization reaction (**Figure 5.4**). Purification of the reaction crude by silica column chromatography, followed by recrystallization in a DCM/MeOH mixture, afforded receptor **1** as white crystals in a 2% yield. The receptor was fully characterized by a set of high-resolution spectra (NMR and HRMS).

The ^{1}H NMR spectrum of a millimolar $CDCl_3$ solution of receptor **1** showed sharp and well-defined signals in agreement with a C_{2v} symmetry (**Figure 5.5**). The pyrrole NH protons of the C4P appeared at δ = 7.0 ppm as a broad singlet. In turn, the β-pyrrole protons resonated at δ = 6.0 ppm as two broad signals. The amide protons of the dicarboxamide strap (Hc) appeared centered at δ = 7.8 ppm. They resonate as a broad triplet due to the scalar coupling with the protons of the methylene group (Hd) resonating at δ = 4.6 ppm. In addition, the protons assigned to the aromatic walls of the receptor (He-h) appeared between 7.5 and 6.8 ppm as four sharp doublets.

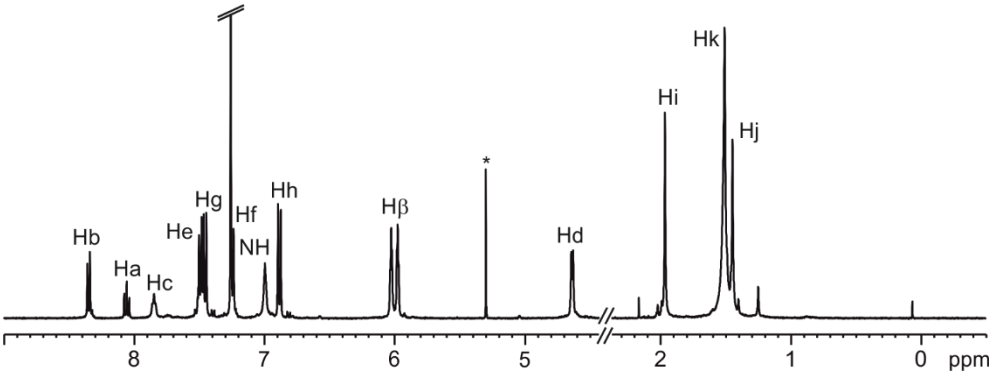

Figure 5.5. ^{1}H NMR spectrum (500 MHz, 298 K, $CDCl_3$) of receptor **1**. See Figure 5.2 for proton assignments.

5.2.2. Binding studies of receptor **1** with ion pairs **2a-c**

The addition of 0.5 equivalent of TBA·Cl **2b** to a 2 mM solution of receptor **1** produced the observation of a new set of proton signals (**Figure 5.6**). This new set of signals was assigned to protons of receptor **1** in a complex of unknown stoichiometry with TBA·Cl **2b**. We observed a sharp singlet centered at δ = 11.1 ppm that was assigned to the NH protons of the C4P core. The dramatic downfield shift experienced ($\Delta\delta$ = 4.1 ppm) by the pyrrole NHs was indicative of their coordination with the Cl^- anion. We also detected a broad proton signal at δ = 8.5 ppm that was assigned to the NH amide protons of the strap (Hc) coordinating also with the Cl^- anion. All the proton signals associated to bound receptor experienced a reduced chemical shift changes along the course of the titration. Interestingly, the amide protons Hc ($\Delta\delta$ = 1.9 ppm) were the ones that most noticeably moved downfield. When one equivalent of the ion pair was added, the integral values of the proton signals assigned to the free and the bound receptor indicated that 50% of receptor **1** was bound with the ion pair **2b**. As the concentration of **2b** was increased, the proton signals assigned to bound receptor **1** grew in intensity at the expenses to those assigned to free **1**. In addition, the proton signal assigned to the methylene protons *alpha* to the nitrogen atom in the TBA^+ appeared upfield shifted with respect to those in the free form ($\Delta\delta$ = - 0.7 ppm). The incremental addition of **2a** caused the downfield shift of the above methylene protons, towards the chemical shift of the free.

Taken together, these results indicated the initial formation of complex **2b**⊂**1**. The complex is involved in a slow exchange on the ^{1}H NMR chemical shift timescale with

free receptor **1**. In this complex, the chloride anion is bound to the pyrrole NHs of the C4P core in cone conformation. This coordination is evidenced by the dramatic downfield shift experienced by the proton signal assigned to the NHs, which are involved in hydrogen bonding interactions with the bound chloride. Almost concomitantly, a new complex is formed in solution as evidenced by the gradual chemical shift changes experienced by the proton signals assigned to the **2b⊂1** complex. Thus, the new complex is involved in a chemical exchange that is fast on the ^{1}H NMR chemical shift with **2b⊂1**. The most noticeable chemical shift changes are experienced by the free amide protons Hc owing to its involvement in hydrogen bonding interactions with a second Cl^- anion. We assigned a 2:1 stoichiometry to the new complex, (**2b**)$_2$⊂**1**. The presence of both complexes in the initial phases of the titration is indicative of similar values for the stepwise binding constants *K*[**2b⊂1**] and *K*[**2b⊂1**↔(**2b**)$_2$⊂**1**]. In addition, when 2 equivalent of the ion pair were added,

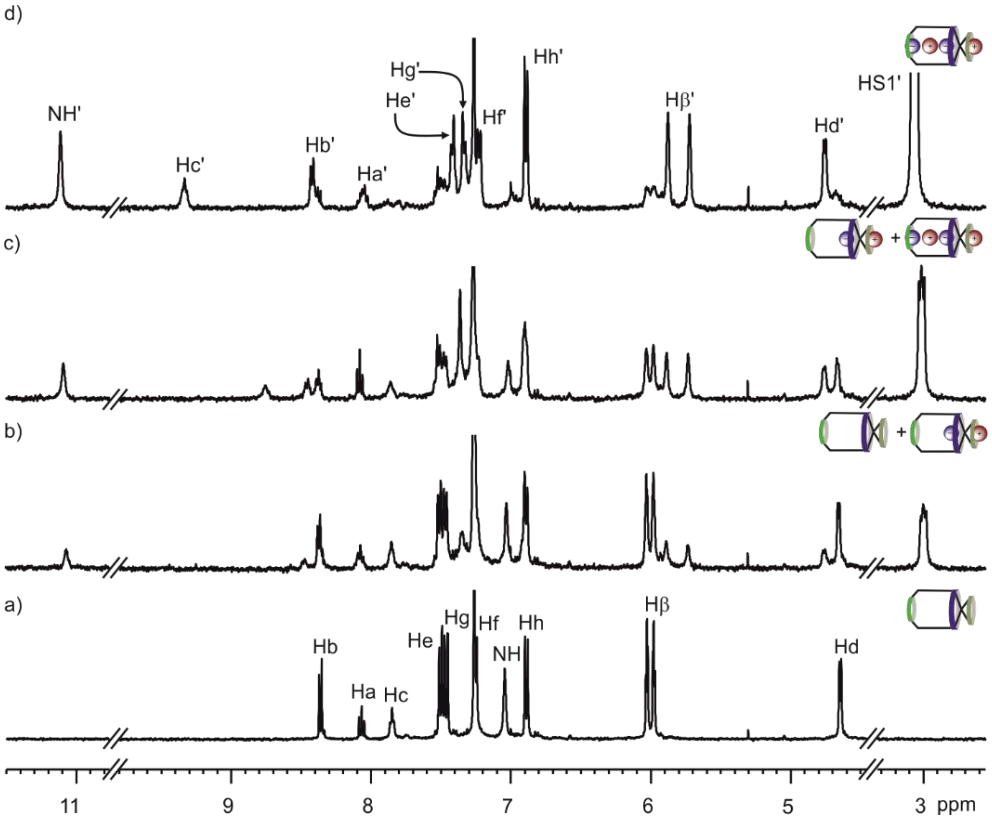

Figure 5.6. Selected region of the ^{1}H NMR spectra (400 MHz, $CDCl_3$, 298 K) of free receptor **1** (2 mM) (a) and incremental additions of TBA·Cl (**2b**): 0.5 (b), 1.0 (c), and 2.0 equivalent (d). Primed letters correspond to protons of **1** binding ion pair **2b**. Schematic models indicate the major species observed. See Figure 5.2 for proton assignment.

we could still observe low intensity signals assigned to the free receptor. This finding suggests a value for the binding affinity constant of $K[(\mathbf{2b})_2 \subset \mathbf{1}] < 10^{8}\ M^{-2}$.

The upfield shifts experienced by the *alpha*-methylene proton signal H1 of the TBA^+ in the initial phase of the titration points out to its coordination in the electron rich aromatic cup generated by the C4P's cone conformation in the **2b⊂1** complex. Even in the presence of two equivalent of **2b** the H1 signal is upfield shifted with respect to free TBA^+, suggesting that in the $(\mathbf{2b})_2 \subset \mathbf{1}$ complex also one TBA^+ is included in the aromatic cavity. In both complexes, one bound TBA^+ is located opposite to the bound Cl^- anion stabilized mostly by π-cation interactions with the pyrrole aromatic panels. We registered a ^1H NMR experiment at 213 K using a mM solution containing a mixture of **2b** and **1** in a 2:1 molar ratio (see Experimental Section). Under these conditions, the formation of the $(\mathbf{2b})_2 \subset \mathbf{1}$ complex is almost quantitative. We observed that the *alpha* methylene proton HS1 splits into two broad signals, which are upfield shifted with respect to free TBA^+. This finding indicates the existence of two chemically non-equivalent bound TBA^+ cations. The two TBA cations are involved in a slow chemical exchange on the chemical shift timescale. Unfortunately, we could not assign the two signals of the alpha methylene protons to specific locations of the bound TBA^+ cations.

In order to investigate the binding geometry of the $(\mathbf{2b})_2 \subset \mathbf{1}$ complex and the location of the two TBA^+ cations, we performed a ROESY experiment using the solution of the mixture discussed above at room temperature (**Figure 5.7**). We observed cross-peaks related to proximity in space between the proton signals assigned to TBA^+ cations and those assigned to the aromatic walls of receptor **1**, as well as its β-pyrrole protons. These observations support the coordination of the two TBA^+ cation in the $(\mathbf{2b})_2 \subset \mathbf{1}$ complex. One TBA^+ cation corresponds to the ion pair bound by the C4P unit displaying a receptor separated binding mode. The second TBA^+ cation corresponds to the counter-ion of the chloride bound by the bis-amide strap. Most likely, this second TBA^+ cation is sandwiched between the two Cl^- anions. The resulting ion triplet should display a cascade-like arrangement (**Figure 5.8**). The two chemically non-equivalent TBA^+ cations are involved in a dynamic chemical exchange that is fast on the ^1H NMR chemical shift timescale at 298 K but slow at 213 K.

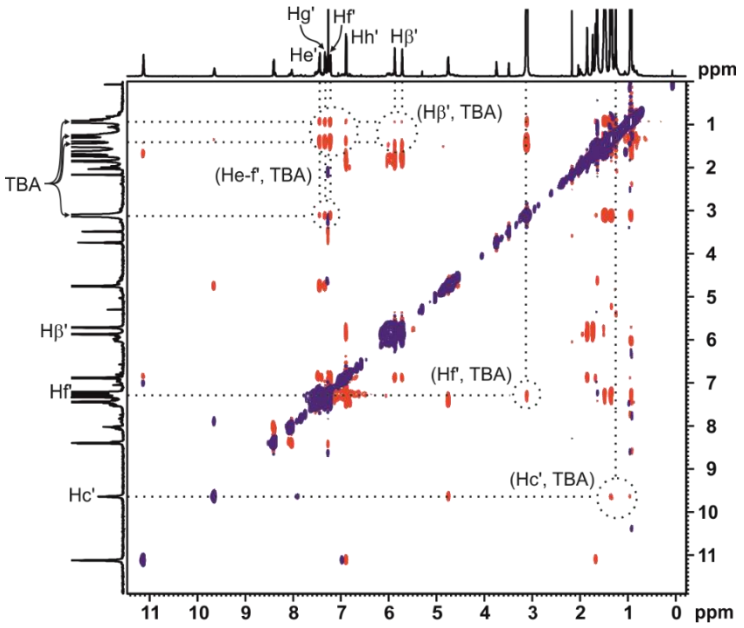

Figure 5.7. Selected region of the ^{1}H-^{1}H ROESY experiment (500 MHz, $CDCl_3$, 298 K, spin-lock = 0.3 s) of a 1:2 mixture of receptor **1** and ion pair **2b** with relevant cross-peaks. See Figure 5.2 for proton assignments.

^{1}H NMR titration experiments of the terminal alkyne derivative of **4**, used as model of the strap unit in **1**, with TBA·Cl **2b** assigned a reduced binding affinity constant of 56 ± 6 M^{-1} to the 1:1, **2b**⊂**4** complex (see Experimental Section).

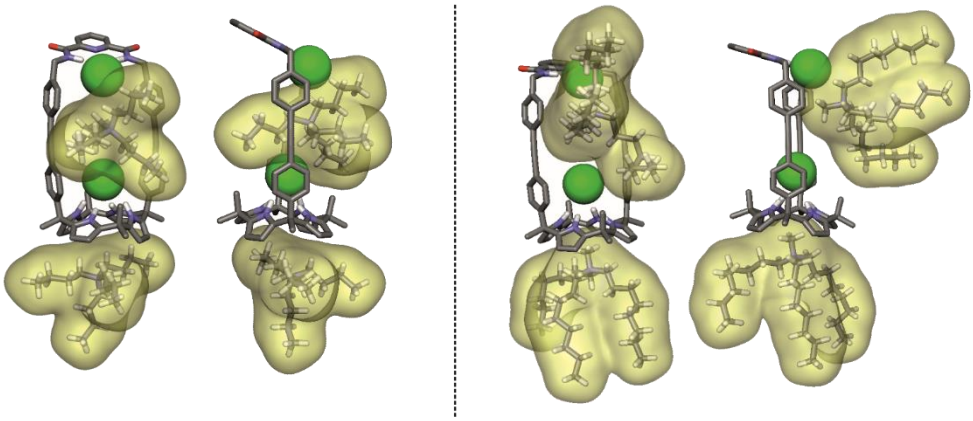

Figure 5.8. Energy-minimized structure (MM3) of complexes (**2b**)$_2$⊂**1** (left) and (**2a**)$_2$⊂**1** (right). TBA^+ and $MTOA^+$ cations are depicted with a van der Waals surface. Non-polar hydrogens were removed for clarity.

The binding affinity constant for the **2b⊂4** complex is more than two orders of magnitude smaller than the ones estimated for the binding of Cl^- to the bis-amide strap of the C4P receptor **1**. [14,15] Based on these results, we did not expect the coordination of the Cl^- anion to the dicarboxamide strap moiety of **1** until the binding site of the C4P core was fully saturated. The concomitant formation of the 2:1 and 1:1 complexes of **2b** with **1** at the initial phases of the titration suggests the existence of positive cooperative binding in the coordination of the second ion pair **2b** by the self-assembled 1:1 complex, **2b⊂1**.

We obtained different results in the ^{1}H NMR titration experiments of **1** with the cyanate salt, TBA·OCN, **2c** (see Experimental Section). Interestingly, the amide proton signal Hc of the strap unit of **1** experienced reduced downfield shifts ($\Delta\delta$ = 0.5 ppm) after the addition of 3 equivalent of the ion pair. This result suggests a weaker coordination of the polyatomic cyanate anion to the dicarboxamide strap compared to the Cl^-.The spread of the negative charge over the three atoms of the OCN^- reduces the electrostatic interaction of the hydrogen-bonds. In short, we surmise that the OCN^- anion binds preferentially the C4P core of receptor **1**.

The ^{1}H NMR titration experiment of receptor **1** with MTOA·Cl **2a** also produced different results to those obtained with TBA·Cl **2b**. The addition of 1 equivalent of MTOA·Cl to the solution containing **1** induced the exclusive observation of the proton signals assigned to bound **1**. Interestingly, the proton signal assigned to the dicarboxamide NH (Hc) broadened beyond detection (**Figure 5.9**). The methyl group of the MTOA cation resonates at δ = 0.2 ppm. Taken together, these results suggest the exclusive formation of a 1:1 complex **2a⊂1**. In this complex, the MTOA cation is located in the aromatic cup defined by the pyrrole ring of the C4P core in cone conformation. Most likely, the chloride anion is bound to the opposite pyrrole NHs. The existence of an intermediate chemical exchange process of the bound chloride between the polar sites of **1** cannot be ruled out and may explain the broadening beyond detection of Hc. However, this hypothesis is not supported by the observation of a sharp singlet for the pyrrole NHs of the **2a⊂1** complex. We are inclined to suggest that the broadening of Hc is a consequence of intermediate dynamic conformational processes of the strap in the **2a⊂1** complex.

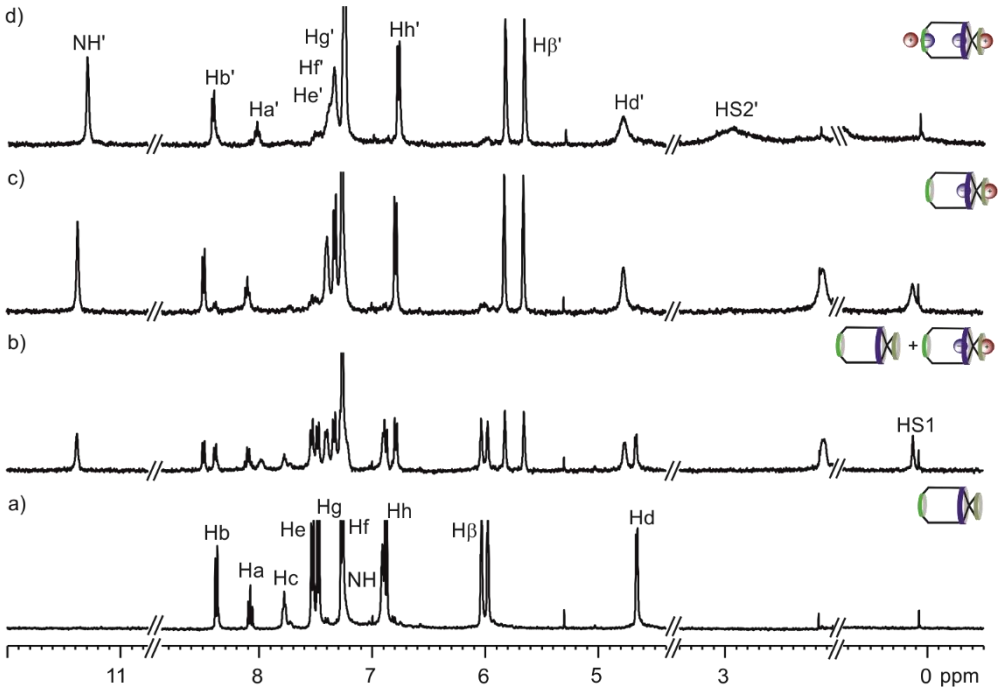

Figure 5.9. Selected region of the ^{1}H NMR spectra (400 MHz, $CDCl_3$, 298 K) of free receptor **1** (2 mM) (a) and incremental additions of MTOA·Cl (**2a**): 0.5 (b), 1.0 (c), and 2.0 equivalent (d). Primed letters and doubled primed letters correspond to proton signals assigned to complex **2a**⊂**1** and (**2a**)$_2$⊂**1**, respectively. Schematic models indicate the major species observed. See Figure 5.2 for proton assignment.

The addition of more than 1 equivalent of **2a**, produces the gradual assembly of the 2:1 complex (**2a**)$_2$⊂**1**. This process induced reduced chemical shift changes to the protons of **1**. These changes are more noticeable for the signals of the pyrrole NHs, *β*-pyrrole protons, methylene protons *alpha* to the amides and some of the aromatic protons. We performed a ^{1}H-^{1}H ROESY experiment using a mM solution containing a 2:1 molar ratio of **2a** and receptor **1** (**Figure 5.10**). Under these conditions, the formation of complex (**2a**)$_2$⊂**1** is almost quantitative. The ROESY spectrum revealed cross-peaks related to spatial proximity between the methylene proton *alpha* to the nitrogen atom in the MTOA$^+$ cation (HS2) and the *β*-pyrrole protons of **1**. No cross-peaks were detected between the cation and the aromatic walls of receptor **1**.

We propose the existence of two chemically non-equivalent MTOA$^+$ cations in the (**2a**)$_2$⊂**1** complex (**Figure 5.8**). Similar to the observation made for TBA·Cl **2b**, the MTOA$^+$ cation of the first bound ion pair is included in the electron rich aromatic cavity of the C4P in **1**, opposite to the bound chloride. The formed **2a**⊂**1** complex

displays a receptor-separated binding mode. We are tending to assign a close contact binding geometry to the second bound ion-pair **2a**. The Cl^- anion will be bound to the dicarboxamide NHs of the strap. Based on the lack of ROESY cross-peaks between the protons of the $MTOA^+$ cation and the aromatic walls of **1**, we hypothesized that the close-contact binding geometry of the second ion-pair **2a** does not involve the sandwiching of the alkyl substituents between the two bound chloride atoms.

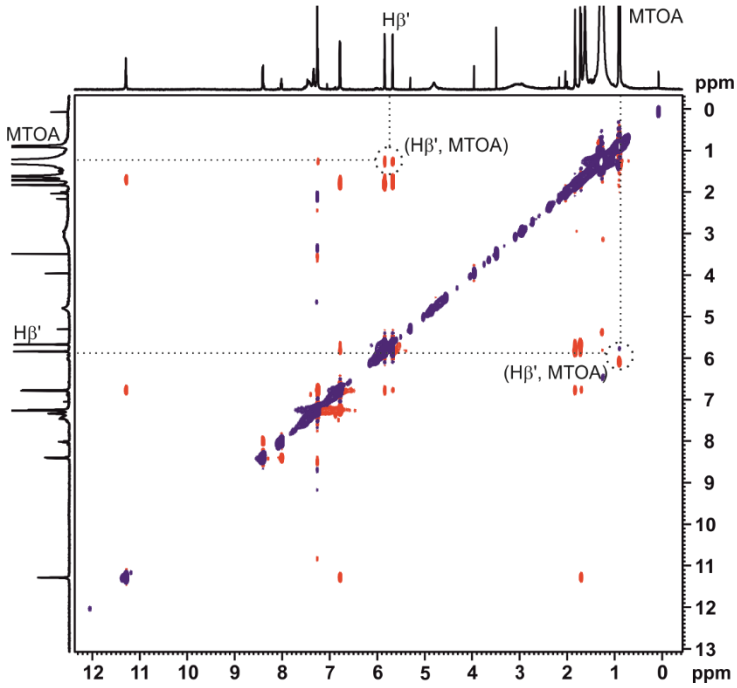

Figure 5.10. ^1H-^1H ROESY experiment (500 MHz, $CDCl_3$, 298 K, spin-lock = 0.3 s) of a 1:2 mixture of receptor **1** and ion pair **2a** with relevant cross-peaks. See Figure 5.2 for proton assignments.

5.2.3 ^1H NMR characterization of pseudorotaxane complexes **2a-c**·**3**⊂**1**

We performed a ^1H NMR titration experiment of receptor **1** in a mM $CDCl_3$ solution by adding incremental amounts of *N*-oxide **3** (**Figure 5.11**). The addition of 1.0 equivalent of **3** produced the appearance of a new set of broad signals that were assigned to the protons of axle **3**. These signals appeared upfield shifted with respect to those of the free guest. Some of the proton signals assigned to receptor **1** (Hb, He, Hg and Hd) also experienced a reduced broadening. In addition, the NH protons of the C4P core of **1** broadened beyond detection. The subsequent addition of **3**, up to 2.0 equivalent, provoked gradual upfield shifts to the protons H2 and H3

of the axle *N*-oxide **3**. Interestingly, the signal assigned to the NH protons of the bis-amide strap moved *ca.* $\Delta\delta$ = 0.2 ppm downfield. We interpreted this result as indicative of the weak coordination of *N*-oxide **3** axle with the bis-amide strap of **1**.

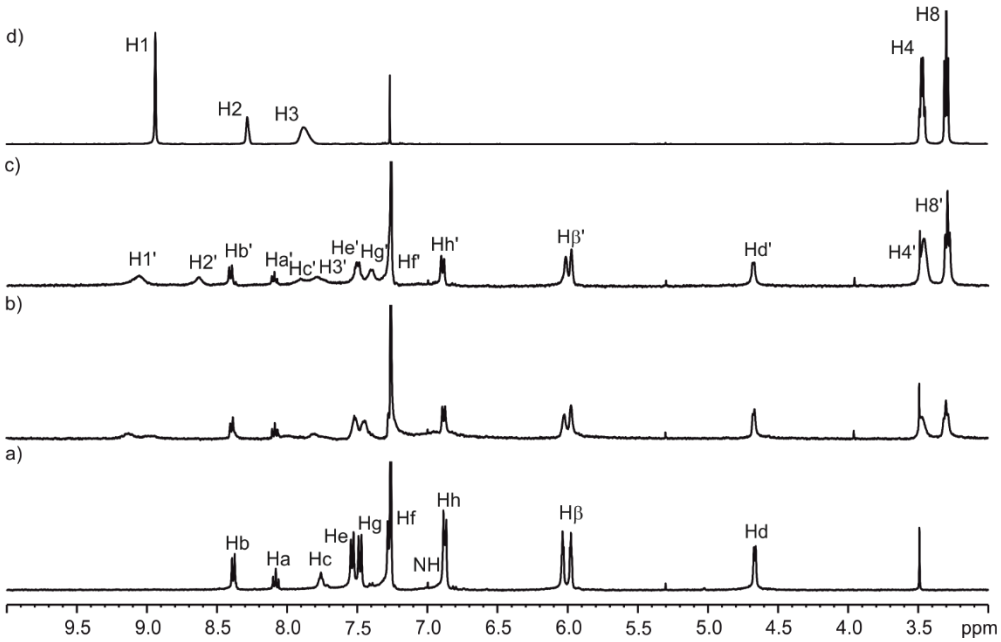

Figure 5.11. Selected region of the ^{1}H NMR spectra (400 MHz, $CDCl_3$, 298 K) of free receptor **1** (2 mM) (a) and incremental additions of *N*-oxide **3**: 1.0 (b) and 2.0 equivalent. Free *N*-oxide **3** shown for comparison (d). Primed letters correspond to proton signals assigned to receptor **1** in the complex formed with **3**. See Figure 5.2 for proton assignment.

The observations made above point out to the formation of a 1:1 complex between receptor **1** and axle **3**. We hypothesize that the **3**⊂**1** complex could involve two isomeric forms. One of them will be mainly stabilized by the establishment of hydrogen bonding interactions between the oxygen atom of the *N*-oxide axle **3** and the four NH of the C4P. The second isomeric 1:1 complex will involve the interaction of the oxygen atom of the *N*-oxide **3** with the two amide NH protons of the bis-amide strap of **1**. The obtained results do not provide evidence for the selective binding of the *N*-oxide axle **3** in one of the two binding sites of **1**. Most likely, the bound *N*-oxide axle **3** experiences a chemical exchange process featuring fast dynamics on the ^{1}H NMR chemical shift timescale between the two isomeric 1:1 complexes. The mechanism of this exchange process may involve the pirouetting of the axle inside **1** or the dissociation and reassembly of the complex. In any case, we

estimate a value for the binding affinity constant of the **3⊂1** complex lower than 10^4 M^{-1}.[16]

The formation of the **3⊂1** complex was further supported by a ^{1}H DOSY experiment performed to a solution containing a 1:1 molar ratio of both components (see Experimental Section). The ^{1}H DOSY experiment assigned similar diffusions constant values for the proton signals corresponding to macrocycle **1** and *N*-oxide **3** (D = 2.41 ± 0.20 x 10^{-9} $m^2 \cdot s$). Taking into account the differences in size and shape of both components, this result points out to the formation of the hydrogen-bonded complex between **1** and **3**.

We proved the binding of the self-assembled **3⊂1** pseudorotaxane complex with tetraalkylammonium ion pairs **2a** and **2c** by means of ^{1}H NMR titration experiments. The resulting four particle aggregates would also feature pseudorotaxane topology.

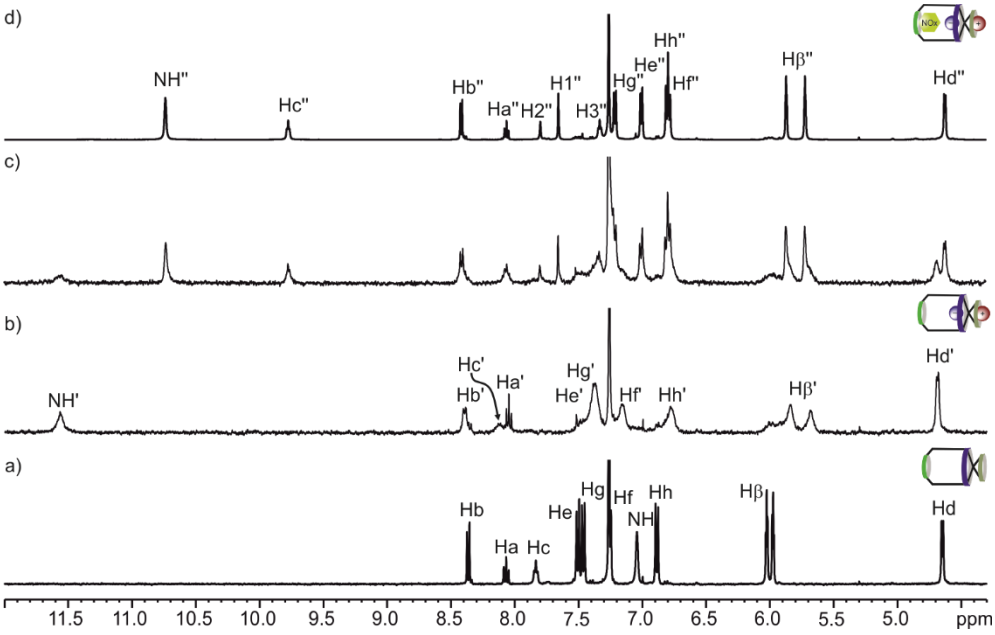

Figure 5.12. Selected region of the ^{1}H NMR spectra (400 MHz, $CDCl_3$, 298 K) of free receptor **1** (2 mM) (a) 1:1 mixture of receptor **1** and **2c** (b) and addition of 0.5 (c) and 1.0 equivalent (d) of **3**. Primed letters correspond to proton signals assigned to receptor **1** in the complex formed with **2c**. Doubled primed letters correspond to proton signals assigned to complex **2c·3⊂1**. Schematic models indicate the major species observed. See Figure 5.2 for proton assignment.

The ^{1}H NMR spectrum of a mM $CDCl_3$ solution containing an equimolar mixture of **1** and **2c** showed broad signals for the majority of the protons (**Figure 5.12**). Under

these conditions, complex **2c⊂1** is almost quantitatively formed. We demonstrated above that the OCN^- anion in the 1:1 complex is preferentially bound to the C4P binding site of receptor **1** (*vide supra*). The addition of 0.5 equivalent of *N*-oxide **3** produced reduced chemical shift changes and some sharpening to most of the proton signals of receptor **1**. In addition, we observed two sharp singlets centered at δ = 7.8 and 7.6 ppm, which were assigned to protons H2 and H1, respectively, of bound *N*-oxide **3**. These signals are significantly upfield shifted with respect to those in the free axle. This observation suggest the binding of the *N*-oxide axle **3** by threading through the macrocycle **1**. The bis-amide of **3** is sandwiched between the two aromatic walls of **1** and experiences its shielding effect. We also detected the appearance of a new set of sharp signals centered at δ = 10.7, 9.7 and 4.6 ppm. These signals were assigned to the bound pyrrole NHs, the bound bisamide NHs (Hc) and the bound *alpha* methylene protons (Hd) of receptor **1**. When 1 equivalent of *N*-oxide **3** was added, only the new set of proton signals assigned to the bound counterparts was detected. This result suggested the quantitative formation of the [2]pseudorotaxane complex **2c·3⊂1**.

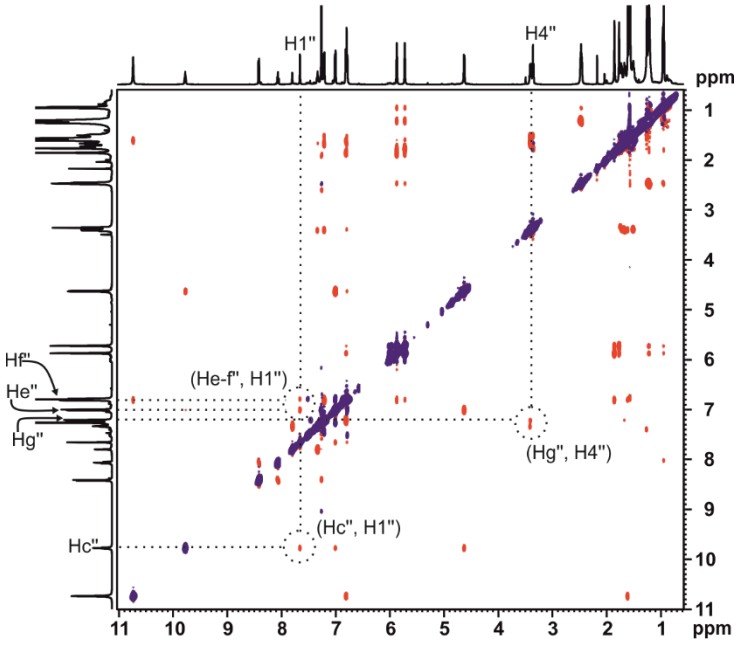

Figure 5.13. ^1H-^1H ROESY experiment (500 MHz, $CDCl_3$, 298 K, spin-lock = 0.3 s) of a 1:1:1 mixture of receptor **1**, *N*-oxide **3** and ion pair **2c** with relevant cross-peaks. See Figure 5.2 for proton assignments.

We performed a ^{1}H-^{1}H ROESY experiment using a mM $CDCl_3$ solution containing an equimolar mixture of receptor **1**, ion pair **2c** and *N*-oxide **3**. The ROESY spectrum showed cross peaks due to proximity in space between protons Hf, He and Hc of **1** and proton H1 of *N*-oxide **3** (**Figure 5.13**). Interestingly, we did not detect any cross-peaks between proton H1 of axle **3** and protons Hg and Hh of **1**, pertaining to the C4P binding site. We detected ROESY peaks between the signal attributed to the methylene proton *alpha* to the nitrogen atom in the TBA^+ cation (HS1) and the β-pyrrole protons of receptor **1**.

These observations are in agreement with the [2]-pseudorotaxane topology of the **2c·3⊂1** complex. The fact that the equimolar ratio of the three components at mM concentration produces the quantitative assembly of the **2c·3⊂1** complex allowed us to estimate a binding affinity constant K[**2c·3⊂1**] > 10^8 M^{-2}. The results obtained in the 2D experiment are also indicative of the formation of the **2c·3⊂1** complex as a single isomer (**Figure 5.14**). This result was expected to certain extent owing to the

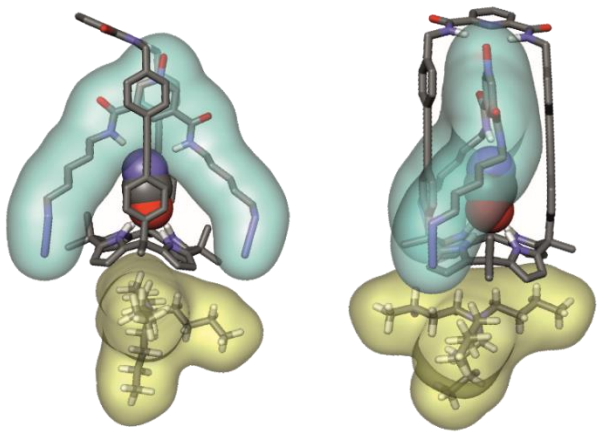

Figure 5.14. Energy-minimized structure (MM3) of complex **2c·3⊂1.** TBA^+ cation and *N*-oxide **3** are depicted with a van der Waals surface highlighted in yellow and blue colors, respectively. Non-polar hydrogens were removed for clarity.

weak coordination of OCN^- to the amide protons of the dicarboxamide unit (*vide supra*). In the **2c·3⊂1** complex, *N*-oxide **3** is coordinated to the 2 NH amide protons of the dicarboxamide strap. This is supported by the downfield shift experienced by the amide protons (Hc) in the **2c·3⊂1** complex ($\Delta\delta$ = 1.5 ppm). At the same time, the OCN^- anion is stabilized by the 6 simultaneous hydrogen bonding interactions between the 4 NH of the C4P and the 2 amide protons of **3**. The proton signal

assigned to the C4P's NH binding OCN^- in the **2c⊂1** moved upfield by approximately 1.0 ppm in the **2c·3⊂1** complex. We attributed this chemical shift change to the establishment of additional hydrogen bonding interactions between OCN^- and the amide protons of axle **3**, as well as to structural changes in the [2]pseudorotaxane complex. The TBA^+ cation in the **2c·3⊂1** complex is bound in the electron rich aromatic cavity generated by the C4P's cone conformation, opposite to the bound anion. The location of the TBA^+ is derived from the upfield shift experienced by the signal of its alpha methylene protons (HS1) ($\Delta\delta$ = - 0.9 ppm). The cross-peaks detected in the ^1H-^1H ROESY experiment of the equimolar solution of **1**, **2c** and **3** also supports the location of the TBA^+ cation (*vide supra*).

We obtained different results in the ^1H NMR titration experiment of an equimolar solution of **1** and **2a** with incremental amounts of *N*-oxide **3**. The ^1H NMR spectrum of the 1:1 mixture of **1** and **2a** showed sharp and well-resolved signals (**Figure 5.15**).

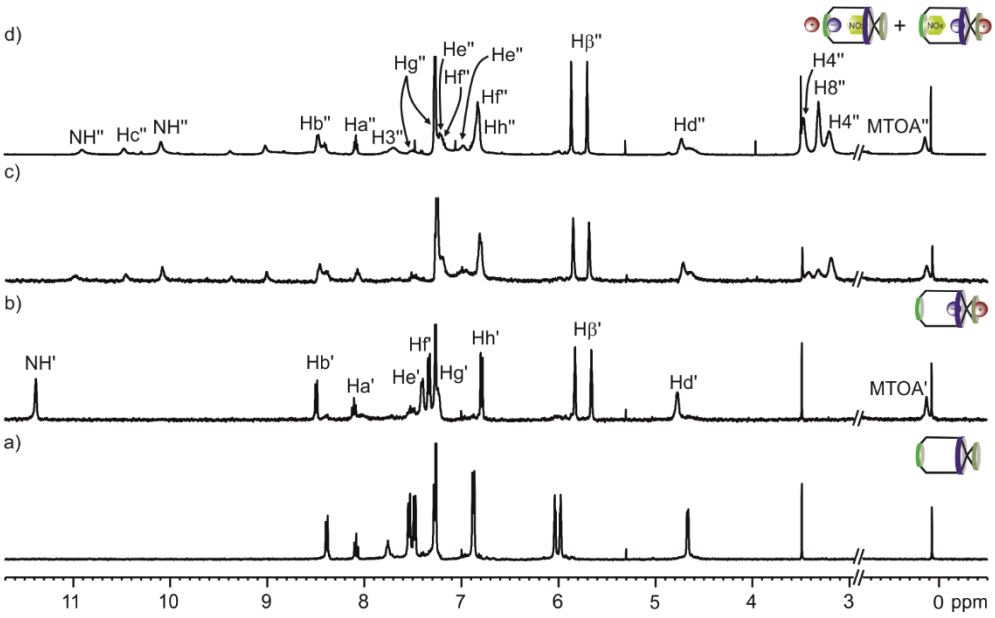

Figure 5.15. Selected region of the ^1H NMR spectra (400 MHz, $CDCl_3$, 298 K) of free receptor **1** (2 mM) (a) 1:1 mixture of receptor **1** and **2a** (b) and addition of 1.0 (c) and 2.0 equivalent (d) of **3**. Schematic models indicate the major species observed. Primed letters correspond to proton signals assigned to receptor **1** in the complex formed with **2a**. Doubled primed letters correspond to proton signals assigned to the two isomeric forms of complex **2a·3⊂1**. See Figure 5.2 for proton assignment.

These signals were assigned to the quantitative formation of the **2a⊂1** complex. The addition of 1.0 equivalent of **3** produced the appearance of a new set of signals for

the protons of **1**. More precisely, we observed three broad signals resonating between δ = 11.0 and 10.0 ppm that were assigned to the C4P's NH and the bis-amide NH protons (Hc) of **1** in the [2]pseudorotaxane complex **2a·3⊂1**. The addition of 2.0 equivalent of *N*-oxide **3** produced only the increase in intensity of the new set of signals. Interestingly, the proton signal assigned to the methyl proton alpha to the nitrogen atom in the $MTOA^+$ cation (HS1) resonated at δ = 0.1 ppm along the course of the titration.

The observations made above point out to the formation of complex **2a·3⊂1**. We attributed the duplicity of the proton signals of the receptor (e.g. the C4P's NH and Hd) to the existence in solution of two geometrical isomers of complex **2a·3⊂1**. The two isomers are involved in a chemical exchange process displaying slow dynamics on the ^{1}H NMR chemical shift timescale for the proton signals assigned to the C4P's NH and Hd and fast for the rest. This was confirmed in the ^{1}H-^{1}H ROESY experiment

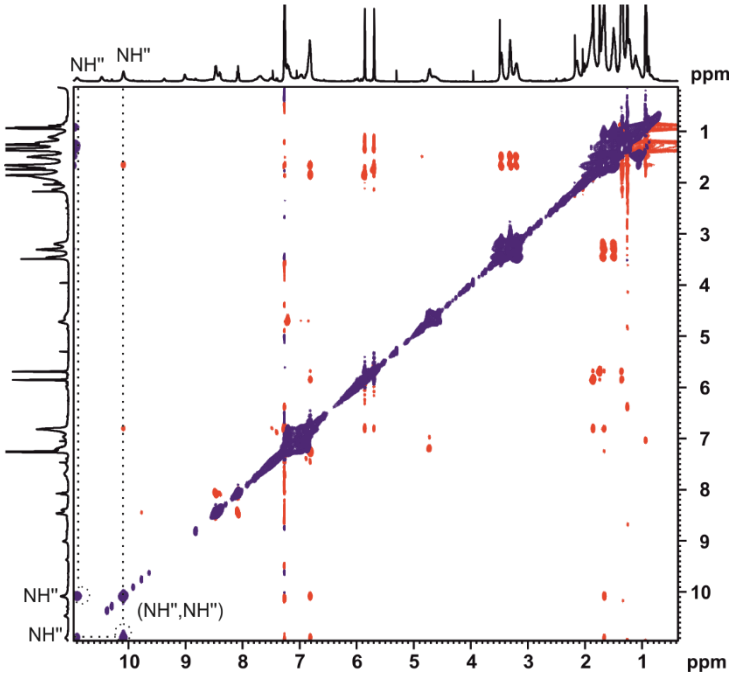

Figure 5.16. ^{1}H-^{1}H ROESY experiment (500 MHz, $CDCl_3$, 298 K, spin-lock = 0.3 s) of a 1:1:1 mixture of receptor **1**, *N*-oxide **3** and ion pair **2a** with relevant cross-peaks. See Figure 5.2 for proton assignments.

performed to the same mixture (**Figure 5.16**). Indeed, cross-peaks related to chemical exchange were observed between the proton signals of the NHs assigned to the two different isomers. However, the obtained results does not allow a

complete assignment of the proton signals of the two isomeric forms of complex **2a·3⊂1**. Hence, the isomeric distribution of the complex could not be accurately determined.

Based on the relative integral values of the two pyrrole NHs, we suspect that the isomer having the axle *N*-oxide bound to the C4P unit is present in a major extent. We rationalize the observation of two distinct isomeric forms of **2a·3⊂1** complex as a consequence of the reduced binding affinity of the Cl^- compared to OCN^- for the cylindrical and polar cavity of the self-assembled receptor **3⊂1** that is defined by the C4P binding site and the axle bisamide. Finally, the quantitative formation of the [2]-pseudorotaxane **2a·3⊂1**complex upon addition of 1 equivalent of the *N*-oxide indicates that the binding constant value can be estimated as K[**2a·3⊂1**] > 10^8 M^{-2}.

5.2.4. Gas phase characterization

We characterized the complexes formed between receptor **1**, ion pairs **2a-c** and *N*-oxide **3** in the gas phase by means of ESI-MS and IMS-TW experiments. The stability of the complexes was also investigated by Collision Induced Dissociation (CID) experiments.

Gas phase characterization of ion-paired complexes

We performed a MS-ESI analysis of a methanol solution containing a mixture of receptor **1** and ion pair **2b** in a 1:2 molar ratio at μM concentrations. In the chromatogram obtained, we detected an ion peak with a m/z value of 1253.6589. We attributed this to the molecular ion [**TBA**·(**Cl**)$_2$⊂**1**]$^-$. The isotopic pattern was in agreement with the simulated one (see Experimental Section). Most likely, the molecular ion is generated upon the loss of the TBA^+ cation bound to the C4P electron rich aromatic cavity in the (**2b**)$_2$⊂**1** complex. The cation is mainly stabilized by cation-π and CH-π interactions. On the other hand, the sandwiched TBA^+ cation is stabilized by stronger electrostatic interactions. We detected similar complexes in the experiments performed with ion pairs **2a** and **2c** (see Experimental Section). In addition, in the experiments performed with **2c** we observed the presence of the heterodimeric complex [**TBA·Cl·OCN⊂1**]$^-$ formed by the complexation of the residual Cl^- anion present in the solution.

We also performed CID experiments in order to investigate the stability in the gas phase of the ion-paired complexes. The gradual increase of the voltage applied at

the entrance of the hexapole produced the loss in intensity of the ion peak attributed to the molecular ion [**TBA**·(**Cl**)$_2$⊂**1**]$^-$(**Figure 5.17**). Simultaneously, we detected an ion peak with m/z= 976.5039. Further increase of the voltage applied produced the appearance of an additional ion peak with m/z = 940.5308, which grew in intensity at the expenses of the previous one. When the voltage applied was

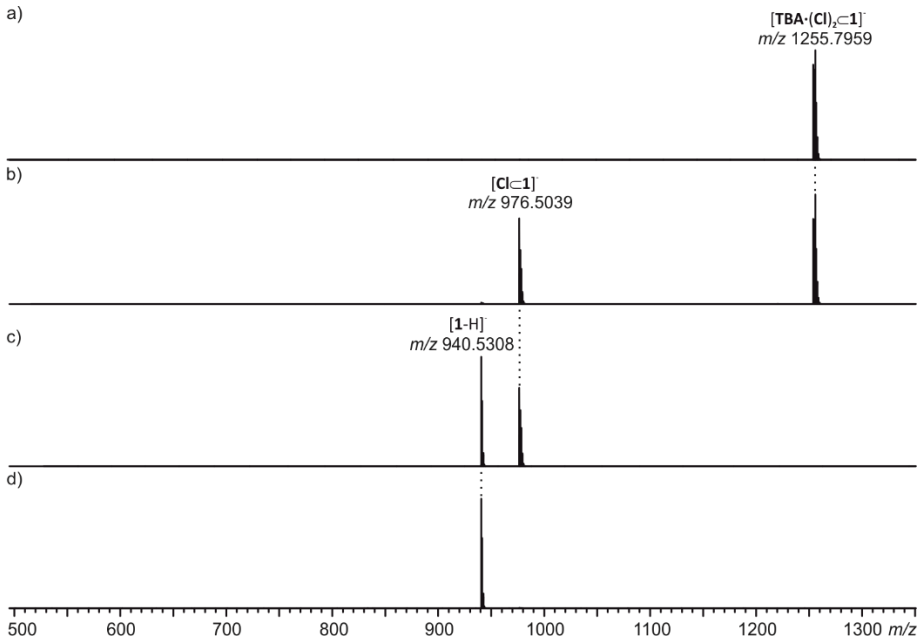

Figure 5.17. CID experiment performed with mass-selected molecular ion [**TBA**·(**Cl**)$_2$⊂**1**]$^-$ a) with CE of 20 V b), 34 V c) and 46 V d).

increased to 46 V, only the later was detected. Based on these observations, we propose that molecular ion [**TBA**·(**Cl**)$_2$⊂**1**]$^-$ is disassembled in the initial phases of the CID experiments by the loss of TBA·Cl. This is evidenced by the detection of a molecular peak that can be attributed to molecular ion [**Cl**⊂**1**]$^-$. We hypothesize that the chloride anion bound to the dicarboxamide unit is lost as ion pair TBA·Cl. This anion is weakly coordinated when compared to the Cl$^-$ anion bound to the C4P core owing to the 2 additional hydrogen bonding interactions established with the C4P NH. Further increase of the voltage applied produces the disassembly of complex [**Cl**⊂**1**]$^-$ to generate the deprotonated receptor, [**1**-H]$^-$. The normalized integrated values of the ion peaks showed the total disassembly of [**TBA**·(**Cl**)$_2$⊂**1**]$^-$ at a voltage value of *ca*. 26 V (**Figure 5.18**). At this point, 100% of the receptor was forming complex [**Cl**⊂**1**]$^-$. Likewise, the complex is completely disassembled after reaching 46 V to generate the free deprotonated receptor [**1**-H]$^-$.

Similar results were obtained in the CID experiments performed to molecular ion [**MTOA**·(**Cl**)$_2$⊂**1**]$^-$ (see Experimental Section).

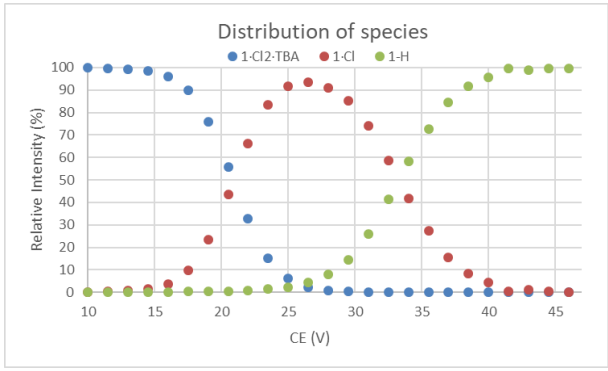

Figure 5.18. Relative intensity of the fragments observed in the CID experiment of complex **[TBA·(Cl)$_2$⊂1]**$^-$ at increasing CE voltages. The intensity was calculated as Intensity = I. Complex / (I. Complex + I. Fragments) x 100%.

Interestingly, the CID experiments performed to molecular ion [**TBA**·(**OCN**)$_2$⊂**1**]$^-$ produced different results (see Experimental Section). In this case, the disassembly of the complex was originated by the loss of H·OCN to generate [**TBA**·**OCN**⊂**1**-H]$^-$. Most likely, the loosely bound OCN anion located in the dicarboxamide strap is lost by the abstraction of an amide proton. Likewise, complex [**TBA**·**OCN**⊂**1**-H]$^-$ disassembles at higher values of applied voltage to generate deprotonated receptor [**1**-H]$^-$ and [**OCN**⊂**1**]$^-$ in a minimal amount.

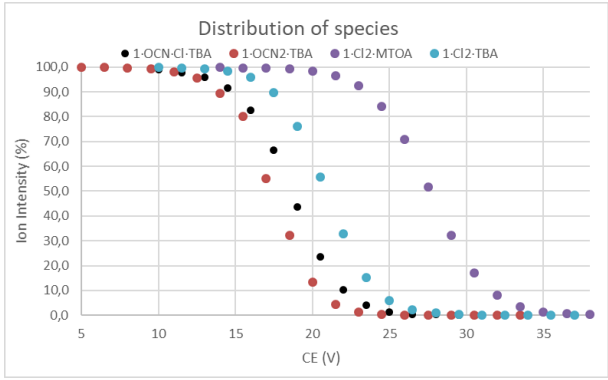

Figure 5.19. Relative intensity of the complexes obtained between receptor **1** and salts **2a-c** observed in the CID experiment at increasing CE voltages. The intensity was calculated as Intensity = I. Complex / (I. Complex + I. Fragments) x 100%.

We plotted the relative intensity of the ion peaks observed in the CID experiments against the applied voltage. The relative stabilities of the ion-paired complexes were investigated by the direct comparison of the collision energies needed to produce the disassembly of the molecular ion to a 50% extent (CE_{50}) (**Figure 5.19**). According to the CE_{50} values calculated, complex [**MTOA**·(**Cl**)$_2$⊂**1**]$^-$ presents a higher stability in the gas phase than the TBA^+ analogues (**Table 5.1**). Most likely, this is a direct effect of the better fit of the methyl group of the $MTOA^+$ cation in the aromatic cup of the C4P in the cone conformation. In addition, complex [**TBA**·(**Cl**)$_2$⊂**1**]$^-$ presented a greater stability in the gas phase than its OCN^- counterpart, again attributed to the weak coordination of OCN^- in the dicarboxamide unit of **1**.

Table 5.1. CE_{50} values obtained in the CID experiments of the complexes formed between receptor **1** and ion pairs **2a-c**.

Complex	CE_{50} (V)
[TBA·Cl$_2$⊂1]$^-$	22
[MTOA·Cl$_2$⊂1]$^-$	27
[TBA·Cl·OCN⊂1]$^-$	19
[TBA·OCN$_2$⊂1]$^-$	17

We also performed IMS experiments to investigate the relative size of the ion-paired

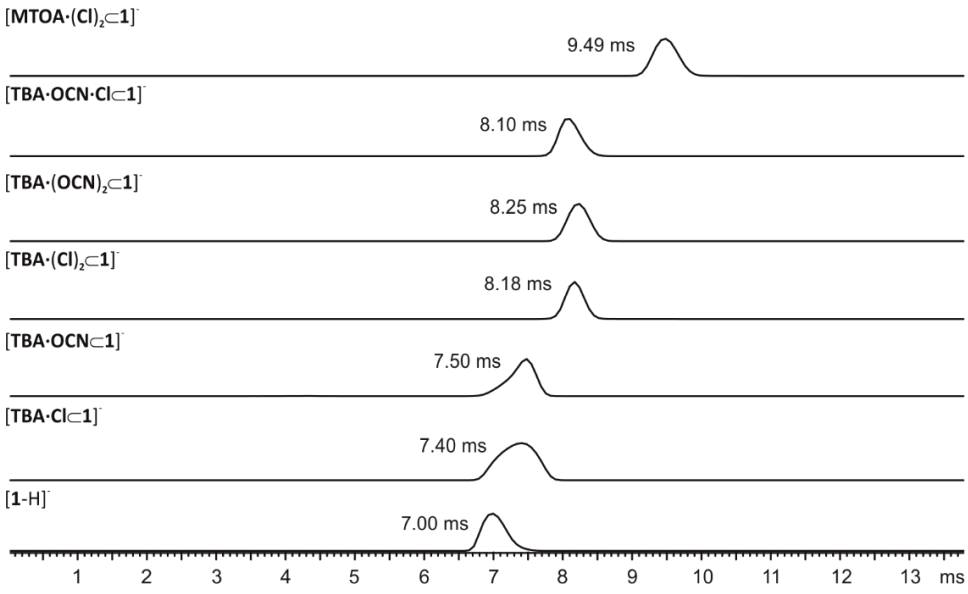

Figure 5.20. Arrival time distribution of most abundant ions obtained in the TW-IM-MS experiments of the different complexes formed between receptor **1** and ion pairs **2a-c**.

complexes (**Figure 5.20**). As expected, we obtained longer arrival times for the complexes with a bound cation i.e. [**MTOA**·(**Cl**)$_2$⊂**1**]$^-$, [**TBA**·(**Cl**)$_2$⊂**1**]$^-$ and [**TBA**·(**OCN**)$_2$⊂**1**]$^-$. Between those, the complex formed with MTOA$^+$ had the longer arrival time due to the greater size of the cation. In addition, the complexes [**TBA**·(**Cl**)$_2$⊂**1**]$^-$ and [**TBA**·(**OCN**)$_2$⊂**1**]$^-$, as well as the 1:1 complexes [**OCN**⊂**1**]$^-$ and [**OCN**⊂**1**]$^-$, showed similar values for the arrival time owing to the similarity in cross-section of the bound anions.

Gas phase characterization of pseudorotaxane complexes

We performed ESI-MS experiments to the μM solutions in methanol containing the equimolar mixture of **1**, **2b**-**c** and **3**. The pseudorotaxane complexes were generated by the dissociation of the loosely bound cation in the transition to the gas phase to generate ion peaks with m/z = 1379.6554 and m/z = 1386.6449 attributed to [**Cl**·**3**⊂**1**]$^-$ and [**OCN**·**3**⊂**1**]$^-$, respectively (see Experimental Section).[17] The isotopic pattern of the molecular peaks detected were in agreement with those simulated for molecular ions [**Cl**·**3**⊂**1**]$^-$ and [**OCN**·**3**⊂**1**]$^-$.

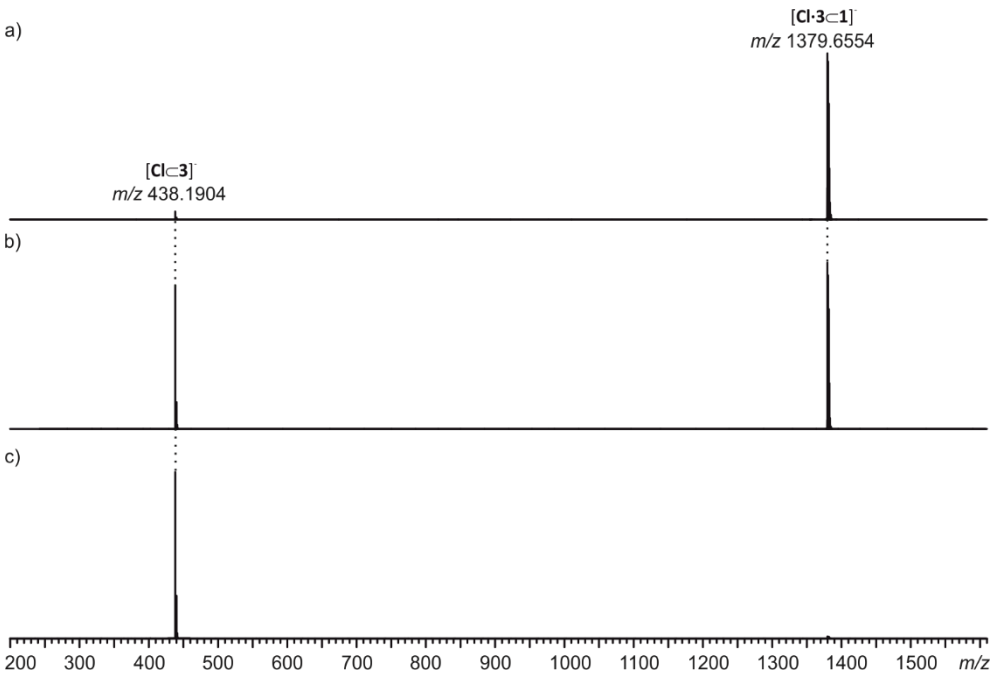

Figure 5.21. CID experiment performed with mass-selected ion [**Cl**·**3**⊂**1**]$^-$ a) with CE of 11 V b) and 17 V.

We performed CID experiments to assess the stability of molecular ion [**Cl·3⊂1**]$^-$. The increase in intensity of the voltage applied at the entrance of the hexapole produced the appearance of a new ion peak with m/z = 438.1904 (**Figure 5.21**). Higher values of applied voltage produced only the increase in intensity of the new ion peak at the expenses of the one assigned to the molecular ion. We attributed this ion peak to complex [**Cl⊂3**]$^-$ generated by the dissociation of *N*-oxide **3** with bound Cl$^-$ (**Figure 5.22**).

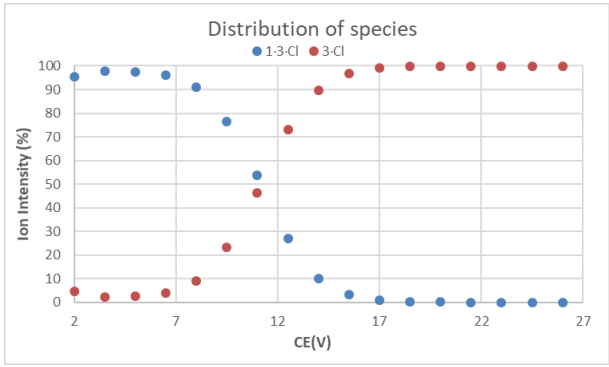

Figure 5.22. Relative intensity of the fragments observed in the CID experiment of complex [**Cl·3⊂1**]$^-$ at increasing CE voltages. The intensity was calculated as Intensity = I. Complex / (I. Complex + I. Fragments) x 100%.

Surprising to us, the disassembly of the molecular ion [**Cl·3⊂1**]$^-$ implied the cleavage of up to 6 hydrogen bonding interactions to generate [**Cl⊂3**]$^-$: 4 between the Cl$^-$ anion and the C4P NH core and 2 between the oxygen atom of **3** and the dicarboxamide strap. On the other hand, the dissociation of axle **3** would imply only

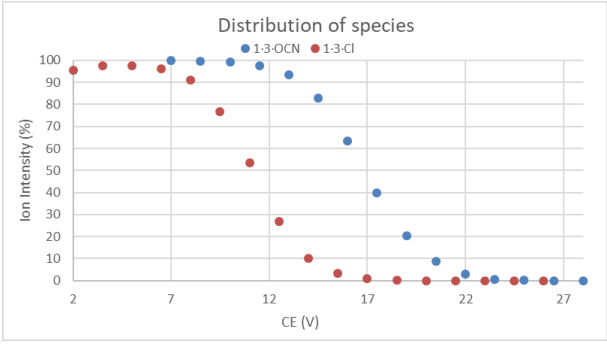

Figure 5.23. Relative intensity of the complexes obtained between receptor **1**, *N*-oxide **3** and salts **2b-c** observed in the CID experiment at increasing CE voltages. The intensity was calculated as Intensity = I. Complex / (I. Complex + I. Fragments) x 100%.

the cleavage of 4 hydrogen bonds: 2 of them with the Cl anion and 2 with the dicarboxamide strap. A similar result was also obtained in the CID experiment of molecular ion [**OCN·3⊂1**]$^-$ (see Experimental Section). Most likely, this can be explained by higher binding affinity of the anions towards axle **3** than with receptor **1**.

The direct comparison of the CE_{50} values obtained in the CID experiments provided information on the stability of the complexes in the gas phase (**Figure 5.23**). The results obtained point out to the greater stability of molecular ion [**OCN·3⊂1**]$^-$ (**Table 5.2**). We rationalize this result by invoking the better fit of the polyatomic anion in the cylindrical binding site generated by receptor **1** and *N*-oxide **3**.

Table 5.2. CE_{50} values obtained in the CID experiments of the complexes formed between receptor **1**, *N*-oxide **3** and salts **2b-c**.

Complex	CE_{50} (V)
[Cl·3⊂1]$^-$	11
[OCN·3⊂1]$^-$	17

We also performed IMS-TW experiments to the separate solutions containing the equimolar mixture of **1** and **3** with ion pair **2b** and **2c** (**Figure 5.24**). As expected, we obtained similar values for the arrival time of molecular ions [**Cl·3⊂1**]$^-$ and [**OCN·3⊂1**]$^-$ owing to the cross-sections of the bound anions.

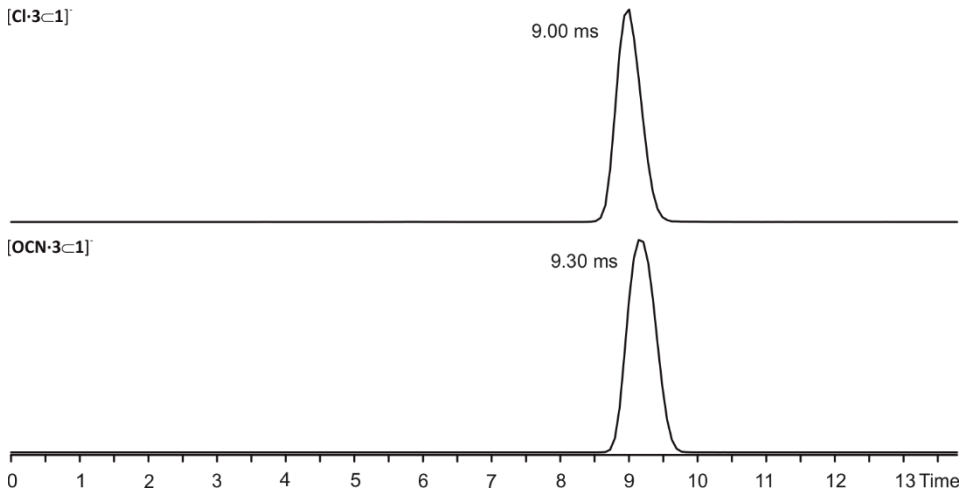

Figure 5.24. Arrival time distribution of most abundant ions obtained in the TW-IM-MS experiments of the different complexes formed between receptor **1**, *N*-oxide **3** and salts **2b-c**.

5.4. Conclusions

In this chapter, we have described the synthesis and binding studies of strapped C4P receptor **1**. The macrocycle consisted on a 2W-SAE-C4P covalently linked in the upper rim to a dicarboxamide strap. Receptor **1** was synthetized through the acid-catalyzed condensation of bis(di-pyrromethane) precursor **7** in acetone. We investigated the properties of receptor **1** to bind tetraalkylammonium salts **2a-c** in chloroform solution and at millimolar concentration by means of 1D and 2D NMR experiments. Remarkably, we obtained thermodynamically and kinetically stable complexes with all the ion pairs studied displaying 1:1 and 1:2 receptor:guest stoichiometry. In the 1:2 complexes obtained, one anion was bound to the C4P NH by establishment of 4 hydrogen bonding interactions. The second anion was coordinated into the amide NH protons of the dicarboxamide strap. In addition, the binding geometry of the ion pairs was highly dependent on the cation. The use of TBA·Cl **2b** and TBA·OCN **2c** generated the formation of cascade complexes displaying an ion triplet bound inside the receptors cavity and a second cation bound in the outer rim of the C4P. In contrast, the complex obtained with MTOA·Cl **2a** displayed a receptor-separated binding geometry. The second cation was bound as a close-contact ion pair next to the Cl^- anion coordinated to the dicarboxamide unit. The CID experiments performed in the gas phase pointed out to the greater stability of the MTOA·Cl complex.

We also studied the formation of pseudorotaxane complexes with *N*-oxide **3** templated by ion pairs **2a** and **2c**. We confirmed the quantitative formation of the pseudorotaxane complex assisted by TBA·OCN by means of 1D and 2D NMR experiments. The complex existed in solution as a single isomer featuring the cyanate anion bound into the C4P's NH core and the *N*-oxide coordinated into the dicarboxamide strap. The use of MTOA·Cl produced the formation of the pseudorotaxane complex as two distant isomeric forms. Most likely, this was due to the greater affinity of the ion pair towards the C4P binding site of **1**. The greater stability of the pseudorotaxane complex assisted by OCN^- was proved by CID experiments. We attributed this increase in stability to the complementarity in size and shape of the cylindrical anion with the anion binding site generated between receptor **1** and *N*-oxide **3**.

5.5. Experimental section

5.4.1. General information and instruments

Reagents were obtained from commercial suppliers and used without further purification unless otherwise stated. All solvents were commercially obtained and used without further purification. Deuterated solvents were purchased from Sigma Aldrich. Dry solvents were taken from a solvent system MB SPS 800. THF was dried, distilled and degassed by three freeze-pump-thaw cycles. Routine ^{1}H NMR and ^{13}C {^{1}H} NMR spectra were recorded on a Bruker Avance 300 (300 MHz for ^{1}H NMR and 75 MHz for ^{13}C NMR), Bruker Avance 400 (400 MHz for ^{1}H NMR and 100 MHz for ^{13}C NMR), Bruker Avance 500 (500 MHz for ^{1}H NMR and 125 MHz for ^{13}C NMR) or Bruker Avance 500 with cryoprobe (500 MHz for ^{1}H NMR and 125 MHz for ^{13}C NMR). Deuterated solvents used are indicated in the characterization and chemical shifts are given in ppm. Residual solvent peaks were used as reference. All NMR J values are given in Hz. COSY, NOESY, ROESY, HMQC and HMBC experiments were recorded to help with the assignment of ^{1}H and ^{13}C signals. High-resolution mass spectra (HRMS) for determination of exact mass of compounds **4**-**8** were obtained on a Bruker HPLC-TOF (MicroTOF Focus) and Bruker HPLC-QqTOF (MaXis Impact) using the ionization mode indicated for each species. IR spectra were recorded on a Bruker Optics FTIR Alpha spectrometer equipped with a DTGS detector, KBr beamsplitter at 4 cm^{-1} resolution using a one bounce ATR accessory with diamond windows. Melting points were measured on a MP70 Melting Point System Mettler Toledo. Column chromatography was performed with silica gel technical grade, pore size 60 Å, 230-400 mesh particle size, 40-63 µm particle size and thin layer chromatography (TLC) analysis on silica gel 60 F254. Ion mobility mass spectrometry and CID experiments were performed with Waters Synapt G2 Q-TOF mass spectrometer. Samples were prepared with 10-20 µM concentration in methanol solution with a 1:2 host–guest ratio. The modified Waters Synapt G2 was equipped with a linear drift cell filled with ~2 Torr nitrogen (298 K). Samples were ionized with a nanoESI ion source. In-house pulled capillary tips were used with inserted platinum wire for nanoESI. Parameters were optimized as follows: Capillary voltage 2.30 kV and source temperature 80 ºC. Data was analyzed using MassLynx v4.1 (Waters Corporation, USA) and Microsoft Excel 2016 (Microsoft, USA).

5.4.2. Synthesis and characterization data

Synthesis of 4. 490 mg of pyridine-2,6-dicarbonyl dichloride (2.4 mmol) in 30 mL of dry DCM are added under Argon via cannula to 20 mL of DCM containing 1.6 g of 4-iodophenylmethanamine (6.7 mmol, 2.8 equivalent) and 1 mL of freshly distilled triethylamine. The solution is left stirring under Argon at room temperature for 8 h. After that, 100 mL of water are added to the solution and the mixture is passed to a separation funnel, extracting the product three times with 75 mL of DCM. The combined organic layers are then washed once with 100 mL of sodium carbonate and twice with 100 mL water, dried with sodium sulfate, filtered and concentrated under reduced pressure to obtain a green/brownish oil. Product is purified by silica column chromatography using a 10% mixture of EtOAc in DCM to obtain a white solid as the pure product (804 mg, 56%). ^{1}H NMR (500 MHz, $CDCl_3$, 298 K) δ 8.39 (d, 2H, J = 6.4 Hz, Hb), 8.20 (t, 1H, J = 6.4 Hz, Ha), 8.05 (br, 2H, Hc), 7.61 (d, 4H, J = 8.5 Hz, He), 7.04 (d, 4H, J_1 = 8.5 Hz, Hf), 4.56 (d, 4H, J = 6.4 Hz, Hd).^{13}C {^{1}H} NMR (125 MHz, $CDCl_3$, 298 K) δ 163.6, 149.0, 139.5, 138.2, 138.0, 130.1, 125.9, 93.4, 43.3. FTIR (ATR): $\bar{\upsilon}_{max}$ (cm^{-1}) = 3307 (amine N-H stretching), 1675 (pyridine C=N stretching), 1647 (pyridine C=N stretching), 1524 (N-H bending), 1004 (alkene C=C bending). HR-MS (ESI-TOF-MS) m/z calculated for $C_{21}H_{17}I_2N_3NaO_2$ $[M+Na]^+$ – 619.9302, found 619.9299.

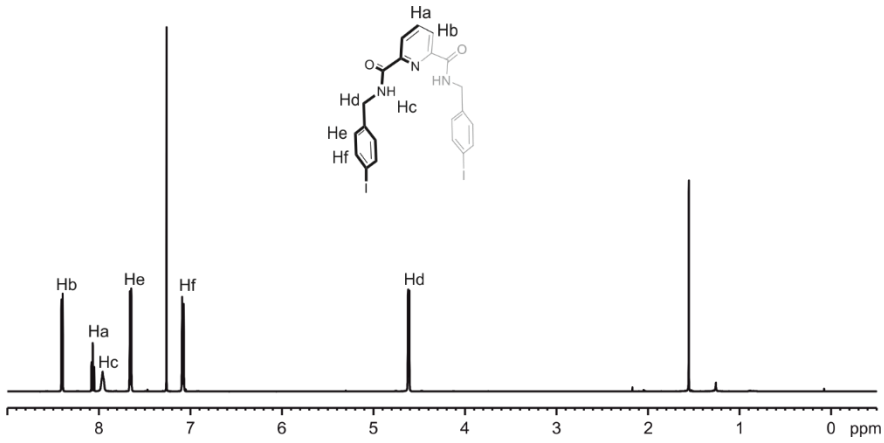

Figure 5.25. ^{1}H NMR spectrum (500 MHz, $CDCl_3$, 298 K) of **4**.

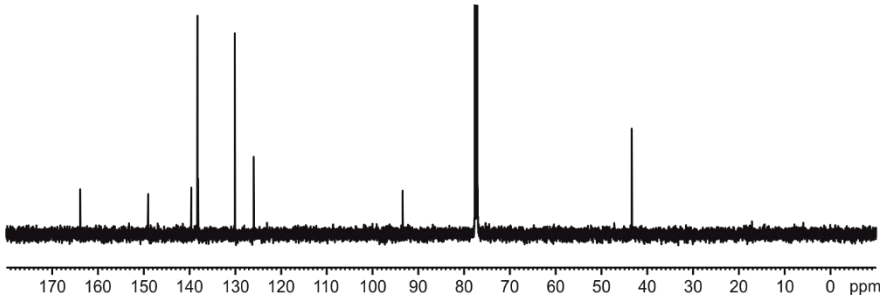

Figure 5.26. ^{13}C NMR spectrum (125 MHz, $CDCl_3$, 298 K) of **4**.

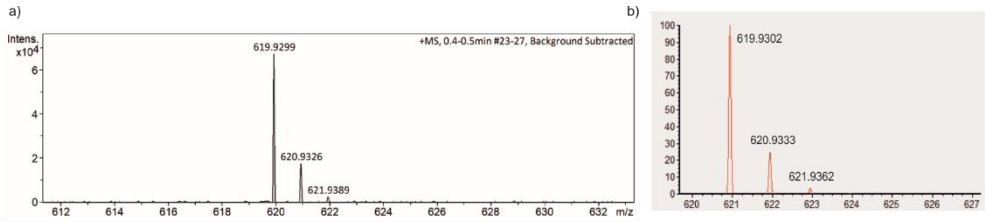

Figure 5.27. Experimental (a) and theoretical (b) isotopic distribution of [**4**+Na]$^+$.

Synthesis of 5. In 30 mL of dry and degassed THF are suspended 2 gr of the iodo-dipyrromethane (5.52 mmol), 194 mg of $Pd(PPh_3)_2Cl_2$ (0.3 mmol, 0.05 equivalent) and 53 mg of CuI (0.3 mmol, 0.05 equivalent). To this suspension are added 20 mL of freshly distilled and degassed triethylamine and 4.6 mL of ethyniltrimethylsilane (33 mmol, 6 equivalent). The solution is left stirring at 50 C under Argon during 4 hours, at which the reaction is stopped and is put into a separation funnel, washing the flask with 50 mL of DCM. The organic phase is washed once with 80 mL of 5% HCl and twice with 80 mL of water, is dried with sodium sulfate, filtered and concentrated under reduced pressure to obtain a black oil (1.8 gr of crude). Product is isolated by purification by silica column chromatography using a 1/1 hexane/DCM mixture and a later precipitation in hexane. Product was obtained as a white solid (1.7 gr, 93%). ^1H NMR (500 MHz, $CDCl_3$, 298 K) δ 7.76 (br, 2H, NH), 7.40 (d, 2H, J = 8.5 Hz, Ha), 7.07 (d, 2H, J = 8.5 Hz, Hb), 6.66 (ddd, 2H, J1 = 1.6 Hz, J2 = 2.5 Hz, J3 = 1.5 Hz, Hβ1), 6.19 (br, 2H, J1 = 2.5 Hz, J2 = 1.6 Hz, J3 = 1.5 Hz, Hβ3), 5.97 (br, 2H, Hβ2), 2.04 (s, 3H, Hc), 0.29 (s, 9H, TMS). ^{13}C {^1H} NMR (125 MHz, $CDCl_3$, 298 K) δ 148.2, 137.3, 132.1, 127.8, 121.8, 117.5, 108.7, 106.9, 105.3, 94.6, 45.1, 29.0, 0.41. FTIR (ATR): $\bar{\upsilon}_{max}$ (cm^{-1}) = 3424 (amine N-H stretching), 2966 (C-C stretching), 2159 (alkyne C≡C stretching), 1249 (pyrrole C-N stretching), 835 (methyl C-H bending). HR-MS (ESI-TOF-MS) m/z calculated for $[M+H]^+$ – 333.1782, found 333.1781.

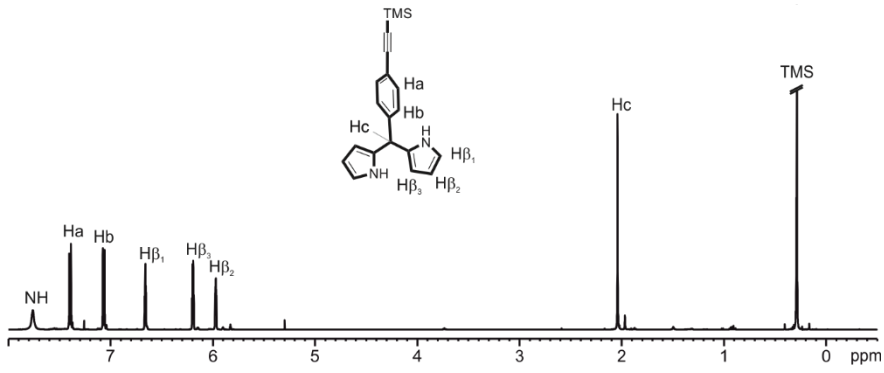

Figure 5.28. ^{1}H NMR spectrum (500 MHz, $CDCl_3$, 298 K) of **5**.

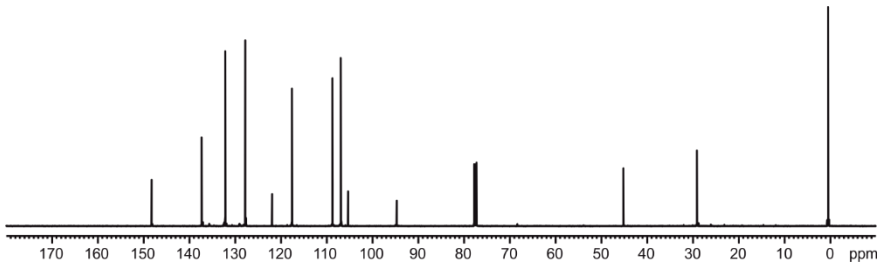

Figure 5.29. ^{13}C NMR spectrum (125 MHz, $CDCl_3$, 298 K) of **5**.

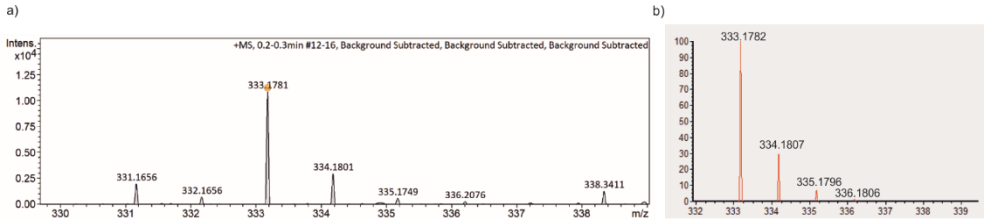

Figure 5.30. Experimental (a) and theoretical (b) isotopic distribution of [**5**+H]$^{+}$.

Synthesis of 6. In 75 mL of THF are solved 1.7 g of **5** (5.1 mmol). To this solution are added 5.6 mL of a 1 M solution in THF of tetrabutylammonium fluoride (5.7 mmol, 1.1 equivalent). The solution is left stirring for 1 h. After that, 100 mL of NH_4Cl are added and the mixture is transferred to a separation funnel with 100 mL of DCM. The aqueous phase is discarded and the DCM is washed three times with 100 mL of water, dried with sodium sulfate, filtered and concentrated under reduced pressure to obtain a brown oil (1.3 g of crude). **6** was isolated by purification by silica column chromatography using a 1/1 hexane/DCM mixture and a later precipitation in hexane. **6** was obtained as a white-yellowish solid (870 mg, 65%). ^{1}H NMR (500 MHz, $CDCl_3$, 298 K) δ 7.77 (s, 2H, NH), 7.40 (d, 2H, J = 8.4 Hz, Ha), 7.08 (d, 2H, J = 8.4 Hz, Hb), 6.68 (m, 2H, Hβ1), 6.18 (ddd, 2H, J1 = 2.5 Hz, J2 = 2.8 Hz, J3 = 3.0, Hβ2), 5.96

(br, 2H, Hβ3), 3.05 (s, 1H, Hd), 2.04 (s, 3H, Hc).^{13}C {^{1}H} NMR (125 MHz, $CDCl_3$, 298 K) δ 148.2, 136.8, 131.9, 127.5, 120.5, 117.7, 108.2, 106.5, 83.4, 44.8, 28.6, 28.3. FTIR (ATR): $\bar{\upsilon}_{max}$ (cm^{-1}) = 3395 (amine N-H stretching), 731 (C=C bending), 533 (C-I stretching). HR-MS (APCI-TOF-MS) m/z calculated for $C_{18}H_{16}N_2$ $[M+H]^+$ – 261.1386, found 261.1385.

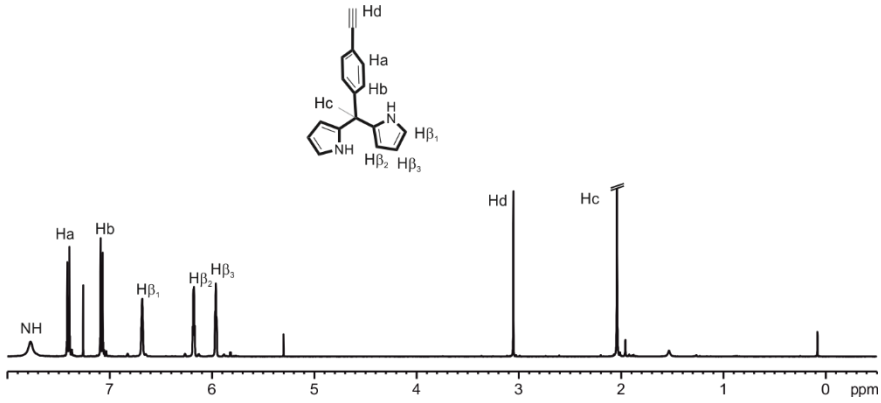

Figure 5.31. ^{1}H NMR spectrum (500 MHz, $CDCl_3$, 298 K) of **6**.

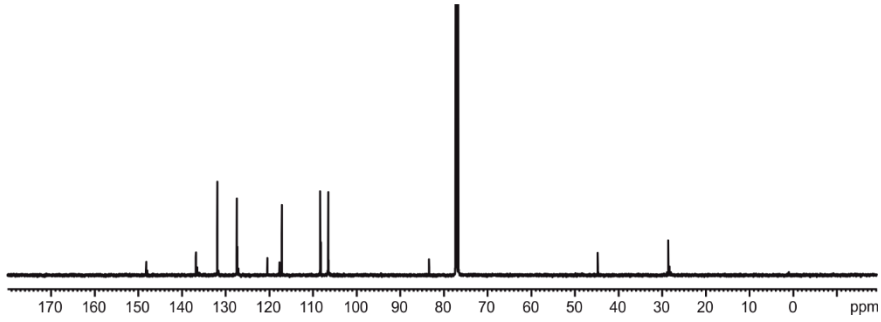

Figure 5.32. ^{13}C NMR spectrum (125 MHz, $CDCl_3$, 298 K) of **6**.

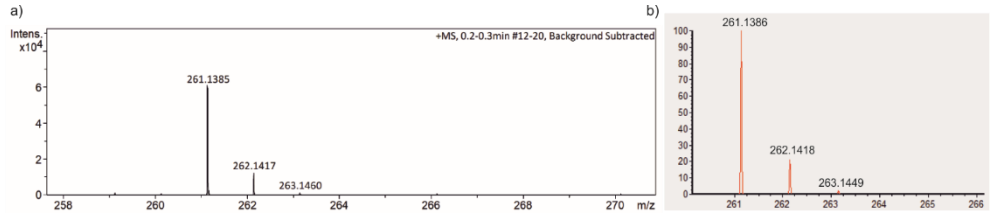

Figure 5.33. Experimental (a) and theoretical (b) isotopic distribution of [**6**+H]$^{+}$.

Synthesis of 7. To a solution of 10 mL of dry and degassed THF containing 250 mg of **4** (59 mmol), 41 mg of $Pd(PPh_3)_2Cl_2$ (0.06 mmol, 0.1 equivalent) and 11 mg of CuI

(0.06 mmol, 0.1 equivalent) are added 5 mL of THF containing 610 mg of **6** (2.3 mmol, 4 equivalent) and 15 mL of dry and degassed triethylamine. The solution is stirred at 40 ºC for 8 h. The reaction crude is transferred to a separation funnel. The flask was washed with 40 mL of DCM. The organic phase is washed three times with 50 mL of water, dried with sodium sulfate, filtered and concentrated under reduced pressure to obtain a brown solid (1.04 g of crude). The product is isolated by purification through silica column chromatography using a 10% mixture of AcOEt in DCM as the eluent, to obtain the pure product as a brown solid (450 mg, 89%). ^{1}H NMR (500 MHz, $CDCl_3$, 298 K) δ 8.40 (d, 2H, J_1 = 7.4 Hz, Hb), 8.07 (t, 1H, J = 7.4 Hz, Ha), 7.99 (t, 2H, J = 6.2 Hz, Hc), 7.79 (br, 4H, NH), 7.47 (d, 4H, J_1 = 7.8 Hz, He), 7.41 (d, 4H, J = 9.0 Hz, Hg), 7.27 (d, 4H, J = 7.8 Hz, Hf), 7.08 (d, 4H, J = 9.0 Hz, Hh), 6.68 (m, 4H, Hβ1), 6.17 (ddd, 4H, J1 = 2.6 Hz, J2 = 3.2 Hz, J3 = 3.5 Hz, Hβ2), 5.96 (m, 4H, Hβ3), 4.67 (d, 4H, J = 6.2 Hz, Hd), 4.67 (d, 4H, J = 6.2 Hz, Hd), 2.03 (s, 6H, Hi).^{13}C {^{1}H} NMR (125 MHz, $CDCl_3$, 298 K) δ 164.0, 148.4, 148.3, 138.0, 137.0, 131.7, 131.4, 127.6, 127.5, 122.4, 121.1, 117.4, 108.1, 106.5, 89.9, 88.9, 44.8, 28,7. FTIR (ATR): $\bar{\upsilon}_{max}$ (cm^{-1}) = 3391 (amine N-H stretching), 1656 (pyridine C=N stretching), 1515 (N-H bending), 720 (C=C bending). HR-MS (ESI-TOF-MS) m/z calculated for $C_{57}H_{48}N_7O_2$ $[M+H]^+$ – 862.3864, found 862.3892.

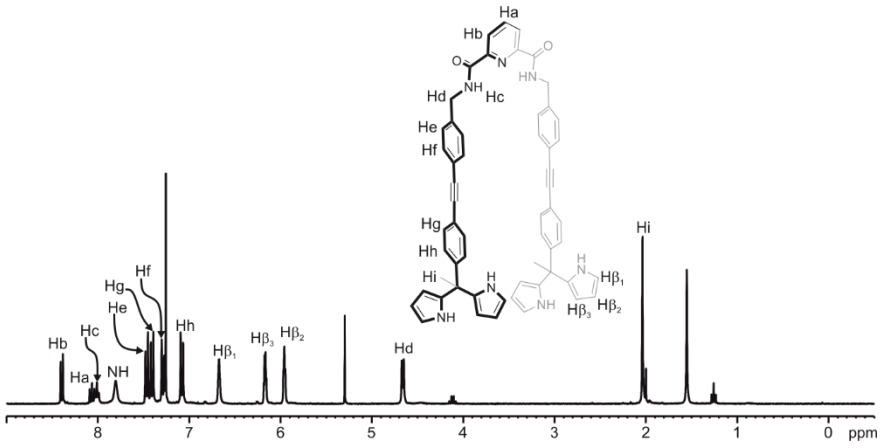

Figure 5.34. ^{1}H NMR spectrum (500 MHz, $CDCl_3$, 298 K) of **7**.

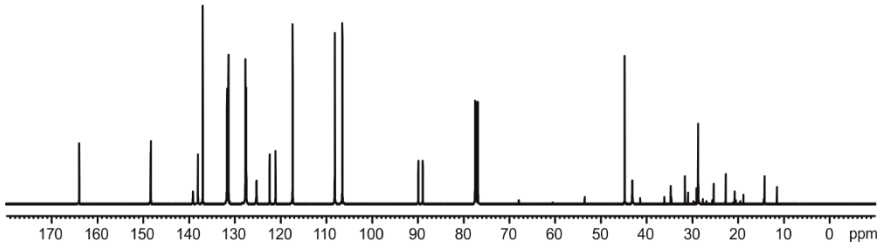

Figure 5.35. ^{13}C NMR spectrum (125 MHz, $CDCl_3$, 298 K) of **7**.

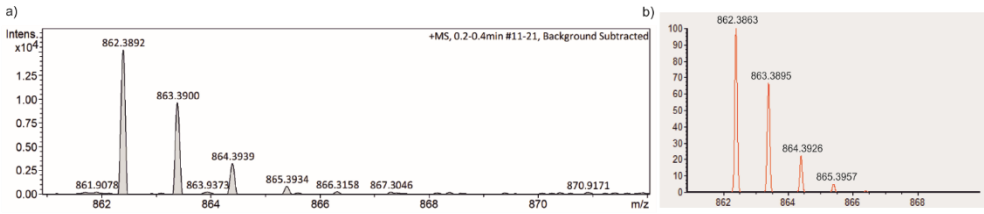

Figure 5.36. Experimental (a) and theoretical (b) isotopic distribution of [**7**+H]$^+$.

Synthesis of 1. 440 mg of **7** (0.51 mmol, 1 equivalent) are solved in 95 mL of a 20:1 mixture of Acetone:DMSO. To this mixture are added 0.36 mL of boron trifluoride diethyl etherate (3 mmol, 5.7 equivalent) in one portion. The solution is stirred under Argon atmosphere for 5 hours at room temperature. A red suspension is obtained, which is transferred to a separation funnel. 100 mL of DCM are added and the organic phase is washed three times with 150 mL of water, dried with sodium sulfate, filtered and concentrated under reduced pressure to obtain 500 mg of a pink solid. Purification by silica column chromatography using a 40% mixture of acetone in hexane, followed by crystallization in a 20% methanol mixture in DCM, gave the pure product as white crystals (9 mg, 2%). ^{1}H NMR (500 MHz, $CDCl_3$, 298 K) δ 8.35 (d, 2H, J = 7.7 Hz, Hb), 8.06 (t, 1H, J = 7.7 Hz, Ha), 7.85 (t, 2H, J = 6.2 Hz, Hc), 7.50 (d, 4H, J = 8.2 Hz, He), 7.46 (d, 4H, J = 8.0 Hz, Hg), 7.24 (d, 4H, J = 8.2 Hz, Hf), 7.00 (br, 4H, NH), 6.88 (d, 4H, J = 8.0 Hz, Hh), 6.00 (m, 8H, Hβ), 4.63 (d, 4H, J = 6.2 Hz, Hd), 1.97 (s, 6H, Hi), 1.51 (s, 6H), 1.45 (s, 6H). ^{13}C {^{1}H} NMR (125 MHz, $CDCl_3$, 298 K) δ 163.0, 148.6, 147.4, 139.3, 137.7, 137.1, 132.2, 131.8, 127.7, 127.6, 127.2, 125.2, 122.8, 121.4, 105.8, 105.1, 89.6, 89.3, 45.0, 43.5, 35.7, 30.6, 30.1, 29.7, 29.1. FTIR (ATR): $\bar{\upsilon}_{max}$ (cm^{-1}) = 3303 (amine N-H stretching), 2921 (C-C stretching), 1688 (ketone C=O stretching), 1516 (N-H bending). HR-MS (ESI-TOF-MS) m/z calculated for $C_{63}H_{55}N_7O_2$ $[M+H]^+$ – 942.4490, found 942.4526.

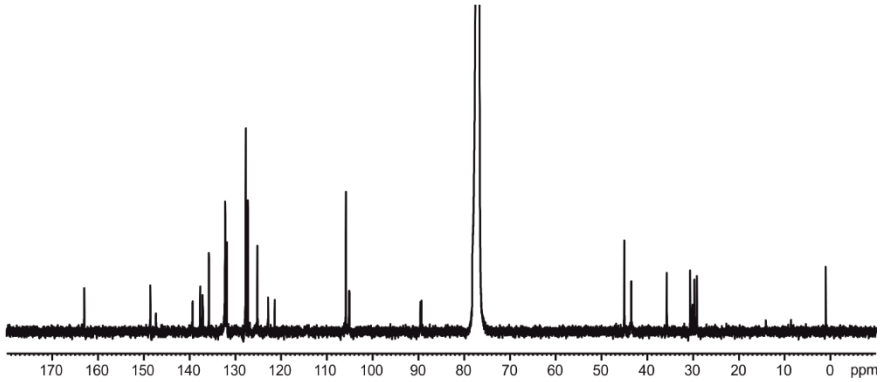

Figure 5.37. ^{13}C NMR spectrum (125 MHz, $CDCl_3$, 298 K) of **1**.

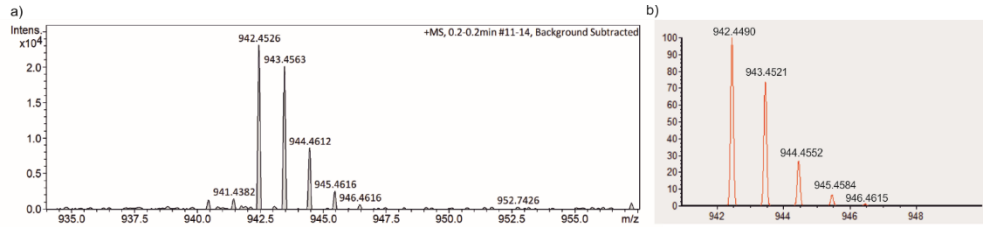

Figure 5.38. Experimental (a) and theoretical (b) isotopic distribution of [**1**+H]$^+$.

5.4.3. ^{1}H NMR Titration Experiments

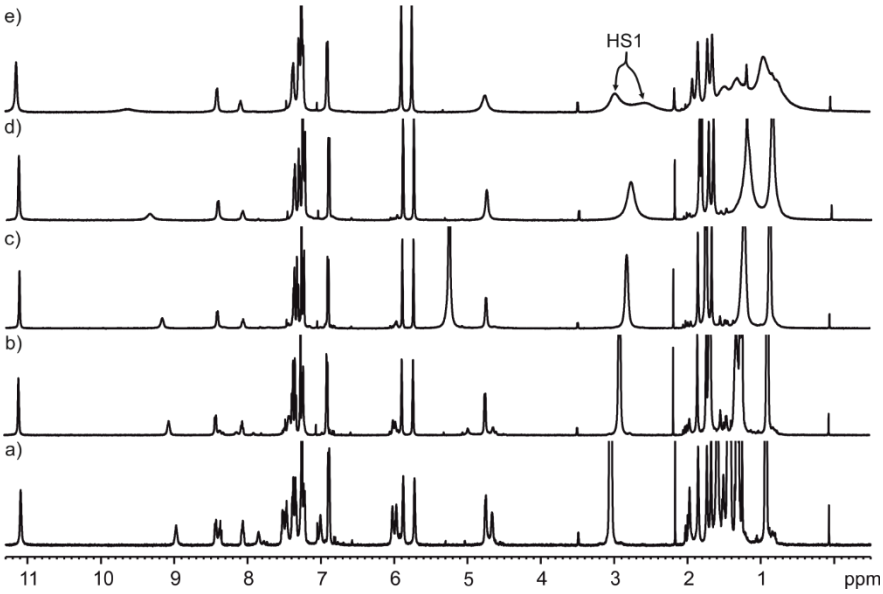

Figure 5.39. ^{1}H NMR spectra (500 MHz with cryoprobe, $CDCl_3$) of a 1:2 mixture of receptor **1** and TBA·Cl **2b** at 298 K a) 273 K b), 253 K c), 253 K d) and 213 K e). See Figure 5.2 for proton assignments.

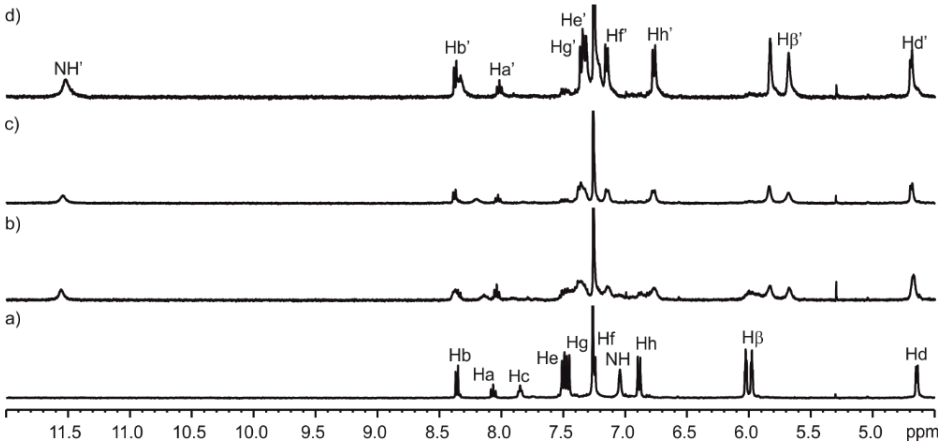

Figure 5.40. Selected region of the ^{1}H NMR spectra (400 MHz, $CDCl_3$, 298 K) of receptor **1** a) after the addition of 0.5 b), 1.0 c) and 3.0 d) equivalent of tetrabutylammonium cyanate **2c**. See Figure 5.2 for proton assignments.

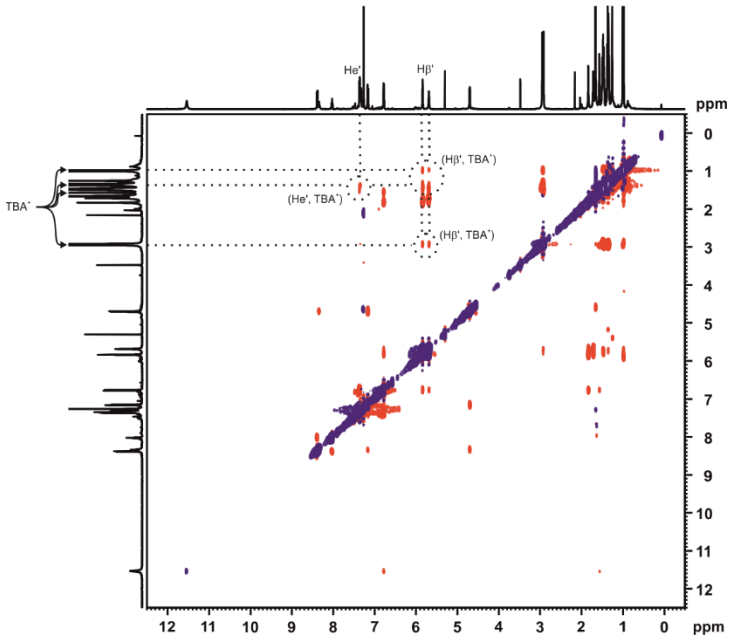

Figure 5.41. ^{1}H-^{1}H ROESY experiment (500 MHz, $CDCl_3$, 298 K, spin-lock = 0.3 s) of a 1:3 mixture of receptor **1** and TBA·OCN **2c**. Cross peaks of interest are assigned. See Figure 5.2 for proton assignments.

5.4.4. DOSY experiments

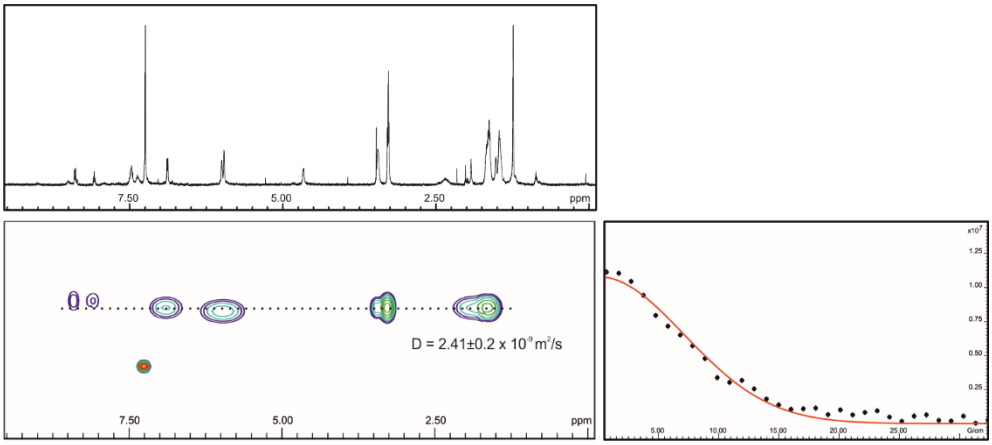

Figure 5.42. (left) ^{1}H pseudo 2D plot of DOSY (500 MHz, 298K, $CDCl_3$) of a 1:1.5 mixture of receptor **1** and TBA·Cl **2b** (D20 = 0.15 s, P30 = 1 ms). (right) Fit of the decay of the signal of proton Hb to a mono-exponential function using Dynamics Center software from Bruker. Error is indicated as standard deviation.

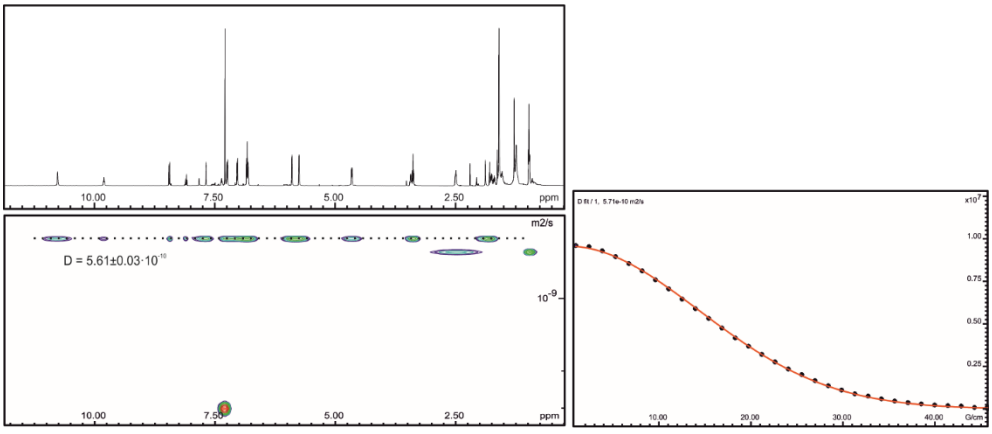

Figure 5.43. (left) ^{1}H pseudo 2D plot of DOSY (500 MHz, 298K, $CDCl_3$) of a 1:1:1 mixture of an equimolar mixture of receptor **1**, *N*-oxide **3** and TBA·OCN **2c** (D20 = 0.15 s, P30 = 1 ms). (right) Fit of the decay of the signal of proton Hb to a mono-exponential function using Dynamics Center software from Bruker. Error is indicated as standard deviation.

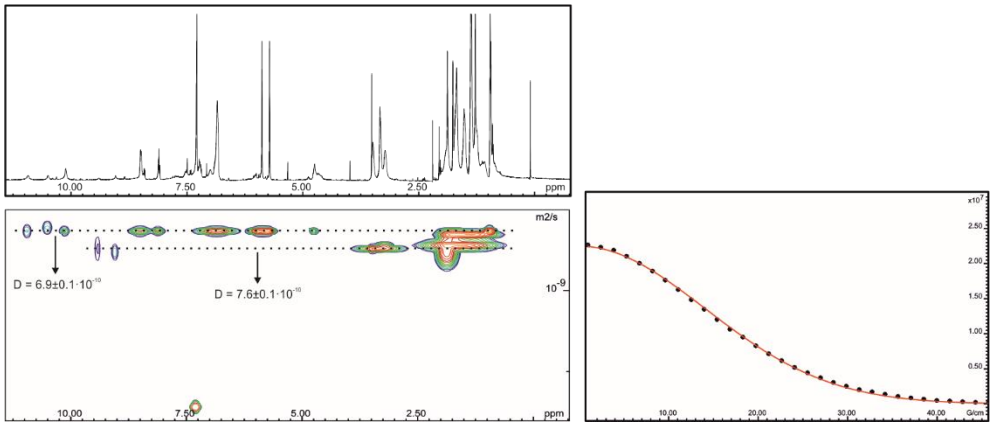

Figure 5.44. (left) ^{1}H pseudo 2D plot of DOSY (500 MHz, 298K, $CDCl_3$) of a 1:1:1 mixture of an equimolar mixture of receptor **1**, *N*-oxide **3** and MTOA·Cl **2a** (D20 = 0.15 s, P30 = 1 ms). (right) Fit of the decay of the signal of proton Hb to a mono-exponential function using Dynamics Center software from Bruker. Error is indicated as standard deviation.

5.4.5. ESI-MS experiments

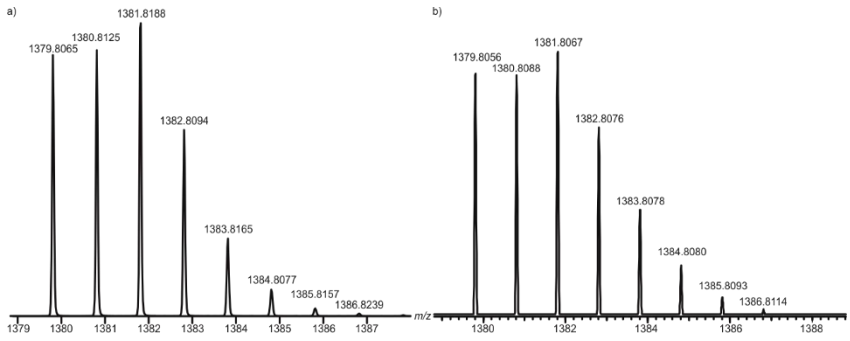

Figure 5.45. Experimental a) and calculated b) isotopic distribution of complex [**MTOA**·(**Cl**)$_2$⊂**1**]$^-$.

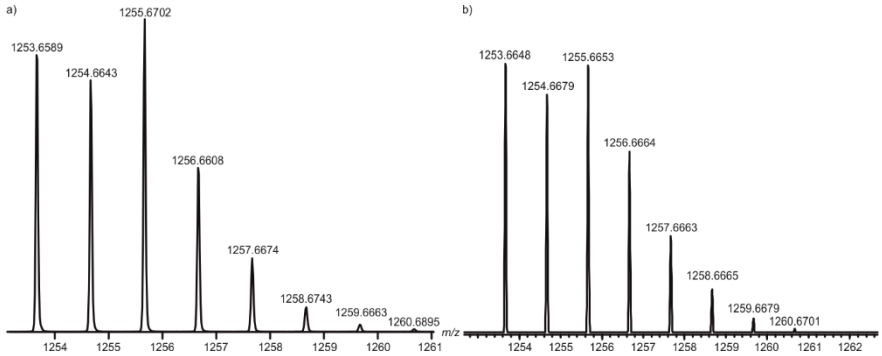

Figure 5.46. Experimental a) and calculated b) isotopic distribution of complex [**TBA**·(**Cl**)$_2$⊂**1**]$^-$.

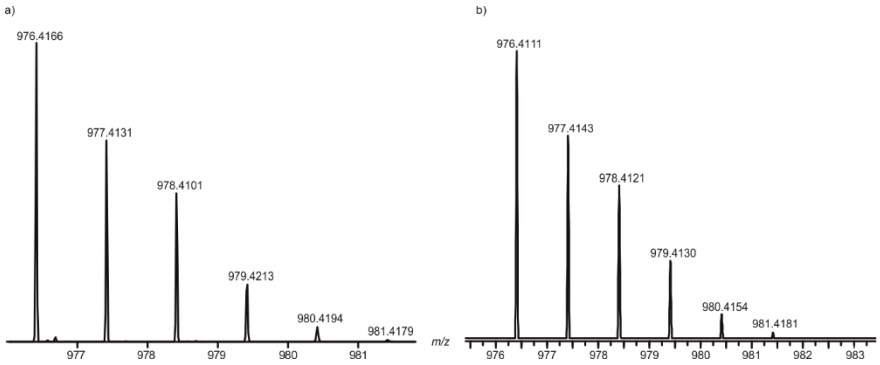

Figure 5.47. Experimental a) and calculated b) isotopic distribution of complex [**Cl**⊂**1**]$^-$.

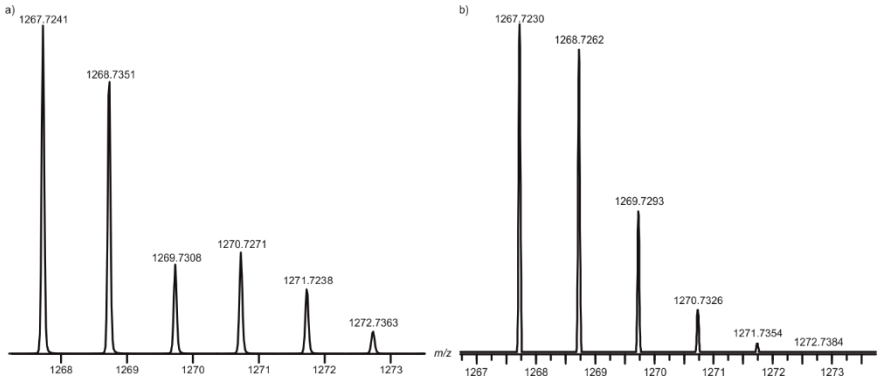

Figure 5.48. Experimental a) and calculated b) isotopic distribution of complex [**TBA**·(**OCN**)$_2$⊂**1**]$^-$.

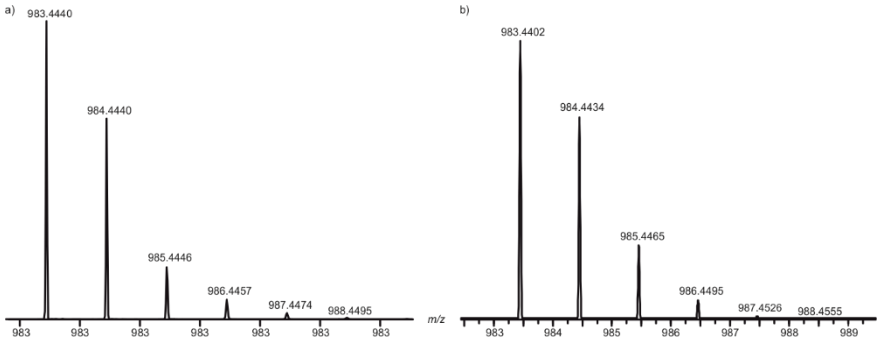

Figure 5.49. Experimental a) and calculated b) isotopic distribution of complex [**OCN**⊂**1**]$^-$.

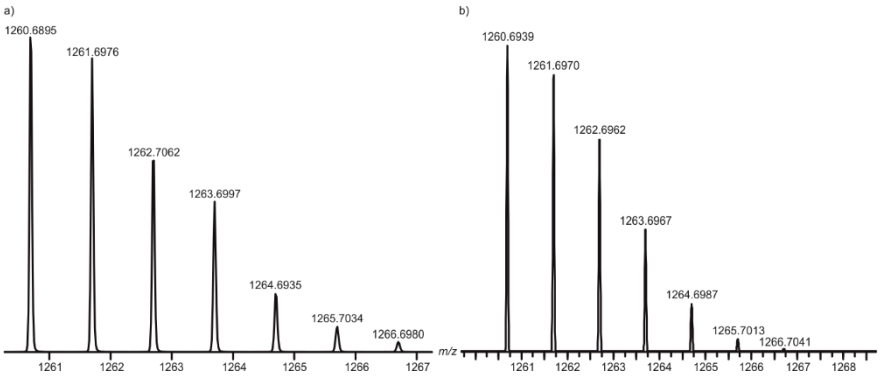

Figure 5.50. Experimental a) and calculated b) isotopic distribution of complex [**TBA·Cl·OCN⊂1**]$^-$.

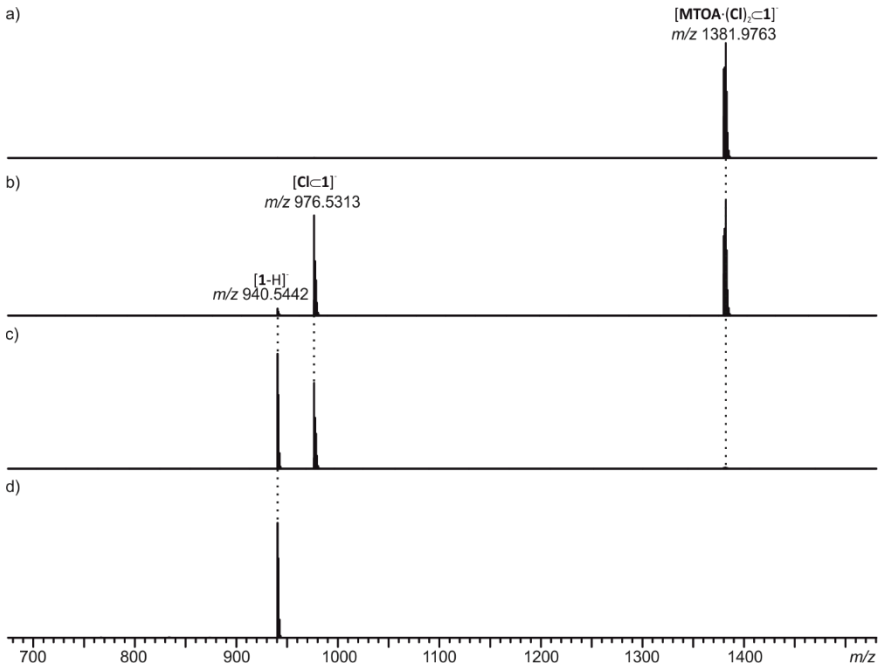

Figure 5.51. CID experiment performed with mass-selected ion [**MTOA·(Cl)$_2$⊂1**]$^-$ a) with CE of 27 V b), 36 V c) and 56 V d).

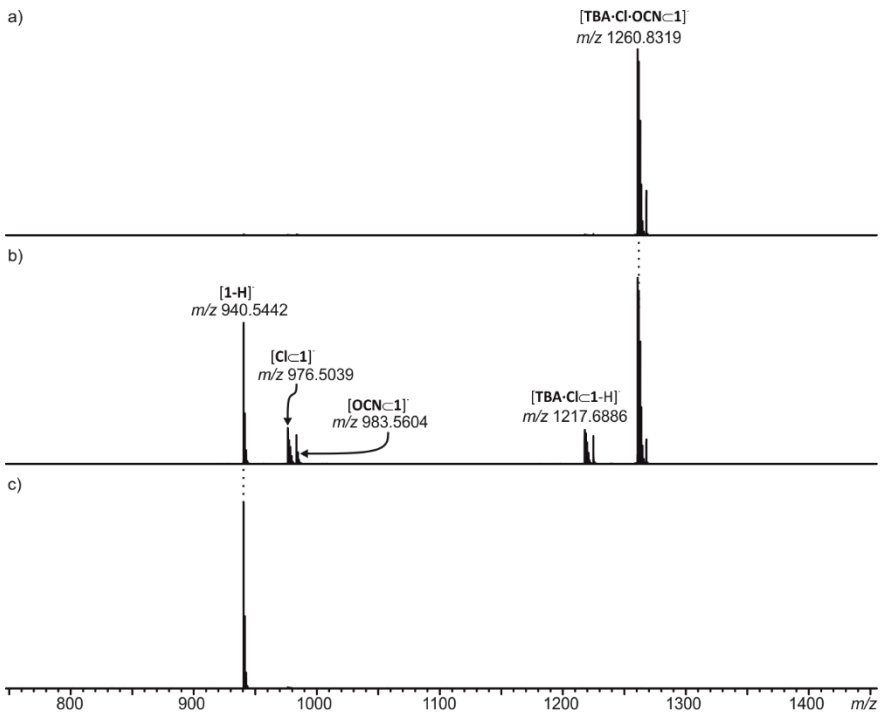

Figure 5.52. CID experiment performed with mass-selected ion [**TBA·(Cl)$_2$⊂1**]$^-$ a) with CE of 19 V b) and 40 V.

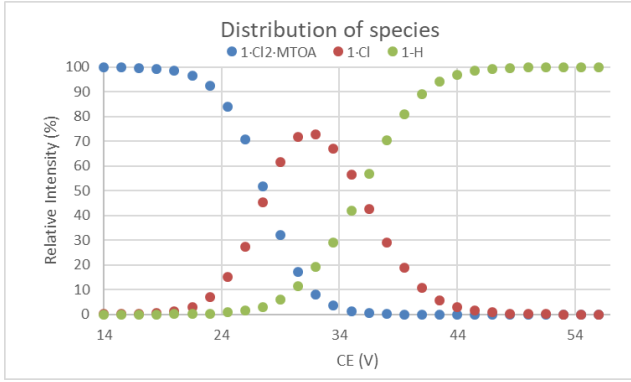

Figure 5.53. Relative intensity of the fragments observed in the CID experiment of complex [**MTOA·(Cl)$_2$⊂1**] at increasing CE voltages. The intensity was calculated as Intensity = I. Complex / (I. Complex + I. Fragments) x 100%.

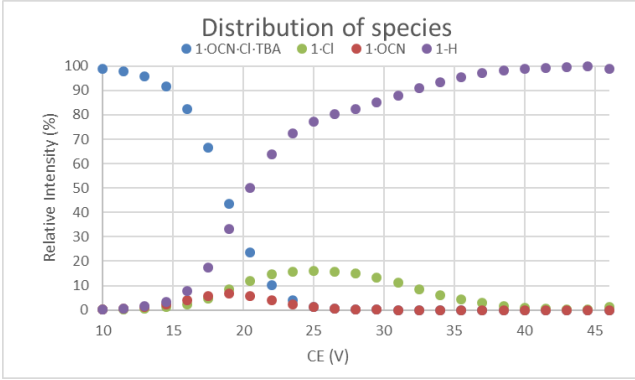

Figure 5.54. Relative intensity of the fragments observed in the CID experiment of complex [**TBA·OCN·Cl⊂1**] at increasing CE voltages. The intensity was calculated as Intensity = I. Complex / (I. Complex + I. Fragments) x 100%.

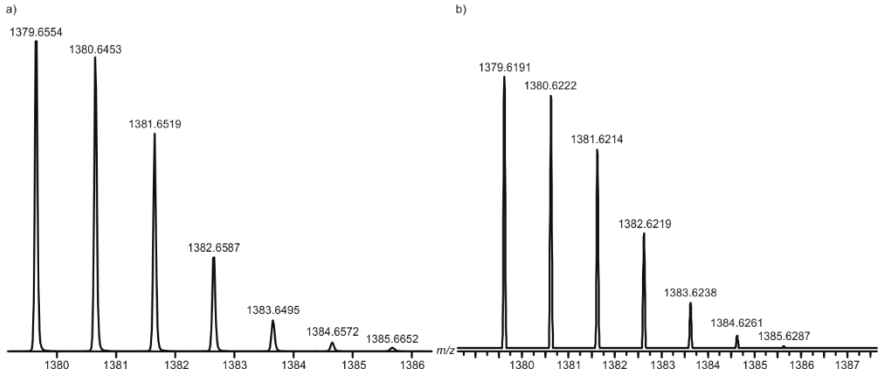

Figure 5.55. Experimental a) and calculated b) isotopic distribution of complex [**Cl·3⊂1**]$^-$.

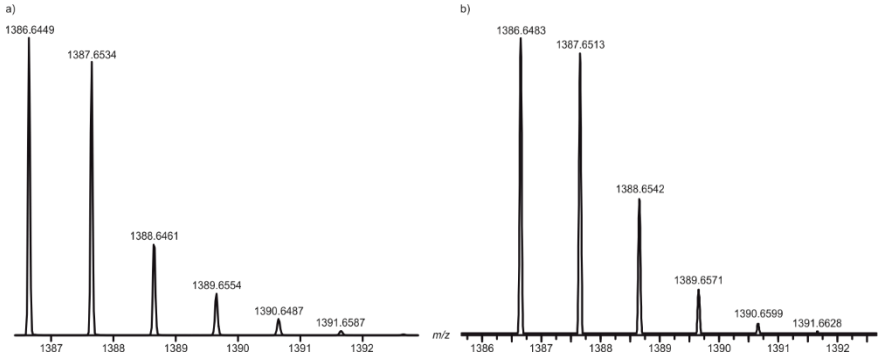

Figure 5.56. Experimental a) and calculated b) isotopic distribution of complex [**OCN·3⊂1**]$^-$.

5.5 References and notes

[1] Kim, S. K.; Sessler, J. L., Calix[4]pyrrole-Based Ion Pair Receptors. *Acc. Chem. Res.* **2014,** *47*, 2525-2536.
[2] Wagay, S. A.; Rather, I. A.; Ali, R., Functionalized calix[4]pyrroles: Emerging class of ion-pair receptors in supramolecular chemistry. *Mater. Today* **2020**.
[3] Peng, S.; He, Q.; Vargas-Zúñiga, G. I.; Qin, L.; Hwang, I.; Kim, S. K.; Heo, N. J.; Lee, C.-H.; Dutta, R.; Sessler, J. L., Strapped calix[4]pyrroles: from syntheses to applications. *Chem. Soc. Rev.* **2020,** *49*, 865-907.
[4] Lee, C.-H.; Miyaji, H.; Yoon, D.-W.; Sessler, J. L., Strapped and other topographically nonplanar calixpyrrole analogues. Improved anion receptors. *Chem. Commun.* **2008**, 24-34.
[5] He, Q.; Williams, N. J.; Oh, J. H.; Lynch, V. M.; Kim, S. K.; Moyer, B. A.; Sessler, J. L., Selective Solid–Liquid and Liquid–Liquid Extraction of Lithium Chloride Using Strapped Calix[4]pyrroles. *Angew. Chem. Int. Ed.* **2018,** *57*, 11924-11928.
[6] Kim, S. K.; Sessler, J. L.; Gross, D. E.; Lee, C.-H.; Kim, J. S.; Lynch, V. M.; Delmau, L. H.; Hay, B. P., A Calix[4]arene Strapped Calix[4]pyrrole: An Ion-Pair Receptor Displaying Three Different Cesium Cation Recognition Modes. *J. Am. Chem. Soc.* **2010,** *132*, 5827-5836.
[7] Park, I.-W.; Yoo, J.; Kim, B.; Adhikari, S.; Kim, S. K.; Yeon, Y.; Haynes, C. J. E.; Sutton, J. L.; Tong, C. C.; Lynch, V. M.; Sessler, J. L.; Gale, P. A.; Lee, C.-H., Oligoether-Strapped Calix[4]pyrrole: An Ion-Pair Receptor Displaying Cation-Dependent Chloride Anion Transport. *Chem.--Eur. J.* **2012,** *18*, 2514-2523.
[8] Miyaji, H.; Kim, H.-K.; Sim, E.-K.; Lee, C.-K.; Cho, W.-S.; Sessler, J. L.; Lee, C.-H., Coumarin-Strapped Calix[4]pyrrole: A Fluorogenic Anion Receptor Modulated by Cation and Anion Binding. *J. Am. Chem. Soc.* **2005,** *127*, 12510-12512.
[9] Heo, N. J.; Oh, J. H.; Lee, J. T.; He, Q.; Sessler, J. L.; Kim, S. K., Phenanthroline-strapped calix[4]pyrroles: anion receptors displaying affinity reversal as a function of solvent polarity. *Organic Chemistry Frontiers* **2020,** *7*, 548-556.
[10] Gross, D. E.; Yoon, D.-W.; Lynch, V. M.; Lee, C.-H.; Sessler, J. L., Anion binding behavior of heterocycle-strapped calix[4]pyrroles. *J. Inclusion Phenom. Macrocyclic Chem.* **2010,** *66* (1), 81-85.
[11] Ko, S.-K.; Kim, S. K.; Share, A.; Lynch, V. M.; Park, J.; Namkung, W.; Van Rossom, W.; Busschaert, N.; Gale, P. A.; Sessler, J. L.; Shin, I., Synthetic ion transporters can induce apoptosis by facilitating chloride anion transport into cells. *Nature Chem.* **2014,** *6* (10), 885-892.
[12] Yoon, D.-W.; Hwang, H.; Lee, C.-H., Synthesis of a Strapped Calix[4]pyrrole: Structure and Anion Binding Properties. *Angew. Chem. Int. Ed.* **2002,** *41*, 1757-1759.
[13] The energy-minimized structure was obtained using the software package Fujitsu Scigress Version 2.2.0. The structure was optimized by performing a geometry calculation using the implemented molecular mechanics force field with augmented MM3 parameters.
[14] See Chapter 3 for the determination of the binding constant between a two-wall aryl-extended calix[4]pyrrole and MTOA·Cl.
[15] Adriaenssens, L.; Gil-Ramírez, G.; Frontera, A.; Quiñonero, D.; Escudero-Adán, E. C.; Ballester, P., Thermodynamic Characterization of Halide–π Interactions in Solution Using "Two-Wall" Aryl Extended Calix[4]pyrroles as Model System. *J. Am. Chem. Soc.* **2014,** *136*, 3208-3218.

[16] Adjustment of the titration data to a 1:1 binding model using HypNMR software 2008 (version 4.0.66) allowed us to estimate a binding affinity constant of ca. $< 10^2$ M^{-1}. The minor chemical shift changes experienced by the proton signals of the receptor made the adjustment troublesome and the values obtained unreliable.

[17] For this reason, the experiments performed with the equimolar mixture of **1**, **2a** and **3** produced analogue results as those obtained with **2b**.

General conclusions

This thesis describes the synthesis and binding properties of a series of supramolecular receptors based on calix[4]pyrrole architectures. The general objective of this work was the recognition of ion-pairs in chloroform solution, which has been achieved with the use of the synthetized receptors. The complexes obtained have been characterized by ^{1}H NMR, ITC and ESI-MS experiments.

The first receptor discussed in this thesis is a two-wall bis(calix[4]pyrrole) macrocycle obtained by the intermolecular coupling reaction of two terminal calix[4]pyrrole units. The obtained results evidence the crucial role played by templating molecules in the synthesis of supramolecular receptors. The formation of open oligocyclic intermediates takes place by random collision of the reacting units. However, the intramolecular reaction necessary to generate the macrocyclic receptor is often facilitated by the use of a template. We concluded that correct choice of a template molecule complementary in size and shape with the macrocyclic receptor is in some cases mandatory. In our particular case, the therephthalate anion facilitated the formation of the macrocyclic receptor by favouring the intramolecular reaction of the open oligocyclic intermediate. In contrast, the use of the longer bis-pyridyl-bis-*N*,*N*-oxide favoured the formation of polymeric products.

We explored the properties of the prepared bis(calix[4]pyrrole) receptor to bind tetraalkylammonium salts TBA·Cl, TBA·OCN and MTOA·Cl. We demonstrated the formation of 1:2 complexes containing two bound ion-pairs. Interestingly, the binding affinity constants obtained for the coordination of the first ion-pair were one to two orders of magnitude higher than the ones obtained with the analogous two-wall versions of the receptor, featuring a single binding site. This finding support the positive effects of the preorganization of rigid supramolecular receptors in the binding of neutral and charged molecules. We also detected the preferred binding of the anions in one of the two non-equivalent binding sites of the bis(calix[4]pyrrole) macrocyclic receptor. From these results, we conclude that reduced differences in the electron density of the *meso* aromatic walls in C4P receptors can greatly affect the anion-π interactions.

The 1:2 complexes obtained displayed two different binding geometries depending on the cation used. In the case of the TBA salts we obtained cascade-like arrangements featuring a close-contact ion triplet. The use of MTOA·Cl produced

the formation of a receptor separated complex. These results support the higher affinity of the $MTOA^+$ cation in the shallow and electron rich aromatic cavity generated by the C4P cone conformation.

The formation of the 1:2 complexes displayed a non-cooperativity allosteric effect in the case of the TBA salts and a negative allosteric cooperativity for MTOA·Cl. Most likely, this is due to the relative short distance of the bound chloride anions. These results also highlight the important role that counter-cation plays in the binding of ion-pairs by synthetic receptors.

We studied the formation of pseudorotaxane complexes assisted by the same tetraalkylammonium salts using a lineal pyridyl-*N*-oxide as axle. We observed the formation of kinetically and thermodynamically stable [2]pseudorotaxane complexes with all the ion-pairs studied. The obtained complexes existed in two isomeric forms depending on which of the two binding sites of the receptor the anion and the axle are bound. From the obtained results, we concluded that TBA·OCN could be used as template for the synthesis of a [2]rotaxane by a stoppering procedure due to the slow dynamics exchange governing the binding process of the precursor [2]pseudorotaxane. Our findings highlight the importance of the pseudorotaxane formation studies for the later synthesis of MIM such as catenanes and rotaxanes. In addition, we obtained higher values for the binding affinity constant of the pseudorotaxane assembled receptors towards TBA·OCN over TBA·Cl, most likely due to the cylindrical shape of the polyatomic cyanate anion. These findings emphasize the relevance of designing suitable three-dimensional binding pockets on supramolecular receptors that match the size and shape of the anion of interest.

The anion templated synthesis of the [2]rotaxane produced the almost quantitative formation of the entangled architecture. However, dissociation of the bound anion proved to be not feasible under the explored conditions. The synthesis in the absence of any template produced the [2]rotaxane receptor in an 8% yield, highlighting the role played by template molecules in the synthesis of supramolecular receptors. As expected, similar results were obtained for the binding studies of tetraalkylammonium ion pairs with the [2]rotaxane receptor as those observed for the [2]pseudorotaxane.

We have also disclosed the synthesis of a strapped 2W-C4P receptor featuring a pyridine-dicarboxamide strap. The macrocyclic receptor featured a larger inner

cavity compared to the strapped 2W-C4P counterparts previously reported in the literature. The strapped macrocycle produced kinetically and thermodynamically stable 1:2 complexes with tetraalkylammonium salts. The binding geometry of the complexes obtained featured cascade and receptor-separated binding geometries for TBA and MTOA salts, respectively. Additionally, the stability and binding exchange dynamics displayed by the pseudorotaxane complexes obtained with a lineal pyridyl-*N*-oxide axle were also dependent on the ion pair used. On the one hand, these results show that increasing the cavity size of synthetic receptors favors the binding of close contact ion triplets. On the other hand, it again emphasizes the role played by the counter cation in the assembly of synthetic supramolecular complexes assisted by ion-pairs.

In summary, we have demonstrated the applications of C4P macrocycles for the design of supramolecular ion-pair receptors. The incorporation into the C4P scaffold of additional polar groups able to engage in molecular recognition processes generate ion-pair receptors with improved affinity and selectivity. In addition, C4P can be incorporated in interlocked receptors in which three-dimensional binding pockets are generated. We believe that the results herein described can help in the design of interlocked molecules of rotaxane topology with multiple stations. The presence of two inequivalent binding sites in the BC4P macrocyclic receptors herein described may impose some level of selectivity towards the different stations of a potential lineal component with multiple binding sites. The transition of these systems into the aqueous media could also generate receptors with potential applications as intermembrane anion transporters.

UNIVERSITAT ROVIRA I VIRGILI
Calix[4]pyrrole Based Receptors for the Recognition of Ion Pairs
Ricardo Molina Muriel

List of Abbreviations

AE-C4P	-	Aryl Extended calix[4]pyrrole
AcOEt	-	Ethyl acetate
ACN	-	Acetonitrile
ATR	-	Attenuated Total Reference
BC4P	-	Bis(calix[4]pyrrole)
BPNOx	-	4,4-bipyridine-N,N-dioxide
C4P	-	Calix[4]pyrrole
CID	-	Collision Induced Dissociation
CIS	-	Complexation Induced Shifts
COSY	-	Correlated Spectroscopy
CPK	-	Corey-Pauling-Koltun model
CuAAC	-	Copper(I)-catalyzed alkyne-azide cycloaddtion
DIPEA	-	*N,N*-Diisopropylethylamine
DCM	-	Dichloromethane
DMSO	-	Dimethylsulfoxide
DOSY	-	Diffusion Ordered Spectroscopy
ESI-MS	-	Electrospray Ionization Mass Spectrometry
FT-IR	-	Fourier Transform Infrared Spectroscopy
HSQC	-	Heteronuclear Single Quantum Correlation
HMBC	-	Heteronuclear Multiple Bond Correlation
HPLC	-	High-Performance Liquid Cromatography

IMS	-	Ion-Mobility Mass Spectrometry
ITC	-	Isothermal Titration Calorimetry
K	-	Kelvin
Kcal	-	Kilocalorie
MALDI	-	Matrix-Assisted Laser Desorption Ionization
MHz	-	MegaHertz
MIM	-	Mechanically Interlocked Molecule
MS	-	Mass Spectrometry
mM	-	Millimolar
MM	-	Molecular Mechanics force field
MTOA	-	Methyltrioctylammonium
NMR	-	Nuclear Magnetic Resonance
NOESY	-	Nuclear Overhauser Enhancement Spectroscopy
ROESY	-	Rotating-frame Enhancement Spectroscopy
r.t.	-	Room temperature
SAE-C4P	-	Super Aryl-extended Calix[4]pyrrole
SPS	-	Solvent Purification System
TBA	-	Tetrabutylammonium
TBACl	-	Tetrabutylammonium Chloride
TBAF	-	Tetrabutylammonium Fluoride
TBAOCN	-	Tetrabutilammonium Cyanate
THF	-	Tetrahydrofuran
TFA	-	Trifluoroacetic acid

TBTA	-	Tris(benzyltriazolylmethyl)amine
TMS	-	Tetramethylsilane
TMA	-	Tetramethylammonium
TPH	-	Terephthalate
TW	-	Traveling wave
UV-Vis	-	Ultraviolet-Visible

UNIVERSITAT ROVIRA I VIRGILI
Calix[4]pyrrole Based Receptors for the Recognition of Ion Pairs
Ricardo Molina Muriel

UNIVERSITAT ROVIRA I VIRGILI
Calix[4]pyrrole Based Receptors for the Recognition of Ion Pairs
Ricardo Molina Muriel

UNIVERSITAT ROVIRA I VIRGILI
Calix[4]pyrrole Based Receptors for the Recognition of Ion Pairs
Ricardo Molina Muriel

UNIVERSITAT ROVIRA I VIRGILI
Calix[4]pyrrole Based Receptors for the Recognition of Ion Pairs
Ricardo Molina Muriel

UNIVERSITAT
ROVIRA i VIRGILI